# Design and Development of Synthetic Nanoparticle Antibodies to Deplete Selected Target Cells for Cancer Immunotherapy

A Dissertation
Presented to
The Academic Faculty

by

Jiaying Liu

In Partial Fulfillment
of the Requirements for the Degree
Doctor of Philosophy in the
Wallace H. Coulter Department of Biomedical Engineering

Georgia Institute of Technology and Emory University
August 2019

# Design and Development of Synthetic Nanoparticle Antibodies to Deplete Selected Target Cells for Cancer Immunotherapy

Approved by:


Dr. Krishnendu Roy, Advisor
School of Biomedical Engineering,
*Georgia Institute of Technology*
*& Emory University*

Dr. Ravi Kane
School of Chemical and Biomolecular Engineering
*Georgia Institute of Technology*

Dr. M.G. Finn
School of Chemistry and Biochemistry,
*Georgia Institute of Technology*

Dr. Susan Thomas,
School of Biomedical Engineering
*Georgia Institute of Technology*
*& Emory University*

Dr. Robert Guldberg
Phil and Penny Knight Campus for Accelerating Scientific Impact,
*University of Oregon*



Date Approved: June 06, 2019

To my family and friends who supported me throughout graduate school.

# ACKNOWLEDGEMENTS

When I first arrived in the United States, I thought I would spent the following several years lonely dealing with science. It turns out that life in the graduate school is completely different from what I expected. Now, when it comes to an end, when I am going to step out with a full six years of harvest in science, skills, friendship and love, I want to express my sincere thanks for the unwavering support from my family, friends and mentors.

First, I'd like to thank my advisor, Dr. Krishnendu Roy. His guidance in my research is instrumental, without which it would not be possible for me to present this two-hundred-page dissertation here. In addition, he is a great mentor in research as well as in life. It is his advice, patience and confidence in me that led me to complete my graduate school. Next, I would like to thank my committee members for their valuable input in my thesis project. Despite of his crazy schedule, Dr. M.G.Finn was always there to give the clearest and useful suggestions that solved the problems I encountered. Dr. Guldberg is the one who knew my project even before my thesis proposal and expressed persisting support throughout the years. Dr. Thomas has been a role model for me as a successful female scientist and she encouraged me in many ways to do a better job in my research. Also, Dr. Kane provided a lot of helpful insights to make my research move forward.

Besides, among the lab members, Pallab, Randy and later Casey have contributed countless ideas, help and time in my projects. They knew all the frustrations and excitement I've had in research and made the "SNAb Lab" experiments less boring. Apart from research, we are also good friends, sharing thoughts about food, life and

future together. Kirsten, Joscelyn and Michael are my closest companions in the journey to Ph.D. We struggled through the Qualifying exams, Proposal, and Defense and celebrated each milestone together. They were always ready to help. Their warmth and friendship are something I want to cherish for the rest of my life. In addition, Jardin, Alexandra A, Delta, Hannah, Nate and Aaron also provided a lot of help in experiments and life. More importantly, we had many joyful moments together in and outside of lab that I will not forget. Lastly, without the participation of many dedicated, intelligent undergraduate students, including Shohini, Andrew, Simran, and Sondos, this thesis would not have been possible. I learnt a lot while I was working with them.

Furthermore, I would like to thank my collaborators, Dr. Gumbart, Zijian and Katie. They did the computational modeling part of the thesis and made the conclusions more solid. Kelsey and Dr. Emelianov also helped tremendously and were extremely patient with the many repetition of the photoacoustic imaging experiments. Besides, I also want to thank Da Huo in Dr. Younan Xia's group for help on ICP-MS, and Andrew, Akia and Simone in Dr.Platt's lab for help on western blotting. At the meantime, I acquired a lot of assistance for the acquisition of data from Sommer Durham, Andrew Shaw, David Smalley, Aaron Liftland, and Steve Woodard in the core facilities and for the animal studies from the PRL staff. Carol Mills and Carla Zachery submitted all my annoying urgent orders of reagents and figured out my stipend issues. I am sincerely grateful for all the help I received outside of the Roylab.

I want to dedicate this paragraph to my friends. Some of them are also students or alumni of Georgia Tech and Emory University. Thanks for their forgiveness of my inflexible schedule and for sharing the happiness and upset with me in the little leisure time we had.

The other friends are in China or other parts of the US. Distance and time didn't diminish our friendship and they made me realize that however much science disliked me sometimes, they still love me.

Finally, thank you my family, especially my parents and husband, Hao. My parents traveled long distance from China to visit me as many times as they could during my graduate school years. I do and I will express my love to them in every way I could. Three of my most important family members passed away when I am in the US and I know all the family members miss me as much as I miss them. Hao is an invaluable gift of my life. We lived and grew together during the past years. I owe him a thank-you for not giving up our love when my depression in research significantly impacted his quality of life. Our marriage should also be listed as an achievement in my graduate school.

# TABLE OF CONTENTS

# LIST OF TABLES

# LIST OF FIGURES

# LIST OF SYMBOLS AND ABBREVIATIONS

| | |
|---|---|
| ADCC | Antibody-Dependent Cellular Cytotoxicity |
| ADCP | Antibody-Dependent Cellular Phagocytosis |
| AF555/647/680 | Alexa Fluor dye with emission peak at 580nm, 665nm or 702nm |
| ALA | Alanine |
| APC | Allophycocyanin |
| AQUA | Absolute quantification |
| ARG | Arginine |
| ASN | Asparagine |
| ASP | Aspartic acid |
| ATP | Adenosine triphosphate |
| SA-AuNP-SA | Gold nanoparticle coated with streptavidin |
| SA-AuNP-SH | Janus streptavidin-coated gold nanoparticle with part of the surface displaying thiol groups |
| BCA | Bicinchoninic acid |
| CFSE | Carboxyfluorescein succinimidyl ester |
| CLEARTM | Crosslinked ethoxylate acrylate resin |
| CTLA-4 | Cytotoxic T Lymphocyte-ssociated Antigen 4 |
| CYS | Cysteine |
| DMEM | Dulbecco's Modified Eagle Medium |
| DMSO | Dimethyl Sulfoxide |
| DTSSP | Dithiobis(sulfosuccinimidylpropionate) |
| DTT | Dithiothreitol |

| | |
|---|---|
| EC50 | The concentration of a drug that gives half-maximal response. |
| ELISA | Enzyme-Linked Immunosorbent Assay |
| EPR | Enhanced permeability and retention |
| FACS | Fluorescence Activated Cell Sorting |
| FBS | Fetal Bovine Serum |
| FcγR | Fc gamma Receptor, including FcγRI, FcγRII(a,b), FcγRIII, FcγRIV |
| FcRn | Neonatal Fc receptors |
| FITC | Fluorescein isothiocyanate |
| Foxp3 | Forkhead box P3 |
| FSC | Forward Scatter |
| G3-SNAbs | Same as Janus G3-AuNP-cp33 nanoparticles |
| G3*-SNAbs | Same as Janus G3*-AuNP-cp33 nanoparticles |
| GLU | Glutamic acid |
| GLN | Glutamine |
| GLY | Glycine |
| Gr1 | Group 1 protein |
| HABA | 4'-hydroxyazobenzene-2-carboxylic acid |
| Her2 | Human epidermal growth factor receptor 2 |
| HEPES | 4-(2-hydroxyethyl)-1-piperazineethanesulfonic acid |
| His | Histdine |
| IC50 | The concentration of an inhibitor where the response (or binding) is reduced by half. |
| ICP-MS | Inductively coupled plasma-mass spectrometry |
| ILE | Isoleucine |

| | |
|---|---|
| IFNγ | Interferon gamma |
| IgG | Immunoglobulin, including IgG1, 2, 3, 4 |
| IL | Interleukin, such as IL-6, IL-12 |
| ITAM | Immunoreceptor tyrosine-based activation motif |
| ITIM | Immunoreceptor tyrosine-based inhibitory motif |
| LEU | Leucine |
| LYS | Lysine |
| mAb | Monoclonal Antibody |
| MACS | Magnetic-activated cell sorting |
| M-CSF | Macrophage colony-stimulating factor |
| MDSC | Myeloid-Derived Suppressor Cell |
| MDSC-SNAb | Peptide modified Janus gold nanoparticles with part of the surface displaying G3 peptides and the rest of the surface displaying cp33. |
| MET | Methionine |
| NFκB | Nuclear factor kappa-light-chain-enhancer of activated B cells |
| NHS | N-hydroxysuccinimide |
| NK | Natural killer cells |
| OPA | O-Phthaldialdehyde |
| PAGE | Polyacrylamide gel electrophoresis |
| PBS | Phosphate Buffered Saline |
| PD1 | Programmed Death 1 receptor |
| PDL1 | Programmed Death Ligand 1 |
| PE | Phycoerythrin |
| PEG | Poly(ethylene glycol) |

| | |
|---|---|
| Pen-Strep | Penicillin – streptomycin |
| PHE | Phenylalanine |
| PI | Propidium iodide |
| PMN | Polymorphonuclear neutrophils |
| PRO | Proline |
| RAW 264.7 | A mouse macrophage-like cell line |
| RAW-Blue | A reporter cell line for NFκB |
| RIPA | Radioimmunoprecipitation assay |
| RPMI 1640 | Roswell Park Memorial Institute 1640 medium |
| ROS | Reactive Oxygen Species |
| SA | Streptavidin |
| scFv | Single-chain variable fragment |
| SDS | Sodium dodecyl sulfate |
| SER | Serine |
| SK-BR-3 | A human adenocarcinoma cell line overexpressing Her2 |
| SMCC | Succinimidyl-4-(N-maleimidomethyl)cyclohexane-1-carboxylate |
| SNAb | Synthetic nanoparticle antibody |
| SPR | Surface plasmon resonance |
| SSC | Side Scatter |
| Syk | Spleen tyrosine kinase |
| TBS | Tris-buffered saline |
| TBST | Tris-buffered saline with tween |
| TCEP | Tris(2-carboxyethyl)phosphine |
| TEM | Transmission electron microscopy |
| TEMED | Tetramethylethylenediamine |

| | |
|---|---|
| THR | Threonine |
| TNFα | Tumor necrosis factor alpha |
| TRP | Tryptophan |
| TYR | Tyrosine |
| VAL | Valine |
| VEGF | Vascular endothelial growth factor |

# SUMMARY

Monoclonal antibodies (mAbs) have shown great promise as immunotherapy of cancer in the past decades. They mediate the antibody-dependent immune responses to eliminate the malignant or suppressive cells and proteins and restore anti-cancer immunity. However, the application of monoclonal antibodies as therapeutics is greatly hampered by its high production cost as well as high dosage required to generate significant therapeutic effect due to limited tissue penetration and retention. Additionally, monoclonal antibodies targeting some important immunological targets, such as myeloid-derived suppressor cells (MDSCs), regulatory T cells, are still waiting to be developed.

Here, we have developed a novel type of artificial antibodies, the synthetic nanoparticle antibodies (SNAbs), which are Janus nanoparticles multivalently displaying both binding ligands for the selected cellular targets and Fc-mimicking ligands that can activate Fc receptors. Our **primary hypothesis** is that the designed SNAbs could induce antibody-dependent cellular cytotoxicity (ADCC) or phagocytosis (ADCP) of cellular targets efficiently both *in vitro* and *in vivo*. A simple chemistry to fabricate Janus gold nanoparticles and to modify these nanoparticles with peptide ligands was designed to generate SNAbs. We evaluated the capability of SNAbs to target MDSCs, as a model cell type in both *ex vivo* assays and *in vivo* tumor model systems. We showed that SNAbs can selectively induce the antibody-dependent killing of MDSCs in the mixture of various types of cells and are also able to deplete MDSCs in a tumor model. The research completed in this thesis demonstrated that the SNAbs are a functional alternative to monoclonal antibodies and hold great promise as a potent immunotherapy for cancer.

# CHAPTER 1 OVERVIEW, HYPOTHESIS AND SPECIFIC AIMS

## 1.1 Overview

Malignant cells utilize several mechanisms to evade the immune system, including recruiting/promoting regulatory cells (e.g. myeloid derived suppressor cells (MDSCs)), up-regulating inhibitory surface ligands, releasing suppressive cytokines or enzymes to repress the activity of immune effector cells (e.g., cytotoxic T cells).[1,2] Monoclonal antibodies (mAbs), comprised of Fab domain for targeting specific antigens and Fc fragment for immune activation, have shown great promise in treatment of cancer in the past decades[3,4]. A handful of available mAbs (e.g.,atezolizumab) take advantages of the antibody-dependent immune responses to eliminate the suppressive cells/proteins and restore anti-cancer immunity.[5–8] On the other hand, some malignant cells express their own cancer-associated antigens (e.g. Her2, CD20). Antibodies (e.g.,trastuzumab, rituximab), which are able to bind to these antigens, can kill tumor targets by eliciting antibody-dependent cellular cytotoxicity/phagocytosis (ADCC/ADCP).[9–11] However, the application of monoclonal antibodies as therapeutics is greatly limited by its high production cost [12] as well as high dosage required to generate significant therapeutic effect due to limited tissue penetration.[12,13] Furthermore, monoclonal antibodies targeting some important immunological targets, such as MDSCs, regulatory T cells, are still waiting to be developed.

Small molecule ligands, such peptides and aptamers, have emerged as potent biotherapeutics for diagnosis, drug or gene delivery and disease treatment.[14–16] Various screening techniques, such as phage display biopanning, exist to accelerate the

identification of effective small molecule ligands for specific biomedical applications.[14,15,17] These ligands were widely applied on particulate systems to facilitate the targeted delivery of drugs or induction of therapeutic responses.[18–20] The particulate systems, on the other hand, are facile presentation platform and carriers for the ligands and drug, and also provide unique, easy tailorable physical and chemical properties to modulate the therapeutic effects.[21–23] We believe that synthetic nanoparticle antibodies (SNAbs), which are Janus nanoparticles multivalently displaying both binding ligands for the selected targets and Fc-mimicking ligands, can activate Fc-receptor-mediated immune responses and serve as a functional alternative to conventional mAbs. By combining the advantages of peptides and nanoparticles, SNAbs could be a promising immunotherapy for cancer via depleting malignant or suppressive cells or proteins. As a flexible platform technology, SNAbs may also have broad application potential in other biomedical areas, such as disease diagnosis, drug/gene delivery, imaging and analytical biotechnology.

### 1.2 Hypothesis

Our **primary hypothesis** is that the designed SNAbs could induce ADCC/ADCP of cellular targets efficiently both *in vitro* and *in vivo*. The overall objective is to develop the chemistry fabrication method of SNAbs as a platform technology. As a proof of concept, a type of SNAbs was designed to target MDSCs, as a model cell target, and deplete these MDSCs by activating antibody-dependent immune responses *in vitro* and in murine tumor models

### 1.3 Specific Aim 1: To design and develop SNAbs that display both target-binding ligands and Fc-mimicking ligands

In this aim**,** we developed a novel fabrication approach to generate SNAbs. We first synthesized Janus nanoparticles by an adapted solid-phase chemistry method[24] and then designed the chemistry to conjugate target-binding peptides as well as Fc-mimicking ligands [25,26] onto their surfaces to make fully functional SNAbs. The physical and surface chemistry properties and peptide modification of these SNAbs were characterized and validated using colorimetric, microscopic and spectrometric methods.

### 1.4 Specific Aim 2: To demonstrate *ex vivo,* the specificity of cell targeting and activation of immune responses by the SNAbs

In this aim, we hypothesized that the surface presentation of target-binding ligands and Fc-mimicking ligands on SNAbs enables them to bind specifically to target cells and trigger antibody-dependent responses. MDSCs were selected as the model cell target. We validated our hypothesis for MDSC-SNAbs through evaluating the binding capability, targeting specificity, and the induction of ADCC/ADCP of MDSCs by effector cells. We also studied the major mechanism of action of MDSC-SNAbs and also investigated the function of Janus structure in the activation of immune responses by MDSC-SNAbs.

### 1.5 Specific Aim 3: To evaluate the therapeutic potential of the MDSC-SNAbs in tumor models

The 4T1 breast cancer murine model is an aggressive cancer model that recapitulated the pathophysiological properties of human triple negative breast cancer.[27,28] MDSCs

accumulated in the spleen, tumor, blood and lymph nodes in the 4T1-tumor bearing mice and promote the metastasis of the tumor cells. In this aim, we hypothesized that the MDSC-SNAbs can deplete the MDSCs *in vivo* and provide therapeutic benefit in the murine tumor model. To evaluate the efficacy of SNAbs to deplete MDSCs, we administered MDSC-SNAbs to 4T1-tumor bearing mice with different dosing frequency and treatment duration and analyzed the major organs for cell composition and immune-cell functions. We also studied the biodistribution of SNAbs *in vivo* with inductively-coupled plasma-mass spectrometry and conducted survival studies with MDSC-SNAbs alone or in combination with immune-checkpoint inhibitors to assess the potential of MDSC-SNAbs as an immunotherapy for cancer.

### 1.6 Outline

This concludes the introduction to the dissertation, which detailed the hypothesis, three Specific Aims and the approaches we used to test the hypotheses in each Aim. A summarization of the aims is provided below in Figure 1. Chapter 2 discusses the background information regarding the monoclonal antibodies, small molecule ligands, nanoparticles and the significance and innovation of SNAbs. Chapter 3 covers the first Aim, specifically how the SNAbs were developed and characterized. Chapter 4 illustrates the capability of SNAbs to kill target cells in *ex vivo* cellular assays with MDSCs as the model system. Chapter 5 demonstrates one application of SNAbs in the treatment of cancer by evaluating the therapeutic efficacy of MDSC-SNAbs in a murine tumor model. Finally, conclusions and future directions are presented in Chapter 6.

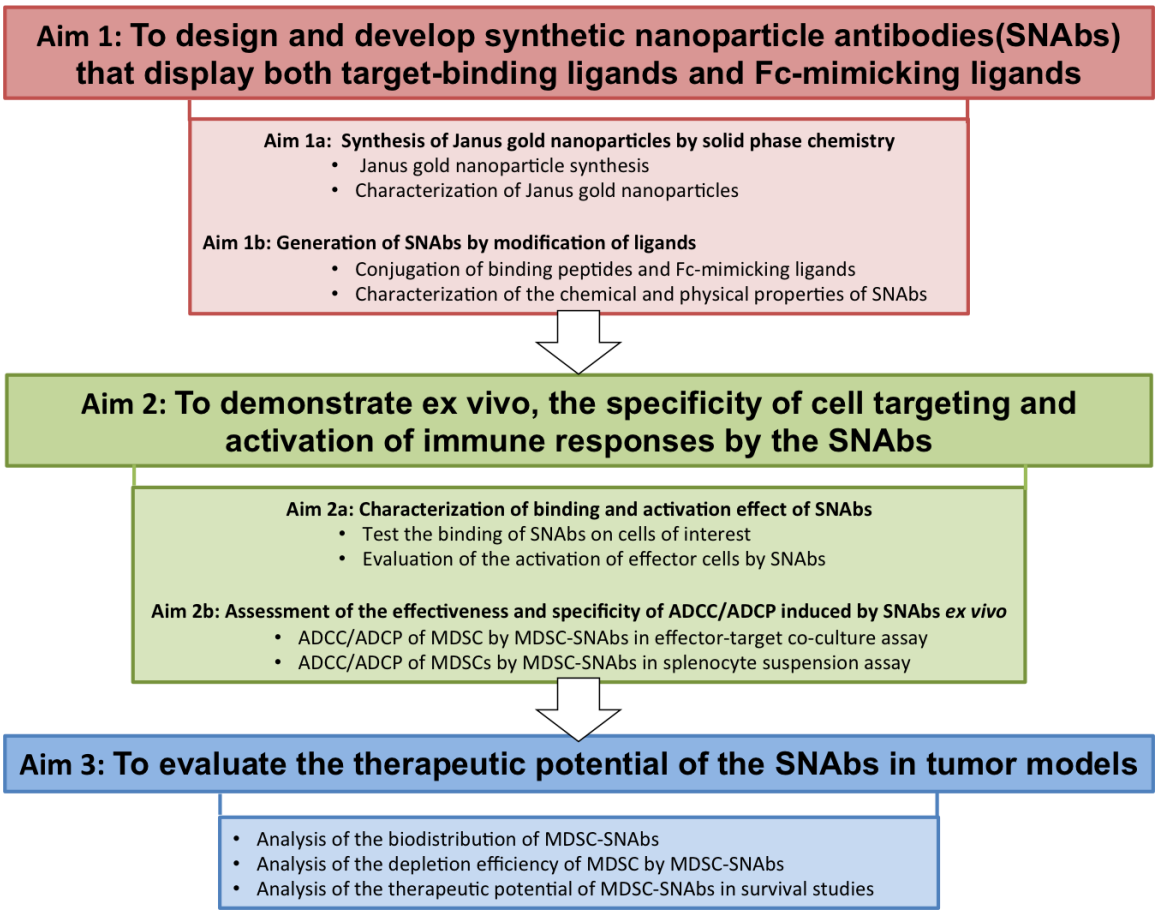


Figure 1. The flow of Aims

# CHAPTER 2 BACKGROUND AND SIGNIFICANCE

During the past decades, monoclonal antibodies have emerged as one of the most potent and specific drug types. So far, over 80 monoclonal antibodies have been approved by the US Food and Drug Administration (FDA) for treatment of diseases, such as cancer, infectious diseases, autoimmune disorders.[29] However, in fact, they are not the perfect "magic bullets" and still face great challenges and limitations in their production and applications. In this Chapter, we will first discuss the functions and problems with monoclonal antibodies, further introduce existing artificial antibody types and the conceptual design of SNAbs. Finally, we will discuss the significance and innovation of our work.

## 2.1 Background

### 2.1.1 Monoclonal Antibodies

Antibodies, also known as immunoglobulins (Ig), are a family of proteins typically secreted by plasma B cells upon exposure to pathogens. They are composed of two heavy chains and two light chains of polypeptides, forming a "Y" shape structure. On the end of the two branches, a tertiary structure of polypeptides establishes the complimentary determining regions (CDRs) in the Fab region, which recognize specific epitopes on the antigen through molecular interaction. The stem of Y structure, also called Fc region, possesses the sequence that can bind the Fc receptors on innate immune effector cells, such as macrophages, natural killer (NK) cells and polymorphonuclear leukocytes (PMN), or interact with complement proteins. As an important player in the immune

defense system, antibodies can neutralize toxins, pathogens (bacteria or virus) or sick cells by attaching to the protein antigen epitopes with Fab region to prevent infections, clear cancerous cells or reject xenotransplanted organs. By engaging the Fc receptors, antibodies can also trigger a cascade of signaling events in the effector cells, which leads to the cytolytic response, phagocytosis of immune complexes, antibody-coated malignant cells or opsonized pathogens. Some antibodies are also capable of activating the complement-dependent cytotoxicity, which kills target cells or microorganisms by damaging cell membrane. There are five major types of immunoglobulins: IgA, IgD, IgE, IgG, IgM, which are distinguished by their constant regions, consisting of part of the Fab and the entire Fc regions. IgA usually helps to defend against germs in the body fluid and IgM is potent at inducing complement pathway activation. IgE is important mediator of allergic reaction and the function of IgD is still under investigation. Among all the five types of immunoglobulins, IgG is the most abundant type and the key contributor to antibody-dependent cellular cytotoxicity (ADCC) and phagocytosis (ADCP), which are the major way how antibody-labeled targets are destroyed or eliminated.[30]

### 2.1.2 Mechanisms of actions of monoclonal antibody therapy work in cancer

Monoclonal antibodies, i.e., antibodies produced by clones of one parent cells or a cell line and composed of identical protein molecules, as treatments for cancer, have been developed for over two decades and has proved their efficacy in a number of hematological malignancies and solid tumors. [10] Over the past 30 years, over 80 monoclonal antibodies have received market approval from US Food and Drug Administration, among which around 30 were indicated for cancer.[31] Generally, monoclonal antibody therapy for cancer can be divided into two categories: (1) directly

eliminates the tumor cells by antibody-dependent immune responses; (2) the other type modulates the immune factors in tumor microenvironements. The success of the first type of antibody-based therapies relies on the expression of tumor-associated antigens (TAAs), which are a group of proteins or molecules that are either selectively expressed, mutated or overexpressed on the malignant cells compared to normal tissues.[32] For example, rituximab, a chimeric IgG antibody for CD20 on malignant B cells, has achieved great clinical response rate in B non-Hodgkin's lymphomas.[33] Upon binding on the CD20 overexpressed on neoplastic B cells, rituximab engages the activating Fc receptors on immune cells and elicits ADCC to kill B cells. An increase in the overall survival of patients with non-Hodgkin's lymphoma is observed after treatment with rituximab with low dose-limiting toxicity.[34] Another successful story is trastuzumab, which targets the overexpressed-antigen Her2 in aggressive breast cancer and a fraction of ovary and stomach tumors. Trastuzumab interacts with macrophages and triggers phagocytic killing of $Her2^{high}$ cancer cells.[35] Other similar examples include Alemtuzumab for CD52 in chronic lymphocytic leukemia and J591 for PSMA in prostate carcinoma.[10] However, the majority of tumor/cancer types do not have a TAA that is suitable for mAb-targeting.

Instead of clearing the malignant cells, the second type of antibody-based therapy depletes immunosuppressive factors or regulatory immune cells and thus restoring the immune attack against cancer cells. For example, Ipilimumab blocks the cytotoxic T lymphocyte-associated antigen 4 (CTLA-4) on T cells, as a result of which regulatory T cell-mediated immune-suppression is impaired.[36,10] Clinical trials in patients with melanoma or prostate cancer showed increase in the diversity of peripheral T cells after

treatment of Ipilimumab.[37] Another major roadblock to successful anti-tumor attack is the interaction between programmed death ligand 1 (PDL1) on tumor cells and programmed death 1 receptor (PD1) on T cells, which leads to dysfunction of antigen-specific T cells. To interrupt this interaction, Atezolizumab (anti-PDL1, Genetech) or nivolumab (anti-PD1, Merck), as two examples, were developed and used in clinic for a number of tumor types. These antibodies achieved good clinical results, showing tolerable toxicity, regression of tumors in patients and improved survival.[38] Despite the encouraging results from the above-mentioned mAb therapies, there are obstacles in cancer treatment that have not been overcome by mAbs.

One of those obstacles is myeloid derived suppressor cells (MDSCs), which are a heterogeneous populations of cells consisting of myeloid progenitors, immature macrophages, immature granulocytes, and immature DCs.[39] Upon the onset of tumor, MDSCs accumulate in tumor, spleen and blood and secrete various cytokines (e.g. IL-10, TGF-β), enzymes and reactive species to inhibit the proliferation, activation of T effector cells, and also regulate the cytokine production of macrophages and impairs the function of nature killer cells.[40,41] Similarly to MDSC, regulatory T cells are required for the protection against autoimmune diseases, which suppresses the reactivity of anti-tumor T cells.[42] It is widely acknowledged that inhibition of MDSC and regulatory T cells is essential to improve the outcome of anti-tumor therapies.[43] Some mAbs (e.g., Ipilimumab) can reduce the number of MDSCs or regulatory T cells in the body; but, because of lack of specific surface antigen, no effective mAbs have been developed specifically for human MDSCs and regulatory T cells.

### 2.1.3 Limitations of monoclonal antibodies

Despite the success of a few types of mAbs, their production and application poses several problems. The first is inherent in the process of their production. A typical process to acquire a new type of mAb involves the immunization of animals (transgenic or non-transgenic) with antigens, the isolation of antibody-producing B cells, hybridoma production, the selection of high binders by screening, cloning, mAb production in a single cell line, purification and validation. Obviously, this is a long, complex process, which usually lasts months and requires large amount of labor and high production cost. To avoid clearance and allergic reaction of murine antibodies and also to be able to activate the antibody-dependent immunity in human, chimeric, humanized and human antibodies must be produced by various antibody-engineering techniques, such as complementarity-determining region grafting and transgenic 'humanized' mice[12], adding difficulty to the process. The advent of antibody (scFv)-phage display screening technique solves parts of the problem by using human DNA in the library.[30] At the same time, this new method reduces the time and amount of effort required by avoiding the immunization and hybridoma production steps.[44] However, the fragments selected through phage display still need to be constructed into a complete antibody followed by mAb production in cell lines. As for the production of mAbs after selection and cloning, sophisticated eukaryotic machinery is required to produce them in active form because antibodies are large protein molecules containing numerous disulfide bonds and post-translational modifications, such as glycosylation.[12] As a result, considerable cell culture work is needed. High expenditure also stems from the following intensive purification

steps of mAbs from cell cultures and validation steps, all of which together make mAb a very expensive drug.

In terms of application, mAbs face several challenges in the following aspects. First, as discussed previously, for a lot of immunological targets and most cancer types, we can hardly develop a type of effective mAbs due to the lack of identified surface antigens. In addition, pharmacokinetics properties of antibodies, which are dictated by their molecular characteristics (e.g.,molecular size, shape, affinity and valency), give them not only an advantage for treating hematological malignancies thanks to the long serum half-life, but also a curse for solid tumors, which make up 85% of human tumors, because of the inefficient tissue penetration and poor retention.[12,13,45] A third possible limitation lies in its mechanism of function. The mAbs have to compete with patient's IgG for binding to Fc receptors and therefore must be injected at a high dose to achieve significant clinical responses, contributing to the high cost of mAb therapy. [12]

### 2.1.4 Alternatives to monoclonal antibodies

To overcome the challenges facing by mAbs therapies, we've been striving to develop functional alternatives during the past few years. There are now limited types of artificial antibodies or antibody-mimetics developed so far (e.g.,nanobody, diabody, minibody, affibody and peptibody), most of which are peptide/protein surrogates of part of or the full structure of monoclonal antibodies. Nanobody is one of the most promising types of artificial antibody, which is single targeting-domain antibody retrieved from an immune library of *Camelida*e.[46] Their advantage lies in better tissue penetration than conventional mAbs because of their small dimensional size (2.5nm in diameter).[46–49] Nanobodies have

been successfully applied in solid tumor treatment, targeted drug delivery and bioimaging, but they cannot trigger antibody-dependent immune responses because of lack of Fc fragments. Their rapid renal clearance and high accumulation in kidney also impeded their advancement in clinical application.[49] Diabody (a dimer of single-domain variable regions of both heavy chains and light chains) and minibody (single-domain antibodies) have similar advantages and drawbacks as nanobody, except that they possess the functional protein fragments to induce immune responses. Affibodies are a library of engineered protein molecules that can be used as tools for molecular recognition, but similar to nanobodies, they do not have Fc fragments.[50,51] Another option is peptibody, which consists of two copies of synthetic peptide ligands for target binding, which are covalently linked to the amino terminus of a recombinant IgG Fc domain. They exhibit potent biological activity and good targeting specificity.[52] Despite better pharmacokinetic properties, they are still subject to renal excretion and face the same production and application problems as mAbs. [52] Patrick McEnaney et al. have developed a chemically synthesized, bivalent molecule functioning similar as anti-PSMA antibodies, called synthetic antibody, by utilizing a PSMA-binding peptide and a human-Fc receptor gamma I binding peptide. The binding peptide cp33 is (AQVNSCLLLPNLLGCGDDK with Cys-Cys cyclization, referred to as cp33 in Ref. 26) utilized in this thesis as well.[53] The molecule they synthesized was able to induce phagocytosis of PSMA-expressing cancer cells *in vitro* with U937 human monocytes, but its function in real tumor is still not tested yet.

### 2.1.5 Crosstalk between mouse and human antibodies

In general, there are four types of monoclonal antibodies most commonly in use for therapy, i.e., murine, chimeric, humanized, and human antibodies. The first type of monoclonal antibody evaluated in the clinic was murine antibody. However, administration of murine antibodies in human induces the development of anti-mAb antibodies and the rapid clearance limited their efficacy.[54] Therefore, it is necessary to use chimeric, humanized and human antibodies, which all have human Fc regions, to treat cancer patients. Mouse models of cancer are the most prevalently used, clinical relevant and economical animal model to evaluate the efficacy of a new type of monoclonal antibodies before undertaking clinical trials in human. Therefore, whether an antibody with human Fc regions can activate an immune response in mouse are intensively studied to discover the best way to design the most effective monoclonal antibody-based treatment strategy for diseases.

Human IgG has four isotypes, IgG1, IgG2, IgG3, and IgG4 and mouse IgG has IgG1, IgG2a, IgG2b, IgG2c and IgG3. Different isotypes have variable specificity and affinity for different Fc gamma receptors (FcγRs) and mediate effector functions in slightly different ways. [55,56] In this thesis, we used a human IgG1-mimicking peptide in mouse systems, and focused on the reactivity of human antibodies in murine models. Human IgG1 is the most commonly used isotype used in antibody therapy of cancer because they are easier to produce and the most potent inducer of ADCC/ADCP by human activating Fc gamma receptor (hFcγRI, hFcγRIIa, hFcγRIIc, hFcγRIIIa, and hFcγRIIIb).[57] Tests in mouse models repeatedly reported that human IgG1 are able to bind on all activating

FcγRs (I, II, III, IV) in mouse with modest affinity and induce ADCC/ADCP by mouse NK cells, macrophages and sometimes polymorphonuclear leukocytes (PMNs). [55,56,58]

### 2.1.6 Small molecule binding ligands

Protein-protein interaction, including the interaction between antibodies and antigens, largely depends on the molecular forces determined by a defined surface composed of a group of spatially adjacent amino acids. In this sense, smaller peptides also have the potential to mimic the binding structures in the original macromolecules. A variety of peptide mimetics (also called peptidomimetics) have been generated by structure-based procedures and exhibits similar biochemical and biological properties to its template proteins.[59–61] In addition to the peptidomimetics, peptide-phage display techniques enable the identification of ligands that have comparable affinity to the relevant antigens as conventional mAbs.[17,62] These peptidomimetics or ligands, usually produced by solid-phase chemical synthesis, can functionally substitute the binding domains and/or the Fc regions in antibodies without the involvement of animal/cell work.

Aptamers are another prevalently used class of small molecule ligands, which are short, single-stranded DNA or RNA molecules. They fold into various secondary structures because of their propensity to form complementary base pairs, as a result of which they form unique three-dimensional structures and are able to bind to their specific cognate targest.[16] One well-known example is pegaptanib, which targets vascular endothelial growth factor (VEGF) and already approved by FDA. Similar to peptides, aptamers are usually selected through screening methods, such as SELEX (systematic evolution of ligands by exponential enrichment).

Both peptides and aptamers have the advantages of small physical size, flexible structure, low immunogenicity, and easier, cheaper and quicker chemical production.[16,17] Their binding capability enables them to be used directly as antagonist or agonist.[63,64] Also, owing to the targeting ability, they were used to guide drug or gene delivery.[18,65,66] The small physical size of them usually results in metabolic instability, so peptide/aptamer-Fc/antibody complexes and particle-conjugates were usually developed to extend the serum half-life.[15,65,67] The small physical size also leads to higher attainable surface density, so multimerization or multivalent-presentation of the peptides/aptamers on carriers (e.g., particles) are possible and brings in advantages of higher avidity, selectivity, and the augmentation of therapeutic effects.[18,68,69,70]

### 2.1.7 Multivalency effect

Another aspect relevant to antibody and antigen interaction as well as antibody-dependent immune responses is the valency of interaction. Multivalent interaction is required in most biological processes, including cell-cell recognition and the induction of signaling transduction after receptor-ligand pairing. Specifically, the initiation of antibody-dependent phagocytosis activity by monocytes relies on the clustering of multiple Fc-receptor molecules on cell membrane by IgGs coated on the pathogens in the immune complexes.[71] A number of previous studies also support the conclusion that a multivalent display of antibodies/binding ligands on the surface of a particle-carrier or construct increases the binding avidity of the conjugates as well as the biological functions of the bound molecules.[68,72,73] For example, multiple copies of RGD peptides displayed on the surface of nanoparticles have decreased EC50 and IC50 on endothelial adhesion by these nanoparticles as well as extended blood half-life compared to free

peptides.[68] Similarly, Irina and her coworker showed that antibody-gold nanoparticle conjugates with different valencies have affinity of three magnitude higher than that of the free antibody to its target virus.[72] Liposomes presenting tetrameric targeting-peptides also delivers more cytotoxic drugs to cells than that with monomeric peptides.[62] In addition, multivalent binding with ligands allows the nanoparticles to distinguish the cell targets with specific receptor density profile on the surface and results in higher targeting specificity. [69,74]

### 2.1.8 Nanoparticles

Synthetic nanoparticles usually refers to particles within the size range of 1-1000nm, made with polymers, metal, lipid, peptides or other biological material through chemical synthetic routes. In the past decades, they have been widely applied in the biomedical field for drug or gene delivery, imaging and treatment of diseases. Unlike monoclonal antibodies, nanoparticles offer some specific physicochemical properties different from large biomolecules, such as tunable size and surface chemistry. They also have a high surface-area-to-volume ratio, which indicates that they may carry a high density of ligands and render high binding efficiency. In addition, sub-50nm nanoparticles exhibit improved tissue penetration and lymphatic trafficking.[75,76] Because of these advantages, nanoparticles have numerous applications in the biomedical field. Some successful examples include the targeted delivery of chemotherapeutic drugs to tumors by antibody-coated nanoparticles,[77] neovasculature imaging by RGD-modified nanoparticles,[78] and the activation of immune responses by adjuvant-carrying nanoparticles.[79]

Among the many types of nanoparticles, gold nanoparticles have the advantages of chemical stability, biological inertness and ease of surface modification and tracking due to their unique optical property. Therefore, it is a favored option to develop tools or nanoparticle-based therapies for biomedical applications.[80–83] For example, the conversion of radiation to heat due to plasmon resonance of gold nanoparticles lead to the hyperthermic damage of cancer cells, so gold nanoparticles are widely applied as radio-sensitizers in the cancer treatment.[84] Oligonucleotides-conjugated gold nanoparticles have been widely used in the diagnosis of diseases combining the DNA hybridization and nanoparticle-facilitated fluorescence, chemi-luminescence or radioactive detection together.[85,86] Similarly, antibody- or ligands-modified gold nanoparticles can easily deliver the drugs to the targeted cells owing to the endocytosis of nanoparticles. [82,87,88]

Janus particles are a group of particles, including polymeric, inorganic or hybrid, micro- or nano-particles, which has anisotropic surface property, named after the two-faced Roman Gold Janus. Typical fabrication methods for Janus particles are phase-separation, microfluidic and electrohydrohynamic jetting, immobilization.[89,90] Janus particles could offer unique optical or catalytic properties owing to the combination of different materials on the same particles, such as a red shift in the UV-vis adsorption of gold nanoparticles after turning into a $SiO_2$-Au Janus particle.[91] Some Janus nanoparticles have the capability to self-assembly into disk-shaped micelles or chain-like structures, presenting distinguished modulating ability for drug delivery and imaging.[92–94] The most promising use of Janus particles relies on their capability to simultaneously and incompatibly present two types of ligands or delivery two types of drugs on different part of the particle surface. However, it was mostly utilized on the Janus microparticles (size

over 1000 nm), for example, anti-CD3 and protein coated Janus microparticles as artificial antigen-presenting cells to activate T cells. [95–97] Few applications in this way were reported using Janus nanoparticles. Despite it is hard to characterize the Janus surface composition on a nano-scale, Janus nanoparticles conjugated with multi-types of ligands or drugs still hold great promise in biomedical applications, such as multi-functional drug delivery and therapeutic modulation.

## 2.2 Overview

Here, we propose to develop a type of artificial antibody using metallic Janus nanoparticle with ligand modifications, called synthetic nanoparticle antibodies (SNAbs). The modification includes two peptide ligands on the opposite surface areas, one of which has binding affinity towards specific surface proteins on the selected target cells, and the other mimic the biological function of Fc region of human IgG1 such that they can bind to human and mouse Fc gamma receptors (FcγRs) and trigger the activation of innate effector cells (e.g.macrophages, NK cells, polymorphonuclear neutrophiles).

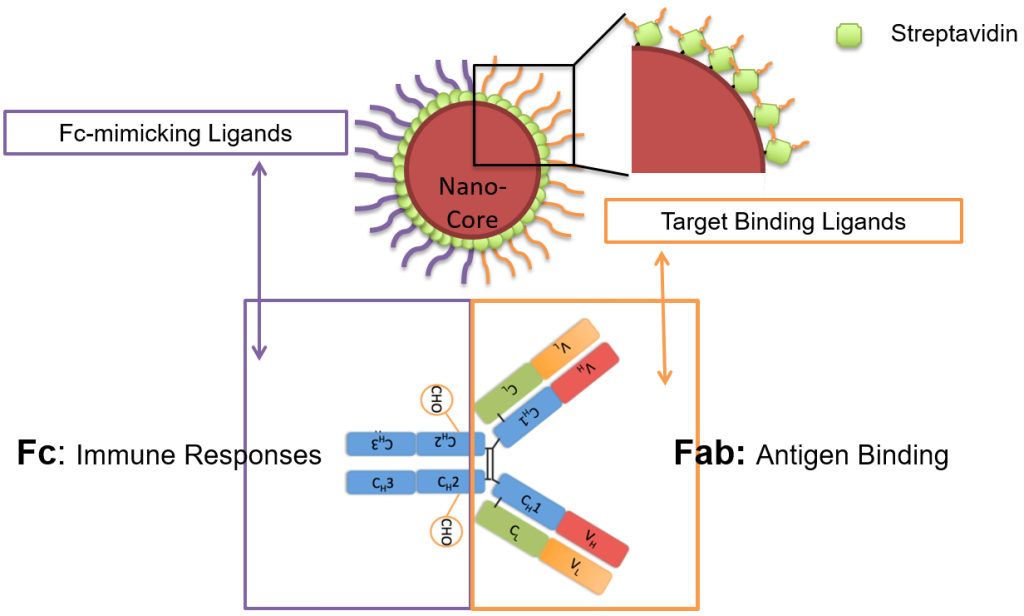


Figure 2. The structural design of SNAbs.

The **primary hypothesis** is: the designed synthetic nanoparticle antibodies (SNAbs) with the mentioned characteristics in Chapter 2 could induce antibody-dependent cellular cytotoxicity (ADCC) and/or phagocytosis (ADCP) efficiently both *in vitro* and *in vivo*. We plan to test this hypothesis by: 1) generating synthetic nanoparticle antibodies that are structurally similar to monoclonal antibodies but displays multiple biologically active ligands on each part of the surface; 2) evaluating the ability of SNAbs to target cells of interest specifically and to activate Fc-receptor-mediated signaling pathways *in vitro* in comparison to mAbs; 3) assessing the degree of ADCC/ADCP induced by SNAbs. The therapeutic potential of the designed SNAbs will also be validated in *in vivo* tumor models. To fully demonstrate the function of SNAbs, we propose to analyze its capability for a murine cell target (myeloid-derived suppressor cell (MDSC)), a cell type that so far does not have a known specific antigen.

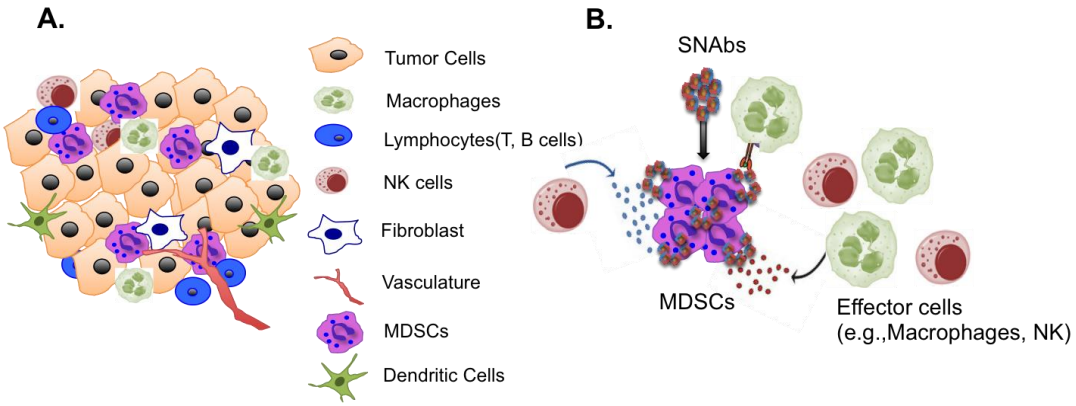


Figure 3. The hypothetical mechanism of action of SNAbs. A. A typical tumor immune-microenvironment. B. A MDSC-targeting SNAb recognizes MDSCs in the microenvironment and engages with the Fc receptors on the effector cells, which subsequently activates the immune responses (e.g., ADCC and ADCP) and kills the MDSCs.

### 2.3 Significance

The **significance of the proposed work** lies in the following aspects: 1) we aim to design optimized synthetic procedure utilizing only peptides and nanoparticles to produce SNAbs that requires lower production cost and shorter production time than conventional mAbs; 2) we aim to develop SNAbs that can be a functional alternative for current antibody therapy of cancer with great translational potential, because these SNAbs can bind on specific antigen and trigger antibody-dependent cytotoxicity as what mAbs do; 3) the SNAbs may have potential advantages over conventional mAbs in terms of application: deeper tissue penetration, longer retention, wider target range than mAbs, and an easily adaptable platform to generate new types of SNAbs by varying the target-binding ligands. In addition, our investigation will yield information as to whether multivalent presentation of peptide ligands (both targeting and Fc-mimicking) on SNAbs can lead to comparable, even stronger or different mechanism of Fc-mediated antigen

specific immune responses in comparison with conventional mAbs, which could benefit the development of new generations of artificial antibodies.

### 2.4 Innovation

There are several aspects that are innovative associated with our work:

**1) New targeted treatment strategy for MDSCs:** MDSCs are selected as the primary cell target to develop the first type of SNAbs. Current options for abrogating MDSC-mediated suppression of anti-tumor immune responses are primarily chemotherapeutics and small molecule inhibitors, which are indirect treatments with severe toxic side effects. The only two monoclonal antibodies available (i.e., anti-Gr1, anti-Tspan33) either have unsatisfactory and toxic side-effects in the animals or are not tested or applicable for diseases models and human.[98–101] Here, we use a completely new targeting strategy for MDSCs, a peptide, identified through phage display library biopanning, on the SNAbs. The SNAbs offers an efficacious while specific depletion method option for MDSCs to restore the immune-competent environment for cancer.

**2) Novel design of an artificial antibody:** All previous artificial antibodies or antibody-mimetics utilize peptide/protein-based conjugates to mimic the structure of antibodies. By contrast, this is the first time that nanoparticles are employed as the scaffold structure of an artificial antibody. This may endow improved tissue penetration and retention property to the SNAbs in solid tumors and deep tissues.[22,23,86] Moreover, metallic particles show better biocompatibility than many polymer particles that presents active terminal chemical groups and also allows imaging without dye-loading, which can benefit the monitoring after *in vivo* treatment of the designed SNAbs.[102,103] Lastly, the use

of nanoparticle also lends us the opportunity to conjugate multiple copies of various ligands on the same construct. All in all, nanoparticle brings in new possibilities for artificial antibody design.

**3) Simpler and more flexible design of artificial antibodies**: Peptides are utilized as both antigen targeting and activation moieties for immune responses, which eliminates the necessity for genetic engineering and cell culturing, making it a simpler artificial antibody to manufacture. Additionally, peptides or aptamers that have specific binding affinity towards various targets can be easily identified through high throughput screening techniques, e.g. phage display biopanning, and thus increased the application potential and target range of SNAbs as an artificial antibody beyond conventional mAbs in terms of cell depletion. By varying the binding peptides, we can easily develop SNAbs for new targets. Again, the multivalent display of ligands on SNAb helps increase the binding avidity and selectivity of the small molecule ligands. [74]

# CHAPTER 3 AIM 1. TO DESIGN AND DEVELOP SYNTHETIC NANOPARTICLE ANTIBODIES (SNABS) THAT DISPLAY BOTH TARGET-BINDING LIGANDS AND FC-MIMICKING LIGANDS

A bacteriophage is a virus of bacteria, whose growth and proliferation relies on a prokaryotic host. With transcriptional fusion with the phage genome, a foreign peptide or protein can be expressed on the phage protein coat. Screening the phage libraries displaying polypeptides against a selected protein, cell type or tissue of interest is a powerful technique, called the peptide phage display biopanning. Several rounds of biopanning against the target (i.e., protein, cell, or tissue) usually leads to the harvest of enriched specific binding phage clones, and by analyzing the genome sequence, we can identify the candidates of targeting ligands with high affinities. Some interesting examples include H2009.1 (RGDLATLRQL) that binds to the restrictively expressed integrin αvβ6 on the non-small cell lung cancer, Peptide P60 (RDFQSFRKMWPFFAM) that can target and inhibit $Foxp3^+$ regulatory T cells, and M2pep (YEQDPWGVKWWY) that can target and induce apoptosis of tumor-associated macrophages.[18,42,104] As we can see, phage display library biopanning enables the identification of ligands for targets that are understudied and lack of known exclusive surface antigens. Sometimes, phage display can even be directly applied *in vivo*, such as in tumor models,[66] to hunt for ligands that bind to a particular type of malignancies in a physiological environment. Cp33, is a peptide ligand, identified with a naïve cyclic peptide phage display library against human FcγRI.[26] The soluble form of cp33 competes with human IgG1 for binding on FcγRI, whereas the dimerized cp33 could trigger phagocytosis of beads[26] or target

cells[53] and superoxide burst by human monocyte-like cells, U937. Cp33 has not been tested for its function in a mouse immune environment, but the crosstalk between human IgG1 antibodies and mouse FcγRs has been well studied. It is reported that hIgG1 binds to all four mFcγRs and was the most potent among all the four types of human IgG1 in inducing ADCC/ADCP with mouse NK cells, polymorphonuclear leukocytes and macrophages.[55,56]

MDSCs are important regulators of the immune responses, consisting of myeloid progenitors, immature macrophages, immature granulocytes, and immature DCs.[105] They are characterized as mainly two subsets, granulocytic MDSCs (G-MDSCs) and monocytic MDSCs (M-MDSCs).[40] In mouse, G-MDSCs are identified $CD11b^{+}Ly6G^{+}Ly6C^{low}$, and M-MDSCs are $CD11b^{+}Ly6G^{-}Ly6C^{high}$.[106] In human, MDSCs are defined as $CD11b^{+}CD33^{+}CD34^{+}$ HLA-$DR^{-}$, with $CD15^{+}$ being G-MDSCs and $CD14^{+}$ being M-MDSCs.[107,108] While it is still under fierce debate which of the two subsets contributes more to the immune-suppression, the majority of the MDSCs in inflammation and cancer are G-MDSCs.[41] In general, MDSCs reduce the essential amino acids (i.e., arginine and cysteine) for T cell proliferation and cytolytic activity. They secrete inhibitory cytokines, such as interleukin-10 and transforming growth factor-beta, to dampen the anti-tumor immune responses.[40,105,109] In addition, MDSCs also secrete reactive nitrogen and oxygen species, which affects the function of T cell receptors and chemokines and thus influencing the T cell migration and inducing NK cell apoptosis.[110,111] MDSCs have high expression of PD-L1 on the surface, which leads to reduced T cell mediated anti-tumor cellular response via the interaction with PD1 receptor.[41] On the other hand, MDSCs help tumor neovascularization and growth through

the secretion of angiogenic factors, growth factors, matrix metalloproteinases and cytokines, which also activates the Th2 response and regulatory T cells.[40] In a word, MDSCs plays a key role in the immune-suppression of tumor. [111–113]

A handful of studies support that the depletion of MDSCs can significantly change the immune environment of tumors, markedly improved the infiltration of T cells in tumor, increased the activation of T cells and inhibited tumor growth. [114,115] MDSC depletion also helped improving the therapeutic effect of other immunotherapies, such as adoptive T cell transfer[116] and immune-checkpoint inhibition.[117,118] However, the options for removing the MDSC population from tumors are quite limited. There are a few chemotherapeutic drugs (e.g. doxorubicin,[116] 5-fluorouracil[119]) and small molecules (e.g., Silibinin,[114] COX2 inhibitor[120]) that can reduce the myeloid cells circulating in the body to some extent, but they are not specific for MDSCs and usually affect the healthy cells and tissue as well. In terms of monoclonal antibodies, group-1 protein (Gr1)-targeting antibody or more specifically Ly6G antibody are the only options for mouse. However, Gr1 antibodies are reported to elicit an effect only in young mice but not in aged mice, fail to deplete MDSCs in liver and affect $CD8^+$ T cells.[99] Anti-Tspan33 is recently reported to recognize suppressive MDSCs in both mouse and human, but yet been validated sufficiently for their therapeutic effects.[100] Tspan33 is also expressed on activated and malignant B cells, increasing the possibility to randomly remove B cells while targeting MDSCs using anti-Tspan33 antibodies. [101] S100A8/A9 proteins are calcium-binding proteins, predominantly expressed by myeloid cells, especially MDSCs.[121,122] S100A9 protein inhibits the differentiation of precursor cells into mature macrophages and dendritic cells and is essential to the recruitment of MDSCs into tumor.

[123] Further, the elevated S100A8/A9 expression supports an autocrine feedback loop that promotes the accumulation of MDSCs in tumors, suggesting the potential of S100A8/A9 as a useful marker for MDSCs.[121,122,124,125] Hong Qin et al. identified a new targeting ligand, G3 peptide, for MDSCs isolated from various murine tumor models with phage display screening.[126] G3 peptide potentially targets the S100A8/A9 heterodimer highly expressed on the MDSCs, which regulates the expansion and migration of MDSCs in both mice and human.[123,124,127] Therefore, G3 is likely to be a good alternative targeting strategy for MDSCs.

Gold nanoparticles are widely used as nano-medicine platforms due to their bio-inertness, facile synthesis method, unique optical properties and surface plasmon resonance peaks that simplify the detection and quantification. We selected 30nm gold nanoparticles as our scaffold structure to leverage the capability of sub-50nm nanoparticles for penetration and retention in tumor. The 30nm gold nanoparticles have streptavidins coated all over the surface to enable the chemistry for making Janus surface structures and conjugation of ligands. Specific segments of the Fc fragments are required to interact with the Fc gamma receptors to elicit a response. Because it is hard to control orientation of Fc fragments either alone or in the form of an antibody during conjugation, we chose to use cp33 to mimic the function of a Fc fragment and as our binding partner for Fc receptors. As the size of the nanoparticle scaffold is very small (30nm in diameter), we are also able to conjugate a higher number of cp33 than Fc protein fragments on the nanoparticles, leading to a higher valency.

In this aim, we propose to develop SNAb that imitate the structure of antibody by conjugating target-binding peptides and Fc-mimicking peptides on Janus nanoparticles.

Our target cell type is myeloid-derived suppressor cells, so we chose G3 as our targeting ligands, and cp33 was used as the Fc-mimicking ligands. To generate the SNAbs, we adapted a solid-phase chemistry methods to product Janus gold nanoparticles and took advantage of highly orthogonal chemical reactions to modify the surface of Janus gold nanoparticles with the above-mentioned two types of peptide ligands (G3 and cp33) that process the required biological functions. The physical and chemical properties of these SNAbs were characterized using fluorescence-based assays and imaging methods.

## 3.1 Methods

### 3.1.1 Materials

Aminomethyl ChemMatrix resin (35-100 mesh size, ~1mmol/g loading capacity, Cat#.68571), tris(2-carboxyethyl)phosphine (TCEP, Cat.#.646547 and C4706), and biotin (Cat#.B4501-1G) were purchased from Sigma Aldrich. The heterofunctional crosslinker, sulfo-NHS-S-S-biotin, was purchased from Thermofisher Scientific (Cat#.21331, and Apexbio Technology.Inc, Cat#.A8005). HABA (4´-hydroxyazobenzene-2-carboxylic acid) (Cat.#.28010) and avidin (Cat.#.21121) were purchased from Thermofisher Scientific, The 30nm streptavidin functionalized gold nanoparticles were made by Nanopartz. Inc and Nanohybrids. Inc. The 10 mL reaction vessel was purchased from Torviq.Inc (Cat#.SF-1000). Human IgG1-Fc functionalized with biotin was purchased from Acrobiosystems (Cat.#.IG1-H82E2). Peptide ligands were synthesized by Genemed Synthesis (See Table 1). N-ethylmaleimide (Cat.#.23030), Alexa Fluor 647 C2-Maleimide (Cat#.A20347), and Slide-A-lyser dialysis cassettes (molecular-weight-cut-off: 2KDa, 3KDa, 10KDa) were purchased from Thermofisher Scientific. The 3nm

biotin-gold nanoprobes were purchased from Nanocs. Inc. (Cat.#.GNB3). PBS buffer was purchased from Hyclone GE Healthcare, Corning Corporation and Sigma Aldrich or made from monobasic and dibasic sodium phosphate from Sigma Aldrich (Cat.#.S9638-250G, S9763-1KG). Whatman Puradisc polyethersulfone syringe filter (0.22 μm) was purchased from GE Healthcare (Cat.#.6780-2502,6780-1302). BD 10 mL syringes with luer lock were purchased from VWR (Cat.#.BD309653). L-Leucine-N-Fmoc (13C6, 97-99%; 15N, 97-99%) for heavy, stable isotype labeled peptide synthesis was purchased from Cambridge Isotope Laboratories, Massachusetts, USA.

### 3.1.2 Preparation of MDSC-targeting synthetic nanoparticle antibodies (MDSC-SNAbs)

*3.1.2.1 Production of Janus streptavidin-coated gold nanoparticles*

To generate Janus gold nanoparticles, aminomethyl ChemMatrix resins were functionalized with biotin groups by reacting with bifunctional, thiolytic cleavable crosslinkers, sulfo-NHS-S-S-biotin in a reaction vessel (Step 1 in Figure 4). Firstly, 110-120 mg of resin was hydrated with 8 mL of pH6.95 1X PBS (0.0067M PO4) in a 10 mL reaction vessel on the shaker shaking at 300 rpm at room temperature for 3-4 hrs. The resins were washed with 5 mL PBS for 7 times. After the resin was hydrated, 100 mg of crosslinker sulfo-NHS-S-S-biotin was dissolved 14 mL of pH 6.95 1×PBS (0.0067M PO4) and filtered with 0.22 μm syringe filters. Three and a half milliliter of the crosslinker solution was added to each reaction vessel. The vessel was rotated at 37 ℃ for 24 hrs, after which the vessel was washed with 5ml of 1×PBS for 12 times. Subsequently, 6-10e11 of streptavidin-coated gold nanoparticles (SA-AuNP-SA)

(Nanopartz. Inc or Nanohybrid Inc, USA) in 3.5 mL of 1×PBS were added to the reaction vessels and reacted with the biotin-functionalized resins for overnight at 37 ℃ on rotator. After reaction, the resins in the vessels were washed with 5 mL PBS with 0.01% Tween-20 twice and 5 mL PBS without tween-20 for another 4 times to remove the unbound and non-specifically bound SA-AuNP-SA (Step 2). Then, 2 mL of 0.05M tris(2-carboxyethyl)phosphine(TCEP) (pH 7) was added into each reaction vessel. Air bubbles were removed and the reaction vessels were rotated at room temperature for 24 hrs.

The resins were then washed again with 3 mL of 1×PBS for 7 times (Step 3). All the wash buffers containing the Janus gold nanoparticles (SA-AuNP-SH) were collected into fresh 50 mL tubes. The solutions of Janus gold nanoparticles were concentrated by centrifugation at 4500 g for 1 hr for three times. The pellets were collected and supernatants were transferred into a new tube after every centrifugation. Finally, the concentrated SA-AuNP-SH solution was dialyzed against PBS in gamma-irradiated, MWCO 10 KDa slide-A-lyzer to remove excessive TCEP for two days and the solution was then retrieved from the cassettes, filtered with 0.22 μm syringe filtered then stored in 4 ℃ until use. The above procedure gave the best yield. To shorten the procedure to one day, some changes in the procedure are acceptable with a compromised yield: the reaction duration of each step can be reduced to 2 hrs; the rounds of concentration centrifugation can be reduced to one time or two times, or be done with ultracentrifuge at higher speed (e.g., 10,000 g) for 15-30 mins; instead of dialysis, the TCEP can be removed from the solutions of concentrated Janus SA-AuNP-SH with ultracentrifugal filters units (e.g., Amicon Ultra-4 MWCO 100 KDa) by centrifuging at 700 g for 5 mins for 4 times.

Table 1. Peptide sequences and functions.

| Name | Sequence | Functionality |
|---|---|---|
| G3-biotin | WGWSLSHGYQVK-biotin | MDSC Targeting |
| G3-SMCC* | WGWSLSHGYQVK-SMCC | MDSC Targeting |
| Scrambled G3-biotin | KSLWVQWSGGHYK-Biotin | MDSC Targeting |
| Cp33-biotin | AQVNSCLLLPNLLGCGDDK-biotin, C6-C15 disulfide bond | FcγR Binding |
| Cp33-SMCC* | AQVNSCLLLPNLLGCGDDK-SMCC, C6-C15 disulfide bond | FcγR Binding |
| IrrelPep-SMCC* | AQTHFDTCSWMYCWDGWWK-SMCC, C8-C13 disulfide bond | Irrelevant peptide control |
| IrrelPep-biotin | AQTHFDTCSWMYCWDGWWK-biotin, C8-C13 disulfide bond | Irrelevant peptide control |
| AHNP-biotin | Biotin-YCDGFYACYMDV-NH2, C2-C8 disulfide bond | Irrelevant peptide control |
| scAHNP-biotin | Biotin-AMFCYGVYDYCD-Amide, C4-C11 disulfide bond | Irrelevant peptide control |
| IrrelG3-biotin | SHSACGDAGWVRCGGGK-biotin, C5-C13 disulfide bond | Irrelevant peptide control |
| $^{13}C$, $^{15}N$-G3-Biotin | WGWS(L)SHGYQVK-biotin | MDSC Targeting, Modification quantification |
| $^{13}C$, $^{15}N$-Cp33-SMCC | AQVNSCLL(L)PNLLGCGDDK-SMCC, C6-C15 disulfide bond | FcγR Binding, Modification quantification |

*SMCC: succinimidyl 4-(N-maleimidomethyl)cyclohexane-1-carboxylate

(L): Heavy, stable isotype labeled-LEUCINE (13C6, 97-99%; 15N, 97-99%)

*3.1.2.2 Synthesis checkpoints for quality control*

The hydrolysis or conjugation of sulfo-NHS releases NHS as a leaving group, which absorbs strongly at 260-280 nm. A sample of the crosslinker solution was measured for absorbance at 260-280 nm before and after adding NaOH (10% by volume) to determine the reactivity of the crosslinker. Another sample (~100 μL) of crosslinker solution before adding to vessels was saved in 0.5 mL tube and rotated at the same time as the reaction vessels at 37 ℃. The saved sample, solutions retrieved from the vessels after reaction with the resin and the washing buffer of the last wash from the vessels were measured for absorbance at 260 nm again to validate the completion of reaction and the removal of free excessive crosslinkers in the vessels after reaction. In general, the crosslinker solution retrieved from the vessels after the reaction should had higher absorbance than the saved sample of unreacted crosslinker. The washing buffer of the last wash should have the same absorbance reading as the PBS solution does.

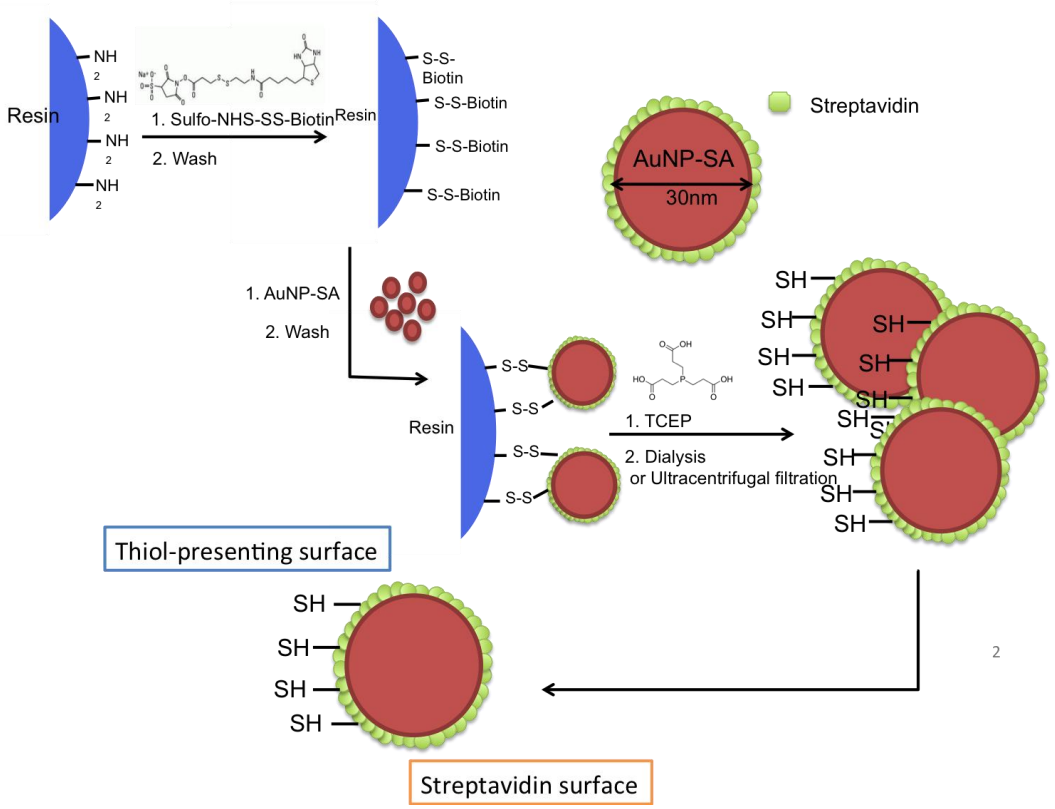


Figure 4. Synthesis procedure of Janus streptavidin-coated gold nanoparticles SA-AuNP-SH. Step 1: Functionalization of resin with sulfo-NHS-SS-Biotin crosslinker; Step 2: Binding of SA-AuNP-SA onto functionalized resins; Step 3; Cleavage of bound SA-AuNP-SA with TCEP and purification of the cleaved Janus SA-AuNP-SH.

*3.1.2.3 Quantification of the SA-AuNP-SA, SA-AuNP-SH particles*

The 30 nm gold nanoparticles have a SPR peak around 522 nm-525 nm. A standard curve was generated with the absorbance of a series of concentration-known SA-AuNP-SA solutions for every new batch of SA-AuNP-SA received from Nanopartz.Inc or Nanohybrids.Inc. We also measured the solutions of the SA-AuNP-SA before adding to vessels, the solution of unbound particles after washing, and the solutions of Janus SA-AuNP-SH before and after dialysis. The calculations was done with the following equations:

$$C = k * (A_{S(522-525)} - A_{P(522-525)}) \quad (1),$$

where C is the concentration of the gold nanoparticles (#/mL), k is the slope generated from the standard curve, $A_{S(522\text{-}525)}$ and $A_{P(522\text{-}525)}$ are the measured absorbance values of sample and PBS at 522-525nm respectively.

$$T = V * C \quad (2),$$

where T is the total number of nanoparticles in the sample, V is the volume of the sample in milliliter.

$$P_B = 100 * (1 - \frac{T_U}{T_I}) \quad (3),$$

where $P_B$ is the percentage of particles bound onto the resins, $T_U$ is the unbound number of particles measured out with the collected washing solution and $T_I$ is the total input number of particles.

$$Y = 100 * \frac{T_C}{T_I} \quad (4),$$

where Y is the yield of Janus SA-AuNP-SH as percentages, $T_C$ is the total number of particles cleaved from the resins.

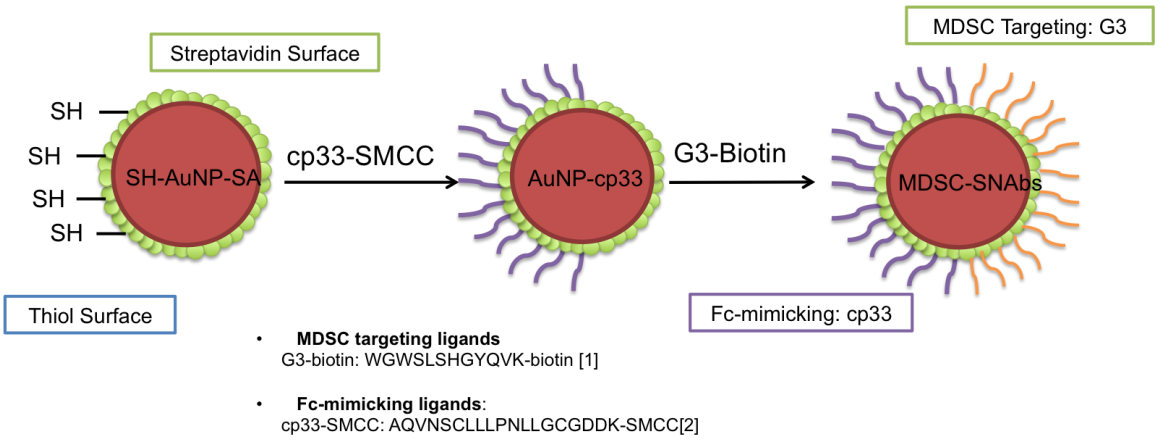


Figure 5. Surface modification of Janus SA-AuNP-SH with peptide ligands to generate MDSC-SNAbs. Cp33-SMCC was conjugated onto the thiol surface of the Janus SA-AuNP-SH through maleimide-thiol specific reaction, while G3-biotin was conjugated onto the streptavidin surface of the nanoparticles through biotin-streptavidin interaction.

*3.1.2.4 Surface modification of the gold nanoparticles with ligands*

To modify the Janus nanoparticles, 1 ×hIgG1-Fc (InvitroGen Inc, Carlsbad, CA, USA), or 30000-molar excess of G3, scrambled G3, cp 33, and/or IrrelPep ligands (Genemed Synthesis Inc., San Antonio, TX, USA) with biotin or SMCC groups were conjugated onto the streptavidin hemisphere or the thiol hemisphere of the nanoparticles through streptavidin-biotin or thiol-maleimide reaction respectively at pH 7.4 in PBS with 0.001% Tween-20 with gentle rotating at room temperature for 4 hrs or 24 hrs at 4 ℃. Excessive ligands were washed out by centrifugation at 4500 g for 50 mins. Modified particles were resuspended in PBS with 0.001% Tween-20 and stored in 4 ℃ until use.

**3.1.3 Verification of asymmetric surface chemistry of the Janus gold nanoparticles**

To verify the existence of the free thiol groups on the Janus particles, an excessive amount of Alexa-fluor 647-C2 maleimide dye (Thermofisher Scientific, USA) was reacted with Janus gold nanoparticles SA-AuNP-SH or nonJanus SA-AuNP-SA for two

hours at room temperature. The unreacted dye was removed by dialysis against PBS with MWCO 6000-8000 tubing (Thermofisher Scientific, USA) for two days. The fluorescence of the dye-conjugated nanoparticle solution was read on a SynergyHT Biotek plate-reader at Ex/Em 635/680. A standard curve made with the known dilutions of Alexa-fluor 647-C2 maleimide dye was also read to enable calculations of the number of dye molecules conjugated on the particles.

To evaluate the topology of each chemistry features on the Janus nanoparticles SA-AuNP-SH or nonJanus nanoparticles, we tagged available biotin-binding pockets of the streptavidins with 3 nm biotin-gold nanoprobes and then obtained the transmission electron microscopy (TEM) images. More specifically, we incubated the Janus or nonJanus nanoparticles with a 2500-molar excess of biotin gold nanoprobes at room temperature for 2 hours. The suspensions were then centrifuged at 4500 g for 30 mins to remove unbound biotin-gold nanoprobes. The TEM samples were prepared by dropping 5 μL of the nanoparticle suspension onto 200-mesh formvar carbon-coated copper grids and dried overnight in air. The TEM images were acquired using Hitachi HT7700 TEM operated at 400 kV.

### 3.1.4 Quantification of peptide modification level on the nanoparticles

G3-biotin and cp33-SMCC with heavy stable isotope-labeled amino acids were synthesized by Genemed Synthesis Inc. (See Table 1) using L-Leucine-N-Fmoc (13C, 97-99%; 15N, 97-99%). G3-AuNP-cp33 SNAb were produced with the normal light peptides, i.e., G3-biotin and cp33-biotin. The SNAbs were concentrated in PBS at a concentration of 1e12/mL and added in the heavy isotope-labeled peptides, i.e., $^{13}C$, $^{15}N$-G3-biotin and

$^{13}C$, $^{15}N$-cp33-SMCC. The final concentration of heavy isotope-labeled peptides added in the SNAb samples were around 503 nM, Control samples were prepared with same concentration of SA-AuNP-SA, or mixture of light and heavy isotope-labeled peptides.

To determine the amount of peptides modified to nanoparticles, an isotope dilution assay was performed.[128] To remove disulfide-bonds in the peptides of interest, the samples were reduced with 5 mM dithiothreitol for 20 mins at 55 ℃, and then alkylated with 15 mM iodoacetamide for 15 mins at room temperature. The samples were then divided in halves and two enzymes, Thermolysin or Asp-N (Promega, Sequencing Grade), were added for the proteolytic cleavage of heavy or light G3 and cp33, respectively. Following desalting, the samples were analyzed by LC-MS/MS as previously described[129] with the following modification: Initially, the sample was run in a data-dependent manner to select the proper settings for parallel reaction monitoring (PRM) of the peptides of interest. Next, PRM analysis was preformed and analyzed using Skyline.[130] The ratio of the light to known amount of heavy isotope-labeled peptide was used to determine the amount of peptides modified onto the nanoparticles in the SNAb samples. This work was supported by Georgia Institute of Technology's Parker H. Petit Institute for Bioengineering and Bioscience, including the Systems Mass Spectrometry Core Facility.

### 3.1.5 Characterization of ligand-modified gold nanoparticles

Sizes of the MDSC-SNAbs and other ligand-modified Janus or nonJanus gold nanoparticles were measured using Zetasizer Nano (Malvern, USA) and transmission electron microscopic imaging. The amount of ligands modified onto the surfaces of the

Janus or nonJanus gold nanoparticles were determined using fluorophore-tagged ligands. Specifically, 10-molar excess of NHS-Alexa Fluor-680 (AF680) dyes were reacted onto the N-terminus of G3-biotin or cp33-SMCC ligands. Unreacted dye molecules were removed by dialysis in MWCO 2000 slide-A-lyzer cassettes (Thermofisher Scientific, USA). A standard curve made with the known dilutions of AF680 dye was read together with the fluorophore-conjugated G3-biotin and cp33-SMCC to quantify the concentration of the peptide solutions. The AF680-tagged G3-biotin and cp33-SMCC were than reacted with Janus nanoparticles SA-AuNP-SHs or nonJanus SA-AuNP-SAs. The unbound peptides were again removed by dialysis against PBS in MWCO 6000-8000 tubing for two days. Fluorescence of the nanoparticle suspension was read by SynergyHT Biotek plate-reader at Ex/Em 635/680nm. The values were used to calculate the number of peptides modified onto the nanoparticles.

## 3.2 Results

### 3.2.1 Validation of the synthesis procedure

We utilized absorbance or fluorescence assays to verify the success of each step of the solid-phase chemistry. First, the presentation of amine groups on the aminomethyl ChemMatrix resin was visualized by reacting NHS-Alex Fluor 647 dye in aqueous solution, which resulted in blue color and fluorescence emission at around 665 nm in plate reader. After the crosslinker-functionalization step (step 1), we quantified the reaction efficiency by either absorbance of NHS leaving group. When the input ratio between amine group on resin and NHS ester on crosslinker is around 2.5:1, almost 100% of the crosslinker will be functionalized onto the resin. To determine the binding

efficiency of streptavidin-coated gold nanoparticles (SA-AuNP-SA) on the biotin-functionalized resin after the 2nd step (Figure 6), we compared the amount of SA-AuNP-SA added into the reaction vessel and the amount remained in the liquid phase after reaction by measuring absorbance of solutions around the surface plasmon resonance (SPR) peak (522 nm-525 nm) of the SA-AuNP-SA. Usually, when the ratio between bound biotin on the resin and total number of streptavidin on the input SA-AuNP-SA is around $10^5$:1, 50-90% of the input gold nanoparticles will be bound onto the functionalized resins (Figure 6). Percentage increases when the number of streptavidin on the surface of SA-AuNP-SA increases.

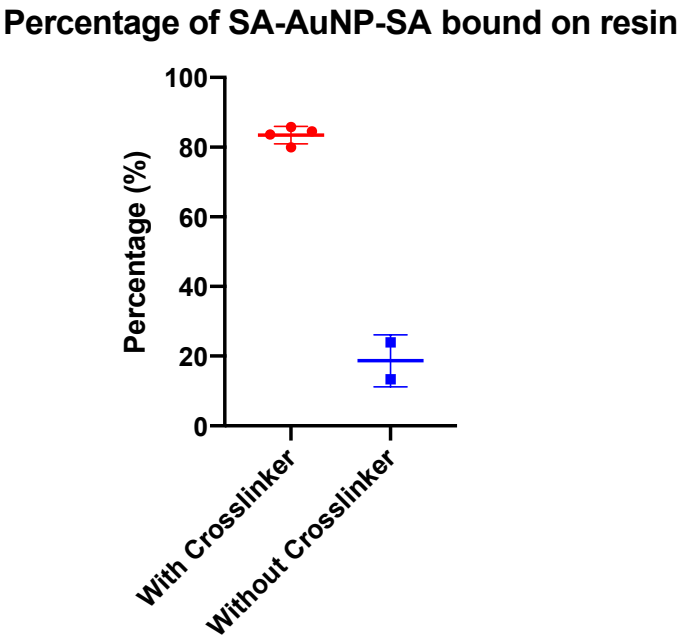


Figure 6. Streptavidin-coated gold nanoparticles bound to crosslinker-functionalized resins. Crosslinker-functionalized resins bound drastically higher amount of gold nanoparticles (SA-AuNP-SA) as compared to resins not functionalized. The results shown in the graph were from a synthesis done with Apexbio batch 14 crosslinker and Nanohybrid Batch 10 particles (96 SA/NP).

Later, the amount of Janus nanoparticles (SA-AuNP-SH) released by TCEP cleavage of disulfide bonds was also measured by absorbance (Figure 7). Twenty to fifty percent of the bound gold nanoparticles, again depending on the number of streptavidin coated on the gold nanoparticles, can be collected. We did these above-mentioned procedures routinely and we are able to get reproducible synthesis outcomes.

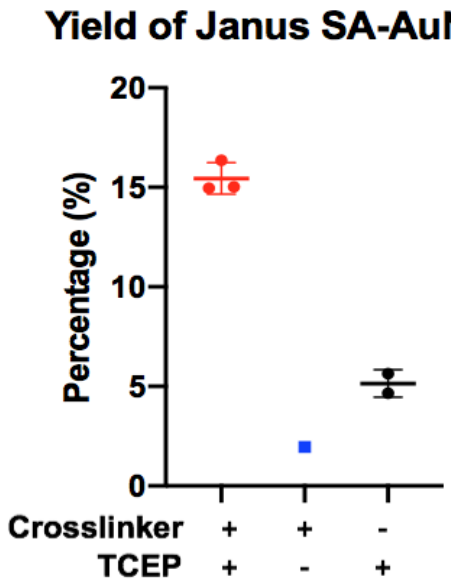


Figure 7. TCEP cleaved the di-sulfide bonds and released the Janus SA-AuNP-SH. Addition of TCEP resulted in the cleavage of di-sulfide bonds in the crosslinker and released Janus SA-AuNP-SH. Without TCEP, nanoparticles also fell off the solid resin to some extent, but they were not Janus nanoparticles. Nanoparticles bound on the resin through crosslinkers were less likely to disconnect from the resin without TCEP because they were more tightly bond on the resin through covalent bonds. The results shown in the graph were from a synthesis done with Apexbio batch 14 crosslinker and Nanohybrid Batch 10 particles (96 SA/NP).

### 3.2.2 Validation of the thiol substitution and surface asymmetry

We reacted fluorescent dye Alex Fluor 647-C2 maleimide with the Janus nanoparticles (SA-AuNP-SH) to verify the existence of thiol groups. The increase in the fluorescence signal at the emission peak of the dye comparing to the original streptavidin-coated gold

nanoparticles (SA-AuNP-SA) indicated the successful thiol-substitution of some of the biotin-binding sites on the nanoparticles (Figure 8).

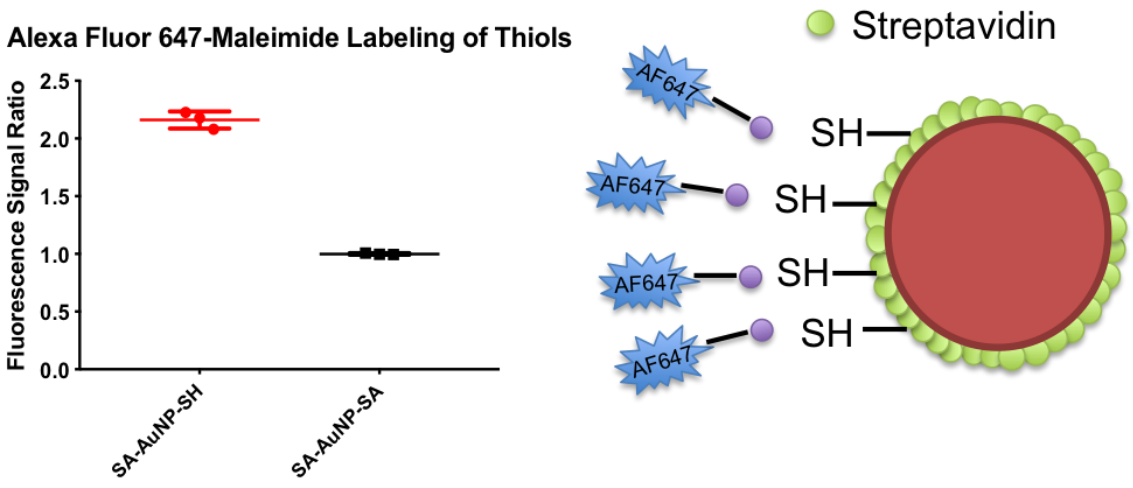


Figure 8. Free thiol groups present on the Janus SA-AuNP-SH. Compared to unmodified SA-AuNP-SA, Janus gold nanoparticles SA-AuNP-SH have higher fluorescence after reaction with Alexa Fluor 647 C2-maleimide, indicating that they have a higher number of available reactive groups, i.e., -SH.

To illustrate the surface asymmetry, we performed TEM imaging with biotin-gold probes (3nm) to visualize the distribution of available biotin-binding sites on the Janus nanoparticles. As shown in Figure 9, biotin-gold probes are only associated with one part of the surfaces, which implies the inaccessible of other part of the surface for biotins.

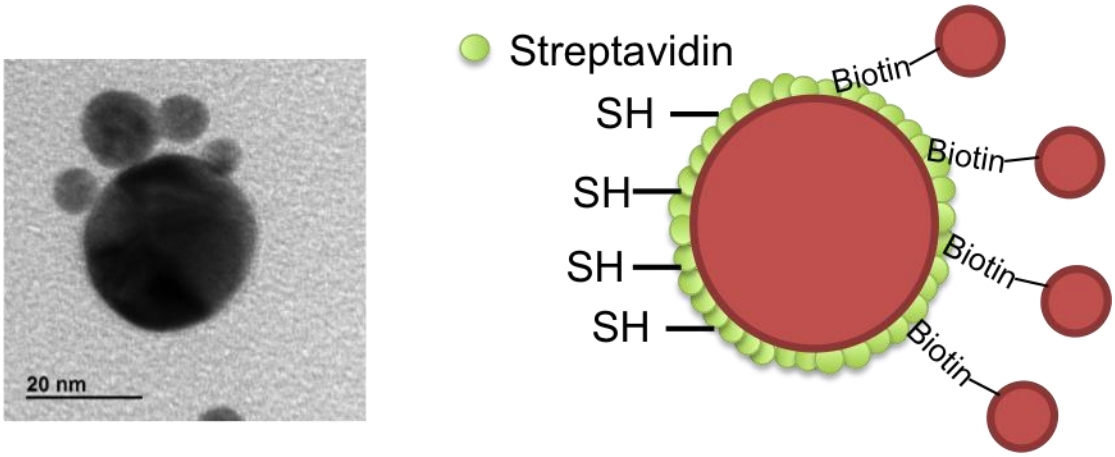


Figure 9. Validation of surface asymmetry by TEM imaging. TEM imaging with 3nm biotin-gold probes showed the asymmetric surface chemistry of SA-AuNP-SH. Biotin-gold nanoprobes (3nm) were only able to bind to part of the surface on the Janus gold nanoparticles (left) as illustrated with TEM imaging.

### 3.2.3 Optimization of yield

First, we separately measured the absorbance of crosslinker and the number of unbound SA-AuNP-SA and cleaved Janus particles collected in each washing step, and confirmed that the elution of both the crosslinker and the nanoparticles are a size-dependent chromatography process. The crosslinkers were small molecule, so the initial elution and first wash after crosslinker functionalization step took away the majority of the crosslinkers. Usually eight washes are good enough to remove all the unbound crosslinker or NHS leaving groups, but we performed twelve washes to eliminate any residuals in the solution to avoid unwanted modification on the SA-AuNP-SA. SA-AuNP-SA and Janus SA-AuNP-SH are relatively large molecules. The initial elution and the following two to three washes all contained a lot of gold nanoparticles. We usually performed more than five washes to collect all the free and loose nanoparticles. By conducting stringent washing, we guaranteed that we collected all of the Janus nanoparticles and the yield measurement was based on this strict criterion.

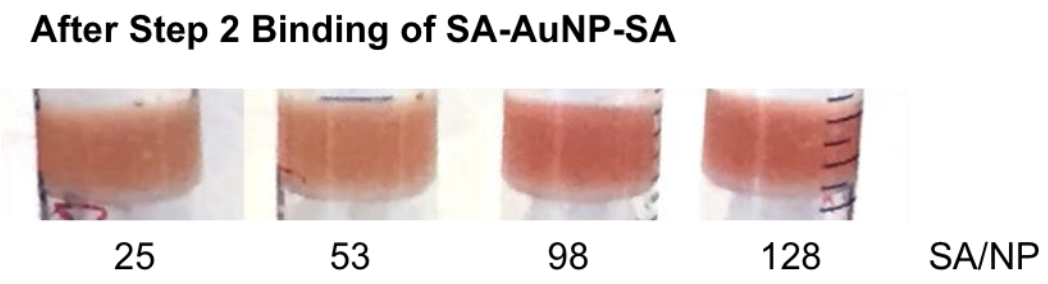


Figure 10. The density of streptavidin affected the binding of SA-AuNP-SA on the functionalized resins. Resin color was darker after binding with SA-AuNP-SA coated with higher density of streptavidin molecules, indicating higher number of SA-AuNP-SA bound onto the resins.

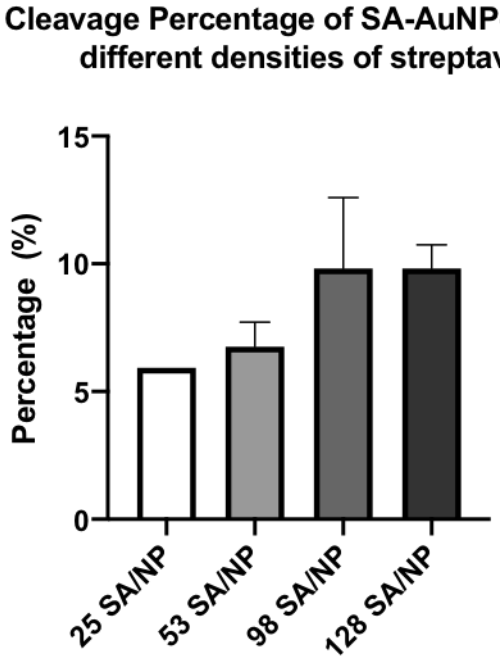


Figure 11. The density of streptavidin affected the binding of SA-AuNP-SA on the functionalized resin. The overall yield of Janus SA-AuNP-SH increased as the density of streptavidin on the SA-AuNP-SA increased, but stabilized after it reached a certain density (~98 SA/NP).

As a way to increase the yield of the solid phase chemistry method, we tested the impact of varying streptavidin density on gold nanoparticles. Specifically, we used gold nanoparticles that had 25, 53, 98, 128 streptavidin per particle in synthesis. The increase

in the number of streptavidin molecules on the particles improved the binding on the resin by increasing the available sites of interaction and also led to a slight increase in the overall yield of the Janus gold nanoparticles, given the amount of resin, crosslinker, TCEP remained the same. The theoretical maximum density of streptavidin on 30nm gold nanoparticles calculated by the surface area is 144 per particle. However, as illustrated by Figure 10 and 11, it doesn't change much after the density of streptavidin reaches 98 per particle. So, we chose around 100 SA/NP as our working density to ensure the highest yield as well as multivalency. To improve yield, we also tested the ratios of resin: crosslinker, concentrations of SA-AuNP-SA and TCEP concentration and pH. The purity of Thermofisher Scientific EZ-link Sulfo-NHS-S-S-Biotin is generally more stable than that of the crosslinker from Apexbio Biotechnology. Usually, for each 110 mg-120 mg of resin, 16.6 mg of crosslinker from Thermofisher Scientific creates the same densely biotin-functionalized surface as that using 25 mg of Apexbio crosslinkers, which is optimized for the binding with 8-10e11 gold nanoparticles, giving the highest yield 30%-40%. On the other hand, for around 110 mg of resins, below 3e11/μL for the binding step with a total of 3 mL, the higher the concentration of gold nanoparticles is, the higher the binding percentage is. Over 3e11/ml, the improvement in the binding percentage is not apparent. TCEP works in a wide pH range. Changing the buffer pH from 5 to 7 does not change the yield. At pH 7, we tried 0.005 M, 0.05 M, 0.5 M TCEP concentration in the last step of Janus nanoparticle production. As long as TCEP concentration was equal to or higher than 0.05 M TCEP, we got the same yield. When the concentration was 0.005 M, we barely collected any Janus nanoparticles. So, we decided

to use 0.05 M pH 7 TCEP in the synthesis. Other reaction conditions (e.g. temperature, volume, reaction duration) for each step were optimized in the same way.

### 3.2.4 Generation of SNAbs by modification with ligands

#### *3.2.4.1 Conjugation of peptides*

To verify the modification of the SA-AuNP-SH with peptides by the described methods in (a), we labeled the binding ligands (biotinylated G3 peptides) as well as Fc-receptor binding peptides (cp33-SMCC) by Alex Fluor 680 (AF680) and reacted the fluorescent peptides with SA-AuNP-SHs as well as SA-AuNP-SAs. By comparing the fluorescence normalized to the amount of nanoparticles, we are convinced that the SA-AuNP-SHs were successfully conjugated with G3 peptides via biotin-streptavidin interaction and with cp33-SMCC through thiol-maleimide reaction and transformed into the designed MDSC-SNAbs. Basically, because the Janus nanoparticles have fewer biotin binding sites than SA-AuNP-SA, we observed lower fluorescence with G3-AF680. The presence of thiol groups to react with maleimide resulted in higher fluorescence intensity of the Janus SA-AuNP-SH and Janus G3-AuNP-SH after reaction with cp33-AF680, also showing no interference between the G3-biotin-streptavidin and cp33-SMCC-SH reactions (Figure 12).

The hydrodynamic size and zeta potential of the unmodified and modified nanoparticles were monitored. The results showed a slight increase in size after peptide modification, part of it possibly resulted from insignificant aggregation of the particles in the buffers (see 3.2.4.3). Little change in zeta after synthesis and modification (See Apendix C and

Figure 13), which indicates that in terms of cellular uptake and in vivo biodistribution, the SNAbs and the parental SA-AuNP-SAs may not be drastically different.

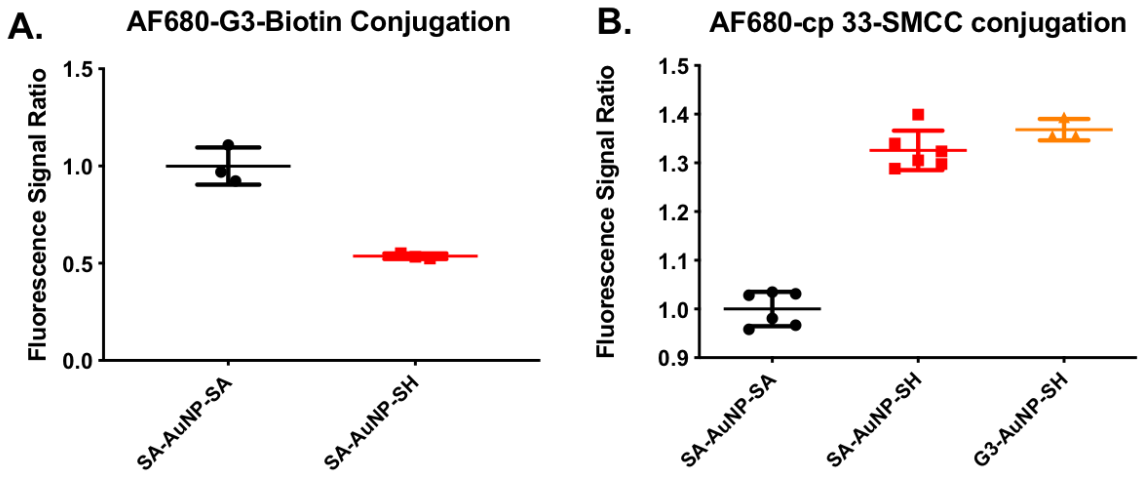


Figure 12. Qualitative analysis of the modification of Janus SA-AuNP-SH with fluorescent-tagged peptides. Janus particles SA-AuNP-SH were only able to conjugate half of the fluorescent G3-biotin on the particle as on the unmodified SA-AuNP-SA (A). At the same time, Janus SA-AuNP-SH has higher fluorescent cp33-SMCC conjugated on the surface because SA-AuNP-SH has free thiol groups available for conjugation (B).

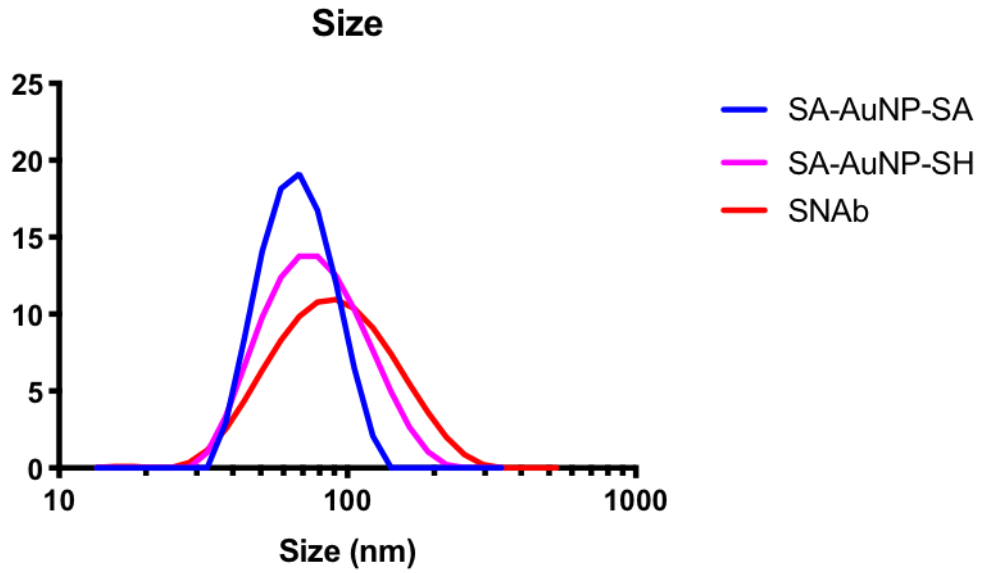


Figure 13. Hydrodynamic sizes of nanoparticles before and after peptide modification. The hydrodynamic size of particles increased from 70nm to 100nm after modification of Janus particles with peptides as measured with dynamic light scattering.

*3.2.4.2 Quantification of the modification level of peptides on the SNAbs*

G3-biotin and cp33-SMCC with heavy, stable isotope-labeled amino acids were synthesized by Genemed Synthesis Inc.. (See Table 1). The numbers of each type of peptide modified onto the surface of the nanoparticles were determined by measuring the relative peak intensity of light peptides (G3-biotin, cp33-SMCC) conjugated on the Janus SA-AuNP-SH to those of the heavy peptides ($^{6}$C, $^{15}$N-G3-biotin and $^{6}$C, $^{15}$N-cp33-SMCC) of known concentration in mass spectrometry. Using this method, on average, each SNAb has 10.63 G3-biotin and 8.81 cp33-SMCC conjugated.

*3.2.4.3 Stability of SNAbs*

We observed particle formulations under optical microscope after synthesis and before use for *in vitro* or *in vivo* study. The particle tends to aggregate after peptide modification because of the increase in hydrophobicity. A study reported that arginine, serine and

tryptophan-ended peptides causes the aggregation of gold nanoparticles of 13 nm and 20 nm in aqueous solutions, which then influence the cellular uptake of these particles. [88] G3 peptide contains an N-terminal tryptophan and an inner tryptophan, and indeed we noticed that non-Janus SA-AuNP-SA particles started precipitating out of the solution, aggregate into pellets and adhered to the wall of the tubes once we added G3-biotin peptides. Janus SA-AuNP-SH seemed to have less of this issue when modifying with G3-biotin probably because they reacted with lower number of G3 and also had localized distribution of G3 (See Figure 9 and 12), reducing the hydrophobic interaction of modified nanoparticles. In Aim 2, we needed to compare the *in vitro* response to Janus G3-AuNP-cp33 particles and nonJanus G3-AuNP-cp33. We tested making nonJanus G3-AuNP-cp33 in different buffers (DI water, 0.9% NaCl solution, PBS, RPMI 1640 complete medium) at the same concentration of nanoparticles (SA-AuNP-SA, 1.25e11/ml) and peptide concentration. NonJanus G3-AuNP-cp33 made in DI water and 0.9% NaCl has a significant increase in the size of the nanoparticle as compared to the size of unmodified SA-AuNP-SA owing to aggregation of the particles (See Table 2). RPMI 1640 complete medium (containing 10% fetal bovine serum) seemed to have prevented or reduced the modification with peptides due to the potential interaction of the serum proteins with the particles, forming a corona on the surface of streptavidin-modified particles. On the other hand, nonJanus G3-AuNP-cp33 made in PBS has detectable increase in size, but are still consistent in quality with the Janus G3-AuNP-cp33 that were not or less aggregated. Our goal is to have control over the influence of aggregation on the cellular response in order to test our hypothesis with nonJanus and Janus peptide modified nanoparticles, so PBS is an appropriate solvent to make the

nonJanus gold nanoparticles. Later, we added 0.001% tween-20 in the PBS for the reactions to reduce the non-specific interaction between particles and particles as well as between particles and tubes. We saw significant improvement in the retention of particles from the tubes after adding the tween-20.

Table 2. Sizes of nanoparticles prepared in different buffers (SA-AuNP-SA from Nanohybrids Inc.).

| **Intensity Peaks** | | **G3-AuNP-cp33** | | | | **Unmodified SA-AuNP-SA** |
|---|---|---|---|---|---|---|
| | | **DI water** | **0.9% NaCl** | **PBS** | **RPMI 1640** | |
| Peak 1 | Ave. Size (nm) | 184.9 | 150.2 | 96.42 | 63.96 | 62.45 |
| | ST.DEV (nm) | 151.6 | 100.2 | 39.83 | 21.45 | 19.32 |
| | Percentage (%) | 98.7 | 98.4 | 97.9 | 100 | 100 |
| Peak 2 | Ave.Size (nm) | 5010 | 4609 | 4789 | N/A | N/A |
| | ST.DEV (nm) | 604.9 | 825.4 | 729.1 | N/A | N/A |
| | Percentage (%) | 1.3 | 1.6 | 2.1 | N/A | N/A |

## 3.3 Discussion

In this chapter, we described the process to develop synthetic nanoparticle antibodies. The first step is to produce Janus gold nanoparticles. The method we used was adapted from a previous publication by Pubudu Peiris, et al., "Assembly of Linear Nano-Chains from Iron Oxide Nanospheres with Asymmetric Surface Chemistry", published on Plos One in 2011. In the paper, they described a method using solid phase chemistry to create an iron oxide nanopshere with two faces, one presenting amine groups and the other presenting thiol groups.[24] It is one type of the immobilization methods widely used to produce inorganic Janus nanoparticles, which meets our goal of generating Janus gold nanoparticles. The method also exhibited a high degree of control over the uniformity of the nanospheres. By step-by-step addition of particles, the same group assembled linear nano-chains and chemically linked drug-loaded liposomes to delivery chemotherapeutics to the tumor sites. The nanochain-liposome conjugates could access the micro-metastatic sites of tumor because of their unique biophysical properties and could release drug on-demand by radio-frequency due to the utilization of iron oxide nanoparticles. [28,93,94,131]

Specifically, Pubudu Peiris, et al. used CLEARTM (crosslinked ethoxylate acrylate resin) resins with amine groups and homobifunctional cleavable crosslinker DTSSP (dithiobis(sulfosuccinimidylpropionate), amine functionalized iron oxide nanospheres and TCEP. In comparison, we use ChemMatrix aminomethyl resin, which has a simpler structure, i.e., PEG network with amine end groups. We used a heterofunctional cleavable crosslinker sulfo-NHS-S-S-biotin and streptavidin coated gold nanoparticles. In this case, the crosslinker prefers to bind the aminomethyl resin through sulfo-NHS and amine reaction, while reacts with the particles through streptavidin-biotin interaction. As

a result, we prevented the quenching of homobifunctional DTSSP by amine groups on the resin or nanoparticles and thus increased the efficiency of synthesis method. On the other hand, sulfo-NHS has the advantage of water solubility, so we could use PBS as solvent to avoid the need to change buffer for downstream biological assays.

Gold nanoparticles are coated with streptavidin through sulfo-NHS-PEG-SH and thiol-gold bonds as reported by the manufacturers' product specification sheet. In contrast to iron oxide nanoparticles, gold nanoparticles cannot be detected by magnetic relaxivity, but instead, the concentration of gold nanoparticles can be measured through surface plasmon resonance. At certain wavelength of light, collective oscillation of electrons on the gold surface after interaction with the photons results in the adsorption and scattering of light, as reflected by the reduction in absorbance reading. This property is easier than magnetic relaxivity to measure, as it is detectable by a common benchtop plate reader or UV-VIS spectrophotometer, while the latter requires a special instrument, e.g., magnetic resonance imaging. The SPR peak of gold nanoparticles depends on the size and shape of the particles and does not change significantly upon surface modification. For gold nanospheres of 20-100nm, the SPR peaks are usually between 520nm to 570nm, resulting in the red color of the solution. As mentioned in the method and results section, for the 30nm streptavidin-coated gold nanoparticle, we use 522-525nm as the wavelengthes for the measurement and calculation.

Pubudu Peiris, et al., tested the impact of particle diameter on the generation of Janus nanospheres. The larger the particle, the smaller the partially modified area (PMA) of thiol-displaying face, with PMA being around 30% of the 30nm ion oxide nanoparticles. We assumed the similar results of our streptavidin coated gold nanoparticles because our

particles are also evenly modified with the reactive groups all over the surface and we utilized the same reaction mechanism. Instead of particle diameter, we tested the effect of variance of streptavidin density on the yield of Janus nanoparticles. There is a limit in the number of streptavidin (~5nm in diameter) that can be conjugated on the gold nanoparticles because of the sensitivity of quantification method used by the manufacturer (Nanopartz. Inc or Nanohybrids. Inc) and the steric hindrance of streptaividin dense-packing. We chose to use 25, 53, 98, 128 streptavidin per nanoparticle (Nanohybrids. Inc) to compare the production of the Janus gold nanoparticles and determined the best working density as 98 SA/NP. Below 98 SA/NP, the binding of SA-AuNP-SA on functionalized resin and the overall yield increased as the SA/NP increased. Although biotin-streptavidin interaction is quite specific and has a low dissociation rate, it is dynamic and non-covalent. Considering the large size of gold nanoparticles, a minimal number of biotin-streptavidin interactions have to occur to form solid binding between the SA-AuNP-SA and resin and to keep the SA-AuNP-SA on the resin. Hence, it is reasonable to have better binding when the number of streptavidin available on the nanoparticle for such interactions increases. However, when the density of streptavidin reaches a certain level, no more streptavidin is needed for each particle to be bond onto the resin, which is why we saw no changes in the binding and yield over 98 SA/NP. In addition to the streptavidin density, the solid phase chemistry was also optimized by varying ratios between resin and crosslinker and SA-AuNP-SA, the concentration of SA-AuNP-SA and TCEP, and other reaction conditions (i.e., temperature, duration, volume, pH).

Generally, each 10 mL-reaction vessel gave us about 1.0-2.0e11 Janus SA-AuNP-SH. After modification, we can concentrate the particles to as high as 5.0-6.0e11/ml, equal to around 1nM. Usually, in *in vitro* antibody-dependent cellular cytotoxicity assays, the antibody concentration is in the range of 0.001 to 10 ug/mL[132,133], corresponding to a molar concentration range of 0.0067-6.7 nM, so we were able to make it to the target working concentration for antibody-dependent response. To do an *in vitro* assay (Chapter 4), we need around 500 μL, and up to 2.0-3.0e11 of Janus nanoparticles. Considering the loss of the modified particles during purification, we usually need to do a batch of four reaction vessels for an *in vitro* assay. In terms of an animal study, previous publications report various different doses and frequencies of mAb administration for different models of tumor in mice. The most frequently used dose is 100-200 μg, which is around 4.0-$8.0\times10^{14}$ molecules, much higher than what we could achieve. Therefore, when we started the first *in vivo* study (Chapter 5), we administered the amount of SNAbs to mice as much as we could manage to fabricate within two-weeks (hypothesized shelf-life of SNAbs considering the instability of peptides at 4 ℃ in PBS) and tested their response. The dosage we used in our study is 0.75e11 per mouse. For each *in vivo* study, we need at least 6e11, in which case we need to do a batch of 6 reaction vessels.

To meet the demand of larger animal studies, we need to figure out the scaling up method of the SNAb fabrication in the future. As discussed, the current scaling up method is to use multiple syringes to achieve the desired amount. Scaling up the process includes two aspects: one is to increase the yield of each round of synthesis, in other words, to increase the efficiency of the method and reduce cost; the other is to reduce the time and effort needed to produce the same yield. For the first aspect, we've optimized most of the

parameters (e.g. temperature, concentration, ratios between reagents, pH) for the resins, crosslinker, particles and TCEP we currently use, but there is still potential for further optimization with the length (number of $CH_2$-) of crosslinker, length of PEG linker between the particle and streptavidin, which affects the reaction efficiency in step 1 and 2. The purity and quality of crosslinker also affects the yield. For the second aspect, as mentioned in the method section (3.1.2.1), we can reduce the reaction and purification time of each step to shorten the entire procedure from 7 days to 1 day. In addition, using larger reaction vessels with higher amount of reagents could be a good option. For example, we have tried 20 mL reaction vessel with double amount of the reagents in the same concentration. We did not see a significant improvement of the yield as per unit amount of input material, but this could be a way to significantly decrease the set-up monetary cost, labor cost and time. Also, for a larger reaction vessel, the amount of reagents and the ratio needs to be optimized again because the volume changes lead to concentration change and may affect the efficiency of reactions. Lastly, other fabrication methods, such microfluidic device and electrohydrohynamic jetting, could be considered.[89] However, a change in fabrication method may require changes in material of the particles and modification chemistry of the ligands as well, which will be discussed later in Chapter 6.

Using fluorescently labeled peptides, we successfully validated the modification of them on the Janus nanoparticles. When it comes to quantification of the number of peptides on the particle surface, we've tried colorimetric assays, including the micro-bicinchoninic acid (microBCA) assay, the fluoraldehyde o-Phthaldialdehyde (OPA) assay, and fluorescence-quantification of the AF647/680-tagged peptides on the nanoparticles.

Unfortunately, both the microBCA and the OPA have a detection lower limit of around 10 μg/mL of protein or peptides. The corresponding concentration of SNAbs required for the assay is around $3.0 \times 10^{13}$ per mL, far higher than what we could achieve because of both the yield of our method and also the expensiveness of gold nanoparticles and peptides. Quantifying the level of modification using fluorescence of the dye-tagged peptides gave us an incredibly high number, in the range of thousands of peptides on each particle. As the total number of available binding sites is only around 400 at most on each particle, we deem this result not reliable, possibly because of the remaining residual of unconjugated peptides in the solution after insufficient purification or the loss and aggregation of nanoparticles. One other method we attempted was analytical ultracentrifugation, which can detect the changes of molecular weight of the particles by measuring the sediment co-efficient during centrifugation. By analytical ultraentrifugation, we confirmed the available binding sites of the streptavidin-coated gold nanoparticles for biotinylated ligands are three per streptavidin on the particles. However, to quantify the number of peptides, we need more accurate detection method other than interference optical measurement in the analytical centrifuge as well as a thorough study of the partial exclusion volume of the particles in the solution, which was unachievable at the moment due to inaccessibility to necessary equipments. Besides, the poly-dispersity of the nanoparticles and large molecular weight of the gold core itself made the measurement of the changes in molecular weight before and after modification unreliable. Finally, we decided to pursue the method of AQUA (absolute quantification) of peptides using mass spectrometry (MS). This method uses the shift of peaks in MS spectrum due to the heavy, stable isotope labels in the peptides to discern between the

normal peptides used in the modification and the heavy peptides of known concentration in the solution. The relative intensity of the two peaks tells us the relative concentration of the normal and heavy peptides and thus yields the accurate level of modification of peptides on the particles. After calculation, each SNAb has around 11 copies of G3 peptides and 9 copies of cp33 on the nanoparticles. Considering the number of streptavidin on SNAbs was on average 100 per nanoparticle and each streptavidin protein molecule has 4 biotin-binding sites, the copy numbers of G3 and cp33 were much lower than the maximum capacity (400) of ligands modification on the streptavidin. We think the reason possibly lies in the either the reduction of reaction efficiency due to the presence of tween-20 detergent and Janus chemistry or the difficulty of proteolytic cleavage of peptides on the nanoparticles by the enzymes. Positive controls of nanoparticles conjugated with known number of peptides need to be tested to confirm the results of the AQUA method. Nevertheless, we could reach a safe conclusion that SNAbs are more multivalent than the bi-valent antibodies and all of the artificial antibodies or antibody biomimetics discussed previously. This multivalent display of ligands could lead to better functionality, which were tested and discussed in Chapter 4 and 5.

When the gold nanoparticles aggregates in the solution, often because hydrophobic interaction between ligands on the surface or high salt concentration in solution, the spectrum of absorbance will have red shift, changing the color of the solution to purple or clear. Therefore, we also use the color and spectrum changes to tell the stability of the particle formulation. In general, both the unmodified SA-AuNP-SAs and Janus gold nanoparticles collected after solid phase chemistry are pretty stable within two to three months. Modified Janus gold nanoparticles, or SNAbs, are less stable because the

hydrophobicity of the peptides and may require addition of detergent, e.g., 0.001% tween-20, to maintain the suspension of particles. We also noticed adhesion of nanoparticles on the tubes as discussed in the 3.2.4.3 section of stability of nanoparticles.

In summary, in this chapter, we have described how we created a solid-phase chemistry based method to fabricate Janus streptavidin-coated gold nanoparticles and modify them with selected ligands to make MDSC-targeting SNAbs. In the next chapter, we will further explore the biological function of the SNAbs *in vitro*.

# CHAPTER 4 AIM 2. TO DEMONSTRATE *EX VIVO*, THE SPECIFICITY OF CELL TARGETING AND ACTIVATION OF IMMUNE RESPONSES BY THE SNABS

Antibody therapies in cancer remove the target cells, such as tumor cells, by antibody-dependent innate immune response, primarily antibody-dependent cellular cytotoxicity (ADCC) and phagocytosis (ADCP). The responses happen after the antibodies bind to the target cells through the interaction between antigen-epitope and Fab region, and are carried out by Fc-gamma receptor-mediated signaling in the effector immune cells, such as natural killer (NK) cells, macrophages and granulocytes, triggered by the engagement with the Fc region of the antibodies.[133] After the bridge is formed, the cascade of events starts with the tyrosine phosphorylation on the intracellular motif of gamma chains, and then induces the release of cytokines, reactive oxygen species (ROS), proteases, perforin and granzyme B, leading to the destruction of target cells.[134–137] In ADCP, the Fc-gamma receptor-mediated signaling in macrophages, which are both phagocytes and antigen-presenting cells, also induce phagocytosis of the opsonized cells and antigen presentation of the killed cells to the adaptive immune effector cells.[134,135]

The major types of effector cells are natural killer cells and macrophages. NK cells in both human and mouse express activating Fc gamma receptors on the surface and can detect the cells opsonized by IgG1, IgG2, IgG3, and IgG4, but at different affinity. NK cells are not phagocytic nor antigen-presenting cells, so it is believed that the way they kill target cells is mainly ADCC by cytotoxic granules, tumor-necrosis factor alpha (TNFα)-family receptor signaling and proinflammatory cytokines.[138] A number of the

successful monoclonal antibody drugs for cancer has been shown to work in a NK-cell dependent way, such as trastuzumab (anti-Her2), Cetuximab (anti-EGFR) and Rituximab (anti-CD20).[138] Macrophages are also important effector cells for antibody-dependent responses. They express all four types of Fc-gamma receptors (FcγRI, FcRIIB, FcγRIII, FcγRIV) in mouse and most of the activating and inhibitory receptors (FcγRI, FcγRIIA, FcγRIIB, FcγRIIIA) in human.[137] Because macrophages are both phagocytes and antigen-presenting cells, they are likely to perform both ADCC and ADCP to kill antibody-labeled cell targets. Interestingly, conflicting results were reported in different studies for which of NK cells and macrophages are dominant effector cells in antibody therapy. Take rituximab as an example, despite previous data showing NK-mediated clearance of $CD20^+$ lymphoma cells in immune-deficient mice,[139] two papers published before 2010 showed that in an immune-competent murine model treated with anti-mouse CD20 monoclonal antibodies, macrophages mediated the ADCC/ADCP of $CD20^+$ lymphoma cells, and no contributions from NK cells or complement pathways were detected.[140,141] The relative importance of different cell types in antibody-dependent responses needs to be discussed case by case. For instance, NK cells are likely to be more efficient in blood leukemia and macrophages works better in solid tumor because they can clear tumor cells and process and present the antigens, leading to the activation of adaptive immune responses. [142] More and more evidence appears to support that cells that co-express both activating and inhibitory Fc receptors, such as macrophages, and granulocytes, mediate the antibody responses, as the deficiency in the FcγRIIB increased the enhancement of ADCC/ADCP.[135,139] Neutrophils, mononuclear cells and granulocytes stimulated with GM-CSF also showed enhanced ADCC capacity *in vitro*.[134] Because macrophages and

monocytes express a variety of Fc-gamma receptors and contribute to both ADCC and ADCP pathways mediated by antibodies, we chose macrophage cell lines as the effector cells of interest in our assays.

The most commonly used method to test the functionality of a newly developed monoclonal antibody is to do ADCC/ADCP assays in target-effector-cell co-culture. Such assays usually quantify the response through one or few of the following methods: $^{51}$Cr (chromium), LDH (lactate dehydrogenase) release from the pre-labeled target cells after killed; staining of the apoptotic/necrotic target cells with propidium iodide (PI), 7AAD (7- amino-actinomycin D) or Annexin V; detect viability by Calcein-AM or MTT/MTS (3-(4,5-dimethylthiazol-2-yl)-2,5-diphenyl tetrazolium bromide/ 3-(4,5-dimethylthiazol-2-yl)-5-(3-carboxymethoxyphenyl)-2-(4-sulfophenyl)-2H-tetrazolium). $^{51}$Cr and other release assays are gradually being replaced by other assays due to the difficulty of radioactive material handling and disposal and the poor reproducibility of release assays. In recent years, new methods were developed for ADCC/ADCP assays, such as using xCELLigence platform and flow cytometry. XCELLigence platform enables measurement of real-time proliferation or cell death in a cell-culture plate by electrical impedance of the adherent target cells. In a typical flow-cytometry-based assay, the effector and target cells are usually labeled with different fluorophores. The advantage of such assays is to be able to tell ADCC and ADCP apart. The ADCC activity is evaluated by the number of dead cells stained with PI, 7AAD or other dead-cell labels and ADCP activity is assessed by the fraction of double-positive cells. In most cases, the effector cells used in such assays are, in human, NK cell line NK-92MI, monocyte cell lines (e.g. U937, THP-1) or peripheral blood mononuclear cells (PBMC), and in mouse,

mouse PBMCs, bone marrow derived macrophages or RAW 264.7 cell line. [35,132,133] In this chapter, we tested our hypothesis using RAW 264.7 cell line as our effector cells in flow-cytometry-based assays. We've also developed a new type of cytotoxicity assay using splenocytes to better recapitulate the responses happening in the physiological environment.

The hypothesis for this aim is that the designed SNAbs can target the cell of interest specifically, activate Fc gamma receptor (FcγR)-mediated intracellular signaling cascade, and trigger ADCC/ADCP of target cells by immune effector cells. Respectively, G3 enabled the specific recognition of MDSCs while multivalent cp33 on SNAbs empowers them to engage with FcγRs on RAW macrophages, which results in down-stream signaling and immune responses. We tested our hypothesis with optimized imaging-, flow-cytometry-based assays and also compared the performance of our SNAbs with mAbs to assess their promise for *in vivo* applications.

## 4.1 Methods

### 4.1.1 Materials

Ebioscience RBC lysis buffer (Cat.#. 00-4333-57), Normocin (Cat.#.NC9390718), RPMI 1640 medium (Cat.#.22400105), DMEM medium (Cat. #.11995-073) and Bovine serum albumin (BSA, Cat.#.23209) were purchased from Thermofisher Scientific. Collagenase D was purchased from Sigma-Aldrich (Cat.#.11088882001). Characterized fetal bovine serum (FBS, Cat.#.SH3007103), USDA FBS (Cat.#.SH30910.03) and 1% Penicillin-Streptavidin (PS, Cat.#.SV30010) were purchased from GE Healthcare. Fixation buffer and Alexa Fluor 647-anti-S100A9 antibodies (Cat.#.565833) were

purchased from BD Bioscience (Cat.#.554655). Cell strainer was purchased from CellTreat.Inc (Cat.#.229481). QuanTI-Blue (Cat. # rep-qb1) for Alkaline phosphatase detection and Zeocin (Cat.#.ant-zn-1) were purchased from InvivoGen. MACS LS columns (Cat. #.130-042-401), anti-biotin beads (Cat.#.130-105-637) and myeloid-derived suppressor cell isolation kit (MDSC-Kit, Cat.#.130-094-538) were purchased from Miltenyi Biotechnology. Purified anti-mouse CD16/32 (Clone 93, Cat.#.101302) for Fc receptor blocking and biotin anti-mouse Ly-6g/Ly-6C (Gr1, clone RB6-8C5, Cat. #.108403) for MDSC sorting was purchased from Biolegend. Antibodies used for cell marker staining includes anti-F4/80-FITC, anti-CD11c-PE, anti-B220-FITC, anti-CD8-FITC, anti-CD4-PE, anti-CD3-PE-Cy7, anti-CD11b-PE-Cy7, anti-Ly6G-PerCP-Cy5.5, anti-Ly6C-APC-Cy7, anti-CD49b-APC, anti-FoxP3-APC and anti-CD25-APC-Cy7, all purchased from Biolegend (Please see Appendix D). Fluorophore (FITC, PE, PE/Cy7, or APC)-conjugated streptavidin for detecting biotin-labeled cells were purchased from Biolegend (Cat.#.405207, 405206, 405204) or Thermofisher Scientific (Cat.#.PI21224). FACS buffer was prepared by adding 10 mL of FBS to 500 mL of PBS. MACS buffer was prepared as PBS buffer (pH7.2) containing 0.5% BSA (bovine serum albumin (BSA)) and 2 mM EDTA.

### 4.1.2 Cells and animals

4T1 breast cancer cell line from American Type Culture Collection (ATCC, Manassas, VA, USA). was cultured in RPMI 1640 medium with 10% characterized FBS and 1% PS. RAW 264.7 macrophages cell line from ATCC (TIB 71) was cultured in DMEM medium with 10% USDA FBS and 1% Penicillin-Streptavidin. RAW-Blue macrophages from InvivoGen.Inc (Cat. #. raw-sp) was cultured in DMEM medium with 10%

characterized FBS and 1% PS. Heat-inactivated fetal bovine serum was made by heating the normal FBS at 56 ℃ for 30mins. All the cells were cultured in 37 ℃, under 5% $CO_2$.

Mice were purchased from Jackson Laboratory. The use of animals was approved by The Institutional Animal Care and Use Committee (IACUC) at Georgia Institute of Technology (Atlanta, GA)

### 4.1.3 Splenocyte suspension preparation from the spleen of 4T1 tumor-bearing mice

Five-to-twelve-weeks old female Balb/c mice were inoculated subcutaneously with 4T1 breast cancer cell line, $0.5\times10^6$ in 50 μL of PBS, at the fourth mammary fat pad. On day 16 post tumor inoculation, mice were euthanized with $CO_2$ gas and cervical dislocation. Spleens were collected and digested using collagenase D, 2 mg/mL for 15-30 mins. The mixture was passed through a 40 μm cell strainer with gentle grinding. The solution was then centrifuged at 500 g for 5mins, followed by red blood cell (RBC) lysis with RBC lysis buffer for 5-10 mins at room temperature. The cell suspension was neutralized with complete medium and washed with PBS by centrifugation at 500 g for 5mins. The cell pellet was resuspended in the desired buffer (e.g. PBS, FACS buffer, MACS buffer) for the following assays.

### 4.1.4 MDSC isolation from splenocyte suspension

MDSCs were isolated using Miltenyi MDSC-Kit from splenocytes of the 4T1-tumor bearing mice. Briefly, 100 million splenocytes was resuspended in 350 μL of MACS (magnetic-activated cell sorting) buffer (PBS, pH7.2, 0.5% BSA, 2mM EDTA), and then incubated with 50 μL of the Fc-receptor blocking reagent (from the kit or anti-CD16/32

antibodies) at 4 ℃ for 10 mins. The cell mixture was subsequently mixed and incubated with 100 μL anti-Ly6G-Biotin in the MDSC-kit or biotin-anti-Gr1 antibodies for 10mins at 4 ℃. Following a wash with 5-10 mL of MACS buffer and 10 mins centrifugation at 300 g, the cells were resuspended in 800 μL buffer and incubated with 200 μL of anti-biotin microbeads for 15 mins at 4 ℃. The cell mixture was washed again with 10-20 mL of buffer and centrifuged at 300 g for 10mins at 4 ℃ and then the pellet was resuspended in 500 μL of MACS buffer. A MACS LS column was placed on a magnet separator and washed with 3 mL of buffer and the 500 μL of cell suspension was passed through the LS column followed by 3×3 mL of buffer to wash the column. The solution can be collected or discarded depending on the desired application. After the column was removed from the separator, 5 mL of buffer was added and using the plunger to flush the column. The solution that passed through was collected in a fresh tube as the isolated $Ly6G^+$ MDSCs or $Gr1^+$ MDSCs. If using anti-Ly6G antibody for the above steps, another round of isolation may be performed on the collected $Ly6G^-$ cells with biotin-anti-Gr1 antibody to get the $Gr1^{dim}Ly6G^-$ cells.

### 4.1.5 Free peptide binding on cells

#### *4.1.5.1 Free peptide binding on isolated MDSCs*

Mouse MDSCs were isolated (see 4.1.4) and added into FACS tubes, 1 million cells per tube. The cells were washed with PBS 1mL/tube by centrifugation at 500 g for 5 mins and then resuspended into 1mL of 0.001% streptavidin-PBS solution and incubated at room temperature for 30 mins to quench the endogenous biotin in the cells. The cells were then washed again with PBS 1mL/tube by centrifugation and incubated with 1mL of

0.001% biotin-PBS solution to quench the streptavidin for 30 mins at room temperature. After another wash, the cells were incubated with different biotinylated peptide solutions (100 μM) in 100 μL PBS for 30 mins at room temperature, at least 3 technical replicates for each type of peptides. The excessive peptide ligands were removed by washing. Subsequently, the ligands-labeled cells were stained with streptavidin-PE or streptavidin-APC at room temperature for 30 mins. After removing excessive staining reagents, the cells were washed and resuspended in 200 μL of FACS buffer (PBS, 2% FBS) and analyzed on BD LSRFortessa flow cytometer.

*4.1.5.2 Free peptide binding on RAW 264.7 macrophage cell line*

Similarly to the procedures of testing peptide binding on MDSCs, RAW 264.7 macrophages 1 million/mL were added to FACS tubes. Cp33-biotin peptide solutions were prepared at different concentration (2 μM, 20 μM, 100 μM) in PBS. The cells were incubated with the cp33-biotin solutions first and then stained with streptavidin-FITC conjugates and then analyzed on BD Accuri C6 flow cytometer.

*4.1.5.3 Free peptide binding on splenocytes*

The experiments were done in a similar way to what's described in 4.1.4.2. Two million cells of the single-splenocytes suspension prepared from the 4T1-tumor bearing mice were added to each FACS tubes. Following the incubation with different peptide solutions, the cells were then stained with antibodies for cell surface markers as well as the fluorescent streptavidins for 30 mins at room temperature. Following washing with FACS buffer, the samples were analyzed on a BD LSRFortessa flow cytometer.

*4.1.5.4 Colocalization of S100A9 and G3 peptides on MDSCs*

Mouse MDSCs were isolated and added into FACS tubes, 1 million cells per tube. The cells were washed with PBS 1mL/tube by centrifugation at 500 g for 5 mins and then resuspended into 1 mL of 0.001% streptavidin-PBS solution and incubated at room temperature for 30 mins to quench the endogenous biotin in the cells. The cells were then washed again with PBS 1mL/tube by centrifugation and incubated with 1 mL of 0.001% biotin-PBS solution to quench the streptavidin for 30 mins at room temperature. Half of the samples were fixed with BD Cytofix buffer for 30 mins at room temperature. After wash with PBS, both the fixed and unfixed cells were incubated with G3-biotin solution (200 μM) in 100 μL PBS for 30 mins at room temperature. Half of the samples were fixed with BD Cytofix buffer for 30 mins at room temperature. The excessive peptide ligands were removed by washing. Subsequently, the ligands-labeled cells were stained with streptavidin-PE and Alexa Fluor 647-anti-S100A9 antibodies at room temperature for 30 mins. After removing excessive staining reagents, the cells were washed and resuspended in 200 μL of FACS buffer (PBS, 2% FBS) and analyzed on BD LSRFortessa flow cytometer.

**4.1.6 Photoacoustic imaging of peptide-modified particles binding on cells**

SNAbs were prepared as described in Chapter 1. Peptide-modified nonJanus nanoparticles were prepared by reacting biotinylated peptides with unmodified AuNP-SA for overnight at 4 ℃ in 0.002% Tween-20-PBS solution. All the particles were washed twice with PBS and resuspended with PBS. The isolated MDSCs were fixed with BD cytofix buffer or without fixation but conditioned to 4 ℃ to minimize endocytosis of

particles. Cells were then incubated with particles at a ratio at $5\times10^{10}$/million cells (for Janus NPs) or $2\times10^{11}$/million cells (nonJanus NPs) in 1mL of PBS for 1 hr (for live cells) or 4 hrs (fixed cells) at 4 ℃. After incubation, cells were washed three times with PBS by centrifugation at 500 g for 5 mins and then fixed with BD cytofix buffer. The cell-NP samples were resuspended into 20 μL per 0.5 million cells in PBS and kept in the fridge until use.

For photoacoustic microscopy, we acknowledge Kelsey Kubelick in Dr. Emelianov's group for the acquisition and processing of photoacoustic images. The gelatin phantom used was composed of a base layer containing 8% gelatin and 0.2% silica. The solution was heated to around 50 ℃ under stirring and after dissolution of the gelatin, the solution was degassed to remove bubbles, poured into a container and solidified at 4 ℃. Each cell-NP sample was mixed with an equal volume of hot 16% gelatin solution (heated and degassed) and solidified on the gelatin phantom in the fridge into dome-like inclusions. The container with the gelatin phantom and the inclusions was filled with degassed ultrapure water and allowed to come to room temperature. The inclusions were imaged with a photoacoustic imaging microscope, the Vevo LAZR (Fujifilm VisualSonics Inc, Toronto, Canada), a combined US/PA imaging system. Three cross-sections of each sample were randomly selected to ensure statistical power of the results. US/PA (ultrasound/photoacoustic) images were acquired at a frame rate of 0.5 Hz with an OPO, Q-switched Nd:YAG pumped laser ($\lambda$ = 532 nm or 680-970 nm) with a 40MHz US/PA linear array transducer (LA550). The data was exported and post-processed in MATLAB (Natick, MA) based on previously described methods. [143]

### 4.1.7 Activation of NFκB signaling pathway by SNAbs

Twenty microliters of SNAbs and control formulations were seeded in 96-well plates. RAW-Blue cells were resuspended in test medium according to manufacturer's protocol and seeded at 100,000 cells/180 μL in each well. The plates were cultured in 37 ℃ for 20 hours in incubator and then 50 μL of the medium from each well was transferred to a new plate for further quantification of the secreted embryonic alkaline phosphatase (SEAP) inducible by NFκB and AP-1 transcription factors from the activated RAW-Blue cells with QUANTI-Blue detection reagents. After 0.5-6 hours of incubation in 37 ℃, the assay plates were read with a SynergyHT BioTek Plate-reader at 625 nm for absorbance.

### 4.1.8 Quantification of ADCC/ADCP of MDSCs triggered by SNAbs

RAW 264.7 macrophages primed with 25 ng/mL of IFNγ overnight at 37 ℃ were used as effector cells and plated in a flat bottom 96 well plate at certain densities between 1 to $5\times10^5$ per well to achieve the desired effector and target ratio. In certain assays, to quantify phagocytosis, the RAW 264.7 macrophages were stained with CellTrace reagents (Thermo Fisher Scientific) before seeding. MDSCs isolated from the spleen of 4T1 tumor-bearing mice were labeled with a different color of CellTrace Reagents (Thermo Fisher Scientific) and incubated with MDSC-SNAbs (i.e., G3-AuNP-cp33), control particles (e.g., AuNP-cp33, SA-AuNP-SA), antibodies (e.g. anti-Gr1 antibody), or buffers respectively for 20 mins at 37 ℃. Following that, the mixture of MDSCs and treatment formulations were dispensed at the required density per well ($0.5\text{-}2\times10^4$/well). The co-culture system was incubated at 37 ℃ for 4 or 24 hrs. Cells were harvested and

stained with viability dyes (e.g. propidium iodide, Zombie UV fixable dye or Annexin V) and then analyzed by flow cytometry.

### 4.1.9 Splenocyte killing of MDSCs triggered by MDSC-SNAbs

RBC-lysed splenocyte suspension was seeded into 96 well plates at $1\times10^6$ cells/well in 200 μL of RPMI 1640 complete medium. MDSC-SNAbs (i.e.,G3-AuNP-cp33), control particles (e.g., AuNP-cp33, SA-AuNP-SA), antibodies (e.g. anti-Gr1 antibody, isotype rat IgG2b,κ), or buffers in 50 μL sterile PBS was added into the corresponding wells respectively. After 20 hrs of incubation at 37 ℃, cells were harvested for flow cytometry analysis using BD LSRFortessa. Viability of cells was evaluated with Zombie UV fixable kit, 7AAD or PI. Antibodies used for cell marker staining includes anti-F4/80-FITC, anti-CD11c-PE, anti-B220-FITC, anti-CD8-FITC, anti-CD4-PE, anti-CD3-PE-Cy7, anti-CD11b-PE-Cy7, anti-Ly6G-PerCP-Cy5.5, anti-Ly6C-APC-Cy7, anti-CD49b-APC, anti-FoxP3-APC and anti-CD25-APC-Cy7.

### 4.1.10 Molecular dynamic (MD) simulation of G3 and G3* peptide interaction with human S100A8/A9 heterodimer

Zijian Zhang and Katie Kuo performed the computational simulation in Dr. Gumbart's group in the school of physics of Georgia Institute of Technology. One S100A8/A9 protein (PDB ID code 1XK4[144]) was placed in a TIP3P water box of dimensions 120×120 ×140 $Å^3$.[145] Sixteen copies of the biotinylated G3 peptide were distributed in the unit cell such that they were at least 10 Å from S100A8/A9. $Na^+$ and $Cl^-$ ions were added to neutralize the system at a concentration of 150 mM, giving a final system size of ~200,000 atoms. Five independent systems were constructed, each with a different

arrangement and orientation of the G3 peptides. Five copies of these systems were also constructed with the G3* peptides replacing G3 peptides. All systems were constructed using Visual Molecular Dynamics (VMD).[146]

The CHARMM36m force field was used for proteins in all simulations;[147] biotin parameters were obtained from CGenFF[148] and used previously.[149] Temperature (310 K = 37 °C) and pressure (1 atm) were kept constant by using Langevin dynamics (damping constant ɣ = 1.0 ps-1) and an isotropic Langevin piston barostat, respectively.[150] The time step was set to 2 fs. Bonded interactions and short-range (12 Å cutoff) nonbonded interactions were calculated at every time step. Long-range interactions were treated with the particle-mesh Ewald (PME) method[151] and were updated every other time step. A total of 10 equilibrium simulations, five for G3 and five for G3*, were run with NAMD[152] for 25 ns each.

We selected 200 frames at equal intervals from the last 20 ns of each equilibrium simulation. Thus, a total of 1000 (200×5) frames were used to calculate the contact probability for each type of peptide (G3 or G3*). A contact was defined as a distance of 3.5 Å or less between heavy atoms. Finally, the number of contacts was divided by 16000 (16 peptides ×200 frames ×5 simulations) to obtain the contact probability.

### 4.1.11 Statistical Analysis

Student's t-test was used to perform statistical analysis between two groups. When comparing more than two groups, normalization tests were performed first to test the distribution of data in each group. One-way analysis of variance (ANOVA) with Tukey post hoc test was used for data with normal distribution and non-parametric methods with

Dunn's post hoc test was used for data that was not in normal distribution. When P value is < 0.05, the difference between groups was considered significant (**** $p<0.0001$, *** $p<0.0002$, ** $p<0.0021$, * $p<0.0332$). *In vitro* experiments were conducted a minimum of two iterations (n=3 or 6 for each sample) to ensure reproducibility.

## 4.2 Results

### 4.2.1 Free peptide binding on isolated MDSCs

In an experiment with live MDSCs (Figure 15), G3 peptides were shown to have much higher binding on both granulocytic and monocytic MDSCs than G3* peptide, a scrambled peptide of G3. Comparably, monocytic MDSCs have higher mean fluorescence intensity (MFI) than granulocytic MDSCs do, indicating a higher expression level of S100A8/A9 proteins on the monocytic MDSCs. In another experiment where we used fixed and permeabilized MDSCs, G3* had much higher binding on a mixture of granulocytic and monocytic MDSCs than G3, indicating there could be some other proteins in the cytoplasma of MDSCs that binds G3* (Figure 14). The above results implied that G3* could be a potential targeting ligand for MDSCs, too. On the other hand, irrelevant-cp33 also binds to MDSCs as well due to the hydrophobic interaction of the tryptophan (W) in the peptides and cell membrane, while all other peptides, cp33, AHNP (a peptide targeting Her2 protein on human breast cancer cells), scrambled AHNP (scAHNP), don't bind to fixed MDSCs at all.

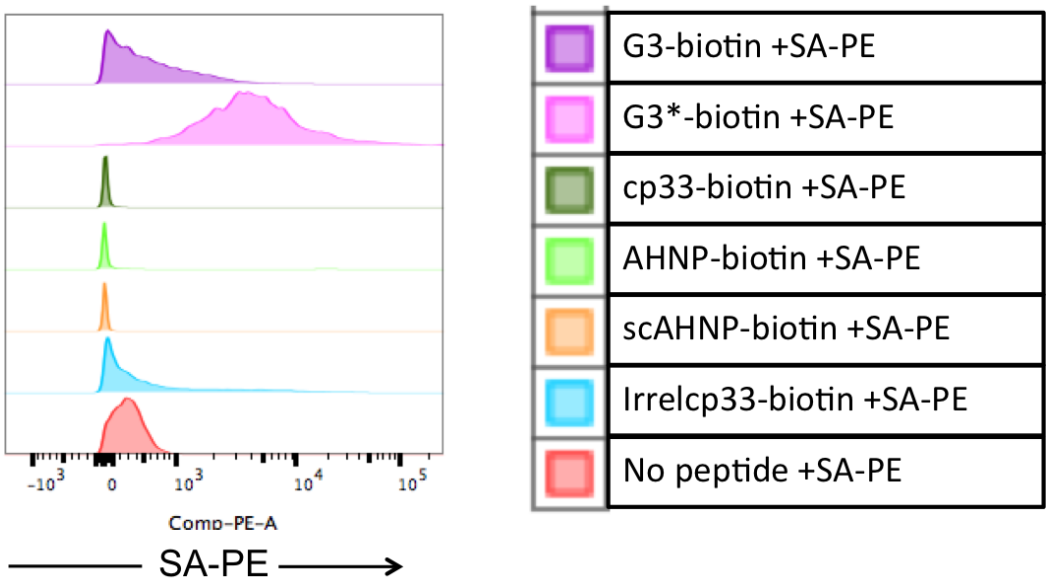


Figure 14. The binding of free peptides on fixed and permeabilized MDSCs. Biotinylated peptides were incubated with fixed and permeabilized MDSCs isolated from the spleen of 4T1-tumor bearing mice after endogenous biotin quenching. Cells were than stained with SA-PE and analyzed on a flow cytometer (n=3).

### 4.2.2 Cp33 binding on RAW 264.7 macrophages

RAW 264.7 is a mouse macrophage cell line that expresses Fc gamma receptors. Cp33 mimics the Fc region of a human IgG1 that binds to mouse Fc gamma receptors on monocytes. In a free peptide-binding experiments (Figure 15), we saw dose-dependent binding of cp33 on Fc gamma receptors, i.e., RAW 264.7 cells that were incubated with higher concentration of cp33 had higher fluorescent intensity than those with lower concentration (100 μM>20 μM>2 μM). This shows the capacity of cp33 to bind on macrophages.

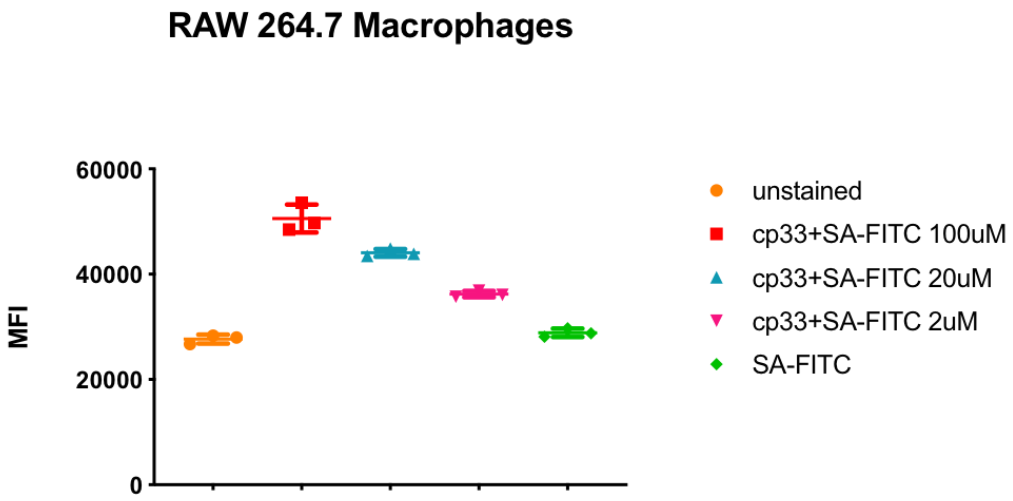


Figure 15. Free cp33-biotin binds on RAW 264.7 mouse macrophages. Cells were incubated with different concentrations of free cp33-biotin. Following the removal of unbound peptides, the peptide-bound cells were labeled with SA-FITC conjugates and analyzed with flow cytometry.

### 4.2.3 Free peptide binding on splenocytes

As with single-cell peptide binding experiments, we tested the binding capability of different peptides on splenocytes. This allows us to assess the specificity of binding of the peptides of interest. As shown in Figure 16 and 17, G3 and G3* have equivalent binding capability on granulocytic while G3 peptide binds better to monocytic MDSCs than G3*.

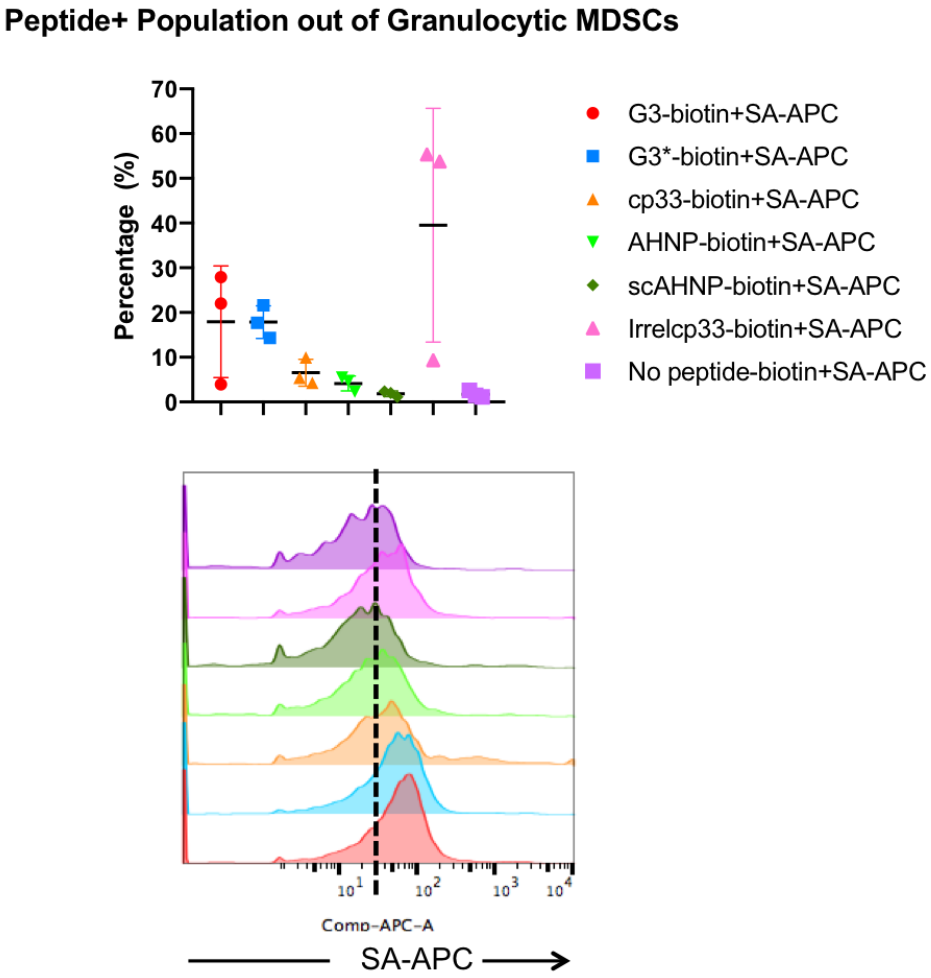


Figure 16. The binding of free peptides on granulocytic MDSCs (G-MDSCs) in a mixed splenocyte suspension. A mixture of splenocytes from 4T1-tumor bearing mice was incubated with different peptide solutions after endogenous biotin quenching. Following the removal of unbound peptides, the cells were stained with fluorescent antibodies against a panel of surface markers and fluorescent streptavidin. Samples were analyzed on a flow cytometer. Top: the percentage of SA-APC$^{+}$ G-MDSCs, i.e., peptide-bound G-MDSCs. Bottom: The representative histogram of the fluorescence of G-MDSCs incubated with the peptides or control solution. The top and the bottom graphs use the same color code for each type of treatment.

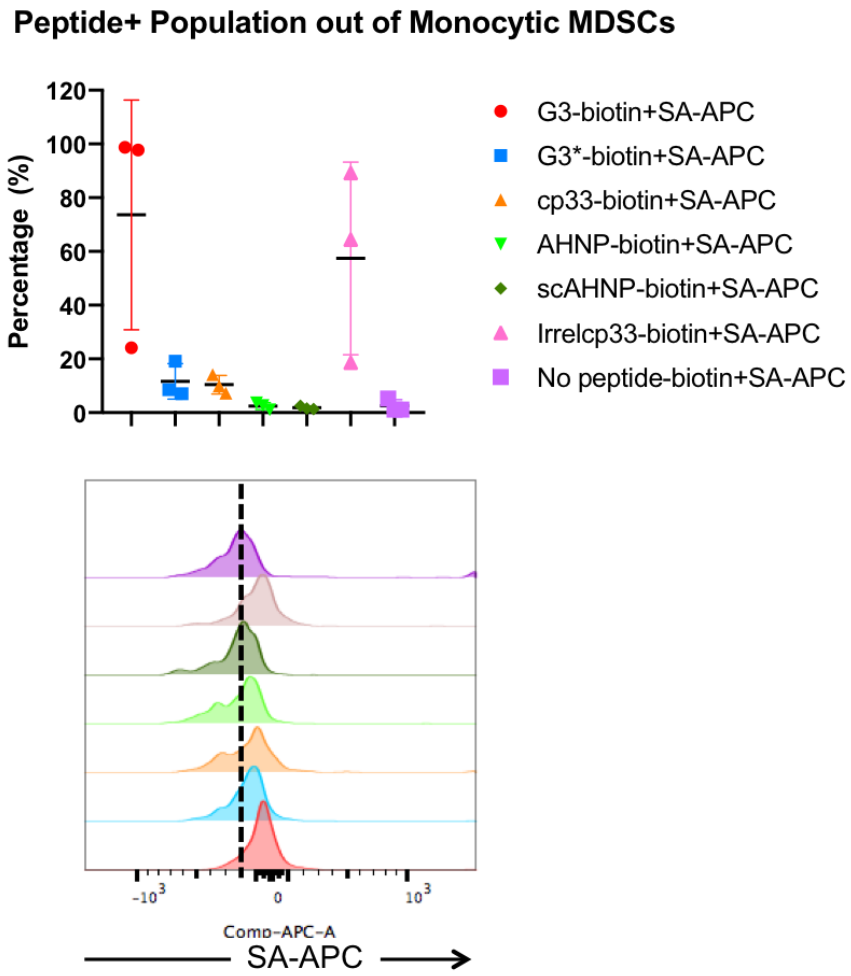


Figure 17. The binding of free peptides on monocytic MDSCs in a mixed splenocyte suspension. A mixture of splenocytes from 4T1-tumor bearing mice was incubated with different peptide solutions after endogenous biotin quenching. Following the removal of unbound peptides, the cells were stained with fluorescent antibodies against a panel of surface markers and fluorescent streptavidin. Samples were analyzed on a flow cytometer. Top: the percentage of SA-APC$^+$ M-MDSCs, i.e., peptide-bound M-MDSCs. Bottom: The representative histogram of the fluorescence of M-MDSCs incubated with the peptides or control solution. The top and the bottom graphs use the same color code for each type of treatment.

As shown in the graphs (Figure 16-17), cp33 also binds to granulocytic and monocytic MDSCs to some extent, illustrating the existence of Fc receptors on the MDSCs. On the other hand, cp33 binds F4/80$^+$ macrophages better than other peptides except Irrelcp33

and AHNP-biotin, showing its selectivity towards Fc receptor-expressing immune effector cells (Figure 18). Surprisingly, AHNP-biotin also binds to macrophages, indicating that there are some potential interaction between the AHNP-peptide and the surface proteins (e.g.,epidermal growth factor receptors) on macrophages. We also tested the MDSC-binding capability of IrrelG3, a peptide used as a negative control for G3 peptide in Hong Qin's paper. However, in our assays, the IrrelG3 also binds to granulocytic MDSCs similarly as G3 peptides, despite less binding to monocytic MDSCs (Figure 19).

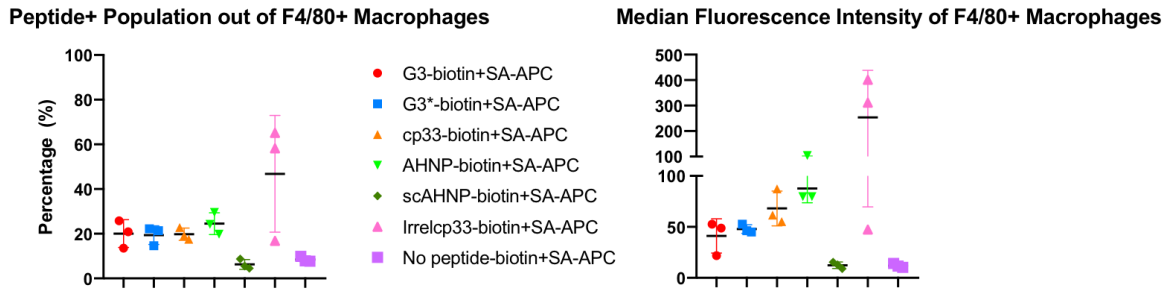


Figure 18. The binding of free peptides on F4/80$^{+}$ macrophages in a mixed splenocyte suspension. A mixture of splenocytes from 4T1-tumor bearing mice was incubated with different peptide solutions after endogenous biotin quenching. Following the removal of unbound peptides, the cells were stained with fluorescent antibodies against a panel of surface markers and fluorescent streptavidins. Samples were analyzed on a flow cytometer. Left: the percentage of peptide-bound macrophages. Right: The median fluorescence intensity of macrophages incubated with the peptides or control solution.

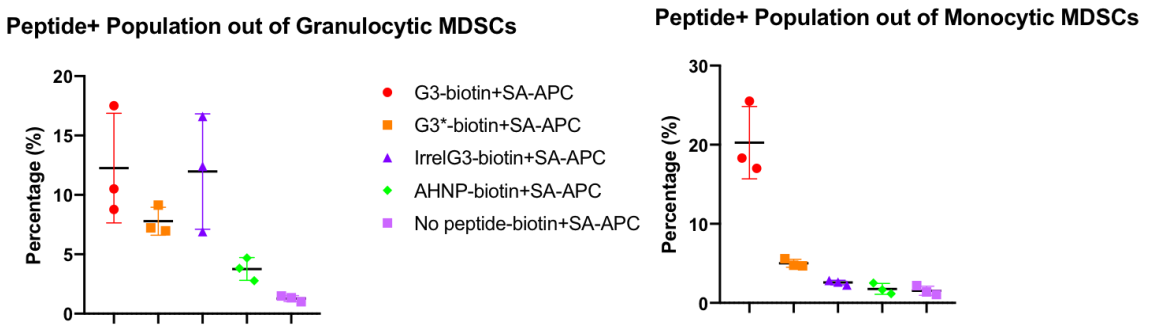


Figure 19. IrrelG3 peptide bound to MDSCs in a mixed splenocyte suspension. A mixture of splenocytes from 4T1-tumor bearing mice was incubated with different peptide solutions after endogenous biotin quenching. Following the removal of unbound peptides, the cells were stained with fluorescent antibodies against a panel of surface markers and fluorescent streptavidin. Samples were analyzed on a flow cytometer. Left: the percentage of peptide-bound G-MDSCs. Right: the percentage of peptide-bound M-MDSCs.

For other cell types, G3 and G3* seem to bind to $CD11c^+$ dendritic cells to some extent (Figure 20). This is expected given that dendritic cells express a good amount of S100 proteins on the surface.[121] NK cells were reported to express the receptor of advanced glycation end product (RAGE) for S100A8/A9 proteins.[153] The binding data shows that G3 binds much more than other peptides to $CD3^-CD49b^+$ NK cells, which reflected the presence of S100A8/A9 protein on the cells. None of the peptides except Irrelcp33 bound to $B220^+$ B cells (Figure 20). G3 and AHNP peptides bind significantly more than other peptides to $CD3^+$ T cells, especially $CD3^+CD8^+$ T cells, indicating some potential interaction between the peptides and the cellular proteins (Figure 21). Unfortunately, Irrelcp33 binds to every cell types strongly, implying that it is not a good negative control peptide for the experiments. Based on the results, scAHNP peptide does not have binding affinity towards any of the major cell types in splenocytes and was selected as the universal negative control peptide for later experiments.

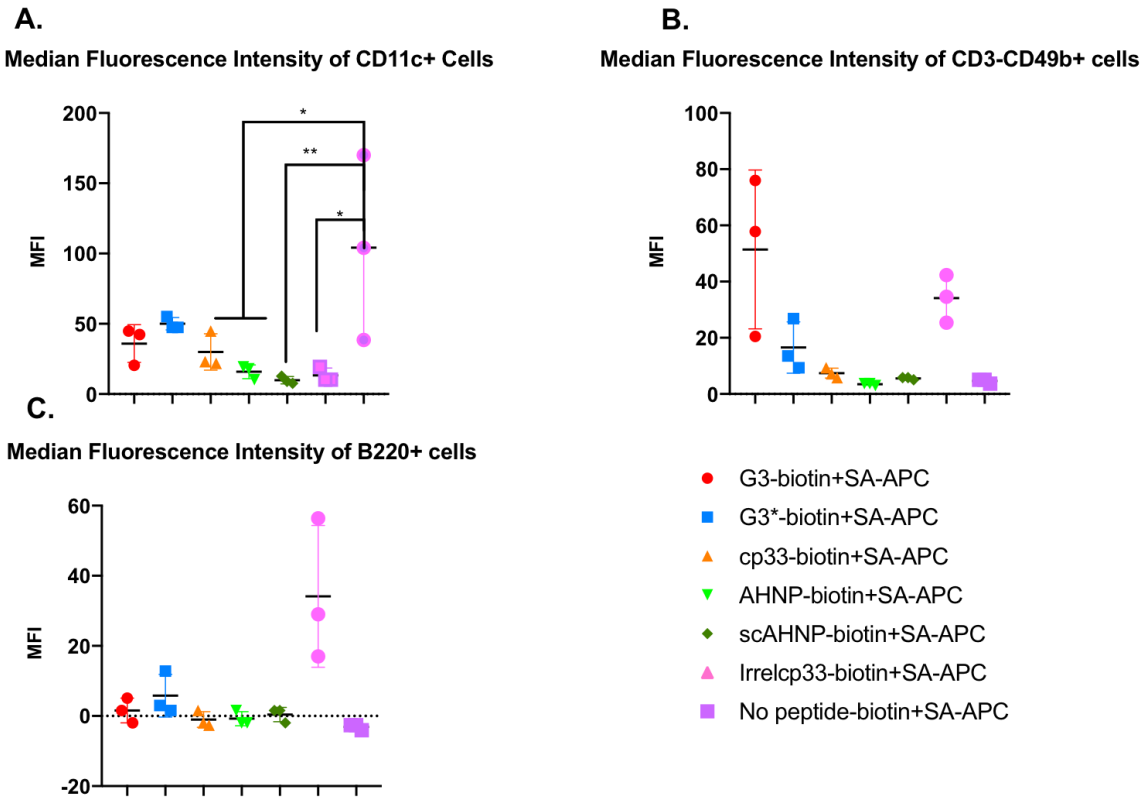


Figure 20. The binding of free peptides on dendritic cells, natural killer cells and B cells in a mixed splenocyte suspension. A mixture of splenocytes from 4T1-tumor bearing mice was incubated with different peptide solutions after endogenous biotin quenching. Following the removal of unbound peptides, the cells were stained with fluorescent antibodies against a panel of surface markers and fluorescent streptavidins. Samples were analyzed on a flow cytometer. Median fluorescence intensities of DCs (A), NK cells (B), B cells (C) after incubation with peptide or control solution are shown on the graphs.

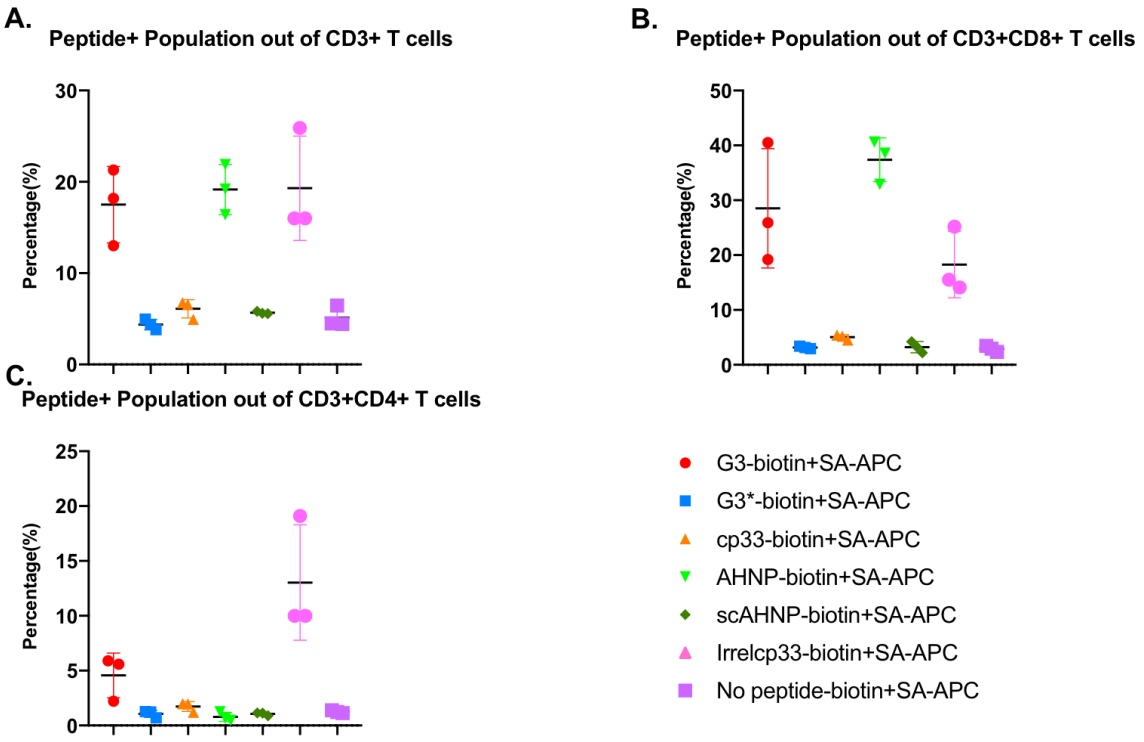


Figure 21. The binding of free peptides on T cells in a mixed splenocyte suspension. A mixture of splenocytes from 4T1-tumor bearing mice was incubated with different peptide solutions after endogenous biotin quenching. Following the removal of unbound peptides, the cells were stained with fluorescent antibodies against a panel of surface markers and fluorescent streptavidins. Samples were analyzed on a flow cytometer. Percentages of peptide-bound cells of $CD3^+$ T cells (A), $CD3^+$ $CD8^+$ T cells (B), $CD3^+$ $CD4^+$ T cells (C) after incubation with peptide or control solution are shown on the graphs.

### 4.2.4 Colocalization of G3 peptide with S100A9 protein on MDSCs

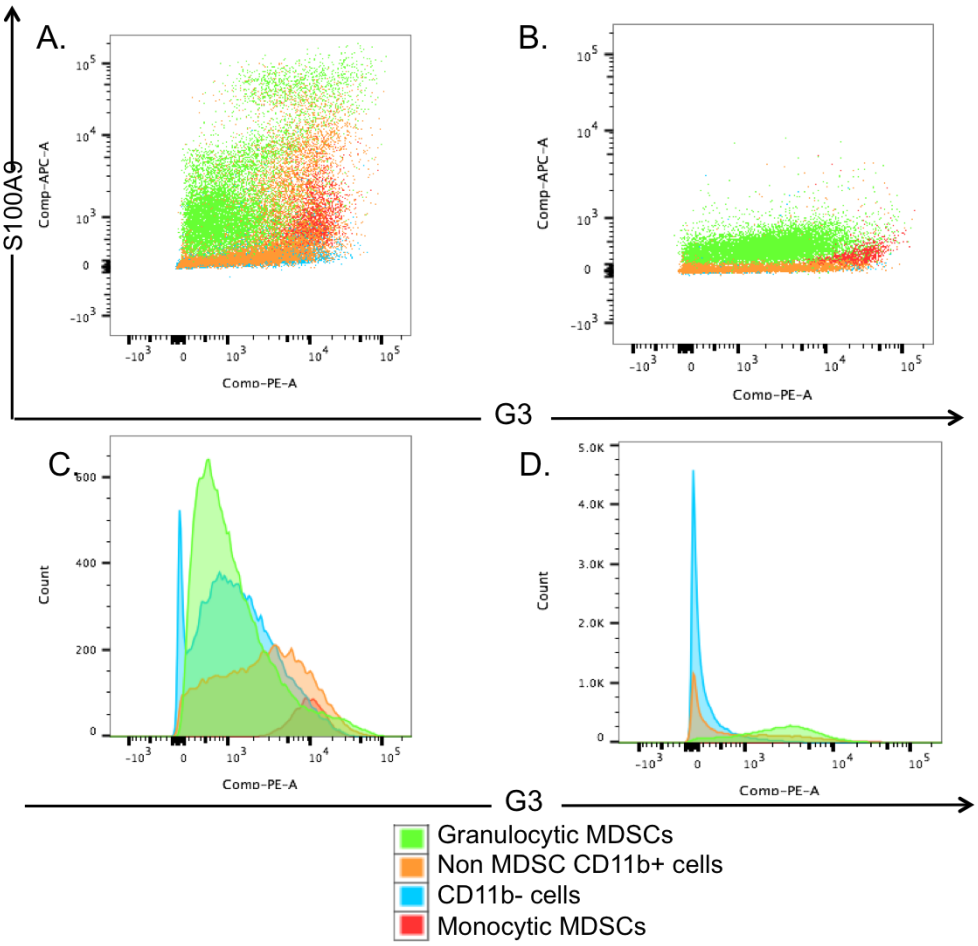


Figure 22. The colocalization of S100A9 protein and G3 on MDSCs and non-MDSC splenocytes. Representative flow cytometry graphs show the colocalization of G3 and S100A9 on MDSCs but not on non-MDSC cells (A, B). Cells were stained with G3 and anti-S100A9 either after fixation and permeabilization (A, C) or before fixation (B,D).

To test whether the target protein of G3 peptide is still S100A8/A9 protein on the MDSCs isolated from 4T1-breast cancer tumor model, which is not verified in the original study of G3,[25] we performed staining with both G3 peptides and anti-S100A9 antibody. Because of the lack of commercially available specific, fluorescent anti-mouse S100A8/A9 antibodies at the moment, we used anti-S100A9 antibodies to study the

colocalization of G3 peptides with its hypothetical target S100A8/A9 proteins in this experiment. Almost all MDSCs, both granulocytic ($CD11b^{+}Ly6G^{+}Ly6C^{low}$) and monocytic MDSCs ($CD11b^{+}Ly6G^{-}Ly6C^{high}$) express S100A9 protein.

As illustrated by this experiment, G3 peptide bound to 89.8% of G-MDSCs and 100% of M-MDSCs. Out of these $G3^{+}$ MDSCs, 99.77% of $G3^{+}$ G-MDSCs and 97.83% of $G3^{+}$ M-MDSCs were stained with anti-S100A9 antibody, showing both surface and intracellular expression of S100A9 (Table 3). On the other hand, 89.83% of $S100A9^{+}$ G-MDSCs and 100% of $S100A9^{+}$ M-MDSCs were bound with G3. These results suggested strong correlation between G3 binding and S100A9 expression on MDSCs. There were some non-MDSC $CD11b^{+}$ cells bound with G3, but only 22.83% of $G3^{+}$ cells among them showed S100A9 positive staining, and 68.7% of $S100A9^{+}$ cells were bound with G3 (Table 4). $CD11b^{-}$ cells did not have G3 binding and had only 2.99% of $S100A9^{+}$ cells in $G3^{+}$ subsets while 84.87% of the $S100A9^{+}$ subpopulation was $G3^{+}$, which tells us that on non-MDSC cells, G3 and S100A9 binding were not co-localized.

Table 3. Colocalization of S100A9 and G3 on MDSCs

| | **Granulotycis MDSCs** | **Monocytic MDSCs** |
|---|---|---|
| **G3+ percentage** | 89.83 | 100 |
| **S100A9+ percentage out** | 99.77 | 97.83 |
| **S100A9+ percentage** | 99.77 | 97.83 |
| **G3+ percentage out of** | 89.83 | 100 |

Table 4. Colocalization of S100A9 protein and G3 on non-MDSC cells

| | S100A9+ percentage of G3+ subset | G3+ percentage out of S100A9+ subset |
|---|---|---|
| **CD11b+** | 72.10 | 88.70 |
| **Non-MDSC CD11b+** | 22.83 | 68.70 |
| **CD11b-** | 2.99 | 84.87 |
| **All cells** | 59.30 | 88.93 |

### 4.2.5 Peptide-modified particles binding on target cells.

To test whether the peptide-modified particles also have the strong binding capacity on the target cells, we performed photo-acoustic imaging with isolated MDSCs and RAW 264.7 macrophages. The acoustic signals quantified the density of cells in the inclusions and photoacoustic signals showed the amount of particles on the cells. As shown in Figure 23, SNAbs bound strongly to MDSCs isolated from 4T1 breast cancer-bearing mice, much more than unmodified SA-AuNP-SA. Not surprisingly, cp33-modified nonJanus particles (AuNP-cp33) also bound very well to MDSCs, indicating the presence of Fc receptors on MDSCs (See Appendix A.2). In terms of RAW macrophages, G3 peptide-modified nonJanus particles bound better than G3* peptide-modified nonJanus nanoparticles. This observation matched the result of free peptide binding on M-MDSCs. The two types of Janus nanoparticles, G3-AuNP-cp33 and G3-AuNP-Irrelcp33, bound equally well to RAW macrophages, indicating the presence of G3 affected the binding

and eliminated the influence of cp33 or Irrelcp33 (Figure 24). All in all, peptide-modified nanoparticles bind to both target cell, MDSCs, and effector cells, macrophages. The limitation of this experiment was that the target cell population, MDSCs, had similar characteristics as effector cells, macrophages, which are both myeloid lineage cells and express S100A8/A9 proteins, leading to targeting effect of G3 to both types of cells. In addition, at the moment, we didn't find a universal negative binding ligands to prove the specificity of the binding of G3- or cp33-modified nanoparticles. As illustrated by the free peptide-binding assay, scAHNP might be a good candidate for negative controls. Future photoacoustic imaging experiment with scAHNP-modified particles is in need for investigating the specificity of the binding of G3-modified and cp33-modified particles on their respective target cell of interest.

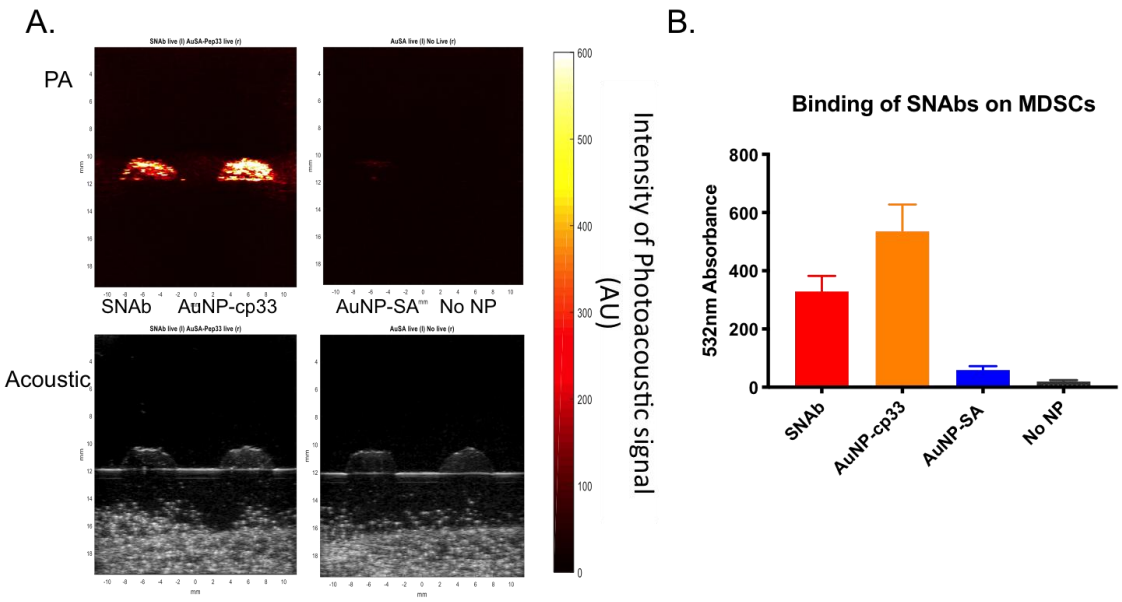


Figure 23. Peptide modified nanoparticles bound on MDSCs isolated from 4T1-tumor model. A. Representative image of photoacoustic imaging. The top images show the photoacoustic signals in the cell inclusions with SNAb-, nonJanus AuNP-cp33, SA-AuNP-SA and no NP-treated samples (from left to right). The bottom images show the acoustic signals of the cell inclusions in the same order. B. The quantified amount of SNAbs bound on each MDSC after normalizing the photoacoustic signals by the cell density calculated with acoustic signals and laser energy.

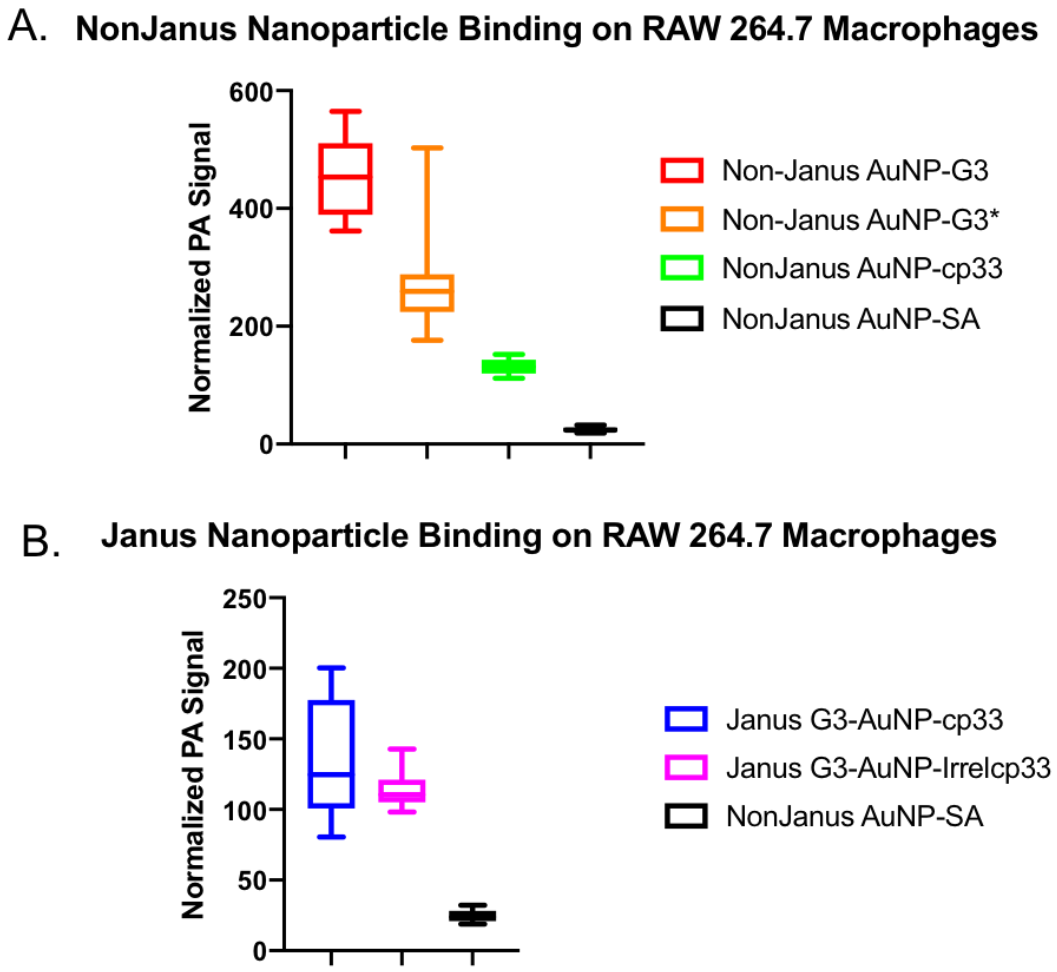


Figure 24. NonJanus and Janus peptide modified nanoparticles bound on RAW 264.7 macrophages. The nonJanus NP to cell ratio was 51,000:1 and the Janus NP to cell ratio was 22,600:1. The quantified amount of nonJanus nanoparticles (A) and Janus nanoparticles (B) including MDSC-SNAbs (G3-AuNP-cp33) bound on each macrophages were calculated by averaging the signals from the randomly-selected three cross-sections from at least two technical replicates after normalizing the photoacoustic signals by the cell density calculated with acoustic signals and laser energy.

### 4.2.6 SNAbs activated NFκB inflammatory pathway in macrophages

High avidity ligation of receptors associated with immunoreceptor tyrosine-based activation motif (ITAM), such as Fc gamma receptors, leads to activation of NFκB pathway in inflammatory cells (e.g. macrophages). [154,155] We used RAW-Blue cells, a

reporter cell line derived from RAW 264.7 macrophages, which were stably transfected with genes for a secreted embryonic alkaline phosphatase (SEAP) inducible by NFκB and AP-1 transcription factors. When these cells were treated with SNAbs for 16-24 hrs, we observed significantly higher secretion of SEAP compared to those in control-particle treated groups, indicating the capability of SNAbs for triggering the activation of NFκB pathway (Figure 25). This effect potentially will lead to the up-regulation of proinflammatory cytokine (e.g. interleukin-1β, IL-6) secretion and the activation of innate immune responses.

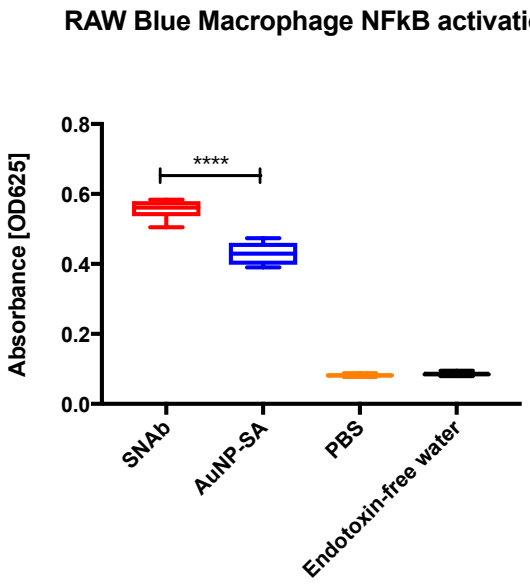


Figure 25. NFκB pathway activation in RAW-Blue macrophages by SNAbs. RAW-Blue macrophages were treated with equal amount of modified and unmodified gold nanoparticles, PBS or endotoxin-free water for 24 hrs. The supernatant was collected and the NFκB activation was measured with QuanTi Blue assay.

### 4.2.7 Toxicity of SNAbs on MDSCs in absence of effector cells

Before we test the function of SNAbs to induce killing of MDSCs with immune effector cells through antibody-dependent immune responses, we wanted to know whether SNAbs

themselves are toxic to MDSCs. MDSCs were cultured with SNAbs and control nanoparticles or buffer (PBS) for 4 hrs and 24 hrs and their viability was stained with Zombie UV fixable viability kit and Annexin V.

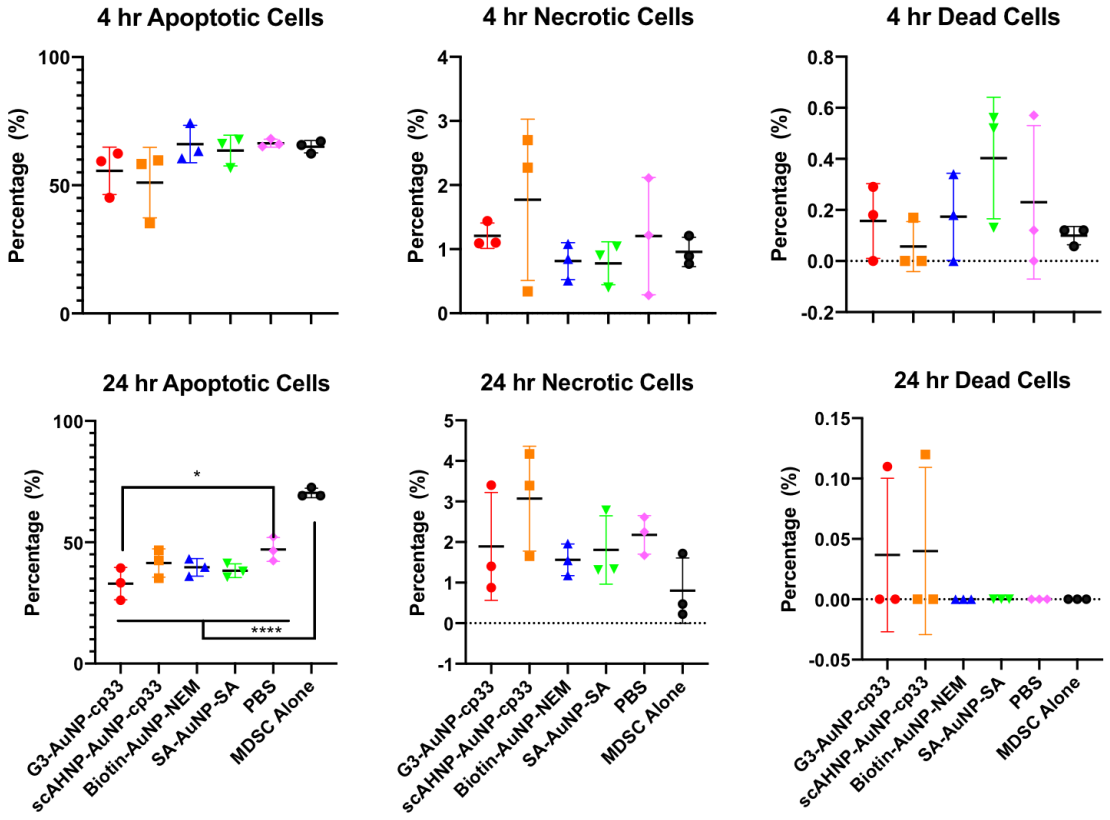


Figure 26. SNAbs by themselves have no toxicity on MDSCs. Isolated MDSCs were treated with various types of Janus nanoparticles. The viability of MDSCs was evaluated with Zombie UV fixable kit and Annexin V-APC at 4 hrs and 24 hrs. The left and right columns show the percentage of apoptotic (Zombie $UV^-$Annexin $V^+$, left), necrotic (Zombie $UV^+$Annexin $V^-$, middle) and dead (Zombie $UV^+$Annexin $V^+$, right) cells at 4 hr (top) and 24 hrs (bottom), respectively.

None of the nanoparticles induced any more apoptosis or necrosis of MDSCs compared to the untreated control groups (MDSC alone) (Figure 26). Therefore, SNAbs and other peptide-modified nanoparticles do not have toxicity themselves for MDSCs. At 24 hr

time point, nanoparticle- or PBS-treated groups had lower apoptosis rate than untreated group did, possibly because the treatments were all in PBS and diluted the medium, which may for some reason supported the survival of MDSCs.

### 4.2.8 SNAbs induced ADCC/ADCP of MDSCs by macrophage *in vitro*

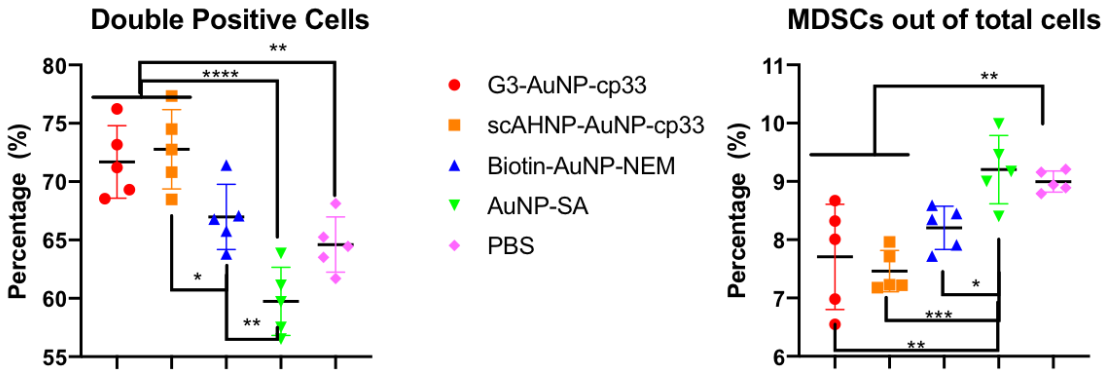


Figure 27. SNAbs induced antibody-dependent phagocytosis of MDSCs by macrophages. Macrophage and MDSCs were labeled with CellTracker Green and Celltrace Yellow respectively and co-cultured for 4 hrs at a ratio of 20:1. The percentages of double-positive (left) and single-positive (right) MDSC cells were analyzed by flow cytometry. Double-positive cells are macrophages that phagocytosed MDSCs.

To test the capability of SNAbs in triggering specific killing of MDSCs, we conducted cytotoxicity assays with MDSCs and RAW 264.7 macrophages co-culture in 96 well plates. In such assays, MDSCs and RAW 264.7 macrophages were labeled with different colors and co-cultured for a certain period of time, after which their percentage and viability were assessed. When the ratio of macrophages and MDSCs were 20:1, at both 4 hr and 24 hr time point, we observed significant increase in the percentage of double-fluorescence cells out of macrophages in the SNAb treated group, indicating the induction of phagocytosis of MDSCs by macrophages (Figure. 27). We also observed

significant reduction in the percentage of MDSCs in the SNAb treated group, resulted from the phagocytosis. However, the single-positive MDSCs were not positive for Zombie UV staining, which stains for the dead cells with permeable cell membrane, and also didn't show higher Annexin V staining, which stains the apoptotic cells. These illustrates that the MDSCs were primarily killed by phagocytosis but not specific lysis via ADCCs. Surprisingly, scAHNP-AuNP-cp33 Janus particles also elicited the same extent of increase in double-positive cell percentage and reduction in the MDSCs population, indicating the G3 is not playing a key role in this response. However, non-peptide-modified Janus particles biotin-AuNP-NEM didn't elicit such response compared to nonJanus SA-AuNP-SA or PBS, showing the importance of peptide modification in the killing of MDSCs by macrophages. In another experiment, we treated the co-culture of MDSCs and macrophages with SNAbs and also nonJanus AuNP-cp33 particles for 24 hrs and stained the cells with PI for viability of cells (Figure. 28). We observed less significant but apparently specific lysis effect induced by the nonJanus AuNP-cp33 nanoparticles, again showing the critical role of cp33 in the killing of MDSCs. The capability of inducing specific lysis by non-Janus AuNP-cp33 is probably owing to the binding of AuNP-cp33 on both MDSCs and macrophages due to presence of Fc receptors (see Appendix A.2).

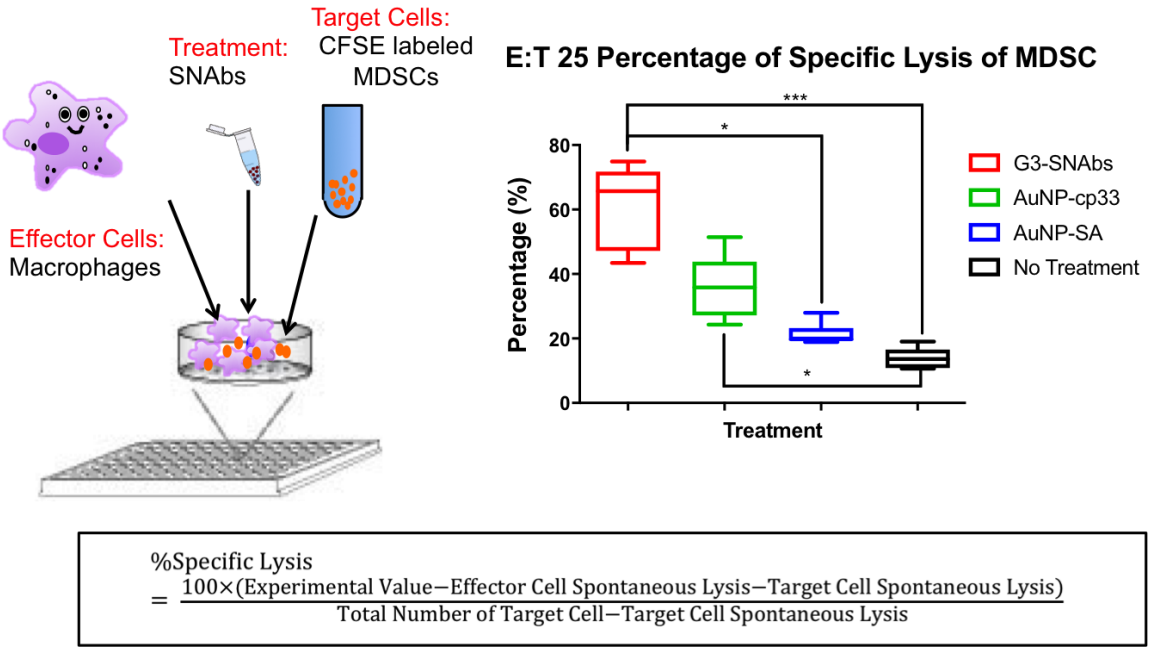


Figure 28. SNAbs triggered specific lysis of MDSCs in a macrophage-MDSC co-culture assay. The MDSCs were labeled with Celltrace CFSE and co-cultured with macrophages at 1:25 ratio for 16 hours. The specific lysis was quantified by staining cells with propidium iodide after culture and analysis with flow cytometry.

### 4.2.9 SNAbs reduced MDSCs in splenocyte suspension

Despite showing effective killing response induced by SNAbs in an effector-target co-culture system, we have yet not enough proved that SNAbs could kill target cells in a physiological relevant condition, where multiple types of immune effector cells are interacting with each other and various secretory factors are changing the immunological environment. Therefore, we devised a splenocyte mixture assay to test the capability of SNAbs to reduce MDSC populations in a complex cancer-relevant environment. We harvested spleens from 4T1-tumor bearing mice on day 16 post tumor inoculation, when massive accumulation of MDSCs already occurred in spleen due to the onset of tumor. The spleens were processed into single cell suspension, which is composed of the

following major cell types: $CD11b^+$ myeloid cells (mainly, $F4/80^+$ macrophages, $CD11c^+$ dendritic cells, $Gr1^+$ cells, including granulogycitc and monocytic MDSCs), $CD3^+$ T cells ($CD4^+$, $CD8^+$), $B220^+$ B cells, and $CD49b^+$ NK cells. In such mixture, macrophage and NK cells were present at a disease-dictated ratio to our target cells, MDSCs. The mixture of splenocytes was treated with equal amount of various types of nanoparticles or control solution (e.g. PBS) for 20-24 hrs and then the percentage of various types of cells were analyzed by flow cytometry. In such assays, we also included positive nanoparticle controls, which is Janus nanoparticles modified with G3 for targeting MDSCs and human IgG1 Fc fragments for Fc-receptor crosslinking. We used dialysed, unmodified SA-AuNP-SA as our negative particle control to exclude the effect generated by nanoparticle treatment, and PBS as our buffer control as all the nanoparticles were formulated with PBS.

First of all, we noticed that both Janus G3-AuNP-cp33 particles (G3-SNAbs) and Janus G3*-AuNP-cp33 particles (G3*-SNAbs) triggered strong killing of G-MDSCs in the splenocyte mixture compared to control particles (SA-AuNP-SA) after 24hrs, even stronger than the positive Janus particle control, Janus G3-AuNP-Fc (Figure 29). This was illustrated by the impressive reduction of the percentage of granulocytic MDSCs and the increase in the percentage of dead granulocytic MDSCs in these two groups. On the contrary, the percentage of M-MDSCs increased after treatment with G3-SNAbs and G3*-SNAbs because of the drastic reduction of G-MDSCs, but meanwhile the percentage of dead M-MDSCs also increased, indicating a killing effect induced by the two types of SNAbs on M-MDSCs as well. The results were consistent across three experiments of the same kind conducted six-months apart. The effect of SNAbs was impressive, considering

that the ratio of macrophages to MDSCs was around 1:3 and the ratio of NK cells to MDSCs was around 1:10 , much lower than that in the effector-target co-culture assay (20:1).

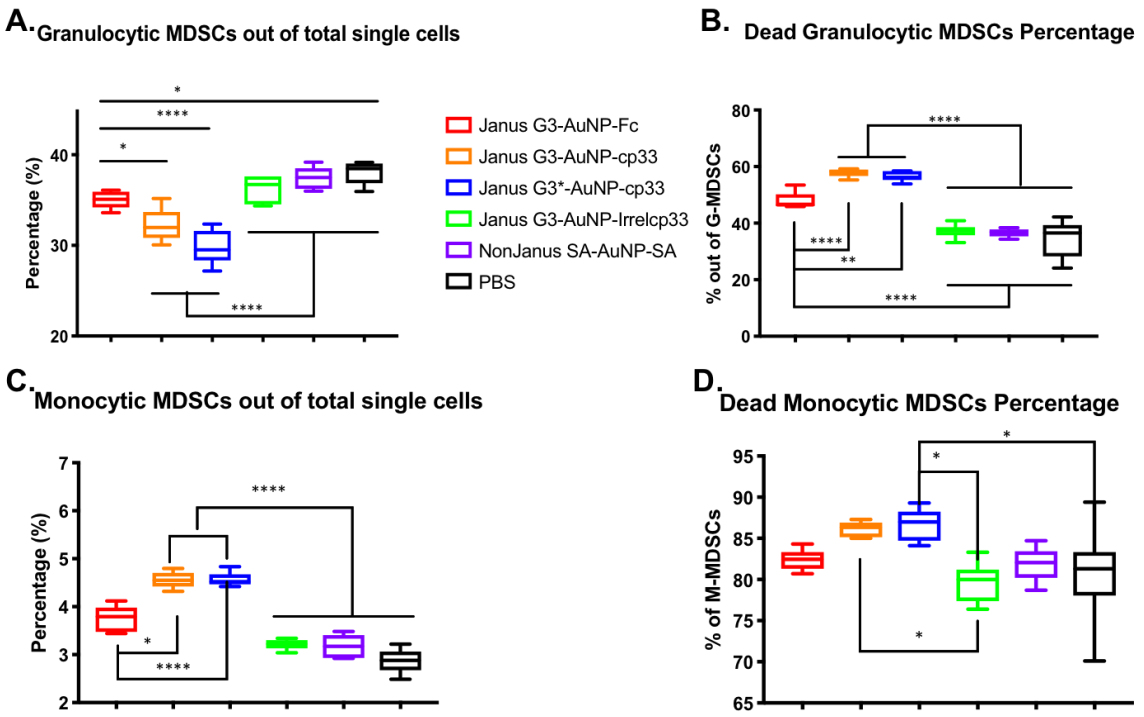


Figure 29. G3-SNAbs and G3*SNAbs triggered killing of MDSCs in a splenocyte suspension.The splenocyte suspension was treated with equal amount of SNAbs and control formulations for 24 hrs. The cells were stained with fluorescent-antibodies for cell markers and Zombie UV dye for viability. The top graphs show the percentages of total G-MDSCs (A) and the percentage of dead cells out of G-MDSCs (B). The bottom graphs show the percentages of total M-MDSCs (C) and the percentage of dead cells out of M-MDSCs (D). One-way ANOVA with Tukey test was performed to analyze the statistical difference among groups (**** $p<0.0001$, *** $p<0.0002$, ** $p<0.0021$, * $p<0.0332$).

In addition, we compared the performance of Janus nanoparticles and nonJanus nanoparticles. The Janus nanoparticles were G3-SNAbs or Janus G3-AuNP-Fc, while nonJanus nanoparticles were SA-AuNP-SA particles modified with G3-biotin and cp33-

biotin or Fc-biotin. On the nonJanus G3-AuNP-cp33, the two peptides randomly distribute all over the surface of the particles in 1:1 ratio. Interestingly, the nonJanus G3-AuNP-cp33 and G3-AuNP-Fc didn't elicit any killing effect of MDSCs, as illustrated by the same percentages of G-MDSCs and dead G-MDSCs as those of particle (SA-AuNP-SA) and buffer-control (PBS) treated groups (Figure. 30). The results were consistent across three experiments of the same kind, indicating that Janus structures are crucial to the specific killing induced by SNAbs.

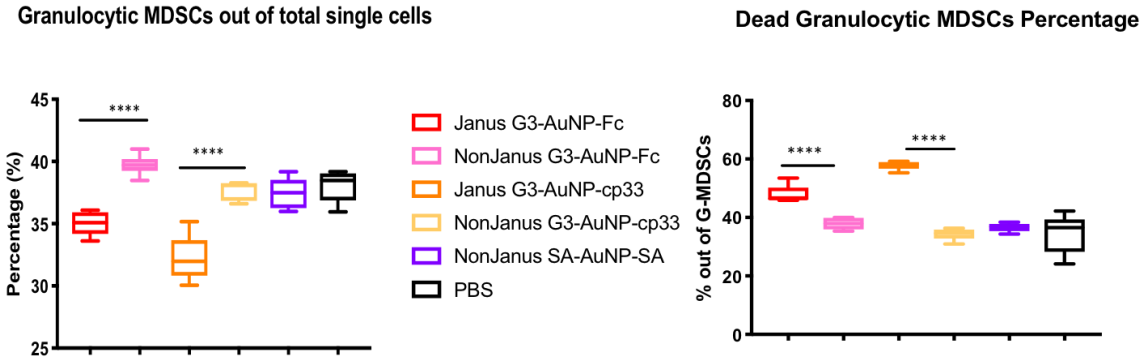


Figure 30. Janus structure is essential for eliciting killing of MDSCs by SNAbs. NonJanus double peptide (G3 and cp33)-modified AuNPs failed to elicit any response in splenocyte suspension assays. Here, we show the percentage of G-MDSCs (left) and the percentage of dead cells out of G-MDSCs (right) as representative results. One-way ANOVA with Tukey test was performed to analyze the statistical difference among groups (**** $p<0.0001$, *** $p<0.0002$, ** $p<0.0021$, * $p<0.0332$).

In terms of specificity, after the SNAb treatment, the percentages of $CD11b^{+}F4/80^{+}$ macrophages, $CD11b^{+}CD11c^{+}$ dendritic cells (DCs), $CD3^{+}$ T cells and $B220^{+}$ B cells significantly increased because of the decrease in the percentages of MDSCs (Figure 31). Surprisingly, SNAbs also reduced the number of NK cells in the mixture of splenocytes,

possibly due to the decrease in the S100A8/A9 factors secreted by MDSCs[153] and the lack of interleukin-2, which is essential growth factors for NK cells in culture.

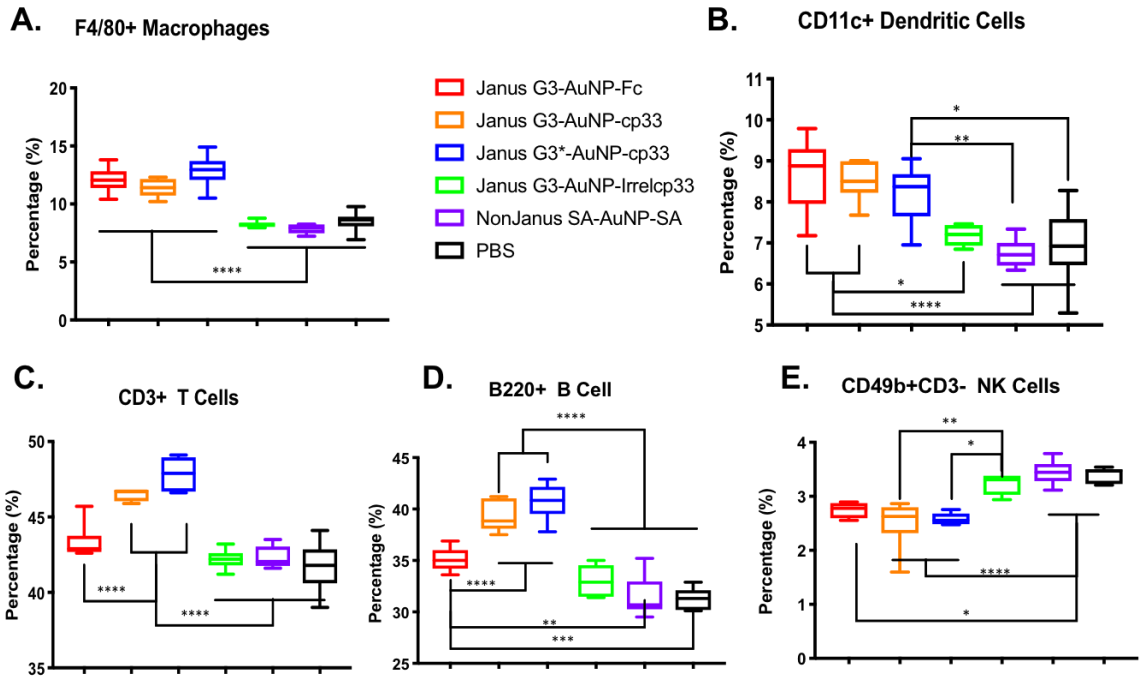


Figure 31. The specificity of SNAb-induced killing of target cells in single splenocyte suspension. SNAbs increased the percentages of F4/80$^+$ macrophages (A), CD11c$^+$ DCs (B), CD3$^+$ T cells (C), and B220$^+$ B cells (D), but decreased that of CD49b$^+$ NK cells (E). The plots are representative of three repeated assays of the same kind. One-way ANOVA with Tukey test was performed to analyze the statistical difference among groups (**** $p<0.0001$, *** $p<0.0002$, ** $p<0.0021$, * $p<0.0332$).

We also compared the efficacy of SNAbs with the most commonly used MDSC-targeting monoclonal antibody, anti-Gr1 antibodies, clone RB6-8C5, which were frequently used in the depletion of MDSCs in murine tumor models.[115,102] We tested two concentrations of the anti-Gr1 antibodies: the low-dose group had a concentration matched that of the gold nanoparticles; the high-dose group used one matched the theoretical concentration of each ligand modified on the SNAbs. We observed influence of the anti-Gr1 antibody

on the staining of anti-Ly6G-PerCP/Cy5.5 antibodies on G-MDSCs and M-MDSCs post treatment in the splenocytes (Figure. 32 left), so we could not directly calculate the percentage of those two types of cells in the anti-Gr1 treated groups. Instead, we examined the percentages of the parent population, the $CD11b^+$ cells. Due to the reduction in G-MDSCs, the percentage of $CD11b^+$ cells also decreased after SNAb treatment. However, neither of the anti-Gr1 treatment groups elicited any reduction in the $CD11b^+$ cells. Anti-Gr1 high-dose group did increase the percentage of dead G-MDSCs and decrease that of dead M-MDSCs, implying different mechanism of action between SNAbs and anti-Gr1 antibodies (Figure. 33) and that concentration of the antibodies matters. At the 24 hr in the splenocyte suspension assay, SNAbs were likely to have induced strong ADCP of MDSCs, while anti-Gr1 antibodies functioned primarily through ADCC, which caused more specific lysis of MDSCs. Further, by presenting ligands multivalently, SNAbs were more effective than anti-Gr1 antibodies at the same dosage (low dose). Lastly, SNAbs targeted both granulocytic and monocytic MDSCs, while anti-Gr1 antibodies worked on only granulocytic MDSCs and seemed to protect monocytic MDSCs from dying.

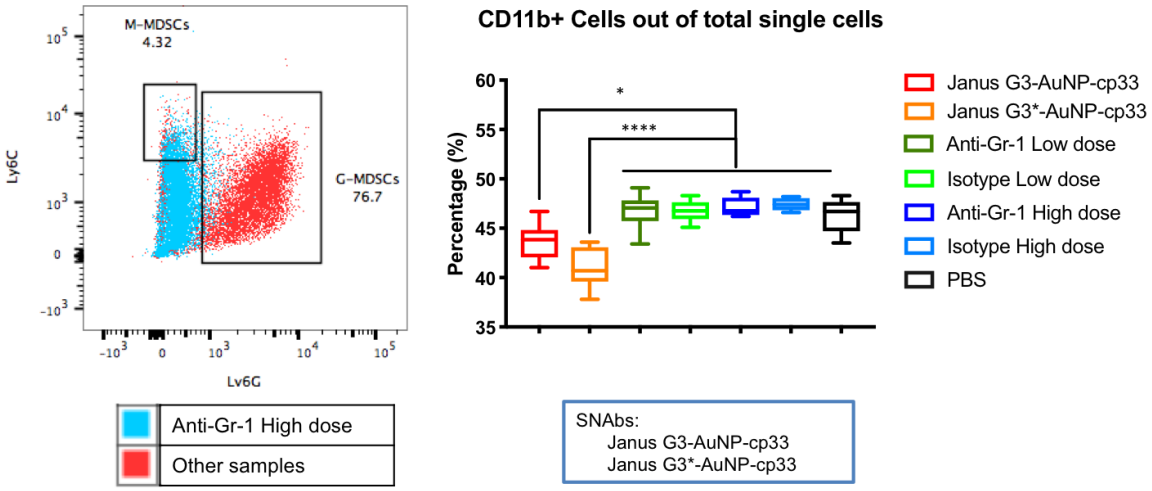


Figure 32. Anti-Gr1 monoclonal antibodies treatment didn't decrease the percentage of CD11b+ cells in the splenocyte suspension. The splenocyte suspension was treated with SNAbs and antibodies (anti-Gr1, IgG isotype) for 24 hrs. The cells were stained with anti-CD11b-PE/Cy7, anti-Ly6G-PerCP/Cy5.5, anti-Ly6C-APC/Cy7 for cell markers and Zombie UV dye for viability. The left graph is a representative flow scattering plot of anti-Gr1 high dose group (red) and other samples (blue). The right is the calculated percentage of $CD11b^+$ cells out of total cells in each group (n=6). One-way ANOVA with Tukey test was performed to analyze the statistical difference among groups (**** $p<0.0001$, *** $p<0.0002$, ** $p<0.0021$, * $p<0.0332$).

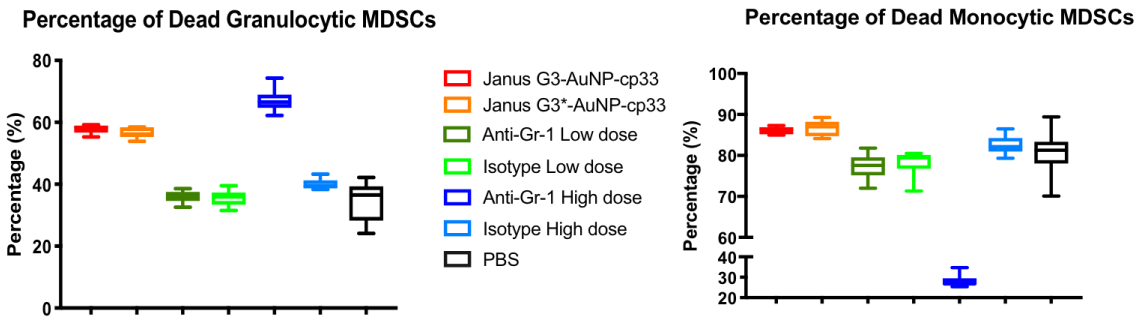


Figure 33. High concentration of anti-Gr1 antibody increased the death of G-MDSCs (left) but decreased that of M-MDSCs (right). The splenocyte suspension was treated with SNAbs and antibodies (anti-Gr1, IgG isotype) for 24 hrs. The cells were stained with anti-CD11b-PE/Cy7, anti-Ly6G-PerCP/Cy5.5, anti-Ly6C-APC/Cy7 for cell markers and Zombie UV dye for viability. The left graph is the percentage of dead G-MDSCs and the right is the percentage of dead M-MDSCs cells (n=6).

Surprisingly, in one assay, we observed inconsistency in the result of the killing of MDSCs in splenocytes (Figure 34). One observation in this assay was that IrrelG3-biotin- or scAHNP-biotin-modified Janus AuNP with cp33-SMCC, basically IrrelG3-SNAb and scAHNP-SNAbs, which should have less strong or no targeting effect for MDSCs, also decreased the percentage of G-MDSCs and increased that of M-MDSCs comparable to G3-SNAbs (Figure 35). The other observation was that G3 and Irrelcp33 modified Janus AuNPs also induced similar killing effect as that of G3-SNAbs, contradicting with the results in other assays. Such accidental failures prompted us to examine the effect of the non-peptide-modified Janus nanoparticles in killing MDSCs in both *in vitro* (see 4.2.8) and *in vivo* (see 5.2.4 and 5.2.5) and the reproducibility of the splenocyte assays.

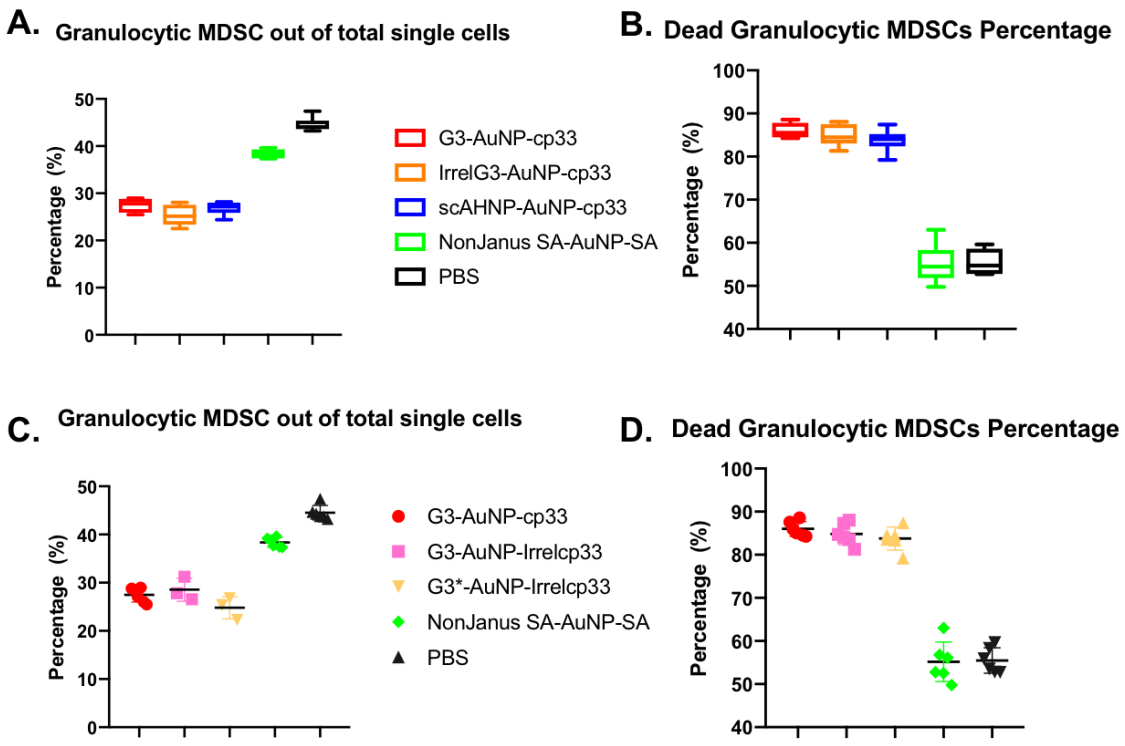


Figure 34. Some inconsistent results of the MDSC killing experiments. The splenocyte suspension from 4T1-tumor bearing mice was treated with equal amount of SNAbs and control formulations for 24 hrs. The cells were stained with fluorescent-antibodies for cell markers and Zombie UV dye for viability. The top graphs compare the percentage of G-MDSCs (A) and the percentage of dead cells out of G-MDSCs (B) after treatment with Janus nanoparticles modified with different targeting ligands. The bottom graphs compare the percentage of G-MDSCs (C) and the percentage of dead cells out of G-MDSCs (D) after treatment with Janus nanoparticles modified with different targeting ligands.

### 4.2.10 MD simulation of the interaction between G3 and G3* peptides and human S100A8/A9 heterodimer protein

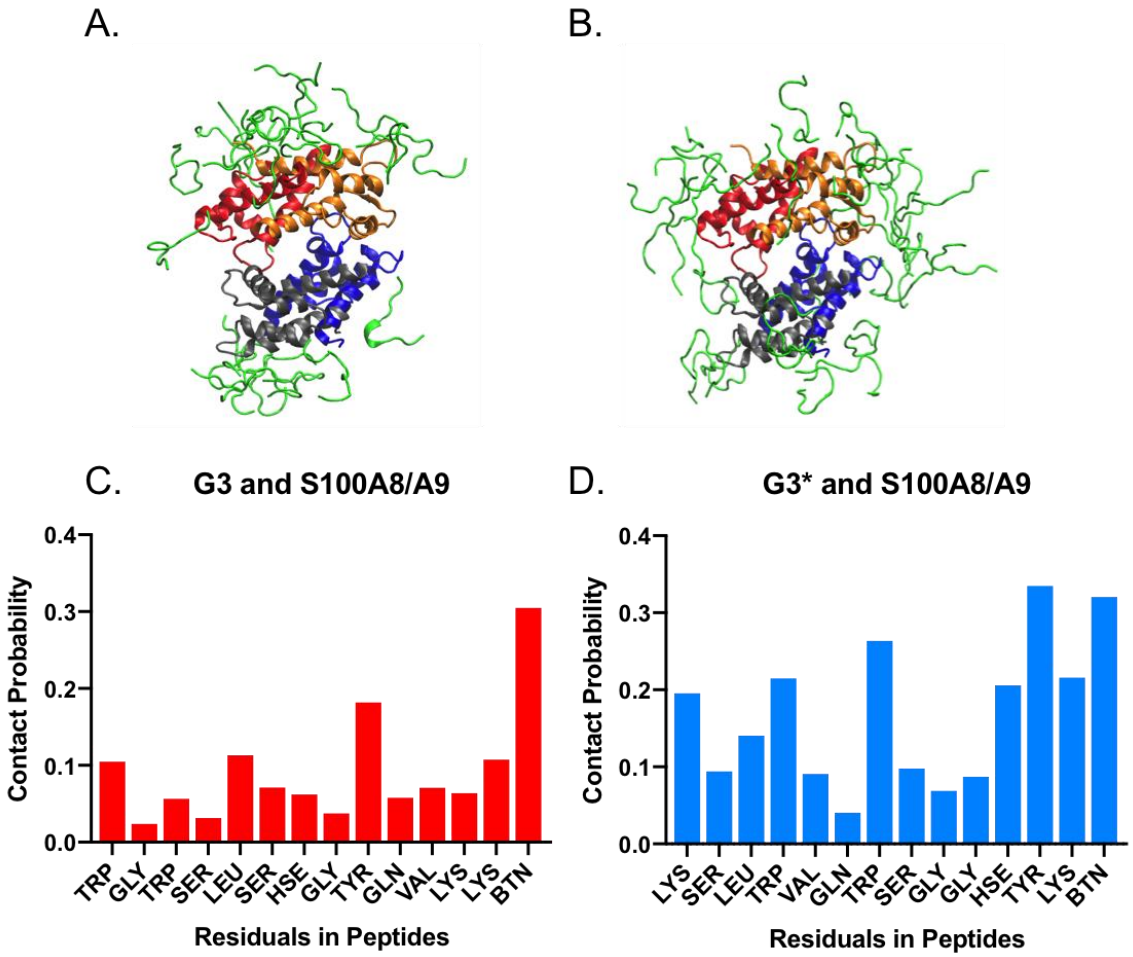


Figure 35. MD simulation of the interaction of G3 and G3* with S100A8/A9 protein. A and B are the superposition of the final frames of the five G3 simulations (A) and G3* simulations (B). C and D are the contact probability (defined as coming within 3.5 Å) determined from all five G3 simulations (C) and G3* simulations (D). The sequence along the x axis is that of each peptide.

As we noticed that both G3 and G3* peptide have strong binding affinity with S100A8/A9-expressing MDSCs in experiments, we collaborated with Dr. Gumbart's group in the school of physics in Georgia Institute of Technology to computationally

predict the binding mechanism. S100A8/A9 mouse heterodimer protein-crystal structure was not determined yet, but human heterotetramer has the similar amino acid sequence (over 50%) as the mouse counterparts and its structure was available from protein data bank. Therefore, the computational modeling was done with human S100A8/A9 heterotetramer protein (PDB ID code 1XK4[144]) and G3-biotin, G3*-biotin peptides in a modeling system to shed some light into the possible binding sites between them.

No unique binding site was observed in any of the simulations; whether this is due to the lack of such a site or the time scale of the simulation being too short is uncertain. However, G3 peptides were observed to interact with two predominant areas on the S100A8/A9 protein, as seen in Fig. 35 A. Since both the distribution of G3 peptides (top and bottom) and the structure of S100A8/A9 heterotetramer are symmetrical, it further supports the preference of G3 for these areas. Contrary to G3, the G3* peptides interact with many different regions of S100A8/A9 in multiple conformations.

At the end of the G3 simulations (Figure 35 A), there are 21 peptides (out of 80 total) within 3.5 Å of S100A8/A9 across all five simulations. In the G3* simulation, there are 30 peptides total within 3.5 Å of S100A8/A9 heterotetramer across all five simulations (Figure 35 B). This suggests that the G3* peptide has a stronger ability to bind with the S100A8/A9 protein.

In order to dissect and further quantify the interactions between the peptides and S100A8/A9, the contact probability between the peptides and S100A8/A9 was measured with a cutoff distance 3.5 Å across all the simulations. Compared to G3 and S100A8/A9, the aggregate binding probability between G3* and S100A8/A9 is notably higher. We

broke down contacts by amino acid in the peptide, revealing which are important for binding to S100A8/A9 (Fig. 35 C-D). Compared to G3 in which the two lysines are next to each other, both with relatively low contact probability, the two lysines of G3* appear separately at the N- and C-termini (not counting biotin), both with relatively high contact probability. This suggests that the location of the lysines in G3* enhances binding to S100A8/A9. In addition, the tryptophan at the N-terminal end of G3 promotes aggregation between the peptides, making it less likely for the G3 peptide to interact with the S100A8/A9 protein.

## 4.3 Discussion

Two of the essential prerequisites for an antibody to function well are the capability to recognize target cell types and the ability to crosslink Fc gamma receptors on the effector cells. We tested the binding capability of both the free peptides and the peptide-modified nanoparticles. The free G3 bound to their target cells, MDSCs, strongly. They also bound to $CD11c^+$ DCs slightly because DCs express S100A8/A9 proteins[121] and Fc receptors as well (See Appendix A.2). Interestingly, G3 also binds to $CD3^+CD8^+$ T cells and NK cells. Although we didn't find any report in previous studies, we cannot exclude the possibility that $CD3^+CD8^+$ T cells also express some S100A8/A9 proteins or have receptors that can engage with such proteins. However, G3 modified-SNAbs didn't affect the viability of $CD3^+CD8^+$ T cells. For NK cells, Kenta, et. al., reported that NK cells express the RAGE receptors on the surface and bind with S100A8/A9 proteins secreted by pancreatic cancer cells.[153] The S100A8/A9 proteins in the tumor stimulated the

proliferation of NK cells, induced interferon gamma (IFN-γ) production and enhanced the NK group 2D ligand-mediated intracellular activation pathway in NK cells. Therefore, G3 could be binding to NK cells via S100A8/A9 engaged with the RAGE receptors. We also observed reduction in the percentage of NK cells in the splenocyte suspension assay. There could be two potential reasons: one is that G3-SNAbs might bind to NK cells and induced phagocytosis of NK cells by macrophages; the other is that the reduction of MDSCs removed the source of S100A8/A9 proteins and the lack of IL-2 factors, resulted in the reduction in viability of NK cells in the culture. Cp33 was shown to bind to RAW 264.7 murine macrophage-like cell line in a concentration-dependent manner, and also preferably bound to $F4/80^{+}$ macrophages in a mixed splenocyte suspension. IFN-γ priming could induce their expression of FcγRIII and FcγRIIb on macrophages (See Appendix A.1), but didn't increase the binding of cp33 on macrophages (Figure A.1.2). Anti-CD16/CD32 antibody treatment also didn't reduce the binding of cp33 on macrophages significantly (Figure A 3), indicating that cp33 possibly favors the FcγRI, which are highly expressed on macrophages, but not so much on PMNs, and are not expressed on NK cells. This observation matches what we saw in the macrophage-MDSCs co-culture assays. In such assays, MDSCs were killed mainly by phagocytosis rather than cytolysis mediated perforin or granzyme B. Cp33 functionally mimics the property of human IgG1, which is evolutionally conservative and similar to mouse IgG1. Both human and mouse IgG1 binds to mouse FcγRI, and human IgG1 actually binds to FcγRI more strongly than to other mouse FcγRs. [55,56] FcγRIs are more efficient at mediating phagocytosis[101,115] and thus cp33-modified nanoparticles can trigger phagocytic process of target cells by macrophages. This conclusion is not only supported

by our own data but also the published results on the ADCP of prostate cancer cells induced by a chemically synthesized small molecule involving cp33.[53]

The nanoparticles we used are 30nm in size, which is challenging to visualize in microscopy. Unfortunately, the available amine groups on the streptavidin molecules were used to functionalize streptavidins on the nanoparticle surface, so they are unavailable for convenient labeling of the particles with amine-reactive dyes. Therefore, we've tried labeling the cp33 peptides with Alexa Fluor 647 dye on the N-terminus and use the fluorophore-conjugated peptides to modify the nanoparticles. When we performed confocal imaging with these particles, we saw clustering of cp33-modified Janus AuNP particles on macrophages (See Figure A 4). Besides confocal imaging, dark-field microscopy can visualize the gold nanoparticles utilizing the optical scattering property of them, but the limited resolution of dark-field microscope (inferior to confocal microscope) and difficulty of thoroughly cleaning and maintenance of cleanness of glass slides impeded the collection of convincing evidence of SNAbs binding on cells. After trials and error, we determined that photoacoustic (PA) imaging is the best way to illustrate the co-localization of nanoparticles and cells. Photoacoustic effect is the conversion of light to sound with a nanosecond pulsed laser. Gold nanoparticles are optical absorbers that absorbs the electromagnetic radiation, leading to localize thermal deposition and the production of a pressure wave, and thus can be detected by PA imaging microscope.[143] Therefore, we can use PA imaging to quantitatively assess the binding of peptide-modified gold nanoparticles on target cells. The significant increase of the PA signals in G3-SNAbs-treated MDSCs and macrophages demonstrated the capability of G3-SNAbs on the target and effector cells. The binding of cp33-modified

nanoparticles on MDSCs can be explained by the expression of Fc receptors on myeloid lineage cells and the binding of G3 or G3*-modified particles on macrophages can be explained by the interaction of S100A8/9 protein with macrophages. Although the cross-binding occurs for G3-AuNP-cp33 particles as shown in PA imaging results, we didn't notice any significant toxicity of the SNAbs on macrophages in the killing assays, indicating that the engagement of two phagocytes could not induce killing of one another.

G3* peptide, which is a scrambled G3 peptide, was originally designed as the negative control peptide for G3. However, G3* sequence was not included in the Ph.D. -12 phage display library, so it was not tested for its binding to MDSCs in the original publication.[25] Both of the flow-cytometry peptide binding assay and the PA imaging experiments proved that capability of G3* to bind to MDSCs, especially G-MDSCs. The experimental results were also supported by the computational modeling of interaction between G3* and human S100A8/A9 heterotetramers. Functionally, G3*-SNAbs was also shown to be able to elicit strong killing of MDSC in the splenocyte suspension. Therefore, we can draw a conclusion safely now that G3* is also a targeting ligand for MDSCs isolated from 4T1 breast cancer-bearing mice.

The clustering of FcγRs by IgG immune complexes will lead to the tyrosine phosphorylation of ITAMs by the Src family tyrosine kinases, which in turn activates multiple signaling pathways, including the activation of spleen tyrosine kinase (Syk), phosphatidylinositol 3-kinase (PI3-K), mitogen-activated protein (MAP) kinases and phospholipase Cγ (PLCγ). These signaling events result in actin polymerization and phagocytic cup formation, the release of various inflammatory mediators, such cytokines and reactive oxygen species (ROS), and eventually the phagocytosis of IgG-coated

particles or the cytolysis of target cells. The entire process is ATP-dependent and involves the refluxes of calcium. Unfortunately, we failed to detect the phosphorylation of Syk by western blotting of cell lysate or the increase in ROS production from RAW macrophages treated with SNAbs (Appendix B). We also could not capture the calcium reflux as it is very transient and time-dependent response.[155,158,159] We could only detected the activation of the downstream signaling events, i.e., NFκB pathway activation, in the highly sensitive reporter cell line, RAW-Blue macrophages, which is highly involved in the transcriptional modulation of inflammatory cytokines. These results prompted us to think about one of our hypotheses, which is that the multivalent presentation of cp33 ligands on the nanoparticles can crosslink the Fc receptors on the effector cells and activate immune responses. Apparently, our SNAbs were not capable enough to elicit antibody-dependent activation of the macrophages without the presence of target cells, which ensures the safety of SNAbs and avoid the unspecific cytotoxicity. In fact, previous studies on the artificial antigen-presenting-cells (aAPCs) for T cell activation have demonstrated that increasing the densities of ligands on the beads alone could not increase the ability to stimulate T cells if the beads were too small (50 nm) and the activation of T-cell receptor (TCR) nanoclusters by multi-receptor ligation is size-dependent for aAPCs (larger than 300nm is required).[160] Given Fc receptor mediated activation of innate immune cells is a similar process as TCR-mediated T cell activation, we think that the 30 nm SNAbs were not large enough to induce the immune response by themselves and thus a target cell is needed to form a large immune complex and trigger the Fc receptor-dependent signaling cascade. Further investigation on the effect of SNAbs of different sizes could provide us with better understanding of how SNAbs work.

In the effector-target cell co-culture assays, we demonstrated that SNAbs could induce phagocytosis of MDSCs by macrophages. Additionally, we developed a new cytotoxicity assay, the splenocyte suspension assay, to test the functions of SNAbs. The splenocyte suspension assay better reflects the physiological events in the following three aspects: one is that it enables us to test the functions of the MDSC-SNAbs at a disease-determined effector-target ratio (macrophage to MDSCs ratio was around 1:3 instead of 20:1 in the co-culture assays), and thus produces more clinically relevant results; a second is that it includes multiple immune effector cells types (e.g. macrophages, NK cells, DCs, T cells and B cells), which is very important for predicting *in vivo* immune responses because innate immunity interacts with adaptive immunity *in vivo* (for example, macrophages are also antigen-presenting cells and can activate cellular immune responses); another aspect is that it allows us to study whether the SNAbs affect other cell types that are either in close proximity spatially with MDSCs or in the similar lineage. Using this assay, we successfully proved that MDSC-targeting SNAbs could still efficiently reduce the MDSCs at a low effector-target ratio after the onset of tumors and this effect was specific for MDSCs, not affecting other cell types *ex vivo*. The G3-SNAbs and G3*-SNAbs did better than the positive Janus control nanoparticles, G3-AuNP-Fc, possibly because the number of Fc fragments conjugated on the nanoparticles were lower than that of cp33 on the SNAbs, leading to the weakened capability of effector activation. Besides, the nonJanus control G3-AuNP-Fc failed to trigger any response, possibly because the competitive binding between G3-biotin and Fc-biotin on the SA-AuNP-SA resulted in a nonJanus nanoparticle mostly covered with G3 ligands. However, our data still undoubtedly demonstrated that Janus structure is essential for induction of such responses

as nonJanus G3-AuNP-cp33, coated with both G3 and cp33, also didn't induce any killing of MDSCs. Moreover, Janus nanoparticles without peptide modification (Biotin-AuNP-NEM) didn't elicit a response, indicating peptide ligands are important as well. Surprisingly, we noticed similar effect in the control SNAb (scAHNP-SNAb) groups and Irrelcp33-modified Janus NP groups inconsistently. Irrelcp33 was excluded from the following experiments or analysis because of its hydrophobicity and strong binding capability on all types of cells. For the control SNAbs, we will see in the next chapter that the *in vivo* experimental results disagreed with the *ex vivo* results and showed that control SNAbs failed to work as well as G3-SNAbs in depletion of MDSCs in murine tumor models.

# CHAPTER 5 AIM 3. TO EVALUATE THE THERAPEUTIC POTENTIAL OF THE SNABS IN TUMOR MODELS

MDSCs are key players in the immunosuppressive microenvironment of tumor, which dampens the anti-cancer immune attack and facilitates the growth and metastasis of tumor. Removing MDSCs from the tumor microenvironment was proven to be an important strategy for restoration of immune-surveillance and the eradication of tumors.[117,161,162] However, as discussed in Chapter 3, there are limited options for depleting MDSCs *in vivo* and therapeutics that work *in vitro* may not necessarily function as well *in vivo*. Therefore, after we validated the capability of SNAbs to induce killing of MDSCs *ex vivo*, we moved forward to test its efficacy in murine tumor models.

Murine tumor models are designed to capture the complexities of human cancer and offer the platform to study the mechanism of therapeutics and evaluate their efficacy and potency before going into human clinical trials. Expansion of MDSCs populations was observed in a variety of murine tumor models, such as EL4 lymphoma, B16 melanoma, EG.7 thymoma and 4T1 breast cancer.[25,105] To test the SNAbs for MDSC depletion, we chose the orthotopic 4T1 breast cancer model, which represent the human triple-negative breast cancer (TNBC) in mouse and is capable of metastasizing efficiently to the sites affected in human.[27,117] The TNBC is defined by a lack of expression of the three human receptors, epidermal growth factor receptors (Her2), estrogen receptor (ER) and progesterone receptor (PR). It accounts for 10%-15% of the breast cancers and has no effective clinical therapy yet. [163,164] Therefore, using 4T1 breast-cancer model to test SNAbs could provide new rationale for TNBC treatment.

In this aim, we tested our hypothesis that SNAbs could deplete MDSCs populations *in vivo* in the orthotopic 4T1 breast cancer model. Myeloid lineage precursor cells mature into suppressive $CD11b^{+}Gr1^{+}$ MDSCs in bone marrow and then enter the peripheral blood and accumulate in the spleen and tumors, and to a lesser extent in the lymph nodes. We evaluated the efficiency of SNAbs in the depletion of MDSCs in blood, tumor, bone marrow and spleen. It is one of the advantages of nanoparticle-based artificial antibody platform that by tailoring size, shape, and surface chemistry, we can enhance the penetration and retention of them in the disease sites. MDSC-SNAbs were designed to be in the size range that they can preferentially accumulate in solid tumors, so we also analyzed the biodistribution of SNAbs after intravenous injection to validate this hypothesis. In the end, we studied whether MDSC-SNAbs could improve the survival of 4T1-tumor-bearing mice by depleting MDSCs.

## 5.1 Methods

### 5.1.1 Material

Aqua regia for dissolving tissue samples in the biodistribution study was prepared by mixing concentrated nitric acid:hydrochloride acid in 1:3 volume ratio; nitric acid was purchased from Sigma Aldrich (Cat.#.695025); hydrochloride acid was purchased from VWR International, (Cat.#.BDH3030). Collagenase D, RBC lysis buffer, and cytofix buffer were the same as described in Chapter 4. Anti-PD1 (Clone RMP1-14) and anti-CTLA-4 (Clone 9H10) were purchased from BioXCell, New Hampshire, USA. The

antibodies used in flow cytometry were the same as those described in Chapter 4, except for some new antibodies for functional markers (See Appendix Table for antibodies)

### 5.1.2 Cell lines and Animals

Murine triple-negative breast cancer cell line 4T1 were purchased from American Type Culture Collection (Manassas, VA, USA). The 4T1 cell lines were cultured in RPMI 1640 (Thermo Fisher Scientific, Waltham, MA, USA) supplemented with 10% FBS (GE Healthcare, Chicago, IL, USA) and 1% PS (Thermo Fisher Scientific) under standard cell culture condition (37 ℃, 5% $CO_2$).

Five to Six-week-old Balb/c female mice were purchased from the Jackson Lab. All mice were maintained in a pathogen-free mouse facility according to institutional guidelines. All of the animal experiments were approved by the Institutional Animal Care and Use Committee (IACUC) at Georgia Institute of Technology (Atlanta, Georgia). The experimental sample sizes ensured adequate statistical power.

### 5.1.3 Biodistribution of MDSC-SNAbs by inductively-coupled mass spectrometry (ICP-MS)

Single-cell-suspension of 4T1 cells before passage 25 was prepared in PBS (Hyclone) at a concentration of $1\times10^7$ cells/mL. Five-to-six-weeks-old Balb/c mice were inoculated with $0.5\times10^6$ 4T1 breast cancer cells orthotopically on the fourth mammary fat pad on day 0. We injected 200 μL of SNAbs ($0.80\times10^{11}$) via tail veins into Balb/c mice with around 3 mm 4T1 breast tumors on day 9 post tumor inoculation. At t=6, 24, 48 hrs, we harvested and weighed the lung, liver, spleen, kidney, tumor, and blood and dissolved

them in aqua regia for overnight at room temperature. Samples for ICP-MS analysis were prepared by boiling aqua regia-tissue solution at 200 ℃ and then diluting the sample with DI water. The debris of tissue samples was removed by going through 0.2 μm syringe filters and the concentration of Au in each sample was analyzed by ICP-MS (NexlON 300Q, Perkin-Elmer). We acknowledge Da Huo in Dr. Younan Xia's group for the acquisition of data with ICP-MS.

### 5.1.4 *In Vivo* Depletion of MDSCs by MDSC-SNAbs

Single-cell-suspension of 4T1 cells before passage 25 was prepared in PBS (Hyclone) at a concentration of $1\times10^7$ cells/mL. Five-to-six-weeks-old Balb/c mice were inoculated with $0.5\times10^6$ 4T1 breast cancer cells in 50 μL sterile PBS orthotopically into the fourth mammary fat pad of each mouse on day 0. MDSC-SNAb (i.e., G3-AuNP-cp33 or G3*-AuNP-cp33) formulation or control SNAbs (e.g., scAHNP-AuNP-cp33, Biotin-AuNP-NEM) or unmodified streptavidin functionalized gold nanoparticles (SA-AuNP-SA) formulation containing $0.75\times10^{11}$ nanoparticles were administrated intravenously through tail vein injection to mice (n=6) according to the designed injection schedule. For single treatment study, at 24 hrs after the injection, mice were euthanized and the spleens, tumors were collected. Spleens and tumors were treated with collagenase D and RBC lysis to make single cell suspensions, as described previously in Chapter 4. We also collected blood by cardiac puncture. A minimum of 100 μL of blood from each mouse was transferred to fresh FACS tubes and treated with 2 mL RBC lysis buffer at room temperature for 10 mins and then centrifuged at 700 g for 10 mins. Cell pellets were resuspended in FACS buffer and kept in 4 ℃ until use. In some experiments, we also collected the bone marrow from tibia and femur. Briefly, the skin and muscle tissue were

removed from the bones and then bone marrow was flushed with medium using a 25 gauge needle and syringe. Red blood cells in the bone marrow were lysed and cells were washed with PBS and resuspended in FACS buffer. All the cell samples from spleen, tumor and blood were stained with antibodies for MDSC (CD11b, Ly6G, Ly6C), macrophages (F4/80), dendritic cells (CD11c), T cells (CD3, CD4, CD8, Foxp3, CD25), B cells and NK cells (CD49b, CD3, B220). Tumor samples were also stained with functional or proliferation markers (Granzyme B, Perforin, CD107, CD69, PD1, LAG3, Ki67, IFNγ). Samples were fixed with BD Cytofix buffer and analyzed on BD LSRFortessa flow cytometer.

### 5.1.5 4T1 breast cancer survival study with MDSC-SNAbs

Single-cell-suspension of 4T1 cells before passage 25 was prepared in PBS (Hyclone) at a concentration of $0.2\times10^7$ cells/mL. Five-to-six-weeks-old Balb/c mice were inoculated with $0.1\times10^6$ 4T1 breast cancer cells orthotopically on the fourth mammary fat pad on day 0. MDSC-SNAbs or control particles SA-AuNP-SA ($0.75\times10^{11}$ NP/200 μL in PBS) were then given intravenously through tail vein injection on day 7, 9, 11. The size of the tumor and the weight of the mice were measured every other day. The mice were sacrificed according to the IACUC protocol when the tumor size reached 1.5 cm in any direction or any of the following was observed: significant weight loss (over > 10%), perforation of skin, or severe cachexia. Tumor volume was calculated by the following equation: $V(cm^3) = l * \frac{w^2}{2}$, where l is the length and w is width of the tumor. Median survival and Kaplan-Meier survival curves were generated, and Log rank (Mantel-Cox)

tests were performed to compare survival between various groups using GraphPad prism 7 software. *P<0.05, ** P<0.01, and *** P <0.001 were considered significant.

### 5.1.6 4T1 breast cancer survival study of the combination therapy of MDSC-SNAbs and immune-checkpoint blockade

Single-cell-suspension of 4T1 cells before passage 25 was prepared in PBS (Hyclone) at a concentration of $0.2\times10^7$ cells/mL. Five-to-six-weeks-old Balb/c mice were inoculated with $0.1\times10^6$ 4T1 breast cancer cells orthotopically on the fourth mammary fat pad on day 0. MDSC-SNAbs or control particles SA-AuNP-SA ($0.75\times10^{11}$ NP/200 μL in PBS) were then given intravenously through tail vein injection on day 7, 9, 11, 13. Anti-PD1 and anti-CTLA-4 antibodies were given 200μg/mouse, intraperitoneally on day 6, 10, 14. The size of the tumor and the weight of the mice were measured every other day. The mice were sacrificed according to the IACUC protocol when the tumor size reached 1.5 cm in any direction or any of the following was observed: significant weight loss (over > 10%), perforation of skin, or severe cachexia. Tumor volume was calculated by the following equation: $V(cm^3) = l * \frac{w^2}{2}$, where l is the length and w is width of the tumor. Median survival and Kaplan-Meier survival curves were generated, and Log rank (Mantel-Cox) tests were performed to compare survival between various groups using GraphPad prism 7 software. *P<0.05, ** P<0.01, and *** P <0.001 were considered significant.

### 5.1.7 Statistical Analysis

Student's t-test was used to perform statistical analysis between two groups. When comparing more than two groups, normalization tests were performed first to test the distribution of data in each group. One-way analysis of variance (ANOVA) with Tukey post hoc test was used for data with normal distribution and non-parametric methods with Dunn's post hoc test was used for data that was not in normal distribution. When P value is $< 0.05$, the difference between groups was considered significant (**** $p<0.0001$, *** $p<0.0002$, ** $p<0.0021$, * $p<0.0332$). *In vitro* experiments were conducted a minimum of two iterations (n=3 or 6 for each sample) to ensure reproducibility. Two-way ANOVA was performed to study the difference among groups in the tumor growth curve. Log-rank (Mantel-Cox) test was used to analyze the statistical difference among groups in the survival curve.

## 5.2 Results

### 5.2.1 MDSCs accumulated in spleen and blood during tumor progression

Our lab has previously established this 4T1 breast cancer model for vaccine studies. Before doing MDSC depletion studies with SNAbs in this model, we examined the accumulation of MDSC in the spleen and blood. Balb/c mice were orthotopically inoculated with $0.5\times10^6$ 4T1 tumor cells in the fourth mammary fat pad and after around 7 days, subcutaneous primary tumors could be seen at the site of injection. MDSCs started to accumulate in spleen, blood, tumor and bone marrow, The percentages of MDSCs could reach 5%-10% and 10%-20% in spleen and blood respectively by day 10 (Figure 36). Healthy mice of age 5-12 weeks will continue to gain weight over time, but

tumor-bearing mice have slower weight growth and scar tissue forms over the site of tumor inoculation typically between day 14-21. Without treatment, tumor dimension will reach the 1.5 cm end-point in about 20-30 days.

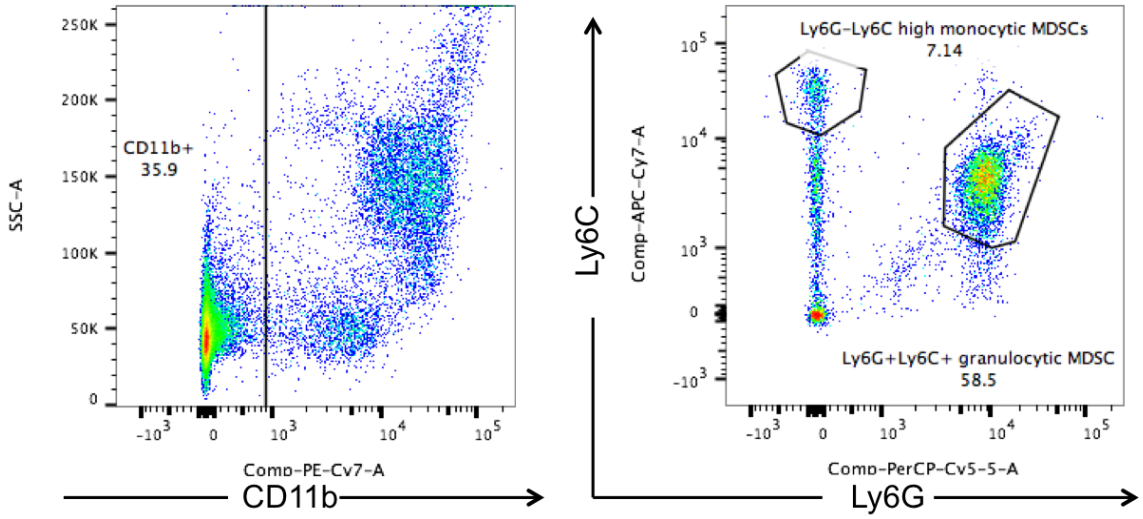


Figure 36. Gating strategy for MDSCs. The graphs are selected from the blood samples of breast cancer tumor-bearing mice. The $CD11b^+$ cells were first gated out from the single cell population. $Ly6G^+Ly6C^{low}$ granulocytic MDSCs and $Ly6G^-Ly6C^{high}$ were then gated in the $CD11b^+$ population.

### 5.2.2 The biodistribution of MDSC-SNAbs in 4T1 breast cancer tumor-bearing mice

As the element Au does not naturally exist in the body of animal, we were able to accurately quantify the amount of gold nanoparticles in the tissues collected from mice to analyze the distribution of MDSC-SNAbs (Janus G3-AuNP-cp33) after tail vein injection. Because they were introduced intravenously, blood was found to have a high concentration of the SNAbs at 6 hr time point after injection (Figure 39). The SNAbs circulated in the blood and travel to other organs over time, resulting in a gradual decrease in the blood concentration of Au over time. At t=48 hr, the concentration of

SNAbs almost returned to zero. The calculated half-life of SNAbs in blood is 26 hrs. After SNAbs left blood vessels, their first destination was liver. At t=6 hr, over 30% of the SNAbs were found to be in the liver, and they remained in the liver for the rest of the time (Figure 37). Spleen was apparently the second favorable organ for SNAbs to accumulate in. In fact, from 6 hr to 48 hr, spleen remained to be the organ with the highest SNAb concentration (ng/g of tissue). Lung and kidney hardly had any retention of SNAbs, but the SNAbs kept accumulating in the tumors. The percentage of SNAbs traveled to tumor increased from around 0.90% at 6hr time point to 3.39% at 48hr time point (Figure 38). The concentration of SNAbs in tumor was the third among all the organ types, being 4645ng/g of tissue.

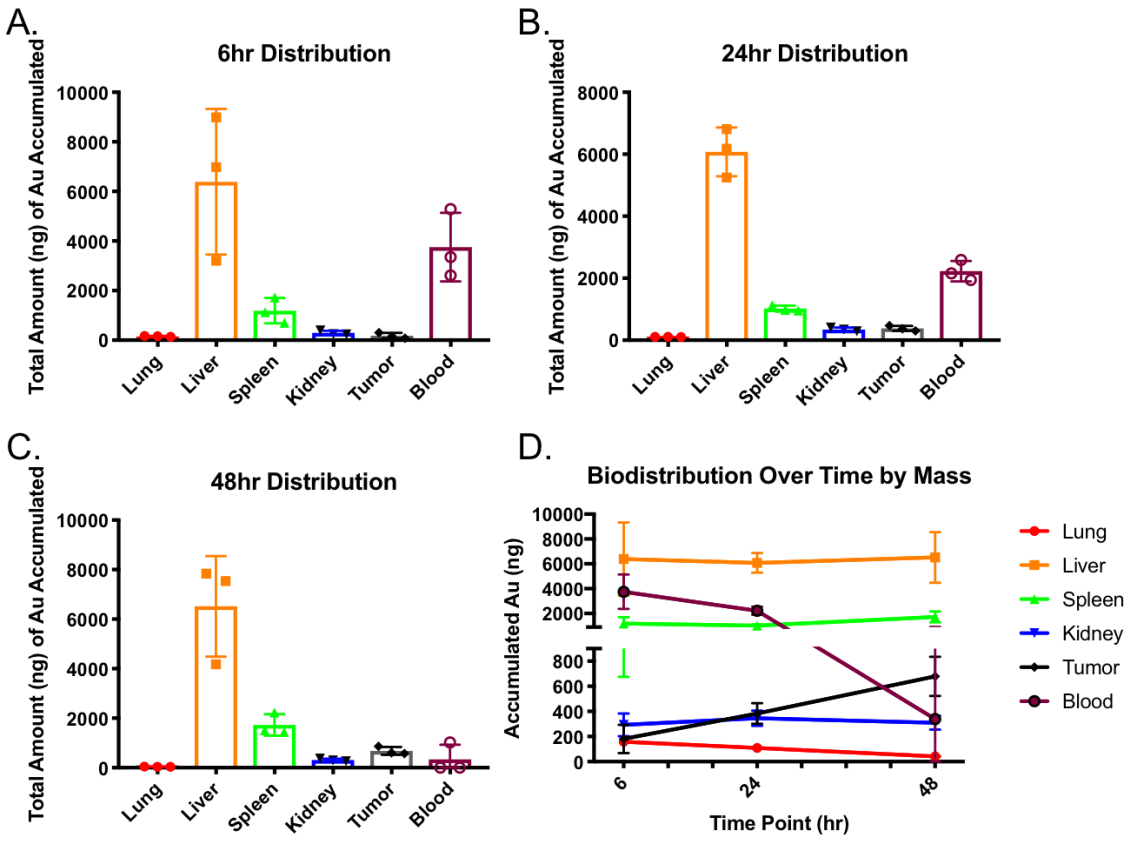


Figure 37. Biodistribution of SNAbs in 4T1-tumor bearing mice by mass of Au. SNAbs were administered by intravenous injection through tail vein. Tissue and blood samples were collected at t=6, 24, 48 hrs post injections. ICP-MS was conducted to analyze the amount of SNAbs in each sample. The graphs show the total amount of Au elements in each type of organs at different time points (A-C) (n=3) and the changes over time (D).

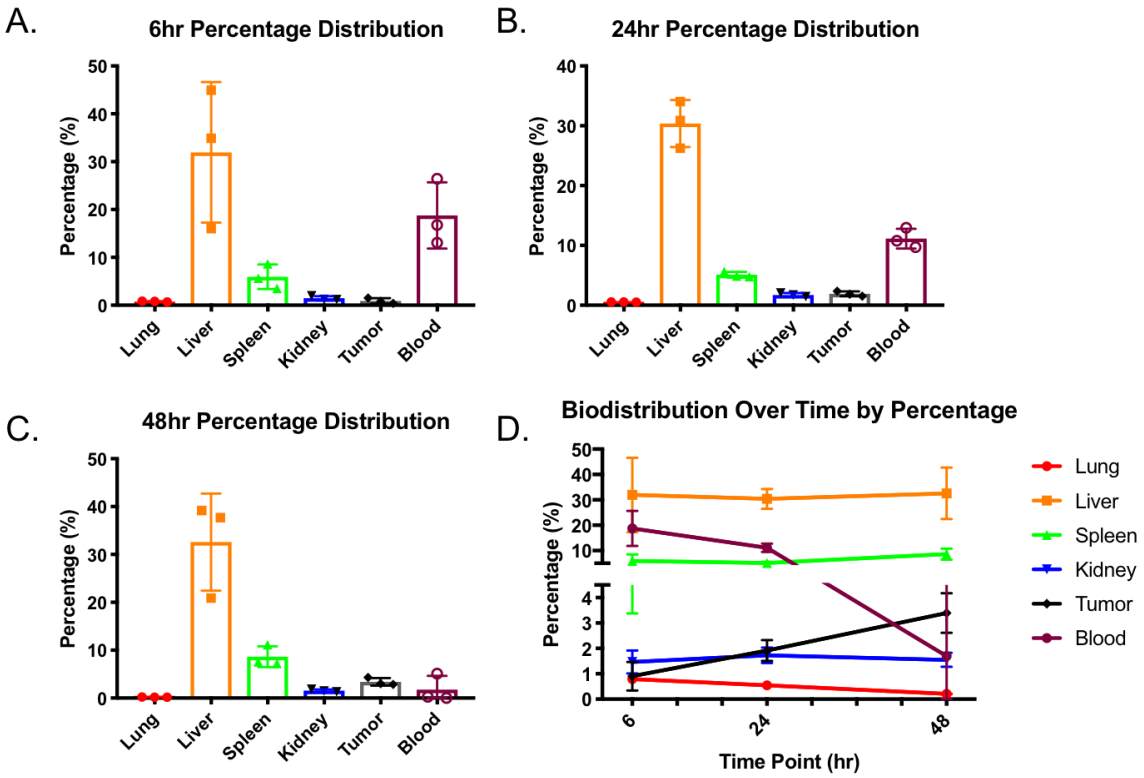


Figure 38. Biodistribution of SNAbs in tumor-bearing mice by percentage. SNAbs were administered by intravenous injection through tail vein. Tissue and blood samples were collected at t=6, 24, 48 hrs post injections. ICP-MS was conducted to analyze the amount of SNAbs in each sample. The graphs show the percentage of SNAbs distributed in each type of organs at different time points (A-C) out of total amount of SNAbs administered (n=3) and the changes over time (D).

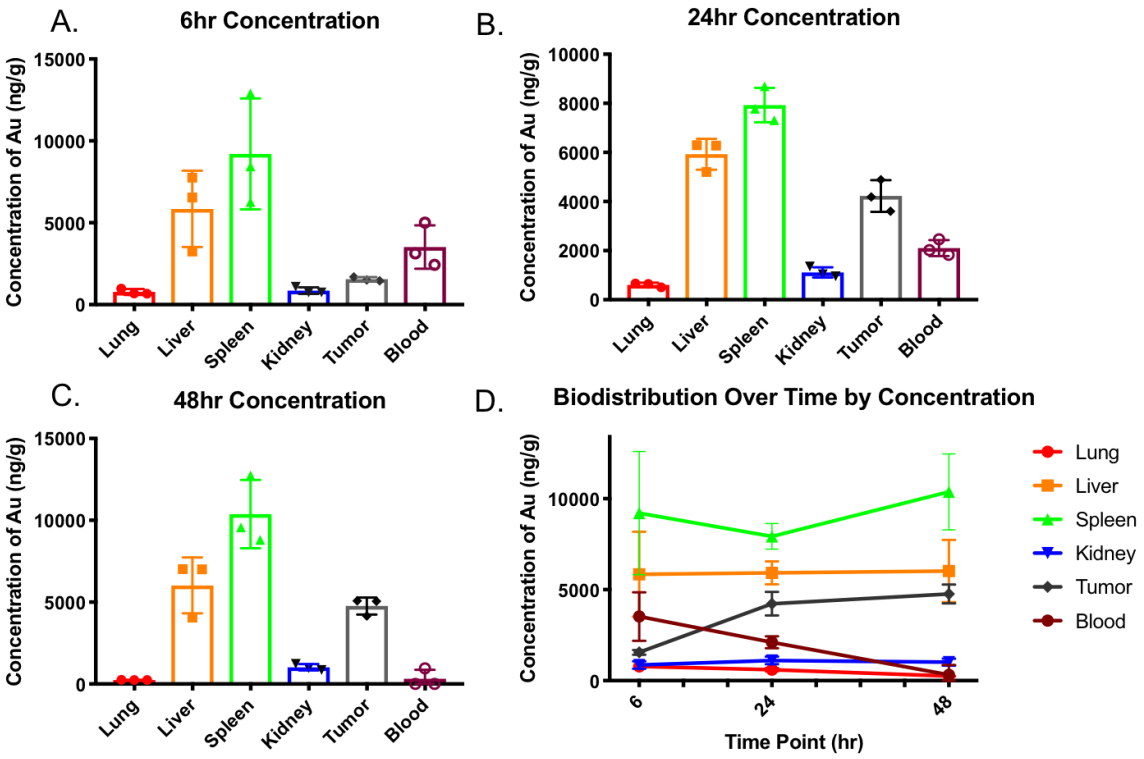


Figure 39. Biodistribution of SNAbs in tumor-bearing mice by concentration (ng of Au per g of tissue). SNAbs were administered by intravenous injection through tail vein. Tissue and blood samples were collected at t=6, 24, 48 hrs post injections. ICP-MS was conducted to analyze the amount of SNAbs in each sample. The graphs show the concentration of SNAbs distributed in each type of organs at different time points (A-C) as nanograms of Au per gram of tissue collected (n=3) and the changes over time (D).

### 5.2.3 MDSC depletion with single treatment of MDSC-SNAbs

In a preliminary study, we administered $0.75\times10^{11}$ of SNAbs or control particles (SA-AuNP-SA) on day 10 post tumor inoculation into the 4T1-breast tumor-bearing mice and after 24 hrs, we analyzed the percentage of major immune cells types in the spleen, blood and tumors.

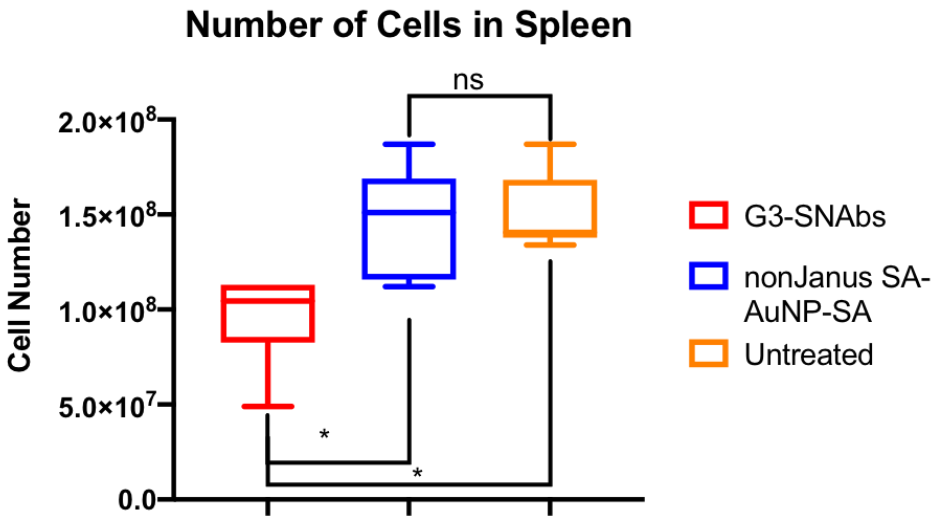


Figure 40. The numbers of cells in the spleens after treatment. Nanoparticles were injected into the 4T1-tumor bearing mice through tail veins on day 10 post tumor inoculation. The spleens were collected 24 hrs after injection and the total number of cells in each spleen was counted with trypan blue. Statistical difference was analyzed with ANOVA with Tukey test (n=6, *p<0.05)

First, we observed significant lower number of cells in the spleen in the G3-SNAb-treated groups compared to the control-particle-treated group or untreated tumor-bearing group (Figure 40), showing an amelioration of splenomegaly, the enlarged spleen symptom resulted from tumor progression. More prominently, we observed apparent reduction in the percentage of granulocytic MDSCs in the spleen and blood, by 55.7% and 46.4% respectively compared to those of the untreated group (Figure 41) and also significant reduction of the number of monocytic MDSCs in spleen by 69.6%. However, SNAbs didn't change the accumulation of MDSCs much in the tumors compared to untreated group. Because of the reduction of MDSCs, the percentage of $CD3^+$ T cells, including $CD3^+CD4^+$ T helper cells, and $CD3^+CD8^+$ cytotoxic T cells in the spleen (Figure 42) after treatment with G3-SNAbs, indicating higher probability of effective anti-cancer

immune responses. Similarly, in blood, $CD3^+CD4^+$ T cells percentage increased and the percentage of $CD3^+CD4^+CD25^+Foxp3^+$ T regulatory cells decreased in the G3-SNAb-treated group by 40.1% compared to the untreated group (Figure 43). Interestingly, the percentage of NK cells increased by 12.4% in the spleen after G3-SNAb treatment, contradicting with the result of the splenocyte suspension assay (Figure 44). Besides, control particle treatment (SA-AuNP-SA) also reduced the percentage of MDSCs to some extent compared to untreated groups, but they do not affect any other cell populations and may not have any treatment effects on cancer progression.

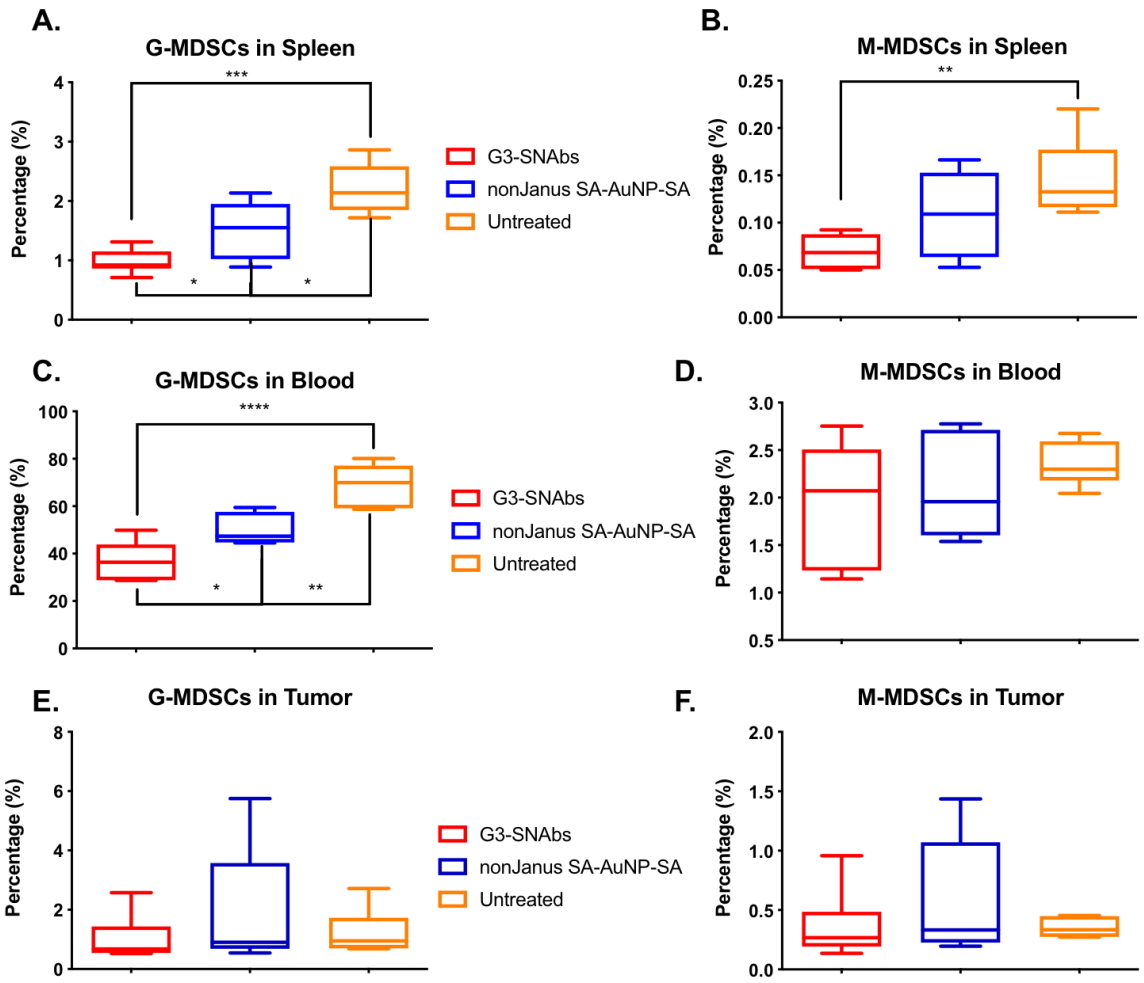


Figure 41. Percentages of G-MDSCs and M-MDSCs in spleen, blood and tumor after treatment. Nanoparticles were injected into the 4T1-tumor bearing mice through tail vein on day 10 post tumor inoculation. The spleens, tumors and blood were collected 24 hrs after injection. The cells in the samples were stained with fluorescent-antibodies against cell surface and intracellular markers and analyzed on a flow cytometer. The graphs show the percentages of G-MDSCs (left column) and M-MDSCs (right column) of spleens (A,B), blood (C,D), and tumors (E,F). Statistical difference was analyzed with one-way ANOVA with Tukey post hoc test or Kruskal-Wallis test with Dunn's multiple comparison, * $p < 0.05$, **$p<0.01$, ****$p<0.001$, n=6.

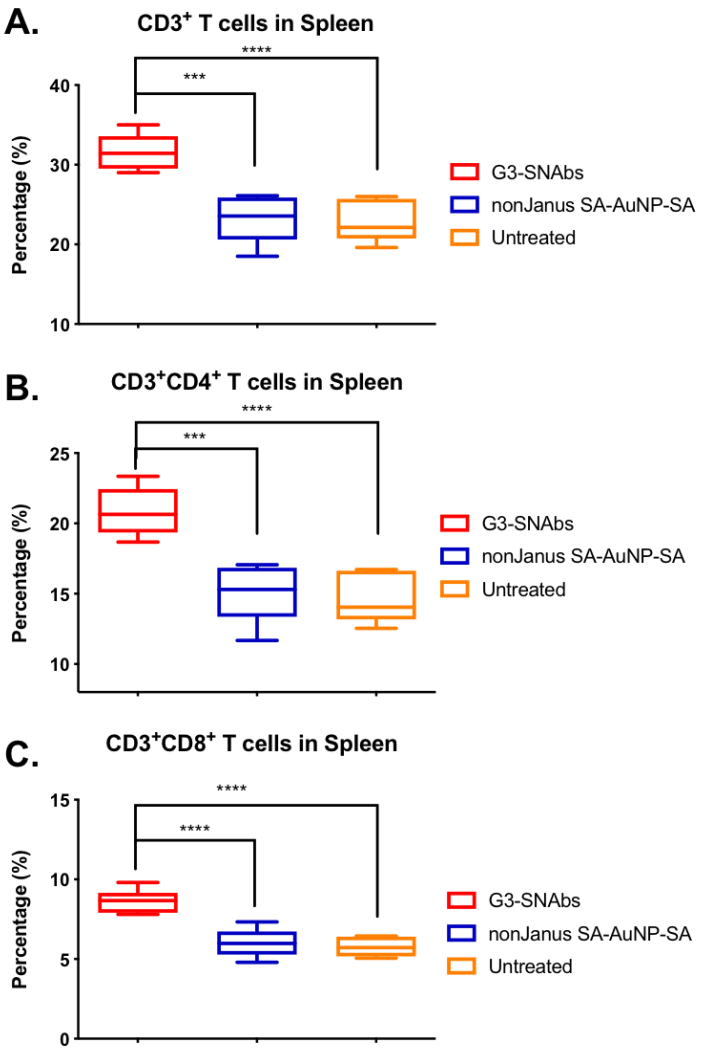


Figure 42. The percentages of T cells in spleens after treatment. Nanoparticles were injected into the 4T1-tumor bearing mice through tail veins on day 10 post tumor inoculation. The spleens were collected 24 hrs after injection. The cells in the samples were stained with fluorescent-antibodies against cell surface and intracellular markers and analyzed on a flow cytometer. The graphs show the percentages of the $CD3^+$ T cells (A), $CD3^+CD4^+$ helper T cells (B), and $CD3^+CD8^+$ cytolytic T cells (C) in the spleens. Statistical difference was analyzed one-way ANOVA with Tukey post hoc test or Kruskal-Wallis test with Dunn's multiple comparison, *p<0.0332, **p<0.0021, ***p<0.0002, ****p<0.0001, n=6.

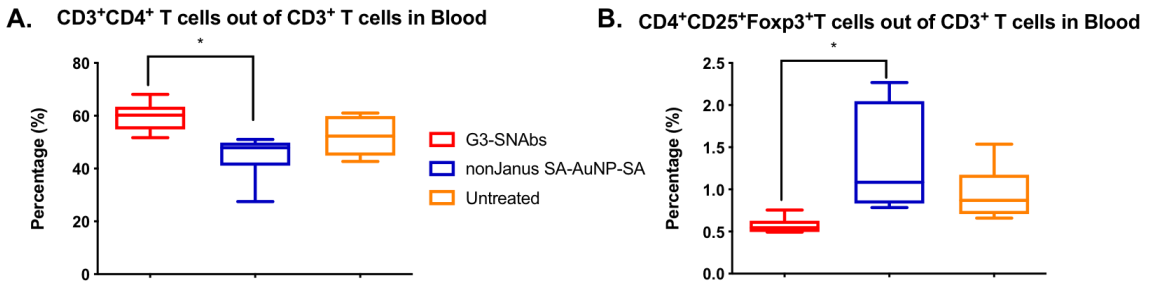


Figure 43. The percentages of $CD4^+$ T cells and T regulatory cells in blood after treatment. Nanoparticles were injected into the 4T1-tumor bearing mice through tail veins on day 10 post tumor inoculation. The spleens were collected 24 hrs after injection. The cells in the samples were stained with fluorescent-antibodies against cell surface and intracellular markers and analyzed on a flow cytometer. The graphs show the percentages of the $CD3^+CD4^+$ helper T cells (A), and $CD3^+CD4^+$ $CD25^+Foxp3^+$ regulatory T cells (B) in the blood. Statistical difference was analyzed with one-way ANOVA with Tukey post hoc test, * $p < 0.0332$, n=6.

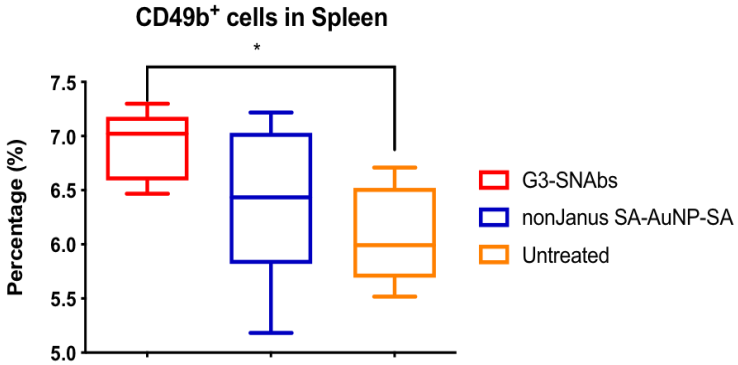


Figure 44. The percentages of $CD49b^+$ NK cells in the spleens after treatment. Nanoparticles were injected into the 4T1-tumor bearing mice through tail veins on day 10 post tumor inoculation. The spleens were collected 24 hrs after injection. The cells in the samples were stained with fluorescent-antibodies against cell surface and intracellular markers and analyzed on a flow cytometer. The graph shows the percentages of the $CD3^-$ $CD49b^+$ NK cells in the spleens. Statistical difference was analyzed with one-way ANOVA with Tukey post hoc test, * $p < 0.0332$, n=6.

### 5.2.4 MDSC depletion with three treatments of MDSC-SNAbs

Single-treatment depletion study didn't affect the accumulation of MDSCs in the tumor, so we tested the therapeutic effects of three treatments in tumor. G3*-SNAbs or other control particles (Janus IrrelG3-AuNP-cp33, G3*-AuNP-Irrelcp33, SA-AuNP-SA) or PBS were administered in the 4T1-tumor-bearing Balb/c mice on day 7, 9, 11 post tumor inoculation. After three treatments with SNAbs, we saw significant enhancement in the depletion of MDSCs in tumor, with 52% and 90% decrease in G-MDSCs and M-MDSCs respectively compared to untreated group, and 69% and 88% decrease compared to SA-AuNP-SA treated group (Figure 45). However, surprisingly, the control SNAbs, IrrelG3-AuNP-cp33, and G3*-AuNP-Irrelcp33 also had strong depletion effect. After we tested the binding of free IrrelG3 peptide and Irrelcp33 on MDSCs (See 4.2), we noticed that both peptides have strong binding capability to MDSCs. Therefore, the Janus particles modified with these two peptides were also capable to affect the MDSC populations *in vivo*. In the following analysis, we will not consider these two types of nanoparticles as control SNAbs any more and in the later depletion study, a non-peptide-modified Janus nanoparticles, biotin-AuNP-NEM, was used as a universal negative Janus nanoparticle control for the SNAbs.

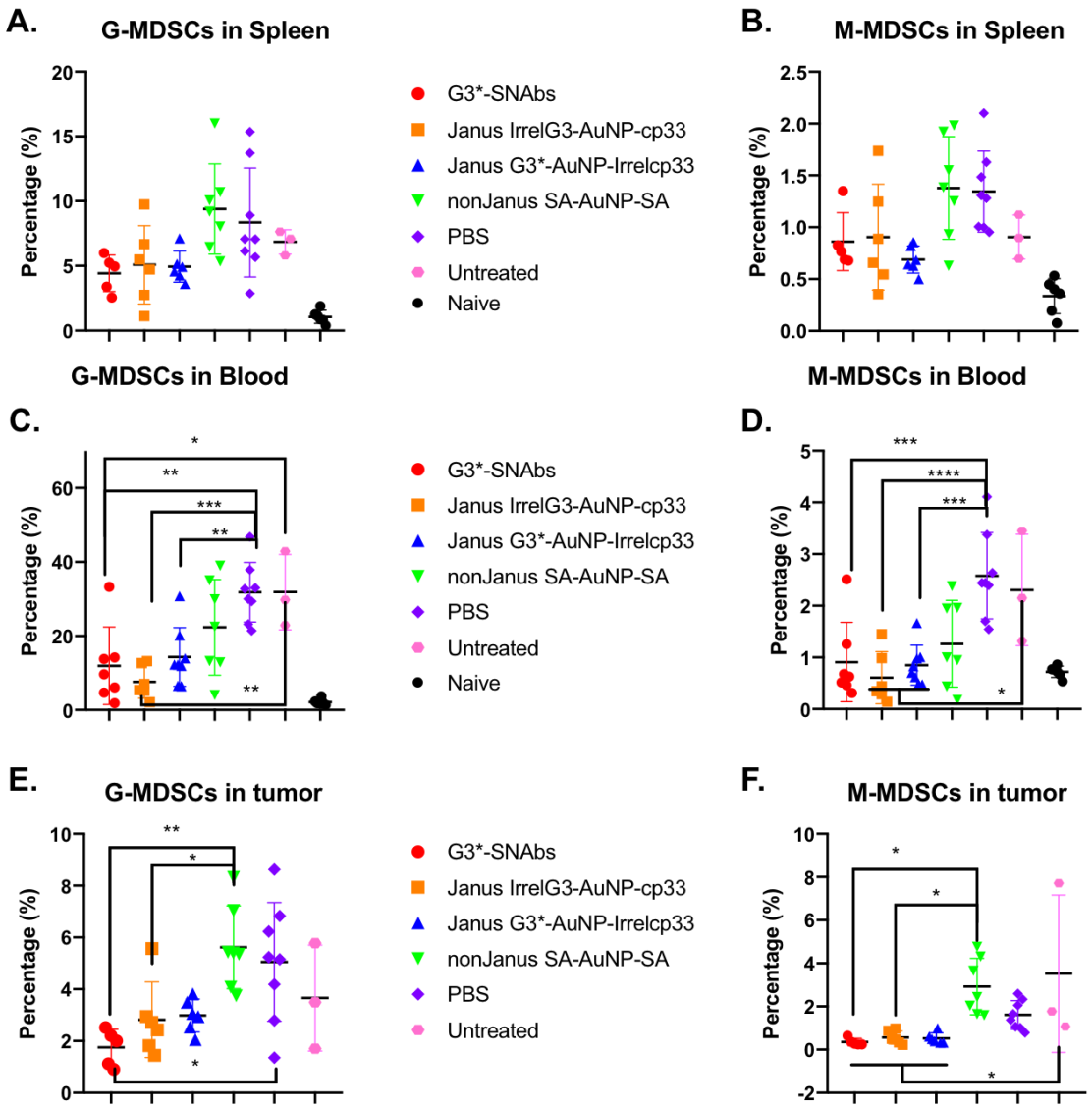


Figure 45. Percentages of MDSCs in spleen, blood and tumor after three injections. Nanoparticles or PBS were injected into the 4T1-tumor bearing mice through tail veins on day 7, 9 and 11 post tumor inoculation. The spleen, tumor, bone marrow and blood were collected 24 hrs after the last injection. The cells in the samples were stained with fluorescent-antibodies against cell surface and intracellular markers and analyzed on a flow cytometer. The graphs show the percentages of G-MDSCs (left column) and M-MDSCs (right column) of spleens (A,B), blood (C,D), and tumors (E,F). Statistical difference was analyzed with one-way ANOVA test with Tukey or Kruskal-Wallis test with Dunn's multiple comparison, * $p < 0.05$, **$p<0.0021$, ***$p<0.0002$, ****$p<0.001$, n=6.

We observed similar reduction in the percentages of G-MDSCs and M-MDSCs in spleen and blood after SNAb treatment as well as compared to PBS-treated and untreated groups (Figure 45). Unlike the first depletion study, SA-AuNP-SA treatment didn't affect MDSCs in tumor and spleen this time, but slightly reduced MDSCs in blood.

Tumor growth significantly increased the percentage of both G-MDSCs and M-MDSCs in the bone marrow, but MDSC-SNAbs failed to deplete any MDSCs in the bone marrow (Figure 46), probably due to the lack of mature effector cells.[25]

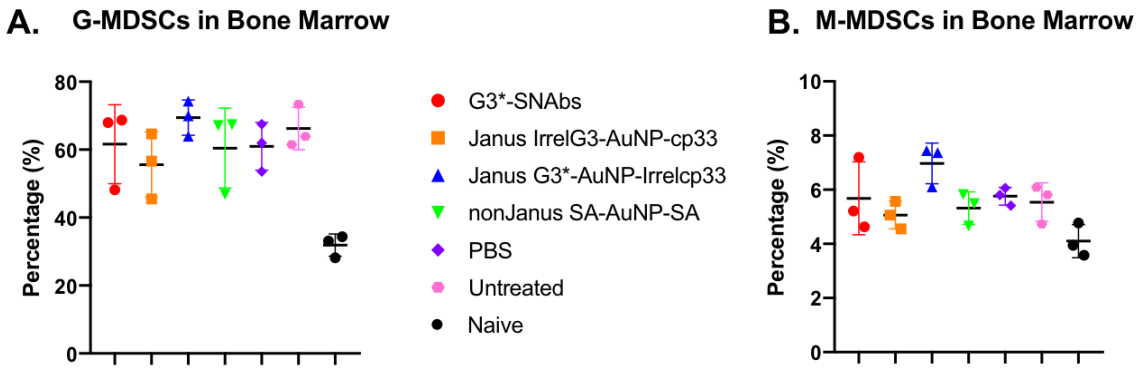


Figure 46. Percentages of MDSCs in bone marrow after three injections. Nanoparticles or PBS were injected into the 4T1-tumor bearing mice through tail veins on day 7, 9 and 11 post tumor inoculation. The bone marrow was isolated 24 hrs after the last injection. The cells in the samples were stained with fluorescent-antibodies against cell surface and intracellular markers and analyzed on a flow cytometer. The graphs show the percentages of G-MDSCs (A) and M-MDSCs (B) in bone marrow. Statistical difference was analyzed with one-way ANOVA with Tukey post hoc test, n=6. Naïve group was significantly different from other groups statistically.

There were no significant changes in T cells in spleen, and blood, but the percentage of $CD3^+CD8^+$ T cells slightly increased in tumors after SNAb treatments. Also, the percentage of $IFN\gamma^+$ cells out of $CD3^+CD8^+$ T cells increased due to SNAb treatment

compared to SA-AuNP-SA-treated and PBS-treated groups, indicating stronger anti-tumor activity in the T cells (Figure 47).

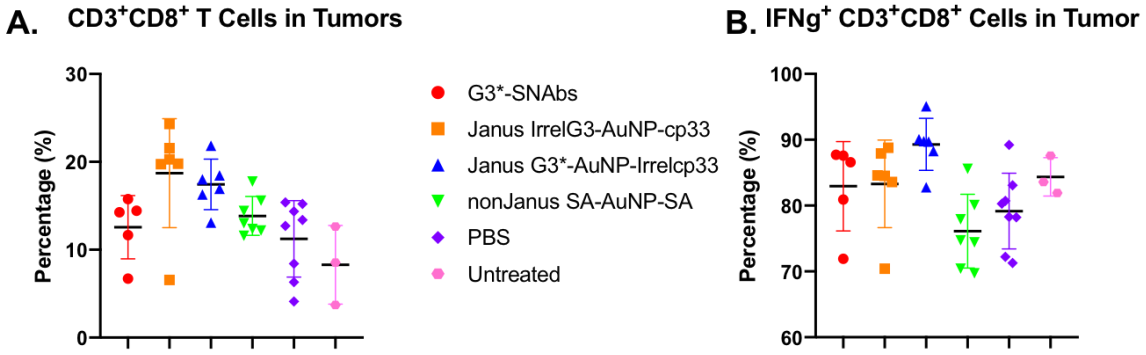


Figure 47. Percentages of cytotoxic T cells in tumors after three injections. Nanoparticles or PBS were injected into the 4T1-tumor bearing mice through tail veins on day 7, 9 and 11 post tumor inoculation. The tumors were collected 24 hours after the last injection. The cells in the samples were stained with fluorescent-antibodies against cell surface and intracellular markers and analyzed on a flow cytometer. The graphs show the percentages of $CD3^+CD8^+$ cytotoxic T cells (A) and IFNγ-secreting $CD3^+CD8^+$ T cells (B) in tumors. Statistical difference was analyzed with one-way ANOVA with Tukey post hoc test, n=6.

Although there were more $CD49b^+$ NK cells infiltrated into the tumors after SNAb injections, all the treatments seemed to have negatively affected the functionality of the NK cells, resulting in lower percentage of $IFN\gamma^+$, $perforin^+$, granzyme $B^+$ cells (Figure 48). It could be that triggered by the treatments, these NK cells have unloaded factors into the tumor microenvironment to kill the malignant cells or the target cells, MDSCs, leading to a reduced percentage of positive cells detected by flow. Otherwise, it could be possible that due to the binding of the Janus nanoparticles to NK cells, the viability and activity of NK cells were dampened.

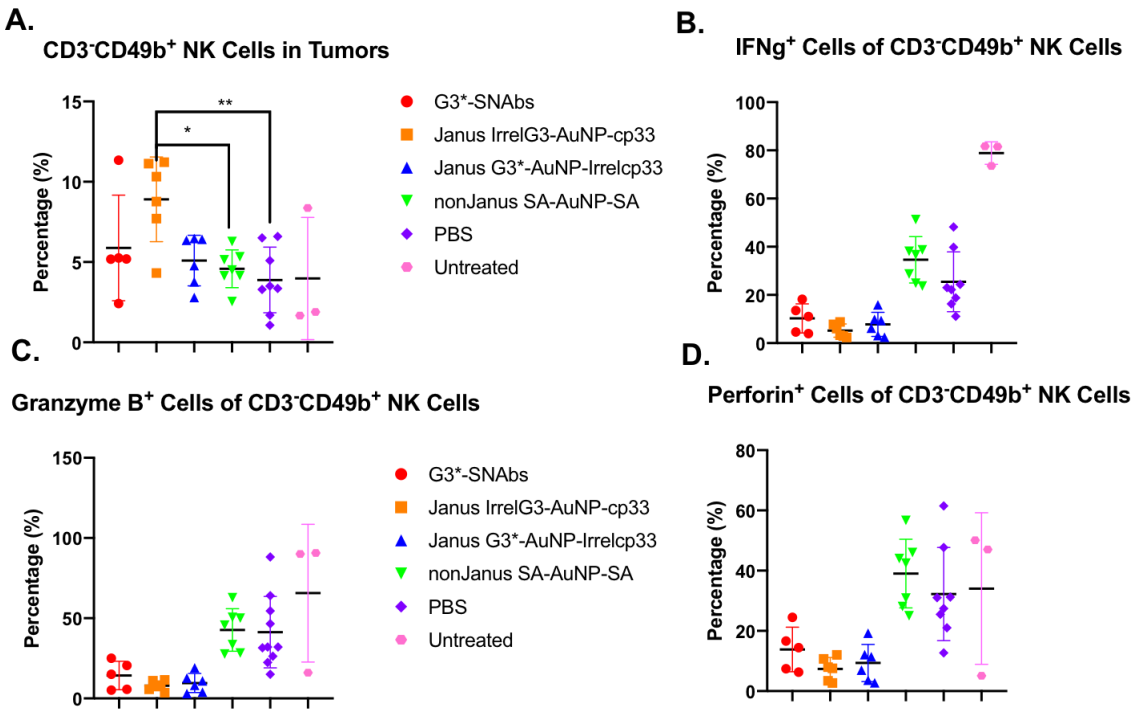


Figure 48. Percentages and functional characterization of NK cells in tumors. Nanoparticles or PBS were injected into the 4T1-tumor bearing mice through tail veins on day 7, 9 and 11 post tumor inoculation. The tumors were collected 24 hrs after the last injection. The cells in the samples were stained with fluorescent-antibodies against cell surface and intracellular markers and analyzed on a flow cytometer. The graphs show the percentages of $CD3^{-}CD49b^{+}$ NK cells (A) and $IFN\gamma^{+}$ (B), Granzyme $B^{+}$ (C), $Perforin^{+}$ (D) NK cells in tumors. Statistical difference was analyzed with one-way ANOVA with Tukey post hoc test, n=6.

### 5.2.5 A comprehensive MDSC depletion study with MDSC-SNAbs

After summarizing the information we got from the previous two MDSC depletion studies, we planned to further investigate whether more dosages of treatment and earlier treatment might have better chances to reduce the MDSC accumulation in tumor. Also, we still haven not reached a conclusion about whether peptide ligands modified on the particles are essential for the selective depletion of MDSCs or not as we got controversial

results from previous *ex vivo* and *in vivo* studies. Therefore, we designed a more comprehensive MDSC depletion study, in which we included a three-injection and a single-injection group of G3-SNAbs, and also single-injection groups of Janus scAHNP-AuNP-cp33 and Biotin-AuNP-NEM. Specifically, the single injections were given on day 10 post tumor inoculation and the three injections of G3-SNAbs were given on day 6, 8, 10 through tail vein. The tissue samples were collected on day 11 post tumor inoculation to study the changes in cell composition in the spleen, blood and tumors. As we didn't see any changes in the bone marrow samples in the last study, bone marrow was excluded from the analysis.

Interestingly, unlike previous results, both single-injection and three-injection groups did not affect granulocytic MDSCs much, but reduced the percentage of monocytic MDSCs in the tumors (Figure 49). The results of single-injection of G3-SNAb group didn't show any difference from those of three-injection group.

Similar to previous results, in the spleens, the treatment with G3-SNAbs resulted in huge reduction (around 69.8%) in the percentage of G-MDSCs in the spleen (Figure 49 C). The single-injection group still had no difference from the three-injection group. While the scAHNP-AuNP-cp33 induced a smaller decrease in the G-MDSC percentage, biotin-AuNP-NEM treated groups didn't change it much. However, due to the decrease in the G-MDSCs, the percentage of M-MDSCs slightly increased in the spleen in the treatment groups. The G3-SNAb three-injection group seemed to have smaller increase in the M-MDSCs groups, indicating a better control in the therapeutic effect.

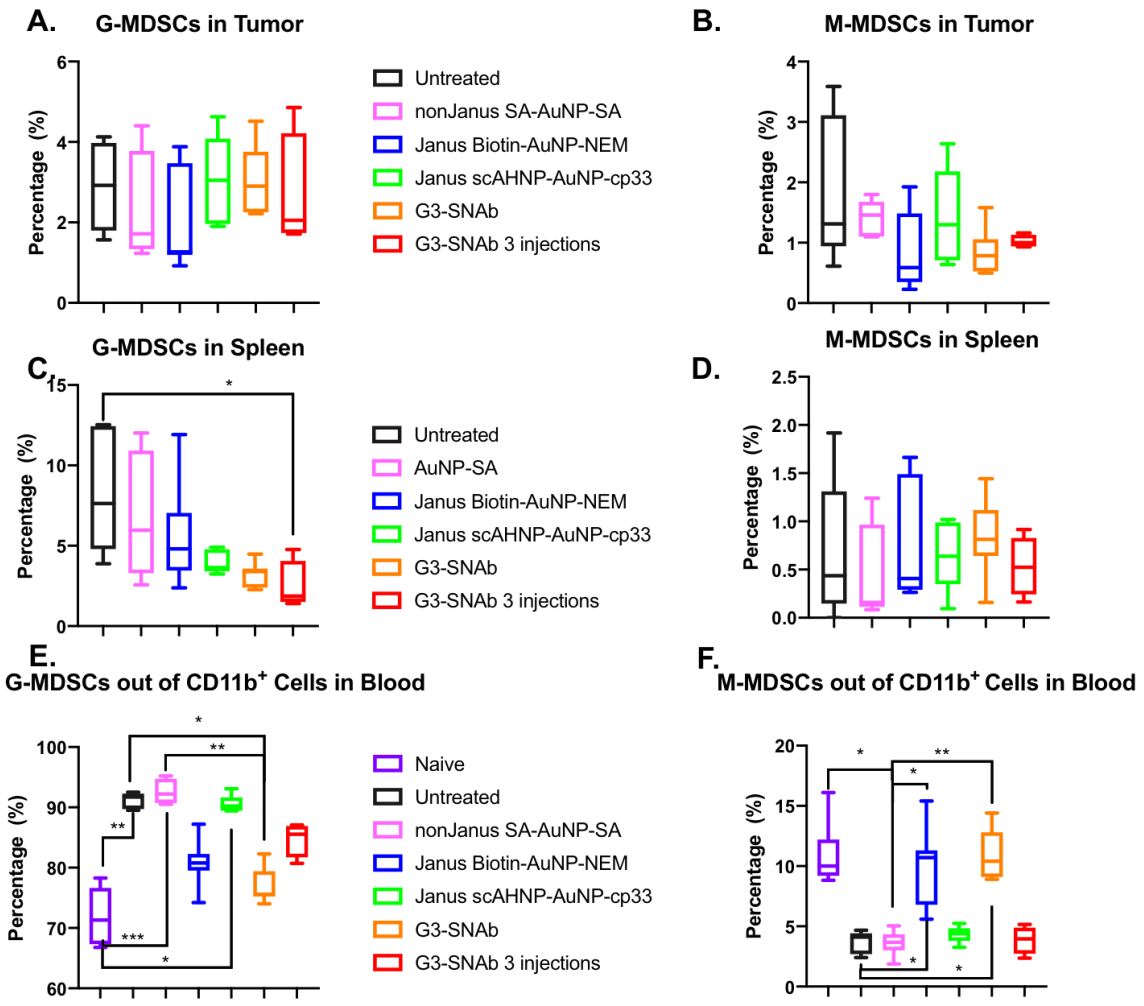


Figure 49. Percentages of MDSCs in spleen, blood and tumors after injections. SNAbs (Janus G3-AuNP-cp33) was injected either one time on day 10 or three times on day 6, 8, 10 through tail vein into the 4T1-tumor bearing mice. Other treatments were given only one time on day 10 to mice. The spleens, blood and tumors were collected on day 11. The cells in the samples were stained with fluorescent antibodies against cell surface and intracellular markers and analyzed on a flow cytometer. The graphs show the percentages of G-MDSCs cells (left) and M-MDSCs (right) out of total cells in tumors (A, B), spleens (C,D) and out of $CD11b^+$ cells in blood (E,F) (n=6). Statistical difference was analyzed with one-way ANOVA with Tukey post hoc test or Kruskal-Wallis test with Dunn's multiple comparison.

However, in blood, the single-injection of G3-SNAbs did better than the three-injection groups in reducing G-MDSCs. ScAHNP-AuNP-cp33 didn't induce any changes in the

percentages of G-MDSCs, suggesting that the targeting-ligands are playing an important role in the depletion of G-MDSCs *in vivo*. Interestingly, the administration of Janus Biotin-AuNP-NEM also affected the G-MDSCs and M-MDSCs as much as the single-injection of G3-SNAbs.

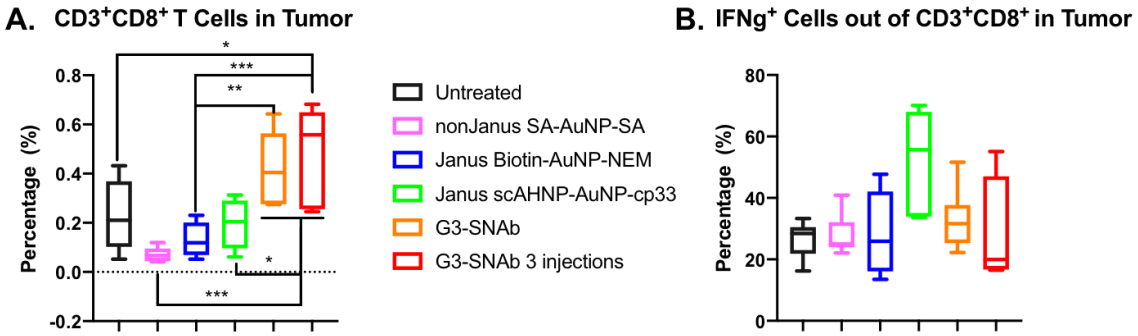


Figure 50. Percentages of $CD3^+CD8^+$ T cells in tumors after injections. The graphs show the percentages of $CD3^+CD8^+$ cytotoxic T cells out of total cells (left) and that of $CD8^+$ out of $CD3^+$ T cells (right) in tumors (n=6). Statistical difference was analyzed with one-way ANOVA with Tukey post hoc test or Kruskal-Wallis test with Dunn's multiple comparison., * $p<0.05$, ** $p<0.0021$, *** $p<0.0002$.

The reduction in MDSCs after G3-SNAb treatment resulted in the remarkable increase in the $CD3^+CD8^+$ T cells in the tumor, as shown in Figure 50. Other Janus nanoparticles didn't elicit the same response, indicating the importance of the targeting-ligand modification on the particles. However, the scAHNP-AuNP-cp33 seemed to be able to activate the few infiltrated $CD3^+CD8^+$ T cells to produce IFNγ more than other groups (Figure 50 B), which we haven't found any explanation yet.

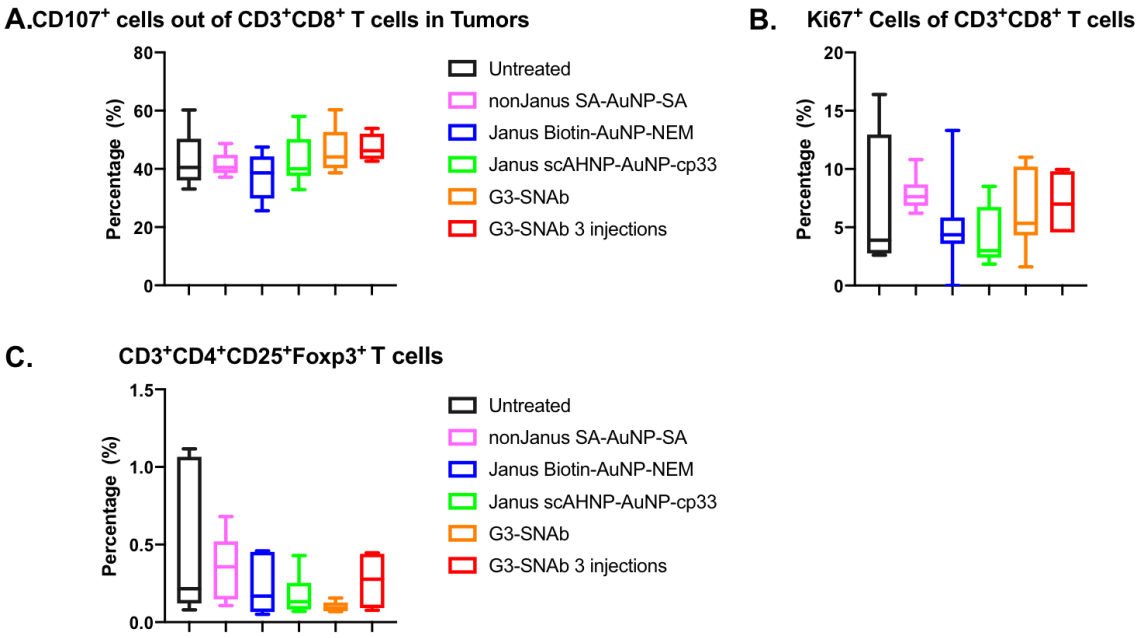


Figure 51. The percentages of activated or regulatory T cells in the tumors after treatment. The graphs show the percentages of $CD107^+$ cells (A) and $Ki67^+$ cells (B) out of $CD3^+CD8^+$ cytotoxic T cells and the percentages of T regulatory cells (C) in tumors (n=6). Statistical difference was analyzed with one-way ANOVA with Tukey post hoc test or Kruskal-Wallis test with Dunn's multiple comparison.

Also noticeably, there was a slightly higher percentage of $CD3^+CD8^+$ T cells being activated in the tumors after G3-SNAb treated compared to control treatments, as those T cells express the CD107 marker representing degranulation during the cytotoxic responses (Figure 51 A). G3-SNAb treatment also seemed to relieve the proliferation inhibition on T cells by MDSCs to some extent compared to control Janus nanoparticle treatments (Figure 51 B). In addition, fewer regulatory T cells were detected in the G3-SNAb groups, indicating the abrogation of immune-suppression due to MDSCs depletion systemically (Figure 51 C).

In terms of T cells in the spleen, we didn't notice any changes except the percentage of the $CD3^+$ T cells (including $CD8^+$, $CD4^+$ and other phenotypes) increased slightly after

treatment with G3-SNAbs (Figure 52 A). Interestingly, in blood, there was a trend of growing percentages of $CD4^+$ T cells out of $CD3^+$ T cells and a trend of decreasing percentages of $CD8^+$ T cells out of $CD3^+$ T cells from the untreated tumor-bearing groups to SNAb-treated groups.

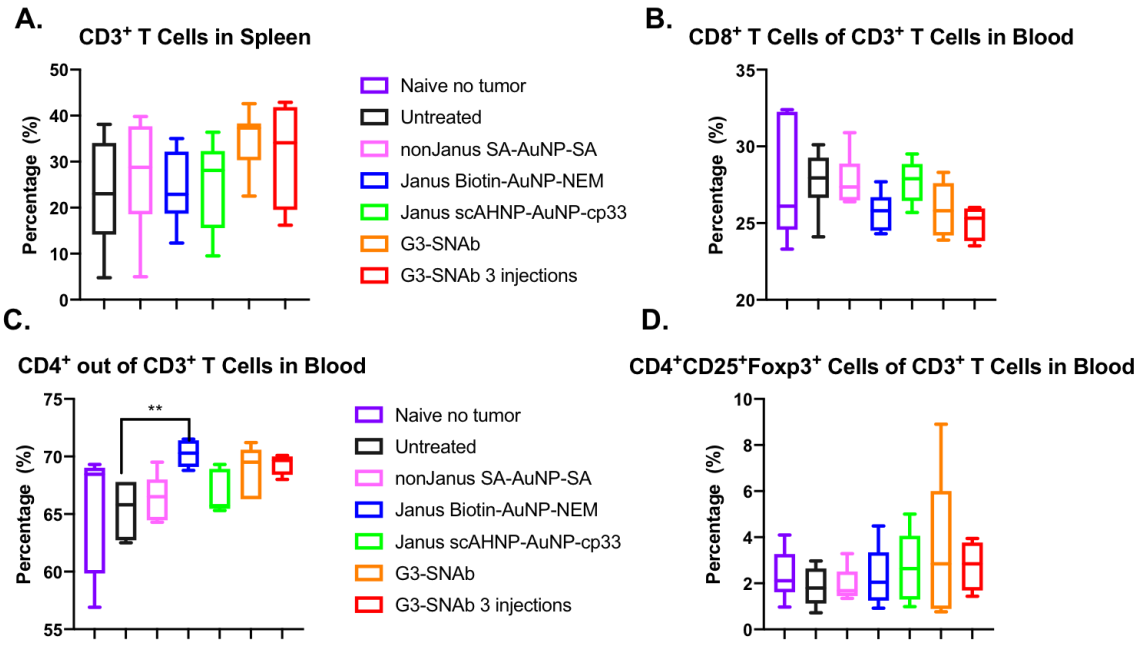


Figure 52. T cell percentages in the spleen and blood after treatment. The graphs show the percentages of $CD3^+$ T cells in the spleen (A), $CD8^+$ T cells (B), $CD4^+$ T cells (C), and regulatory T cells (D) out of $CD3^+$ T cells in the blood after treatment (n=6). Statistical difference was analyzed with one-way ANOVA with Tukey post hoc test or Kruskal-Wallis test with Dunn's multiple comparison, **$p<0.0021$.

Although the G3-SNAb treatment reduced the percentages of B cells and $IFN\gamma^+$ cells out of NK cells in the spleens (Figure 53) and blood (Figure 54), but G3-SNAb single treatment remarkably increased the percentage of NK cells infiltrated in the tumors (Figure 55). No enhancement or reduction of NK cell function or activation in tumors was observed. Interestingly, biotin-AuNP-NEM increased the percentages of B cells out

of CD3- cells and SA-AuNP-SA increased in percentages of IFNγ$^+$ cells out of NK cells in blood (Figure 54).

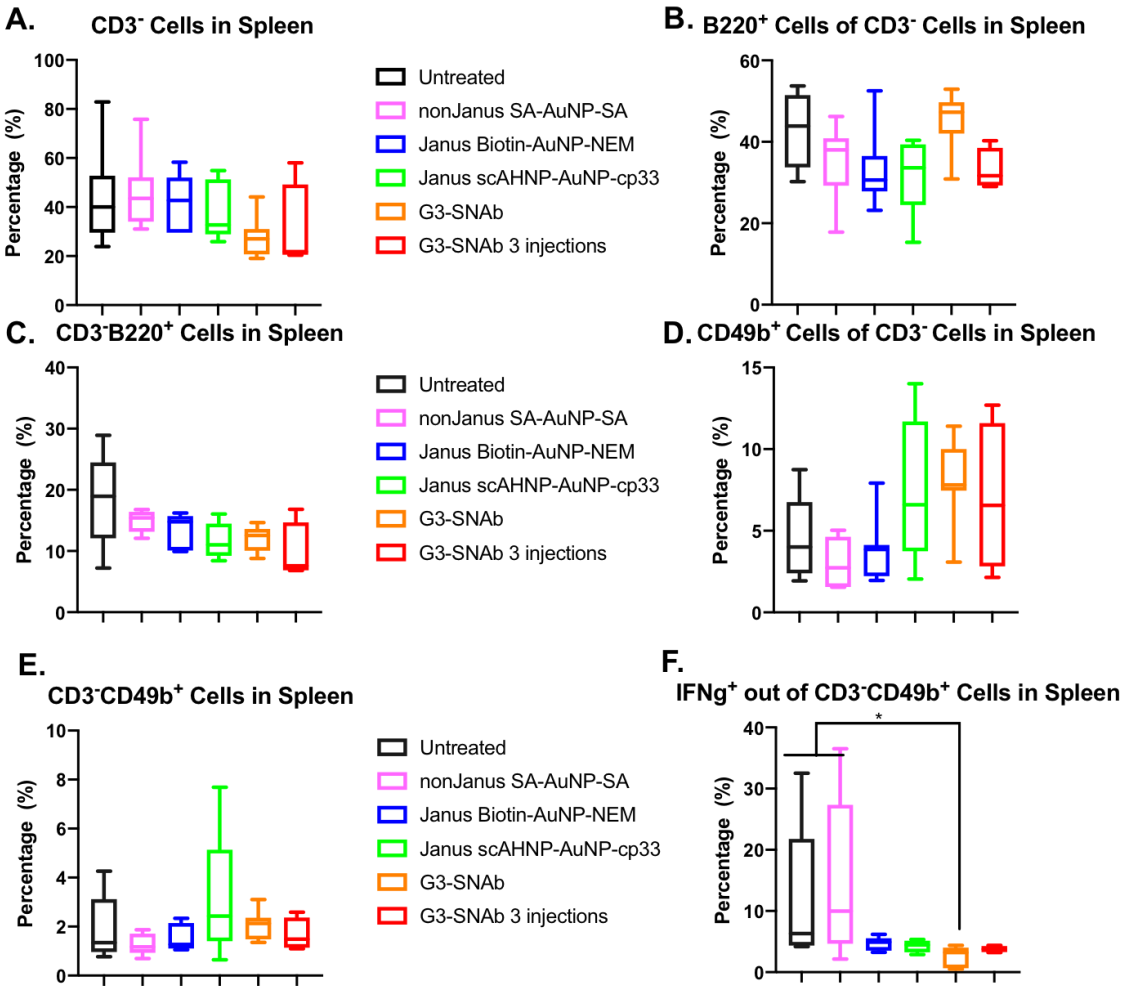


Figure 53. Percentages and characterization of B and NK cells in the spleens. The graphs show the percentages of CD3$^-$ cells (A), B220$^+$ B cells out of CD3$^-$ cells (B), CD3$^-$B220$^+$ B cells out of all cells (C), and CD49b$^+$ NK cells out of CD3$^-$ cells (D), CD3$^-$CD49b$^+$ NK cells out of all cells (E), and IFNγ$^+$ cells out of NK cells (F) in the spleens after treatment (n=6). Statistical difference was analyzed with one-way ANOVA with Tukey post hoc test or Kruskal-Wallis test with Dunn's multiple comparison, *p<0.05.

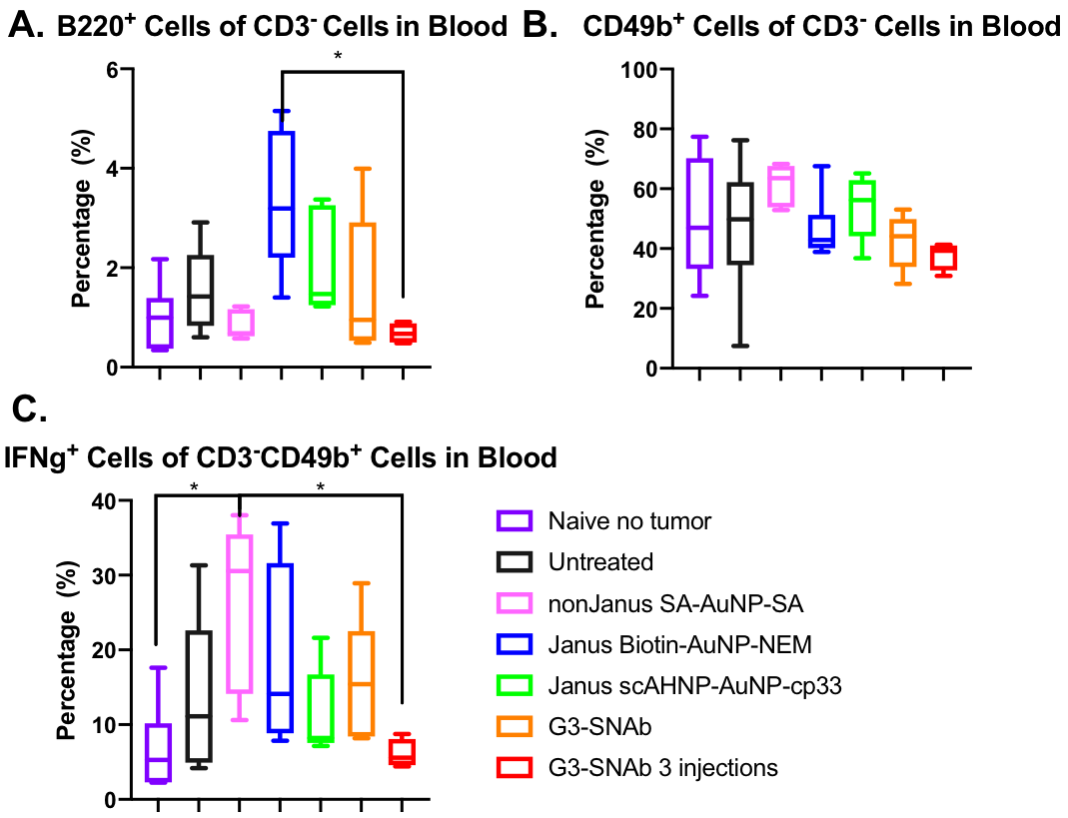


Figure 54. Percentages and activation of B cells and NK cells in blood after treatment. The graphs show the percentages of $B220^+$ B cells out of $CD3^-$ cells (A), $CD49b^+$ NK cells out of $CD3^-$ cells (B), and $IFN\gamma^+$ cells out of NK cells (C) in the blood after treatment (n=6). Statistical difference was analyzed with one-way ANOVA with Tukey post hoc test or Kruskal-Wallis test with Dunn's multiple comparison, *$p<0.05$.

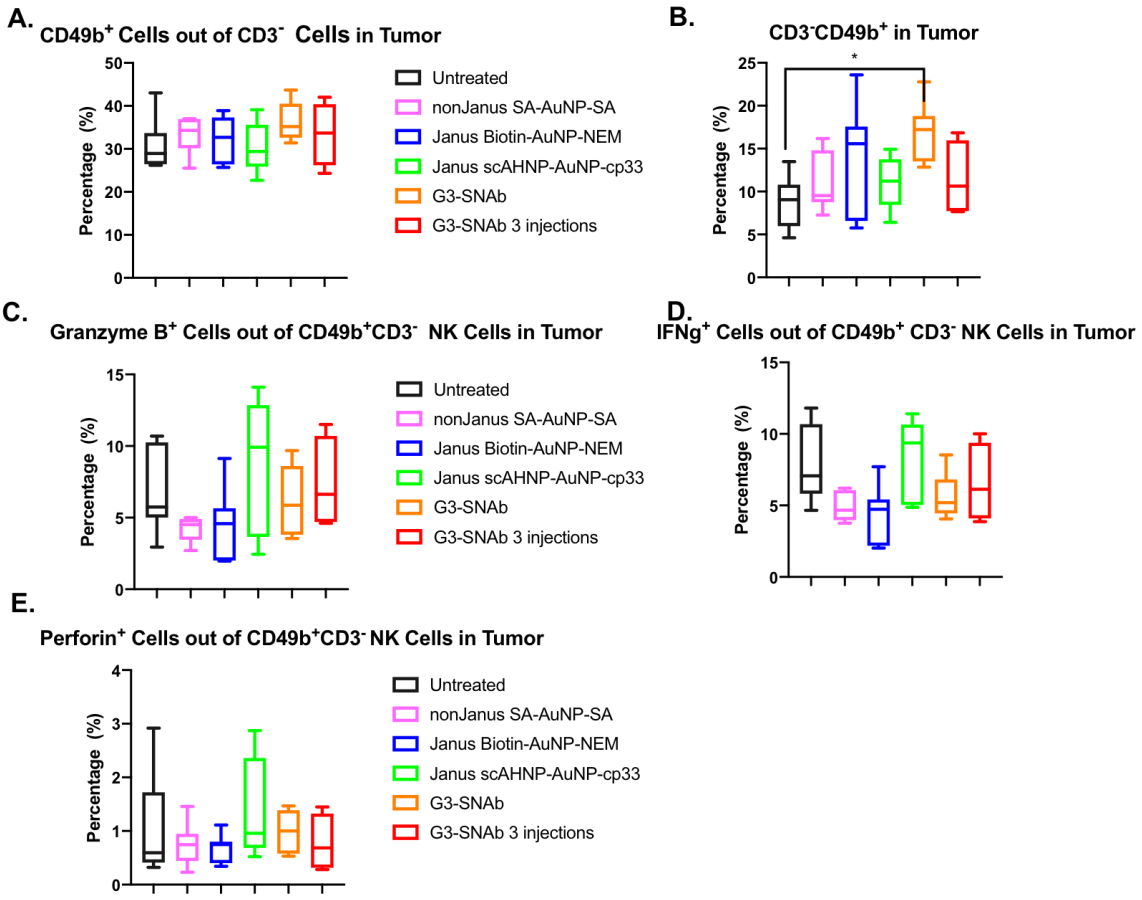


Figure 55. Infiltrated NK cells increased in the tumors after G3-SNAb single injection. The graphs show the percentages of $CD49b^+$ NK cells out of $CD3^-$ cells (A), $CD49b^+$ NK cells out of total cells (B), Granzyme $B^+$ cells out of $CD49b^+$ NK cells (C), $IFN\gamma^+$ cells out of NK cells (D), and $Perforin^+$ out of $CD49b^+$ NK cells (E) in the tumors after treatment (n=6). Statistical difference was analyzed with one-way ANOVA with Tukey post hoc test or Kruskal-Wallis test with Dunn's multiple comparison, **p<0.01.

### 5.2.6 MDSC-SNAb treatment prolonged the survival of 4T1-tumor bearing mice

As shown in the depletion studies, MDSC-SNAbs not only deplete MDSCs in the tumor, spleen, and blood, but also affect other cell types. Therefore, we wanted to investigate how these changes after MDSC-SNAb treatment translate into therapeutic effects in

tumor models. We administered MDSC-SNAbs through tail vein injections to 4T1-tumor bearing mice on day 7, 9 and 11 post tumor inoculation.

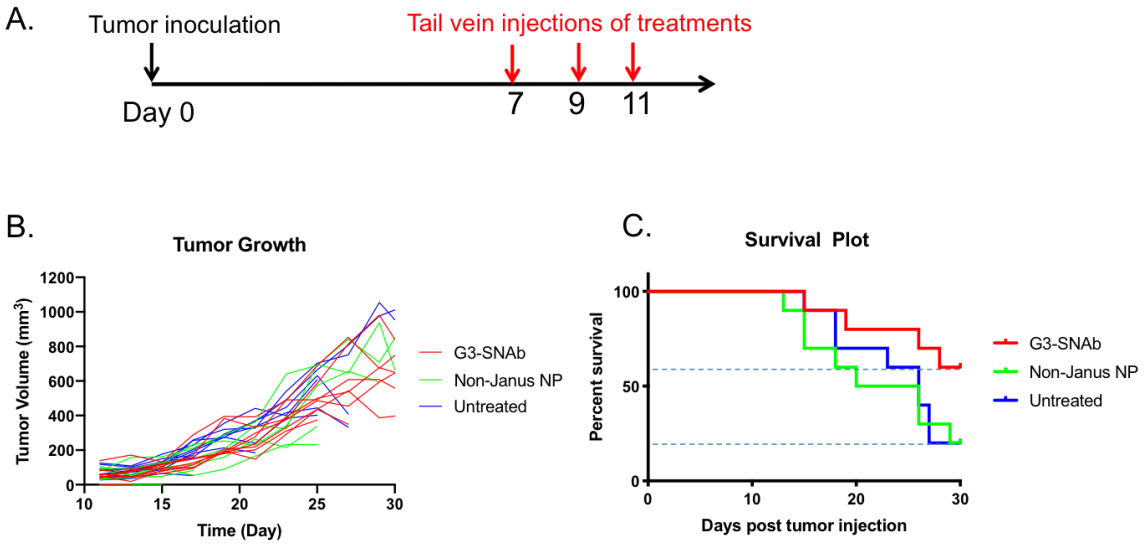


D.

| | SNAbs | AuNP-SA | Untreated |
|---|---|---|---|
| Median Survival (days) | 30 | 23 | 26 |

Figure 56. MDSC-SNAb treatments prolonged the survival of 4T1-tumor bearing mice. MDSC-SNAbs (Janus G3-AuNP-cp33) or control nanoparticles were administered into 4T1-tumor bearing mice on day 7, 9, and 11 post tumor inoculation (A). The graphs and table show the growth curve of tumors in each group (B), the survival plot (C) and median survival of each group (D) (n=10). Two-way ANOVA was performed to study the difference among groups in the tumor growth curve. Log-rank (Mantel-Cox) test was used to analyze the statistical difference among groups in the survival curve.

We observed that MDSC-SNAbs prolonged the survival of mice by delaying tumor growth significantly compared to the control-particle treatment after day 27 (Figure 56). We were requested to end the study on day 30 because of the onset of skin perforation on the primary tumors causing pain in the mice. At day 30, 60% of the mice were still alive (didn't meet any criteria for euthanization) in the MDSC-SNAb-treated group, but only

20% of mice remained alive in the control groups. The median survival of MDSC-SNAb group is 30 days, while that of SA-AuNP-SA-treated group and untreated group is 23 and 26, respectively. These confirmed that depleting MDSCs by SNAbs conferred survival benefits to 4T1-tumor-bearing mice.

### 5.2.7 MDSC-SNAb treatment had little enhancement over the immune-checkpoint blockade therapy in 4T1-breast tumor model.

Anti-PD1 and anti-CTLA-4 antibodies are the most well-known immune-checkpoint inhibitors (ICIs), which were shown to induce remarkable therapeutic responses in various cancers, but had limited effects in poor immunogenic tumors, such as 4T1 breast cancer. Previous studies have shown that MDSC depletion could enhance the therapeutic effects of immune-checkpoint inhibitors, so we tested the combination of MDSC-SNAb and anti-PD1, anti-CTLA-4 treatments in our 4T1-tumor models.[117,118] We administered the nanoparticles and antibodies according to the treatment schedule described in Figure 57 and tracked the growth of tumors in the mice every other day. Although we didn't observe noticeable difference in the tumor growth rate between the group treated with antibodies plus G3-SNAbs and the group treated with antibodies plus control particles or only antibodies, the MDSC-SNAb treated group had longer median survival time (37 days) compared to the control groups (See Figure 57 C). MDSC-SNAbs had a therapeutic effect in the early period of disease progression after adminstration, but the effect was lost after 39 days and mice in MDSC-SNAb-treated groups were euthanized when they met the end-point criteria.

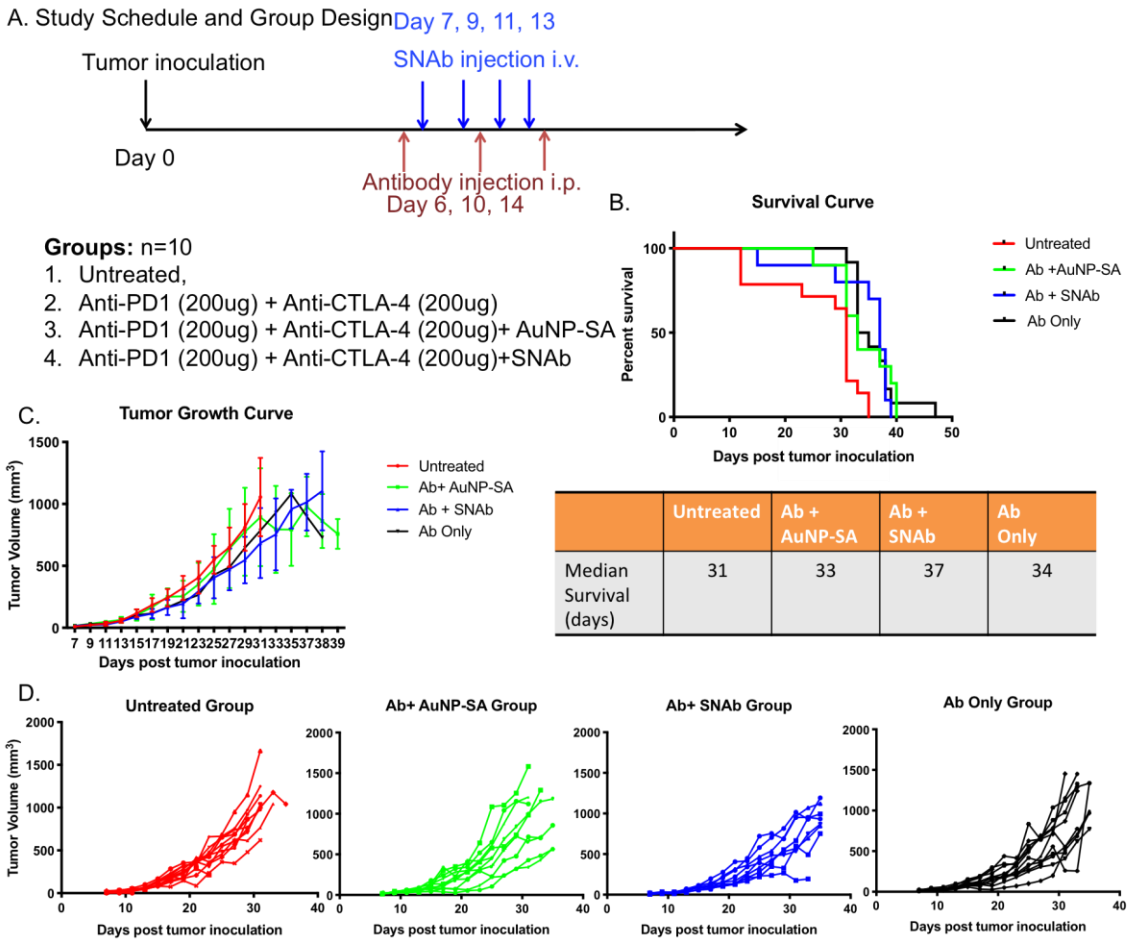


| | Untreated | Ab + AuNP-SA | Ab + SNAb | Ab Only |
|---|---|---|---|---|
| Median Survival (days) | 31 | 33 | 37 | 34 |

Figure 57. Survival study of the combination therapy with immuno-checkpoint inhibitors and MDSC-SNAbs. A. MDSC-SNAbs (Janus G3-AuNP-cp33) or control nanoparticles were administered into 4T1-tumor bearing mice on day 7, 9,11 and 13 post tumor inoculation via tail vein injections (A). Anti-PD1 and anti-CTLA-4 antibodies were administered on day 6,10, 14 via i.p. injections. The graphs and table show the survival plot and median survival (B) and the growth curve of tumors in each group (C, D) (n=10). Two-way ANOVA was performed to study the difference among groups in the tumor growth curve. Log-rank (Mantel-Cox) test was used to analyze the statistical difference among groups in the survival curve.

## 5.3 Discussion

Among all the tumor models, 4T1 is one of the few that is highly metastatic and closely recapitulates the properties triple-negative breast cancer in human, which affect millions

of women in the world and lack effective treatment strategy.[27] The syngeneic 4T1 mouse model also have the advantage of normal immune functions, which provides more translational information for human breast cancers.[28,117] Meanwhile, according to our observation, once inoculated on the mammary fat pad orthotopically in mice, the 4T1 cells establish primary tumors fast and rapidly metastasize to other organs, such as bone marrow, lymph nodes and lung, within 20 days. As a result, the window of treatment and analysis in 4T1-tumor model is short, allowing fast study completion. Also taken into consideration that 4T1-breast cancer strongly promotes the expansion of MDSCs, 4T1-orthotopic murine tumor model is a good choice to evaluate the therapeutic efficacy of MDSC-SNAbs.

Intravenous (i.v.) injection is the most common route of administration for monoclonal antibodies, followed by subcutaneous (s.c.) and intramuscular (i.m.) injection.[13] Adsorption of monoclonal antibodies after s.c. and i.m. injections are slower process compared to that after i.v. injections, because it is dependent on the convective transport of antibodies through interstitial space into the lymphatic system and the flow rate of lymphatic fluid is slow.[165] By i.v. injection, monoclonal antibodies can distribute into the tissue from the blood through convective transport, which relies on the flux of fluid by the blood-tissue hydrostatic gradient and sieving effect of the para-cellular pores.[13] We selected intravenous injection as the route of administration for MDSC-SNAbs to match the common practice used for monoclonal antibodies and also to take advantage of the fast distribution of SNAbs into the tissues, such as spleens and tumor, which are two major sites where MDSCs resides. In addition, after getting out of the bone marrow, MDSCs circulate in the blood to the spleen and tumor following the inflammation cues,

so capturing the blood MDSCs in circulation early by i.v. injection would help enhance the therapeutic effect of MDSC-SNAbs by reducing the systemic immune-suppression of cancer.

To investigate the biodistribution of SNAbs after i.v. injection in the mice, we have tried the following method: 1. Quantifying the fluorescence of organs isolated from mice injected with SNAbs labeled with fluorescent probes at desired time points using IVIS *in vivo* imaging system; 2. Imaging the whole mice with photoacoustic imaging microscope at 680-970 nm after injection with unlabeled SNAbs at desired time points; 3. Using inductively-coupled plasma-mass spectrometry, quantifying the amount of Au element in the tissues collected from the mice injected with unlabeled SNAbs at desired time points. For the first method, we labeled the SNAbs with Vivotag 647-NHS ester dye. Although the fluorescence of the labeled-SNAbs were detectable in the Biotek microplate reader, we failed to acquire any signal distinctly higher from the organs collected from the SNAb-injected mice compared to the untreated mice. Vivotag 647 dye covalently binds to the amine groups. However, the amine groups on the streptavidin were occupied for the conjugation of them onto the gold nanoparticles and the number of available amines on the peptides were also limited, so the nanoparticles were able to produce enough signals to penetrate through the tissue and be detected in the IVIS system. Despite other chemically active groups exist in the structure of SNAbs, they do not present in high enough numbers to enhance the fluorescent signals of the nanoparticles. For the second method, the photoacoustic imaging microscope failed to discern the signals of SNAbs from those of the oxygenated hemoglobin at around the SPR peak (532nm) of 30nm gold nanospheres. As a result, we cannot tell whether the increased signal from the organs of

the nanoparticle-treated animals was caused by more blood flow in the same area or not. Photoacoustic imaging actually works better with gold nanorods, which have optical absorption spectra in the near infrared range and thus distinguishable from the optical adsorption of hemoglobin.[103,166,167] Therefore, we moved on with the third method, quantification of the gold element in the tissues by ICP-MS.

The plasma half-life is a key factor in the pharmacokinetics to be considered when designing the dosage and frequency for drug administration.[168] Monoclonal antibodies usually have elimination half-life in days (for example, 18-21 days for IgG1, IgG2, IgG4[13,168]), because of the recycling by binding onto the neonatal receptor, FcRn, that express on the surface of blood cells and mediate the internalization of IgG by cells and returning of the antibodies to the cell surface under certain physiological conditions. As shown in the ICP-MS results, the SNAbs extravasated the circulation within 48 hrs. Seemingly, the SNAbs have a much more rapid clearance rate from the circulation than monoclonal antibodies, with the half-life being 26 hrs. In this case, SNAbs should be dosed more frequently than monoclonal antibodies. However, they preferentially accumulated in the spleen after they left the blood, which are the of the main target organs for MDSC-SNAbs to deplete MDSCs. This observation matches the remarkable decrease of MDSCs in the spleen of 4T1-tumor bearing mice after treatment of SNAbs. MDSC population expands rapidly in the spleen after tumor onset, constituting as high as 80% of the myeloid-derived cells and up to 40% of the total cells in the spleen (data not shown). Therefore, the capability of SNAbs to accumulate in the spleen and deplete splenic MDSCs could lead to significant reduction of MDSC migration to the tumors, and further ameliorate immunosuppression in tumor and metastasis.[105]

More promisingly, SNAb concentration in tumors was observed to keep increasing from 6 hr to 48 hr post injection. The size of the SNAb (actual size 30-50nm, hydrohynamic size 70-100nm) definitely is playing a critical role in the process as previous literatures suggested nanospheres in the size range of sub-50nm are better at escaping from the tumor vasculature, penetrating and retaining in the tumors by the EPR (enhanced permeability and retention) effect. The favorable accumulation and long retention of SNAbs in the tumor definitely projects greater response and better long-term therapeutic efficacy, and potentially reducing the dosage and treatment duration requirements. Indeed, the dosage we administered of SNAbs in the MDSC depletion studies was 10,000 times lower than those used in previous reports for anti-Gr1 monoclonal antibodies[98,115,156,169] , but we achieved comparable level of MDSC depletion in the blood, spleens and tumors as anti-Gr1 monoclonal antibodies. One other observation is that MDSC-SNAbs also accumulates in the liver to a great extent. It is important that a novel antibody-like therapeutic is safe to patients. So, a future step is to evaluate the liver and hematological toxicity of SNAbs.

The results from the three depletion studies clearly verified our hypothesis that the SNAbs can specifically deplete MDSCs *in vivo*. The first depletion study used the SNAbs generated with the SA-AuNP-SA from Nanopartz.Inc, on which only 21 streptavidins were coated, while in the later two studies, we used the SA-AuNP-SA from Nanohybrid.Inc, on which 100 streptavidins were coated. In other words, the first depletion study used a batch of SNAbs with theoretically lower valency of ligands than the later two studies did. However, we achieved similar level of depletion of G-MDSCs in these studies in the spleens and blood. This result indicates that either the change in the

number of streptavidins on the nanoparticles didn't alter the valency of SNAbs or the change in valency of SNAbs does not impact the capability of them to induce targeted responses for granulocytic cells, which necessitates further investigation on the valency effect of SNAbs with accurate quantification of ligand modification. On the other hand, compared to the first study, the later studies with the theoretical higher-valency SNAbs showed greater reduction in the percentages of M-MDSCs in the collected samples and better depletion effect of both MDSC subsets in the tumors. The valency of the ligands on the SNAbs could possibly be an important reason for it, since the increase in avidity may lead to higher affinity and specificity of SNAbs on the target cells and regulate the penetration and retention of the nanoparticles in the tumors.

We did see some unexpected results elicited by the control Janus nanoparticles unmodified or modified with peptides other than G3 or G3*. One possible explanation for these observations is that the surface property (e.g., hydrophobicity, electrostatic charges) of the Janus nanoparticles after modification changed their interaction with the blood cells. Different Janus nanoparticles would be taken up and cleared by cells in the blood differently, leading to completely different pharmacokinetics of them. Apparently, G3-SNAbs are more prone to get around with blood clearance and get into the tumor and spleens to take an effect. More *in vitro* and *in vivo* investigations need to be carried out to study how the surface property changes after ligand modification impact the nanoparticle-cell interaction, protein corona composition of the nanoparticles and how it translates into the *in vivo* responses elicited by the nanoparticles. This information is crucial for the design of SNAbs as a versatile artificial antibody platform.

MDSCs were known to suppress the adaptive immune responses by reducing the proliferation and activation of cytotoxic T cells and promoting the differentiation of T cell into T regulatory cells. Repeatedly in our MDSC-depletion studies, we observed increased infiltration of $CD3^{+}CD8^{+}$ T cells, higher percentage of activated, IFNγ-secreting T cells and lower numbers of regulatory T cells in the tumors in the MDSC-SNAb treated groups. These all suggested that MDSC-SNAbs are capable of restoring anti-tumor cellular immune responses by depletion of MDSCs. In our preliminary single-therapy *in vivo* study, the MDSC-SNAb-treated group had a much higher percentage of mice remained alive at the end of the study compared to the control groups, which validated that MDSC-SNAbs has therapeutic potential to prolong the survival of 4T1-breast tumor-bearing mice. In the ICI-MDSC-SNAbs combination studies, we didn't see a statistically significant difference in the tumor growth rate among the groups, but from the survival curve, MDSC-SNAbs helped to improve the therapeutic effects of the ICIs in the early times points (before day 39). Previous studies by KiBem Kim et al. and by Olivier De Henau et al. both showed significant improvement in survival in the combination therapy groups with both ICIs and MDSC depletion compared to ICI alone group.[117,118] The reason why we didn't achieve similar results could be that MDSC-SNAbs affected the functions of NK cells to some extent, as shown in the depletion studies. NK cells are the major effector cells for ADCC elicited by IgG2a and IgG2b (anti-PD1: IgG2a, anti-CTLA4: IgG2b), and previous studies report ADCC of regulatory T cells as one of the mechanism of anti-CTLA4 antibodies and potentially for anti-PD1 antibodies.[6,170] Therefore, a dampened NK cell response may affect the therapeutic efficacy of ICIs and thus leading to no improvement in the combination therapy group.

Lastly, based on the collected results from the above-discussed in vivo studies, some other studies would be interesting and important for the evaluation of therapeutic potential of SNAbs. Instead of intravenous injection, intratumoral injection of MDSC-SNAbs could possibly enhance the depletion effect of MDSCs in the tumor and thus more effective inhibit the growth and metastasis of tumors. An imagable 4T1-luc cell line could be used to track the metastasis of the tumor and study whether depletion of MDSCs could delay or inhibit the metastasis of the 4T1 cancer cells to lung, lymph nodes and bone marrow.[27,28,94] Breast cancers were usually surgically removed before treatment with medicines, but the residuals of malignant cells in the original sites will lead to the re-occurrence of tumor and more rapid progression and metastasis of cancer. So, it would be interestingly to see if MDSC-SNAbs treatment after the surgery could decrease the chances of re-occurrence of tumor or improve the prognosis by removing the immunosuppression microenvironment. In addition, the aggressiveness of 4T1-breast tumor model limited the design of the *in vivo* studies in terms of injection schedule. We were only able to inject the SNAbs before day 12 post tumor inoculation due to the collapse of tail vein caused by dehydration of the mice. Therefore, a less aggressive model of 4T1 with a decreased dose of tumor inoculation could be useful to allow wider treatment window and study the effect of late SNAb treatment. We would also like to validate the therapeutic effect of MDSC-SNAbs in other cancer models, such as B16 melanoma, A20 lymphoma, C26 colon carcinoma, pancreatic or prostate cancers, and human breast cancer models in humanized mice.

# CHAPTER 6 CONCLUSION AND FUTURE DIRECTION

## 6.1 Concluding Summary

Over the past decade, we saw an increasing number of monoclonal antibodies being tested in clinical trials and approved by the US Food and Drug Administration (FDA) for use in metabolic disorders, autoimmune diseases, infectious diseases, and various malignancies. Out of the fifty-nine drugs approved in 2018, eleven of them are monoclonal antibodies and they are forecasted to be the potential blockbusters in sales [29]. While we are celebrating the success of monoclonal antibody therapy, we have to keep their limitations in mind. Humanized and human monoclonal antibodies (mAbs), which are the two popular types of mAbs because of their safety in human, are difficult to develop and produce, causing an extremely high price of these mAbs.[12,171] Moreover, their molecular properties resulted in the unsatisfactory therapeutic effects in treating deep, solid tumors due to a lack of penetration and retention.[12,23,172,13,45,168] It is also challenging to develop mAbs towards cellular targets that do not have known unique surface protein markers because of the challenges in the immunization and screening process.[10,12] Therefore, there is still a need for antibody engineering or the development of alternative artificial antibodies to meet the clinical demand.

During the past decades, particulate systems have gained huge attention as promising platform for delivering a variety of synthetic and biological therapeutics and the ease to modulate their functions by tailoring physical parameters makes them a good choice in a wide range of immunotherapeutic applications.[1,21,22,173] On the other hand, synthetic small molecules, such as peptides and aptamers, have emerged as advantageous targeting and

binding ligands for guided and targeted therapies.[16,17,174] Because of the advent of various screening platforms, for example, phage display biopanning, we are allowed to identify such small molecular ligands directly with the isolated target protein or cells and tissues in animals.[17,67,175] A combination of the particulate system and small molecule ligands enables the design of synthetic therapeutics to mimic the functions of macromolecular biologics, such as antibodies, but with much lower developmental cost, higher flexibility and versatility. [18,19,173,176] Therefore, we designed a novel type of artificial antibody with Janus nanoparticles and synthetic ligands, named synthetic nanoparticle antibodies (SNAbs).

To development SNAbs, we first examined whether there are appropriate ligands for the engagement with Fc receptors on the immune effector cells and the specific binding of target cells. Cp33 is a ligand identified through phage display system that can block the binding of human IgG1 and FcγRI by docking onto the binding pockets on the receptors.[26] It was also shown to be able to trigger super-oxide burst and phagocytosis by phagocytes when constructed into dimers.[53] Therefore, cp33 is a good option as Fc-mimicking ligand. For the proof of concept, we selected myeloid-derived suppressor cells as our first target cell type. MDSCs are important therapeutic targets in cancer, which suppresses the innate and adaptive immune responses by various mechanisms.[41,162] The depletion of MDSCs was shown to be able to augment the anti-tumor attack and inhibit tumor growth.[115,117] G3 peptide was selected as the targeting ligand for MDSCs, as it is capable of recognizing both granulocytic MDSCs and monocytic MDSCs isolated from various murine tumor models, potentially through binding to S100A8/A9 heterodimer

proteins on the surface of MDSCs.[126] G3* peptide, a scrambled form of G3 peptide, was also found to have specific binding capability on MDSCs.

To generate SNAbs, we started with streptavidin gold nanoparticles and designed a solid-phase chemistry method to fabricate Janus nanoparticles with the capability to react with biotinylated ligands and maleimide-conjugated ligands on spatially segregated parts of the nanoparticle surface. Subsequently, we modified the Janus gold nanoparticles with biotinylated targeting ligands (e.g.,G3, G3*) and maleimide-terminated Fc-ligands (cp33) to make various functional nanoparticle-ligand conjugates, i.e., MDSC-targeting SNAbs (MDSC-SNAbs). In Aim 1 (Chapter 3), we completed the design, fabrication and characterization of MDSC- SNAbs, and validated that the chemistry method we developed can produce the desired Janus gold nanoparticles, or say SNAbs, that present both targeting and Fc-mimicking ligands on the two segregated areas on surface and form the antibody-like structure.

In Aim 2 (Chapter 4), the functions of SNAbs were evaluated in *ex vivo* systems. Firstly, the results of both free peptide-splenocyte binding assay and photoacoustic imaging supported the strong binding of G3 peptide on MDSCs and that of cp33 on macrophages, for both free peptides and peptide-conjugated nanoparticles. G3*, which is a scrambled G3 peptide, also stood out as an effective binding ligand for MDSCs, especially G-MDSCs. The calcium-binding, proinflammatory protein S100A8/A9 is highly expressed on myeloid cells, and is a potential marker for tumor-associated MDSCs. Further computational simulation of the interaction between G3, G3* and human S100A8/A9 heterodimmer not only verified the binding capability of G3 and G3* on the S100A8/A9

protein, but also suggested their applicability in human therapies as well. Therefore, both G3-SNAbs and G3*SNAbs are considered efficient MDSC-targeting SNAbs.

In general, antibody mediates the elimination of target cells mainly in two ways, ADCC and ADCP. SNAb-treatment alone does not kill MDSCs, meaning that SNAbs do not have cytotoxicity on these cells, but in the effector-target cell co-culture assay, we observed strong specific lysis of MDSCs by macrophages induced by MDSC-SNAbs compared to that by control nanoparticles. The results also illustrated that macrophages primarily relies on phagocytosis to kill target cells in the presence of MDSC-SNAbs. Another strategy we developed to study the function and specificity of MDSC-SNAbs is the splenocyte suspension assay. In this assay, even at an extremely low effector:target ratio (1:3), the MDSC-SNAbs were still able to successfully reduce the MDSC population in the culture to a great extent and increase the percentage of dead MDSCs compared to control treatments. Moreover, MDSC-SNAbs didn't affect other cell types, including macrophages, dendritic cells, T cells and B cells. A negative impact on the numbers of NK cells was observed. However, this possibly was due to the decrease of S100A8/A9 proteins caused by MDSC depletion. These results validated our hypothesis that MDSC-SNAbs can mediate antibody-dependent responses to specifically kill MDSCs in the presence of immune effector cells. Interestingly, G3 and cp33 modified non-Janus gold nanoparticles failed to induce any responses towards MDSCs, indicating that the spatial arrangement of the ligands is crucial to the induction of ADCC or ADCP.

The fact that MDSC-SNAbs can induce antibody-dependent specific killing of MDSCs in an *ex vivo* environment does not legitimate them as effective therapeutic antibodies for treatment of diseases. In Aim 3 (Chapter 5), we further tested the efficacy of MDSC-

SNAbs in a 4T1 murine tumor model, which recapitulates the properties of human triple-negative breast cancer. MDSC-SNAbs had a short half-life in circulation, but accumulated favorably to the spleen and tumors after intravenous injection. Spleen and tumors are the two major sites of interest for MDSC-targeting therapy as MDSCs proliferate in the spleen and then migrate to the tumor to suppress the anti-tumor immune responses. The retention time of MDSC-SNAbs in these two sites are over 48 hrs, suggesting a promising, long-term therapeutic effect on the MDSCs in these organs. The preferentially distribution in tumor also matches the previous observations by other studies on nanoparticles of sub-50nm in size, showing good tumor-targeting effect. The depletion studies proved our hypothesis about the therapeutic effect in spleens and tumors. MDSC-SNAbs eliminated the majority of MDSC populations in the spleen and also affected the MDSCs in the tumors after one or three injections. Following the depletion of MDSCs, we observed an increase in the infiltrated and activated cytotoxic $CD8^+$ T cells. In other words, MDSC-SNAbs mitigated the immune-suppression in the tumor microenvironment and thus strengthened the cellular responses towards tumor. Additionally, despite the short half-life in blood, MDSC-SNAbs were able to remarkably reduce the circulating MDSCs within 24 hrs of treatment, leading to systemic amelioration of immune-suppression and reduction of MDSC accumulation in tumors. The therapeutic efficacy of SNAbs in terms of MDSC depletion was comparable to that reported in literature achieved with anti-Gr1 antibodies at a dose that is 10,000 times higher than that of SNAbs in our study. Furthermore, when the 4T1-tumor bearing mice were treated with MDSC-SNAbs, we observed significant inhibition on the tumor growth rate and a longer median survival time than that of the group treated with control particles

or left untreated. In summary, with MDSCs as a model target cell type, we have successfully proved our hypothesis that SNAbs, Janus nanoparticles with targeting ligands and Fc-mimicking ligands presented multivalently on the opposite surface areas, are an effective type of artificial antibody that can elicit specific depletion of target cells by antibody-mediated immune responses both *in vitro* and *in vivo*. The encouraging results obtained in this thesis research also prompt us to believe that SNAbs as a platform technology could be a functional alternative to monoclonal antibodies and widely applied in targeted immunotherapies for cancer.

## 6.2 Future Directions

Although we have successfully developed a new type of artificial antibody, the synthetic nanoparticles antibodies (SNAbs), there are still a number of limitations in the design of SNAbs that need to be addressed and further investigations on parameters that affect the function of SNAbs are also needed to make SNAbs a more powerful immunotherapeutic for cancer and various other diseases.

First of all, the generation of SNAbs relies on the production of Janus particles, whose yield from the solid-phase chemistry we designed so far is unable to meet the demand of studies in large animal models (e.g., dogs, primates) or human with a reasonable cost of time, money and labor. Scaling-up method using larger reaction vessels or bioreactors are possible solutions to increase the efficiency of the production process, as discussed in Chapter 3. Other technologies for Janus nanoparticle fabrication, such as, other immobilization method, electrohydrodynamic jetting and microfluidic systems, should be approached as an alternative method. The immobilization methods are widely used for producing inorganic Janus nanoparticles and require solid substrates to enable specific modification on certain area of the particles.[89] A side-by-side configuration was usually used in the electrohydrodynamic jetting and the microfluidic method and merging of two flows of polymers with delicate control of fluidic parameters yields Janus particles.[90,177] These methods all have the potential to produce large amount of Janus nanoparticles continuously, but different methods have weaknesses in different ways, such as the limitation in size of the particles produced and in the cost. [89,90,97,177,178] Besides, a change in Janus nanoparticle fabrication method may require switching to different nanoparticle materials (e.g., polymer, lipid).[89,90,178,179] The interaction between the material and

biological systems should be taken into consideration when making the choice, as some particulate systems themselves are immunogenic or toxic to cells. [180–182]

Another limitation of the designed SNAbs lies in the material selected to make the construct. Streptavidin-biotin specific reaction enables the easy conjugation of ligands on the SA-AuNP-SA nanoparticles. Streptavidin also endows negative charges to the nanoparticles, reducing the electrostatic interaction between the SNAbs and cell membranes. However, surface-coating of protein complexes the structure of SNAbs, and increased the instability of particles, resulting in a short shelf-life. Therefore, substituting streptavidin-biotin interaction with other chemistry, such as click-chemistry, could be a feasible option to improve the stability and structural simplicity of the SNAbs.[183–186] On the other hand, despite of their advantages due to the unique optical properties, gold nanoparticles are expensive starting materials, which increased the cost of SNAbs. Polymer particles (e.g.,poly(lactic-co-glycolic acid), PLGA) could be a potential good alternative option as they are cheaper in price and validated for safety in biomedical applications. [1,19] In fact, PLGA has already been used in fabricating Janus particles for drug delivery. [179,187,188]

Further investigation on the effect of nanoparticle size on the function of SNAbs is necessary as it is playing a key role in the biodistribution of SNAbs and interaction with cells, including immune cells.[23,189,190,191] Despite nanoparticles around 50 nm in size provide benefit in animal models, such as ease at reaching lymph nodes if injected subcutaneously or tumors if injected intravenously,[23,192] a larger size in similar size dimensions to the receptor patches on the cell surface could possibly be better at triggering Fc-receptor mediated signaling.[160] The size of the particles also determined the

distance of the effector cells and 'opsonized' target cells, which is likely to affect the induction of the immune responses.[193] So, it would be interesting to learn how the particle scaffold of different sizes (from nano- to micro-particles) affect the strength of responses triggered *in vitro* or *in vivo* by SNAbs. The constraints of size should be considered in terms of organs to target and toxicity for *in vivo* applications. For example, the larger SNAbs (>100 nm) could be applied in targeting cell types that primarily reside outside tumor or lymph nodes (e.g., liver, lung) or in diseases other than cancer (e.g., cystic fibrosis, autoimmune arthritis).

A consensus has already been reached that nanoparticles by themselves can interact with the immune systems, stimulating or suppressing both the innate and adaptive immune responses. Material, surface chemistry, charge, size and shape are factors that can be used to interpret and predict such interactions. For example, SiO2, TiO2, ZrO2, and Co nanoparticles were all shown to increase the expression of toll-like receptors and production of inflammatory cytokines of macrophages, while PLGA nanoparticles were shown to have immunosuppressive properties.[194,195] Due to the negatively charged sialic acid on the surface of macrophages, positively charged nanoparticles generally has higher potential to induce inflammation by interaction with macrophages and cationic particles in general has stronger capability to induce cellular response than anionic particles.[191,195] Nanoparticles could be rapidly internalized by phagocytes by interacting with scavenger receptors,[196] and could be taken up by non-phagocytes via via caveola- or clathrin-mediated processes, influenced by the size and shape of the particles.[195] Spherical particles are more readily to be taken up than rod-like particles and smaller particles (<100nm) tend to trigger more respiratory and gene toxicity in cells than larger ones. [195]

A corona composed of a large number of serum proteins on the surface of particles will be formed during circulation in the blood. Because of their specific surface chemistry, some particles, such as imidazole-modified chitosan and dextran-coated ionic oxide nanoparticles, absorb more C3, a complement protein, in the corona than unmodified chitosan or ionic oxide nanoparticles, as a result of which complement pathway activation was observed following the *in vivo* administration of those particles in mice.[196] Also, as mentioned in Chapter 3, surface chemistry influences the aggregation of nanoparticles, leading to different extent of particle agglomeration and different ways of interaction with the immune systems. Relevant to SNAbs, gold nanoparticles were shown to induce production of TNFα, IL-1β and IL-6 by phagocytes in a size-dependent manner, possibly through toll-like receptors.[84,197] Colloidal gold nanoparticles also increases the production of antibodies when introduced together with antigens in the animals, the mechanism of which is still unclear. [198] In addition, a significant fraction of PEGylated, 50 nm gold nanoparticles was reported to distribute in MDSCs after intravenous injection in mice.[80] However, the known immunogenicity properties of gold nanoparticles could not explain our findings that SNAbs, a Janus gold nanoparticles of 80-100 nm in hydrodynamic size coated with MDSC-targeting and Fc-mimicking ligands, could induce specific killing of MDSCs both *in vitro* and *in vivo*, while non-Janus of similar size and coated with same ligands did not. However, we could not exclude the possibility that material, surface chemistry, charge, size and shape of the SNAbs are contributing to the induction of MDSC-specific response. Therefore, it is definitely necessary to conduct further investigation using various approaches (e.g., computational simulation, signaling study) on the interaction between SNAbs and immune systems with

various types of control nano-constructs and optimize the physical and chemical properties of SNAbs for MDSC depletion. The knowledge acquired from such investigation will also guide the rational design of SNAbs targeting other cells of interest in the future.

Previous studies also suggested that Fc-receptor mediated responses are sensitive to the density of IgG molecular presented[159,199,200] Within a certain range, the higher the density of IgG on beads was, the stronger phagocytosis by macrophages was elicited through sequential ligation of Fc receptors.[200] However, a specific valency of Fc in the form of immune-complexes may actually block the activation of the FcγR systems.[159] Therefore, studying the stimulatory capability of SNAbs with various densities of Fc-mimicking ligands on the surface is necessary to elucidate the optimal valency for targeted depletion of cells in diseases.

In another aspect, the treatment strategy with MDSC-SNAbs in 4T1 breast cancer model still needs to be optimized in terms of route of administration, dosing, frequency and treatment duration. As discussed in Chapter 6, besides intravenous injection, subcutaneous, intratumoral and intramuscular injection could also be attempted for SNAbs for enhanced local therapeutic effect. Although we have achieved satisfactory level of target-cell depletion in spleen at the current dose of MDSC-SNAbs, we would like to test whether higher dosage could increase the efficacy of SNAbs in tumors and blood and further ameliorate the immunosuppression in tumor microenvironment to inhibit tumor growth and prolong survival. Lastly, frequency, treatment duration and time-points are key factors that influence the long-term treatment effect of SNAbs on cancer, so it is absolutely necessary to optimize these parameters in murine models.

Although ICI-MDSC-SNAbs combination therapy does not confer therapeutic benefit to the tumor-bearing mice over single ICI therapy, but SNAbs, as an artificial antibody, could potentially boost the therapeutic efficacy of other immunotherapies (e.g. adoptive T cell transfer), chemotherapy and radiotherapy in cancer. For example, doxorubicin-mediated MDSC depletion enhanced the effect of adoptive T cell transfer in a breast cancer murine model. [116] Trastuzumab (anti-Her) antibody was used in combination with first-line chemotherapy in metastatic breast cancer that overexpresses Her2 and achieved improved clinical response in patients.[201] Radiotherapy was proved to stimulate the immune system by broadening the T cell repertoire, activate DCs and making the radiated cells more vulnerable to T cell attack.[202] It is believed that the combination of radiotherapy and antibody-based immunotherapy could trigger stronger immunogenic cell death and achieve both local and abscopal effect.[203,204] Therefore, it is a good idea to combine MDSC-SNAb treatment with adoptive T cell transfer, chemotherapy or radiotherapy and evaluate whether these combinations has synergistic therapeutic effect in murine breast cancer models.

Moreover, encouraged by the exciting results in 4T1 breast cancer model, we would like test the potency of MDSC-SNAbs in other tumor models as well to expand the applications of MDSC-SNAbs. Actually, previous studies in mouse models have observed remarkable tumor regression after treatment with drugs that reduces MDSCs in melanoma[118], colon cancer[117] and lung cancer[115], so more specific targeting strategies to deplete MDSCs, like SNAbs, are likely to have therapeutic benefit in these tumors as well.

Lastly, we would like to develop a multitude of SNAbs targeting various other types of cells and proteins. SNAbs are designed as a flexible platform to mimic the function of monoclonal antibodies to remove the factors (i.e., proteins, cells) that cause the physiological disorders or playing a promoting role in the progression of the diseases, such as cancer and autoimmune disease. Some examples of such targets are Her2-expressing human breast cancer cells and IL-4 protein in the autoimmune disorders. By activating the innate immune responses to remove such targets, SNAbs can either be a single therapy or a part of a combination therapy to improve the current treatment strategies for diseases. In the long run, SNAbs could also be used as antibodies in diagnosis of diseases and detection technologies, such as enzyme-linked immunosorbent assay (ELISA). All in all, we believe that SNAbs are a novel, promising type of artificial antibody that has wide application possibilities and strong therapeutic potential.

# APPENDIX A. MORE INVESTIGATION ON THE BINDING OF PEPTIDES OR NANOPARTICLES ON CELLS

## A.1 Cp33 binding on Fc receptor-expressing macrophages

Macrophages have high Fc receptor expression and are important mediators of antibody-mediated responses. We have repeatedly validated the binding of cp33 peptides on macrophages. It is also necessary to know whether the binding of cp33 on macrophages is dependent by the relative expression level of specific Fc receptor types and the activation of macrophages to determine the condition for *in vitro* effector-target cell co-culture assays used to test the biological function of SNAbs.

### A.1.1 Materials and methods

#### *A.1.1.1 Materials*

DMEM complete medium for the cell culture and FACS buffer were prepared in the same way as described previously in chapter 4. The recombinant murine interferon gamma (rmIFNγ) protein was purchased from PeproTech. Inc. The anti-CD16-PE antibodies were purchased from R&D Systems and anti-CD32-PE antibodies were purchased from eBioscience, Thermofisher Scientific. Streptavidin-FITC conjugates, CellMask Orange plasma membrane stain kit, and ProLong Gold antifade mountant were purchased from Thermofisher Scientific. The Corning Poly-L-lysine coated-12mm diameter, round coverlips were purchased from Fisher Scientific.Inc.

*A.1.1.2 Fc receptor expression on macrophages primed with rmIFNγ*

RAW 264.7 macrophages were passaged and resuspended into DMEM complete medium with rmIFNγ 25 ng/mL. Cells were cultured for overnight at 37 ℃. The rmIFNγ-primed and unprimed macrophages were then transferred into separate FACS tubes, 1 million/tube. Following washing with PBS by centrifugation at 500 g for 5 mins, the cells were stained with anti-CD16-PE antibodies or anti-CD32b-PE antibodies in FACS buffer at 4 ℃ for 30 mins in dark and then washed again with FACS buffer. After resuspension in 200 μL of FACS buffer, the samples were analyzed using a BD Accuri C6 benchtop flow cytometer.

*A.1.1.3 Quantitative evaluation of cp33 binding on macrophages primed with rmIFNγ.*

RAW 264.7 macrophages were primed in the same way as described in A.1.1.2 or keep unprimed. After transferring to FACS tubes, the cells were incubated with 10 μM cp33-biotin for 1 hr at 4 ℃ in PBS followed by washing with FACS buffer. The control samples were left untreated until the next step. After incubation, all the cells, except the control samples, were stained with streptavidin-FITC conjugates 5 μg/tube in PBS for 1 hr at 4 ℃. After washing, the cell samples were resuspended in 200 μL of FACS buffer and analyzed on BD Accuri C6 flow cytometer.

*A.1.1.4 Quantitative evaluation of cp33 binding on macrophages blocked with anti-CD16/CD32 antibodies*

RAW 264.7 macrophages were primed in the same way as described in A.1.1.2 or keep unprimed. After transferring to FACS tubes, half of the tubes were treated with anti-

CD16/CD32 antibodies 2 μL /tube in 50 μL of FACS buffer for 10 mins in 4 ℃. Then, all the cells, except the control samples, were incubated with 10 μM cp33-biotin for 1hr at 4 ℃ in PBS followed by washing with FACS buffer. The cells were then stained with streptavidin-FITC conjugates 5 μg/tube in PBS for 1 hr at 4C. After washing, the cell samples were resuspended in 200 μL of FACS buffer and analyzed on BD Accuri C6 flow cytometer.

*A.1.1.5 Confocal microscopic imaging of cp33-modified nanoparticles binding on macrophages*

Janus gold nanoparticles SA-AuNP-SH were modified with the cp33-biotin and Alexa Fluor 647-maleimide (AF647) using the method described in chapter 2. The modified particles were purified with dialysis to remove the excessive ligands and dye. RAW 264.7 macrophages were seeded on poly-L-lysine coated cover slips at 200,000 cells per well in 1mL DMEM complete medium and treated with 25 ng/mL rmIFNγ in 24 well plates for overnight at 37 ℃. After priming with rmIFNγ, the cells were washed with PBS and stained with 1×CellMask Orange solution 300 μL /well for 10 mins in 37C. Following another wash with PBS, the particles, i.e., SA-AuNP-SH-AF647 or cp33-AuNP-SH-AF647, were added to the cells, and incubated at 4 ℃ for 1 hr. The cells were then fixed with cytofix solution for 30 mins at 4 ℃ in dark and stained with DAPI (1:1000 dilution) for nucleus at 10 mins in dark. The coverslips were mounted with ProLong Gold antifade mountant on glass slides and then sealed with nail polish. The slides were imaged with a Perkin-Elmer spinning disk microscope.

### A.1.2 Results

#### *A.1.2.1 The effect of rmIFNγ on Fc receptor expression on macrophages*

CD16 and CD32b are the two Fc receptors that have high binding affinity with mouse IgG1, the possible most relevant mouse IgG isotype to cp33. We evaluated whether priming with rmIFNγ could affect the expression of CD16 and CD32b on macrophages by flow cytometry and this information was used to guide the design of experiments for ADCC and ADCP with macrophages. The mean fluorescence intensity showed the average expression level of each type of receptors on the cells. Clearly seen from the results, overnight priming with rmIFNγ increased the amount of CD16 and CD32b on the macrophages by over three folds. Meanwhile, the expression of F4/80, which is the M1 macrophage marker, and CD11b, which is the monocyte marker, were decreased due to rmIFNγ priming.

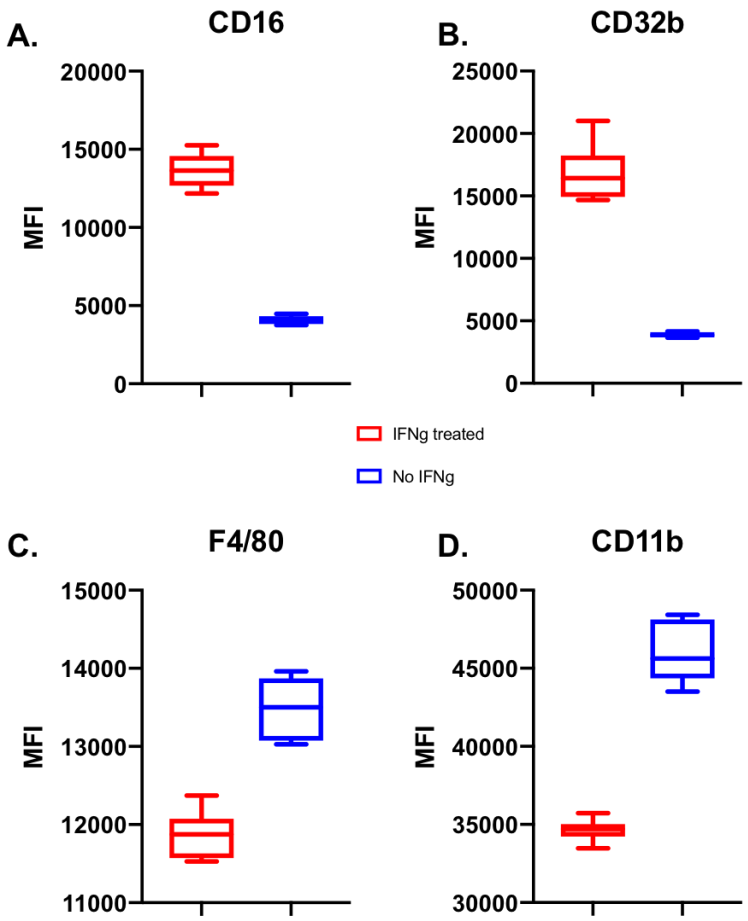


Figure A 1. RmIFNγ treatment affected the expression of CD16, CD32b, F4/80, and CD11b on RAW 264.7 macrophages.

*A.1.2.2 The binding of cp33 on macrophages unprimed or primed with rmIFNγ*

As shown in A.1.1, rmIFNγ priming changes the expression of CD16 and CD32b, which are likely to be the binding partner of cp33. We wanted to see if this in turn affects the binding level of cp33 on macrophages. By probing the biotinylated cp33 with fluorescent streptavidin, we saw that cp33 clearly bound strongly to macrophages. However,

rmIFNγ-boosted increase in CD16 and CD32b didn't enhance the binding of cp33 on the cells.

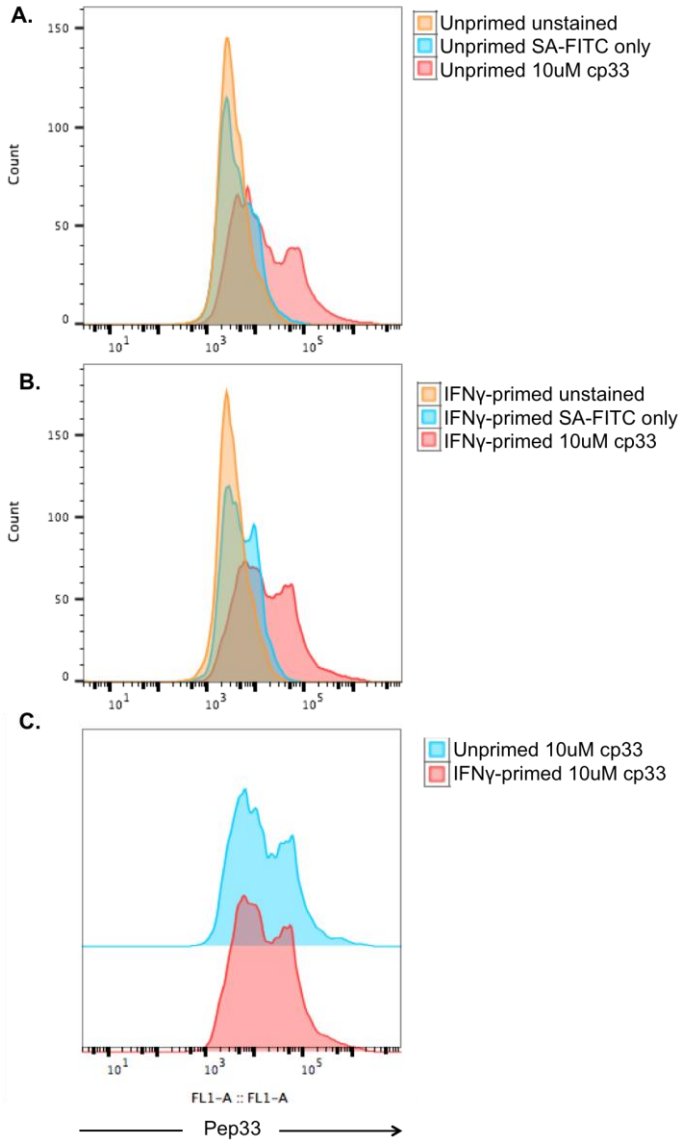


Figure A 2. RmIFNγ-primed and unprimed macrophages have similar cp33 binding profile. RAW macrophages were primed with rmIFNγ 25ng/mL or left unprimed in medium for overnight and then treated with cp33-biotin and probed with streptavidin-FITC. The unprimed (A) and primed macrophages (B) were analyzed on a BD Accuri C6 flow cytometer. The samples treated with cp33 (red) were compared with samples untreated (blue) and unstained sample (yellow). The cp33 binding profiles on rmIFNγ-primed samples (red) and unprimed samples (blue) were compared side by side in C.

*A.1.2.3 The binding of cp33 on macrophages treated with anti-CD16/CD32 antibodies*

To further study whether CD16 and CD32 are important for cp33's binding on macrophages, we tested the binding of cp33 with or without the presence of anti-CD16/32 antibodies. Interestingly, the blockade of CD16 and CD32 also didn't affect the binding of the peptides.

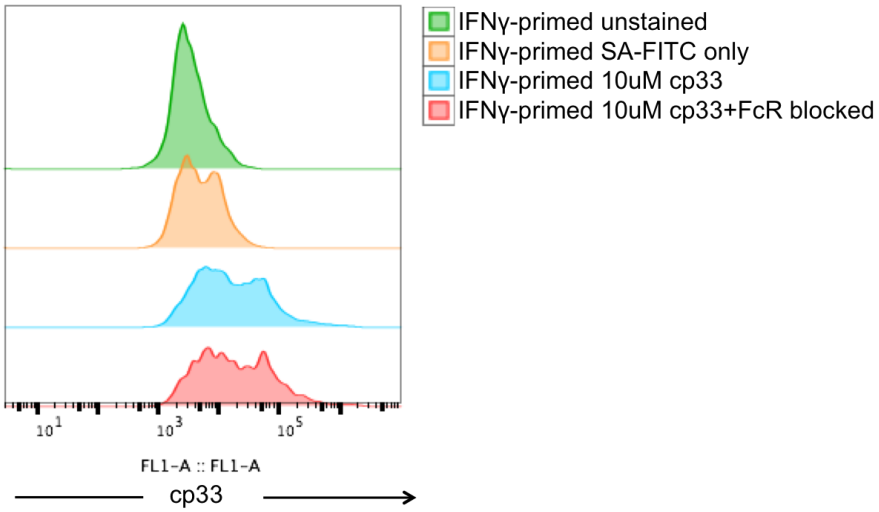


Figure A 3. Anti-CD16/CD32 treatment didn't affect the binding of cp33 on RAW 264.7 macrophages. Red: cp33-biotin (10 μM) binding on RAW macrophages primed with rmIFNγ (25ng/mL) for overnight and treated with anti-CD16/CD32 antibodies; Blue: cp33-biotin (10 μM) binding on RAW macrophages primed with rmIFNγ (25 ng/mL) for overnight and untreated; Orange: SA-FITC control without cp33-biotin on RAW macrophages primed with rmIFNγ (25 ng/mL) for overnight and untreated; Green: unstained RAW macrophages primed with rmIFNγ (25 ng/mL) for overnight.

*A.1.2.4 Cp33-modified Janus gold nanoparticles bound on RAW 264.7 macrophages*

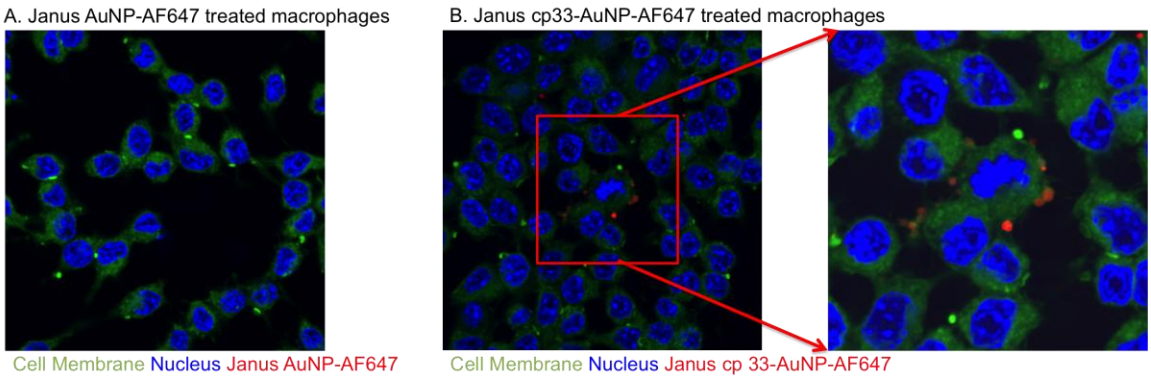


Figure A 4. Cp33-modified Janus AuNP bound on macrophages. A. Janus AuNP-AF647 control particle-treated macrophages; B. Janus cp33-modified AuNP-AF647 particles-treated macrophages. Red: Janus nanoparticles; Blue: Nucleus; Green: Cell Membrane.

As described in the method section, we imaged the particle-treated macrophages under confocal microscope. Because the size of the nanoparticles (30nm) was under the detection limit of the confocal microscope, only clustered nanoparticles can be seen on the image. Clearly, the unmodified Janus AuNP-AF647 didn't bind on the cells, while the Cp33-AuNP-AF647 crosslinked the Fc receptors and circled around the cell membrane. The binding on the Fc receptors by Cp33 forced the nanoparticles to cluster together and gave detectable signals on the confocal images.

### A.1.3 Discussion

CD16 is FcγRIII, the activating receptors highly expressed on macrophages and NK cells that mediate the antibody-dependent cellular responses, while CD32b is the only inhibitory receptors that also bind with IgG strongly but negatively regulates the antibody responses. CD32b was not expressed on NK cells. As shown in A.1.2.1, rmIFNγ treatment increased the expression of both CD16 and CD32b, as a result of which it is

hard to tell whether the macrophages would become more or less activated after priming. However, more and more evidence emerged that the effective antibody-mediated immune responses on monocytes have to do with both activating and inhibitory Fc receptors,[5,132,134] so in the experiments where we tested the functions of MDSC-SNAbs with macrophages, we usually primed the macrophages with rmIFNγ before the assay. $CD11b^{+}F4/80^{+}$ defines the classically activated M1 macrophages and rmIFNγ plus LPS (lipopolysaccharide) treatment was usually used to polarize the macrophages and dendritic cells towards the M1 phenotype.[205] However, what we observed was contradictory to it. After rmIFNγ treatment, the expression level of F4/80 and CD11b was decreased. Taking into consideration that we didn't treat the macrophages with LPS and the RAW 264.7 is a stable M1-like cell line, the observation is not completely unreasonable. Also, the down-regulation of expression of F4/80 and CD11b does not necessarily mean the reversion of M1 polarization. Therefore, the observation was regarded as an important side-effect to know of rmIFNγ-treatment on RAW 264.7 macrophages.

Anti-CD16/CD32 antibodies were used to block the binding of cp33 onto CD16 and CD32. However, the blockade didn't decrease the amount of cp33 bound onto macrophages. Two possible reasons are that cp33 mainly bind to FcγRI and cp33 is a small molecule whose binding sites on CD16 and CD32 were not blocked by the anti-CD16/CD32 antibodies. While we were not able to test the blockade of all four FcγRs due to the unavailability of the blocking reagents, we could further investigate if CD64 (FcγRI) blockade significantly affect the binding of cp33 on macrophages. Lastly, the

confocal imaging clearly indicated that cp33 is important for the binding of Janus nanoparticles on the macrophages.

## A.2. Fc receptor expression on splenocytes

FcγRs are essential for the antibody-dependent immune responses and the targeted depletion of cells by SNAbs. Splenocyte suspensions are used in Aim 2 to evaluate the functions of MDSC-SNAbs for specific killing of MDSCs. However, the majority of splenocytes have FcγR expression, including MDSCs themselves. Therefore, it is important to assess the level of expression of each type of FcγRs to shed light on the possible impact of SNAbs on these different types of cells in the system *ex vivo* as well as *in vivo*.

### A.2.1 Materials and methods

#### *A.2.1.1 Materials*

For cell type sorting, the anti-Gr1-biotin, anti-F4/80-biotin, anti-CD11c-biotin, anti-CD49b-biotin, anti-B220-biotin, anti-CD3-biotin antibodies were purchased from Biolegend. The anti-biotin microbeads and LS column were purchased from Miltenyi Biotechnology. For staining in flow cytometry, the purified anti-mCD32, anti-mCD64-APC, anti-mCD16.2-PE/Cy7, Armenian Hamster IgG-PE/Cy7, mouse IgG1,k-APC, rat IgG2a,k-PE were purchased from Biolegend. The anti-CD16-PE antibodies were purchased from R&D Systems. The anti-FcRn was purchased from Sigma Aldrich. The secondary antibodies anti-rat IgG Alexa fluor 555 (AF555) and anti-rabbit Alexa fluor

647 (AF647) were purchased from Thermofisher Scientific. The MACS buffer and FACS buffer were prepared as described in Chapter 4.

*A.2.1.2 Isolation of different cell types with magnetic activated cell sorting (MACS).*

The spleens of 4T1-tumor bearing mice were harvested on day 16 post tumor inoculation and then processed into single cell suspension using the same method as described in chapter 4. The resulting cell suspension was divided into six equal parts in six tubes. Cells were spun down and resuspended in MACS buffer, followed by incubation with biotinylated antibodies at 20 μg/mL for each cell type, i.e., MDSCs (anti-Gr1-biotin), macrophages (anti-F4/80-biotin), DCs (anti-CD11c-biotin), NK cells (anti-CD49b-APC), B cells (anti-B220-biotin), T cells (anti-CD3-biotin) for 10 mins at 4 ℃. The cells were then washed with 5 mL of MACS buffer, resuspended into 800 μL and then incubated with anti-biotin beads 200 μL /tube for 10mins at 4 ℃. Cell sorting was performed for each cell type according to the manufacturer's protocol with LS columns. The concentration of collected cell suspensions was counted with hemocytometer and trypan blue.

*A.2.1.3 Flow cytometry analysis of Fc receptor expression on immune cells in spleen*

The cell samples were divided into two panels for the staining with different anti-Fc receptor antibodies. The first panel of the cell samples was stained with anti-mCD64-APC, anti-mCD16.2-PE/Cy7, and anti-CD16-PE and fluorescent antibodies for each cell marker (Gr1, F4/80, CD11c, CD49b, B220, CD3). Isotype controls were prepared with the corresponding isotype antibody. The second panel of the cell samples were stained with anti-mCD32 followed by staining with anti-rat IgG-AF555 and anti-mFcRn

followed by staining with anti-rabbit IgG-AF647. For the second panel, no-primary-antibody control and no-secondary-antibody control samples were prepared as well to help with data analysis. After removing excessive antibodies, the cells were fixed with cytofix buffer and analyzed on a BD LSRFortessa flow cytometer.

### A.2.2 Results

*A.2.2.1 CD64, CD16, and CD16.2 expression on the splenocytes.*

In accordance with literature reports, macrophages and DCs express the most CD64 (FcγRI) on the cell membrane, while other cells almost have no expression of CD64 (Figure A5).

In terms of CD16, a higher percentage of NK cells expresses this Fc receptor, however, macrophages, MDSCs, as well as DCs all have a considerable population of cells expressing CD16 (Figure A6).

Interestingly, a part of DCs has a highest abundance of CD16.2 receptors, followed by macrophages and MDSCs, which have a moderate expression of CD16.2. Surprisingly, we also detected CD16.2 expression on NK cells and a little bit on T cells and B cells, which is not reported in previous published literatures[206] (Figure A7).

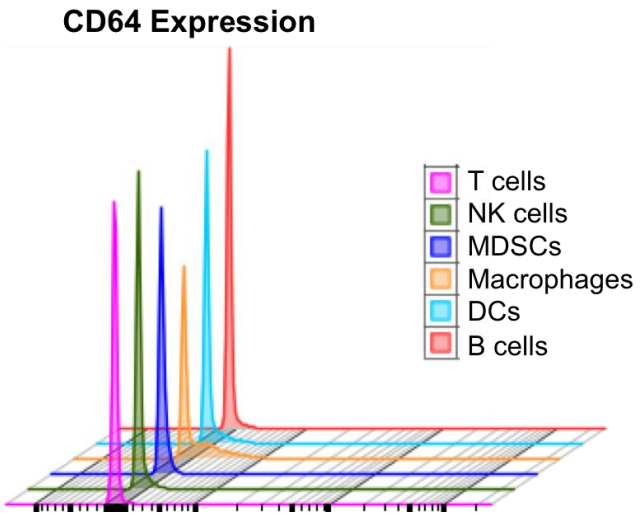


Figure A 5. Expression of CD64 on major cell types in splenocytes.

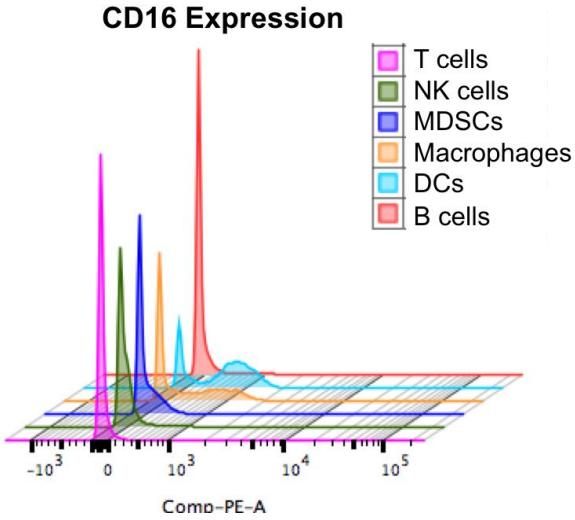


Figure A 6. Expression of CD16 on major cell types in splenocytes.

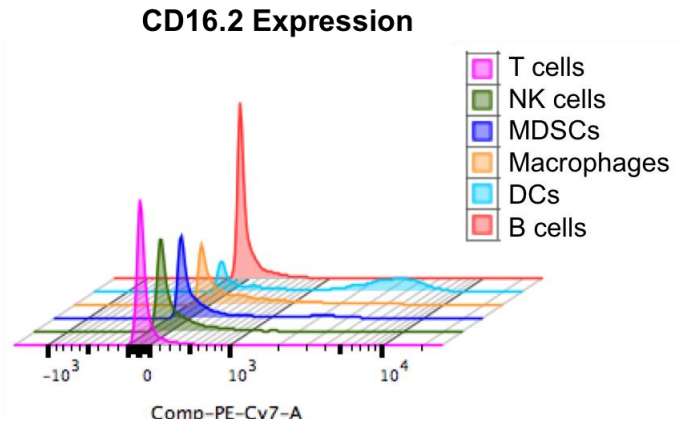


Figure A 7. Expression of CD16.2 on major cell types in splenocytes.

*A.2.2.2 CD32, FcRn expression on the splenocytes*.

CD32 and FcRn expression are so minimal that we could hardly detect any on most of the cells types (MDSCs, macrophages, DCs, NK cells and B cells). However, we did see a significant percentage (10% or so) of $CD3^+$ T cells showing signals in PE channel, indicating expression of CD32, but we could not exclude staining error because the control samples also have high fluorescence. Therefore, we concluded that the expression of CD32 and FcRn are not strong on splenocytes.

**A.2.3 Discussion**

A summary of Fc receptor expression on the major cell types in splenocytes were given below in Table 5:

Table 5. Expression of Fc receptors on the major cell types of splenocytes

| | MDSC | NK | Macrophage | B cell | DCs | T cells | CD4 T cells | CD8 T cells |
|---|---|---|---|---|---|---|---|---|
| CD64 (FcRI) | ++ | - | +++ | + | ++ | - | - | - |
| CD32 (FcRII) | N | N | Y | N | Y | Y | Y | Y |
| CD16 (FcRIII) | ++ | ++ | +++ | ++ | ++++ | + | Y | Y |
| CD16.2 (FcRIV) | ++ | - | ++ | + | ++++ | - | - | - |
| FcRn | N | N | Y | Y | Y | Y | Y | Y |

Two important things to note in the above table are: one, for CD64, CD16, CD16.2, the number of "+" indicates the level of expression, and "-"means no expression; second, for CD32 and FcRn, because the signal detected on cells were very little, we could not quantitatively compare the expression level. Here, Y means expression observed, N means no expression.

In mouse, there are four major types of FcγRs, i.e.,CD64 (FcγRI), CD32 (FcγRIIa, FcγRIIb),, CD16 (FcγRIII),, CD16.2 (FcγRIV), and one neonatal Fc receptors, FcRn. Among them, FcγRIIb is the only inhibitory receptors that contain an intracellular immunoreceptor tyrosine-based inhibition motif (ITIM) to suppress the antibody-mediated immune responses. All other types of Fc receptors are important mediators for ADCC and ADCP with antibodies. Mouse IgG1 binds more strongly to FcγRIIb and FcγRIII, while human IgG1 bind to all four types of Fc gamma receptors modestly.[56,155] The FcRns are main regulators of the serum half-lives of IgG and bind with all types of isotypes.[13] Our results are in accordance with the literature reports on the Fc receptor expression pattern of macrophages and dendritic cells. Both dendritic cells and macrophages have high expression of FcγRI, FcγRIII, FcγRIV and some expression of FcγRIIb and FcRn, showing the potential of these two cell types being effector cells for ADCC and ADCP. NK cells only has strong expression of FcγRIII and can mediate robust ADCC with IgG1, IgG2a and IgG2b. B cells were detected to have little expression of FcγRI, FcγRIII and FcγRIV, and it is still under debate whether B cells can also conduct antibody-dependent innate immune responses. What was conflicting in our results with previous studies is that we saw light expression of CD16 and CD32. As the staining results on surface markers showed that the purity of cells isolated with the biotinylated antibodies were not 100%, we cannot exclude the possibility of false signal from other cell types in the T cell samples. Last but more importantly, MDSCs were observed to have expression of FcγRI, FcγRIII and FcγRIVs. This testified the binding of cp33 and cp33-modified nanoparticles on MDSCs. It is also one of the factors that complicated the results of killing assays and mechanism *in vivo* studies. Despite the

possibility of MDSCs quenching the cp33 on SNAbs due to the expression of the Fc receptors, we can conclude from the above discussed experiment that macrophages, NK cells and possibly DCs are the major effector cells of ADCC/ADCP induced by SNAbs.

# APPENDIX B. MECHANISM OF ACTION STUDIES

An antibody-opsonized cell crosslinks the FcγRs and triggers ADCC or ADCP to remove the cell targets by phagocytes or other effector cells, such as NK cells. Different FcγR will signal slightly differently, and different cells will mediate the ADCC/ADCP in different ways. However, there are common signaling events occurring in the process. The process elicited by the clustering of FcγRs includes the release of cytokines, production of reactive oxygen or nitrogen specifies, secretion of enzymes, proliferation, phagocytosis and antigen presentation.[134] The majority of these events are mediated by the ITAM phosphorylation with the support of calcium fluxes and ATP. As the Fc-mimicking peptides, cp33, are multivalently presented on the surface of the nanoparticles, we hypothesized that the SNAbs by themselves can crosslink FcγRs and induce the signaling cascades. In Appendix B, we documented the signaling studies we did with SNAbs and macrophages as a model type of effector cells and discussed how the results proved the hypothesis is incorrect.

## B.1 Materials and methods

### B.1.1 Materials

2',7'-Dichlorodihydrofluoroscein Diacetate (DCFH-DA), phorbol 12-myristate 13-acetate (PMA), hydrogen peroxide ($H_2O_2$), ionomycin,and vanadium (III) chloride ($VCl_3$) were purchased from Sigma Aldrich. Rat anti-mouse CD16/32 and AF647 anti-mouse CD64 antibodies were purchased from Biolegend. AF555- and AF633-conjugated Goat anti-rat IgG (H+L) secondary antibodies, Indo-1, AM calcium binding dye, Griess

reagent kit, Celltrace CFSE, propidium iodie (PI), RNAse I, Dihydrorhodamine 123 and microBCA kit were purchased from Thermofisher Scientific. Recombinant human IFN-gamma protein (rhIFNγ) and the mouse TNFα ELISA kit were purchased from R&D Systems. The recombinant mouse IFN-gamma protein (rmIFNγ) and recombinant murine M-CSF were purchased from PeproTech.Inc. The anti-Her2 human IgG1 was purchased from InvivoGen. Rabbit anti-SYK 352 or 525/526 antibody, anti-actin antibodies and Tris-buffered-saline solution were purchased from CellSignaling Technology.Inc. The RIPA lysis buffer was purchased from Boston Bioproducts. Inc. The LaemmLi sample-loading buffer was purchased from Amresco. Inc. The Platt Lab in Georgia Institute of Technology was acknowledged for providing SDS-PAGE gels and donkey anti-rabbit secondary monoclonal antibodies, IRD-800CW conjugated, from LI-COR Biosciences. The phosphotase inhibitor, PhosStop, was purchased from Sigma-Aldrich. The protease inhibitor mini tablets and PVDF membrane were purchased from Thermofisher Scientific. The pre-stained Chamleon DUO protein standard and Odesey TBS buffer were purchased from LI-COR Biosciences. U937 human monocyte-like cell line was purchased from ATCC and cultured in RPMI 1640 medium supplemented with 10% FBS and 1% PS. RAW 264.7 macrophages were cultured in DMEM medium supplemented with 10% FBS and 1% PS. Bone marrow derived macrophage (BMDM) culture medium is high glucose DMEM supplemented with 10% heat-inactivated FBS and 1×beta-mercaptoethanol, 1mM sodium pyruvate, 1×non-essential amino acid and 10 nM HEPES.

### B.1.2 Western blotting of Syk phosphorylation

RAW macrophages and U937 cells were passaged and washed with cold 1% BSA in PBS solution. The cells were then resuspended in $4.6\times10^7$/mL, $1.9\times10^7$/mL for RAW

macrophages and U937 cells respectively. The resuspended cells, 50 μL of RAW macrophages and 100 μL of U937 cells, were added to eppendorf microcentrifuge tubes and treated with 50 μL of 10 mM $H_2O_2$ or SNAbs ($3\times10^{11}$/mL) or left untreated for 5 mins, 10 mins or 30 mins at 37 ℃. The cells were then washed with 1% BSA in PBS solution and lysed with 50 μL RIPA buffer on ice, shaking at 150 rpm for 30 mins. The lysed cells were centrifuged at 16000 g for 20 mins at 4 ℃. The supernatant containing proteins were transferred to a new tube. Part of it was used for measurement of protein concentration with a microBCA kit. The protein samples were stored at -20 ℃ until use. A 10% SDS gel was prepared according to the Platt Lab recipe with Protogel, TEMED, 1-Butanol and DI $H_2O$. The sample buffer was prepared with RIPA buffer, PhosStop and protease inhibitors and the protein samples. SDS-PAGE was run with 30 μL of the collected protein samples or the pre-stained Chamleon DUO protein standards. Afterwards, the protein in the gel was transferred to the PVDF membrane using semi-dry method. The protein left on the gel was stained with Ponceau S staining solution. The membrane was washed with TBS-0.05% Tween solution and blocked with Odessey TBS blocking buffer for 1 hr at room temperature. The membrane was then stained with 1:1000 dilution of primary antibodies, i.e.,anti-SYK-352 (Zap 70) or anti-SYK-525/526 and anti-β actin antibodies at 4 ℃ for overnight. After washing, the membranes were stained with donkey anti-rabbit IRD-800CW secondary antibodies at a 1:5000 dilution in TBS-0.1% Tween buffer for 1 hr at room temperature. After washing, the membranes were imaged with an Odyssey Imaging System.

### B.1.3 Calcium refluxes

RAW 264.7 macrophages were primed with rmIFNγ 25 ng/mL for overnight. Alternatively, U937 cells were primed with rhIFNγ 1000 U/mL for 72 hrs. For antibody-mediated Fc receptor crosslinking, macrophage cells were coated with anti-CD16/CD32 antibodies for 30 mins at 37 ℃ followed by washing with calcium-free PBS. The primed cells, including the anti-CD16/CD32-treated cells were resupsended into 1 million/mL in complete medium with 5 μM Indo-1, AM and incubated at 37 ℃ for 1 hr. Cells were then washed and resuspended with PBS buffer. Afterwards, cells were seeded in FACS tubes or black-bottom 96-well plates and treated with peptide-modified nanoparticles (1-5 $\times 10^{10}$/sample), ionomycin (10 μg/mL), or secondary antibodies (15 μg/mL). The samples were analyzed on a BD LSRFortessa flow cytometer or a Biotek Cytation 5 plate reader immediately after adding treatment for the kinetic changes in the intracellular or overall calcium concentration.

### B.1.4 Production of reactive oxygen species

RAW 264.7 cells or U937 cells were passed and resupended in PBS at $1 \times 10^6$/mL for RAW macrophages and at $5 \times 10^6$/mL for U937 cells. Cells were seeded into FACS tubes, 150 μL per tube, and incubated with 150 μL of 40 μM DCFH-DA in PBS solution for 30 mins at 37C in dark. Following washing with 1 mL of PBS, RAW macrophages were either treated with anti-CD16/CD32 antibodies or peptide-modified nanoparticles for a desired period of time (30 mins, 1 hr, 2hrs). Similarly, the U937 cells were treated with anti-human CD64-AF647 or peptide-modified nanoparticles. As positive controls, the RAW macrophages or U937 cells were treated with $H_2O_2$ 100 mM for at least 1hr in 37C.

The anti-CD16/CD32 antibodies-treated RAW cells or the anti-CD64-treated U937 cells were washed and subsequently treated with AF633-conjugated goat anti-rat IgG (H+L) secondary antibodies for RAW cells and AF647-conjugated goat anti-mouse IgG (H+L) secondary antibodies for U937 cells at 37 ℃ for 1hr. The cells were further washed and analyzed with three methods: 1. flow cytometry analysis on a BD LSRFortessa cytometer; 2. fluorescence measurement on a Biotek Synergy HT plate reader;3.imaging of the samples on a Biotek LionHeart FX automated microscope. Dihydrorhodamine 123 (DHR) was also used in some experiments according to the protocol of the manufacturer to detect the oxidative burst of the macrophages or monocytes.

**B.1.5 Production of reactive nitrogen species**

RAW 264.7 macrophages were primed with rmIFNγ 25ng/mL for overnight and then seeded into a clear bottom 96 well plate at $0.5\times10^5$ per 150 uL in each well. The macrophages were treated with $1\times10^{10}$ peptide-modified nanoparticles or unmodified SA-AuNP-SA in 50 μL of PBS for 16-24 hrs. $VCl_3$ solution was prepared by dissolving 51.1 mg of $VCl_3$ in DI water and then mixed with 20 mL of 1M HCl solution. The Griess reagent solution was prepared by adding 770 μL of component A and component B in a tube and mixed with 10 mL of the prepared $VCl_3$ solution. The supernatant from the treated macrophages was added to a fresh 96 well clear-bottom plate, 150 μL/well, followed by adding 150 μL of the prepared Griess reagent solution. A standard curve was prepared on the same plate with a series of dilutions of the 1M nitrite solution provided in the Griess reagent kit. The plate was incubated at RT for 30 mins in dark and read at 548nm for the quantification of nitrate in the supernatant.

### B.1.6 Culture of bone marrow derived macrophages

Bone marrow derived macrophages were differentiated from the bone marrow cells isolated from femurs and tibias of naïve Balb/c or C57BL/6 mice of 6-16 weeks old. Briefly, the bone marrow cells were isolated from the bones using the method described in chapter 5 and then seeded in a petri dish, 3 to 4.5 million cells per 20 mL of BMDM medium with 20 ng/mL M-CSF. Ten milliliter of old medium was aspirated and replaced with 10 mL of fresh BMDM medium containing 40 ng/mL of M-CSF on day 3 and day 6 after seeding. The cells were ready to use on Day 7.

### B.1.7 Proliferation of bone marrow derived macrophages

According to a paper published by Yong Luo, et. al.,[207] bone marrow derived macrophages (BMDM) were starved for M-CSF for two days from day 5 after seeding. On day 7, the BMDMs were harvested and then stained with Celltrace CFSE 10 μM in PBS at 37 ℃ for 30 mins. CFSE staining was quenched by incubating the cell suspension with DMEM medium for 5 mins at room temperature and then the cells were washed with medium by centrifugation at 500 g for 5 mins twice. Cells were resuspended in DMEM at $0.5\times10^6$/mL and seeded in a coated 12 well plates, 1mL/well. Twelve-well plates were pre-coated with human IgG1 or BSA at 10, 20, 40 μg/mL for overnight at 4 ℃ and washed with PBS. At desired time-point (2,5,8 hr), cells were harvested and fixed with BD cytofix buffer. Fixed cells were subsequently stained with 1 μL /ml PI with 10U of RNAse for 20 mins at room temperature. The cells were analyzed on a BD LSRFortessa flow cytometer within 2 hours after staining.

## B. 2 Results

### B.2.1 Syk Phosphorylation

Previous studies reports strong phosphorylation of Syk at Tyrosine 525/526 position and Zap70 (Syk-Tyrosine 352) triggered by the crosslinking of FcγRs by immune-complexes, and the event was time-dependent and hard to capture.[155,158,159,200] We chose the specific time points, 5, 10 and 30 mins tested by the above-mentioned studies to detect the phosphorylation of Syk induced by the SNAbs. However, we only observed strong upregulation of phosphorylated Syk-Tyrosine 362 by the positive treatment, $H_2O_2$, but no difference between the SNAb-treated samples and negative controls at all time points.

### B.2.2 Calcium fluxes

The calcium refluxes in monocytes triggered by FcγR crosslinker is usually reported as the maximum relative fluorescence units detected during the measurement. The events happen within minutes after FcγR crosslinking. As it was hard to control the start of signal acquisition by manually addition of treatment (ionomycin, nanoparticles or buffer), for the trials with both RAW macrophages and U937 cells, we only got fluctuating signals, which was hard to distinguish from noise. Longer kinetic measurement introduced bleaching of the Indo-1, AM calcium-binding dye. The Biotek Cytation 5 plate reader and the LionHeart automated imaging microscope allows automated addition of treatments. However, we could not prepare enough nanoparticle formulations to rinse, wash and fill the injection tubing and the automated injection system only allows two types of treatment at a time, which did not satisfy the needs of the experiments.

### B.2.3 Production of reactive oxygen species

DCFH-DA is freely permeant to cell membranes and will be oxidized to green-fluorescent calcein after reacting with reactive oxygen species (ROS) in the cell, so the fluorescence intensity of the cell after labeling with DCFH-DA is a measurement of the intracellular ROS concentration. We didn't observe significant changes in ROS production upon treatment with nonJanus AuNP-cp33 particles or G3-SNAbs compared to DCFH-DA stained untreated cells (Figure B1). Also, the induction of ROS production by crosslinking of Fc receptors using anti-FcγR primary antibodies (anti-mouse CD16/CD32 for RAW macrophages, anti-human CD64 for U937 cells) and secondary antibodies (anti-rat IgG and anti-mouse IgG antibodies) was also not significant compared to single primary- or secondary-antibody-treated samples. We also tried dihydrohodamine 123 (DHR) for the oxidative burst in the macrophages after treatment with SNAbs and didn't observe any detectable changes.

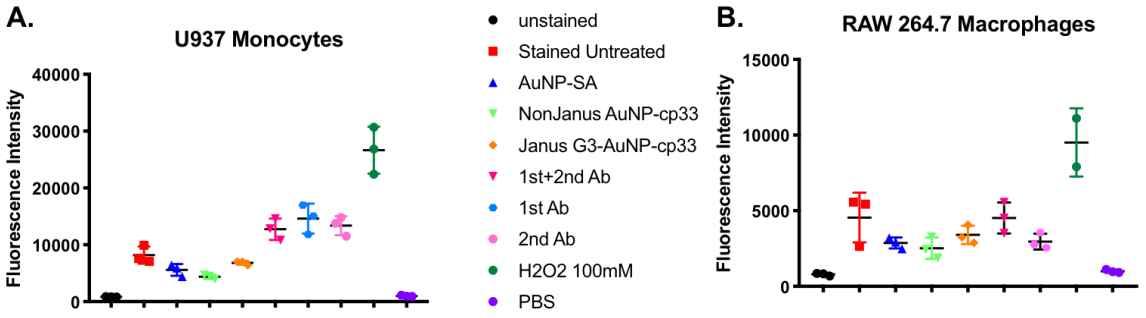


Figure B 1. ROS production by U937 monocytes and RAW 264.7 macrophages after treatment. U937 cells and RAW 264.7 macrophages were stained with DCFH-DA and seeded in 96 well plates. The production of ROS was measured by quantification of the fluorescence in FITC channel of each sample on the plate reader after 1 hr treatment with the indicated formulations shown on the legend. A shows the ROS production of U937 monocytes and B shows that of the RAW 264.7 macrophages.

### B.2.4 Production of reactive nitrogen species.

In the assay, we used $VCl_3$ to reduce all the nitrate into nitrite for the quantification of reactive nitrogen species (RNS) production with a Griess Reagent kit. The calculation of the RNS concentration was enabled with a standard curve prepared by diluting the known-concentration nitrite solution. During the optimization of the SNAb fabrication method, we tested the reliability of RNS production as one of quality control methods for SNAb fabrication. Obviously, the treatment of SA-AuNP-SA alone induced increase in the production of RNS by macrophages, but G3-SNAbs didn't augment the response consistently (Figure B2). The PBS buffer also contributed to the noisiness of the results. As the RNS production results varied a lot from time to time and from batch to batch, we determined that it is unreliable for testing the functionality of SNAbs.

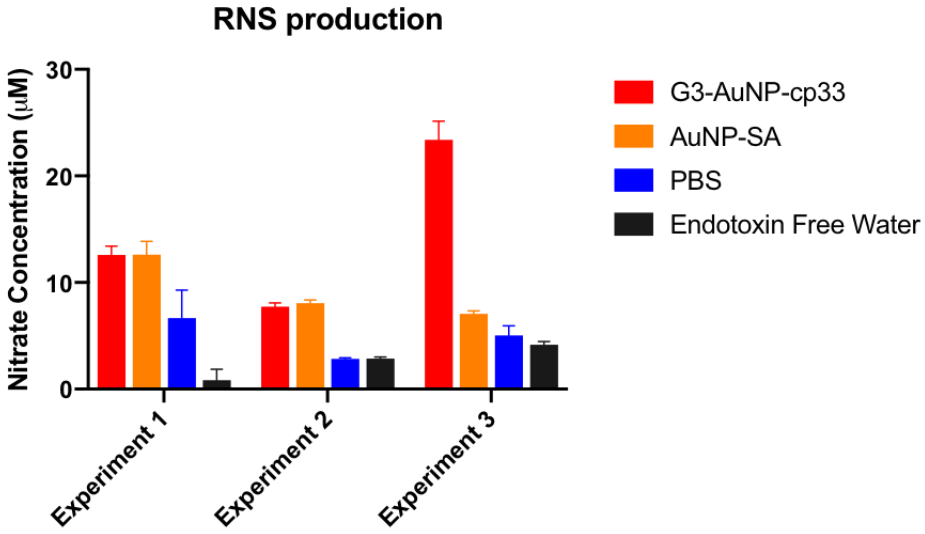


Figure B 2. The variable results of RNS production assay.The experimental results were from three separate experiments with different batches of nanoparticles. The graphs show the nitrite concentration (μM) in the supernatant of macrophages cultured with the treatment shown in the legends. Results were all produced with nanoparticles formulations prepared with SA-AuNP-SA from Nanopartz Inc.

### B.2.5 Proliferation of bone-marrow derived macrophages.

Yong Luo et al. reported the proliferation of macrophages after the activation of ERK pathway by Fc receptor-crosslinking.[207] They observed an increase of the percentage of division and decreased percentage of G1-phase cells in bone marrow-derived macrophages (BMDM) after 5 hr treatment with plate-bound IgG1. We followed the protocol described in their paper, but didn't observe any changes in the DNA content in the cells as suggested by the consistent PI staining profile among various treatment groups. A very minimal decrease in the CFSE fluorescence of BMDMs was noticed upon treatment with high-density IgG1-coated plate. Because we failed to reproduce the results reported in the paper, we didn't continue the assay with SNAbs.

## B.3 Discussion

Here, we documented the attempts to capture the signaling mediated by FcγR-crosslinker to elucidate the mechanism of actions of SNAbs. The signaling cascade is time-dependent and sensitive to the assay conditions, such as the presentation method of Fc, concentration of Fc and buffer components.[200] We failed to produce meaningful results and thus could not conclude whether SNAbs were able to crosslink FcγRs efficiently to induce antibody-mediated responses by themselves. However, as we discussed previously, the receptor-clustering stimulation of immune cells are highly dependent on the size of the particles presenting the stimuli and a nanoparticle of 50 nm in diameter could be too small and of too high curvature that it could not crosslink a sufficient high number of receptors to induce the FcγR-mediated response.[160,190] Therefore, the lack of changes in the signaling after treatment by SNAbs could be attributed to the lack of target cells,

which are responsible for amplifying the interaction between the cp33-presenting SNAbs and FcγRs on the effector cells. As the addition of MDSCs drastically increases the complexity of the assays, we turned to the effector-target co-culture assay and the splenocyte suspension assay for the evaluation of antibody-dependent responses induced by SNAbs. Clearly, our hypothesis that the multivalent presentation of Fc-mimicking ligands on the nanoparticle could induce FcγR-mediated signaling cascade was proved wrong. Indeed, as we reflect back on the application of SNAbs, the inability to trigger FcγR response avoids the non-specific activation of the immune system and is an advantage of SNAbs in terms of safety in clinical treatment.

To further explore the mechanism of action of SNAbs *in vivo*, *in vitro* assays of granzyme B and perforin production by NK cells and complement activation in the presence of both effector cells and target cells would be helpful. In addition, an "artificial target cell" made of cell-sized microbeads coated with antigens would also be useful to investigate the ADCC/ADCP process (e.g., phagocytosis, cytokine production) of SNAbs with macrophages or NK cells as effector cells *in vitro.*

# APPEXDIX C. SIZES AND ZETA POTENTIALS OF THE NANOPARTICLES

Here lists the sizes and zeta potential of modified Janus and non-Janus nanoparticles. The sizes listed are representative of all experiments using SA-AuNP-SA from Nanohybrid.Inc.

Table 6. Typical hydrodynamic sizes of the Janus nanoparticles

| Size | Janus Nanoparticles | | | | | Unmodified SA-AuNP-SA |
|---|---|---|---|---|---|---|
| | G3-AuNP-Fc | G3-AuNP-cp33 | G3*-AuNP-cp33 | scAHNP-AuNP-cp33 | G3-AuNP-Irrelcp33 | |
| **Ave. Size (nm)** | 178.9 | 95.04 | 92.14 | 90.80 | 115.00 | 73.79 |
| **ST.DEV (nm)** | 103.7 | 41.5 | 39.93 | 34.73 | 52.6 | 22.15 |

Table 7. Typical hydrodynamic sizes of modified nonJanus nanoparticles.

| Size | NonJanus Nanoparticles | | | Unmodified SA-AuNP-SA |
|---|---|---|---|---|
| | G3-AuNP-Fc | G3-AuNP-cp33 | AuNP-cp33 | |
| **Ave. Size (nm)** | **84.08** | **83.69** | **79.96** | **73.79** |
| **ST.DEV (nm)** | **26.32** | **28.87** | **29.58** | **22.15** |

Table 8. Zeta potential of peptide-modified Janus nanoparticles

| Zeta Potentials | Ave. Zeta Potential (mV) | ST.DEV (mV) |
|---|---|---|
| **Unmodified SA-AuNP-SA** | -3.50 | 2.17 |
| **Janus G3-AuNP-cp33 (SNAbs)** | -3.54 | 0.47 |
| **Janus scAHNP-AuNP-cp33** | -2.31 | 0.64 |
| **Janus Biotin-AuNP-NEM** | -3.68 | 0.87 |

# APPENDIX D. ANTIBODIES USED IN FLOW CYTOMETRY AND MACS SORTING

Table 9. Antibodies used in flow cytometry and MACS sorting experiments.

| Flow Cytometry | | | |
|---|---|---|---|
| Name | Clone | Company | Function |
| ANTI-FCRN (FCGRT) | Polyclonal | Sigma-Aldrich | Neonatal FcRn |
| Anti-mouse CD32 (Fcγr2) | S17012B | Biolegend | Fc gamma receptor II |
| Alexa Fluor 647 Rat Anti-Mouse S100A9 | MRP-14 | BD Bioscience | S100A9 protein |
| APC Annexin V | Annexin A5 | Biolegend | Apoptotic cells |
| APC Anti-Foxp3 | FJK-16s | eBioscience | Treg |
| APC anti-mouse CD49b (pan-NK cells) | DX5 | Biolegend | NK cells |
| APC Anti-CD64 | X54-5/7.1 | Biolegend | Fc gamma receptor I |
| APC/Cy7 Anti-mouse CD4 | RM4-5 | Biolegend | T cell |
| APC/Cy7 Anti-CD49b (pan-NK cells) | DX5 | Biolegend | NK cells |
| APC/Cy7 anti-mouse CD25 | 3C7 | Biolegend | Treg |
| APC/Cy7 anti-mouse Ly-6C | HK1.4 | Biolegend | MDSC |
| FITC anti-mouse CD8a | 53-6.7 | Biolegend | T cell |
| FITC anti-mouse/human CD45R/B220 | RA3-6B2 | Biolegend | B cell |
| FITC anti-mouse F4/80 | BM8 | Biolegend | Macrophages |
| PE anti-mouse CD4 | RM4-5 | Biolegend | T cell |
| PE anti-mouse CD11c | N418 | Biolegend | DC |

**Table 9 Continued**

| | | | |
|---|---|---|---|
| PE anti-mouse CD32b | AT130-2 | eBioscience | Fc gamma receptor Iib |
| PE anti-mouse CD16 | 275003 | R&D Systems | Fc gamma receptor III |
| PE anti-mouse CD279 (PD-1) | 29F.1A12 | Biolegend | T cell exhaustion |
| PE Anti-Ki-67 | SolA15 | eBioscience | Proliferation |
| PE anti-mouse Perforin | S16009A | Biolegend | Cytolytic function |
| PerCP/Cy5.5Anti-CD223 (LAG-3) | C9B7W | Biolegend | T cell exhaustion |
| PerCP/cy5.5 anti-human/mouse Granzyme B | QA16A02 | Biolegend | Cytolytic function |
| PerCP/Cy5.5 anti-mouse CD107a (LAMP-1) | 1D4B | Biolegend | Degranulation |
| PerCP/Cy5.5 anti-mouse Ki-67 | 16A8 | Biolegend | Proliferation |
| PerCP/Cy5.5 anti-mouse Ly-6G | 1A8 | Biolegend | MDSC |
| PE/Cy7 anti-mouse CD3ε | 145-2C11 | Biolegend | T cell |
| PE/Cy7 anti-mouse/human CD11b | M1/79 | Biolegend | Myeloid cells |
| PE/Cy7 anti-mouse CD16.2 (FcγRIV) | 9E9 | Biolegend | Fc gamma receptor IV |
| Purified anti-mouse CD16/32 | 93 | Biolegend | Blockade of Fc receptors |
| **MACS Sorting** | | | |
| Biotin anti-mouse CD3ε | 145-2C11 | Biolegend | T cell |
| Biotin anti-mouse CD11c | N418 | Biolegend | DC |
| Biotin Anti-CD49b | DX5 | Biolegend | NK |
| Biotin Anti-mouse F4/80 | BM8 | Biolegend | Macrophages |
| Biotin anti-mouse Ly-6G/Ly-6C (Gr1) | RB6-8C5 | Biolegend | MDSCs |

For antibodies used in depletion assays as treatments or *in vivo* experiments, please refer to the material and method sections in the corresponding chapters.

# REFERENCES


1. Jiaying Liu, P. P. & Roy, and K. Synthetic Polymeric Nanoparticles for Immunomodulation. in *Nanomaterials in Pharmacology, Methods in Pharmacology and Toxicology,* (eds. Lu, Z.-R. & Sakuma, S.) 413–438 (Springer Science+Business Media, 2016). doi:10.1007/978-1-4939-3121-7

2. Lesterhuis, W. J., Haanen, J. B. A. G. & Punt, C. J. A. Cancer immunotherapy – revisited. *Nat. Rev. Drug Discov.* **10**, 591–600 (2011).

3. Bru, M., Ma, B., Hayre, J. & Avis, S. Human Antibody Production in Transgenic Animals. 101–108 (2015). doi:10.1007/s00005-014-0322-x

4. Chaigne, B. & Watier, H. Pharmacology & Therapeutics Theranostic of biopharmaceuticals. *Pharmacol. Ther.* (2017). doi:10.1016/j.pharmthera.2017.02.035

5. Stewart, R., Hammond, S. A., Oberst, M. & Wilkinson, R. W. The role of Fc gamma receptors in the activity of immunomodulatory antibodies for cancer. *J. Immunother. Cancer* **2**, 29 (2014).

6. O'Brien, E. L. S. and E. M. Investigating the effect of anti-CTLA-4 on tumor-infiltrating effector T cells. *J Immunol* **198**, (2017).

7. Scheiermann, C., Gibbs, J., Ince, L. & Loudon, A. Clocking in to immunity. *Nat. Rev. Immunol.* **18**, 423–437 (2018).

8. Galluzzi, L., Chan, T. A., Kroemer, G., Wolchok, J. D. & López-soto, A. The hallmarks of successful anticancer immunotherapy. **7807**, 1–15 (2018).

9. Boross, P. & Leusen, J. H. W. Mechanisms of action of CD20 antibodies. *Am. J. Cancer Res.* **2**, 676–90 (2012).

10. Scott, A. M., Wolchok, J. D. & Old, L. J. Antibody therapy of cancer. *Nat. Rev.* **12**, 278–287 (2012).

11. Sievers, E. L. & Senter, P. D. Antibody-Drug Conjugates in Cancer Therapy. *Annu. Rev. Med.* **64**, 15–29 (2013).

12. Chames, P., Van Regenmortel, M., Weiss, E. & Baty, D. Therapeutic antibodies: Successes, limitations and hopes for the future. *Br. J. Pharmacol.* **157**, 220–233 (2009).

13. Ryman, J. T. & Meibohm, B. Pharmacokinetics of monoclonal antibodies. *CPT Pharmacometrics Syst. Pharmacol.* **6**, 576–588 (2017).

14. McGuire, M. J., Samli, K. N., Chang, Y. C. & Brown, K. C. Novel ligands for cancer diagnosis: Selection of peptide ligands for identification and isolation of B-cell lymphomas. *Exp. Hematol.* **34**, 443–452 (2006).

15. Ning, L., He, B., Zhou, P., Derda, R. & Huang, J. Molecular Design of Peptide-Fc fusion Drugs. *Curr. Drug Metab.* **19**, 1–7 (2018).

16. Zhou, J. & Rossi, J. Aptamers as targeted therapeutics: Current potential and challenges. *Nat. Rev. Drug Discov.* **16**, 181–202 (2017).

17. Molek, P., Strukelj, B. & Bratkovic, T. Peptide phage display as a tool for drug discovery: Targeting membrane receptors. *Molecules* **16**, 857–887 (2011).

18. Brown, K. C., Gray, B. P. & Li, S. From Phage Display to Nanoparticle Delivery: Functionalizing Liposomes with Multivalent Peptides Improves Targeting to a Cancer Biomarker. *Bioconjug Chem* (2012). doi:10.1021/bc300498d

19. Li, J. *et al.* Targeting the brain with PEG-PLGA nanoparticles modified with phage-displayed peptides. *Biomaterials* **32**, 4943–4950 (2011).

20. Jung, S. N. *et al.* Targeted delivery of vaccine to dendritic cells by chitosan nanoparticles conjugated with a targeting peptide ligand selected by phage display technique. *Macromol. Biosci.* **15**, 394–404 (2015).

21. Gao, W., Thamphiwatana, S., Angsantikul, P. & Zhang, L. Nanoparticle approaches against bacterial infections. *Wiley Interdiscip. Rev. Nanomedicine Nanobiotechnology* **6**, 532–547 (2014).

22. Trigueros, S. Nanoscale Metal Particles as Nanocarriers in Targeted Drug Delivery System. *J. Nanomedicine Res.* **4**, 2–7 (2016).

23. Tang, L. *et al.* Investigating the optimal size of anticancer nanomedicine. *Proc. Natl. Acad. Sci.* **111**, 15344–15349 (2014).

24. Peiris, P. M., Schmidt, E., Calabrese, M. & Karathanasis, E. Assembly of Linear Nano-Chains from Iron Oxide Nanospheres with Asymmetric Surface Chemistry. *PLoS One* **6**, (2011).

25. Qin, H. *et al.* Generation of a new therapeutic peptide that depletes myeloid-derived suppressor cells in tumor-bearing mice. *Nat. Med.* **20**, 676–681 (2014).

26. Stephane Bonetto, Loredana Spadola, Andrew G. Buchanan, Lutz Jermutus, and J. L. Identification of cyclic peptides able to mimic the functional epitope of IgG1 -Fc for human FcγRI. *FASEB J.* **23**, 575–585 (2009).

27. Tao, K., Fang, M., Alroy, J. & Gary, G. G. Imagable 4T1 model for the study of late stage breast cancer. *BMC Cancer* **8**, 1–20 (2008).

28. Peiris, P. M. *et al.* On-Command Drug Release from Nanochains Inhibits Growth of Breast Tumors. 1460–1468 (2014). doi:10.1007/s11095-013-1102-8

29. Mullard, A. *2018 FDA drug approvals*. *Nature Reviews Drug Discovery* **18**, (2019).

30. Murphy, K. *Janeway's ImmunoBiology*. (GS Garland Science, Taylor & Francis Group, LLC, 2012).

31. Kaplon, H. & Reichert, J. M. Antibodies to watch in 2019. *MAbs* **11**, 219–238 (2019).

32. Scott, A. M., Allison, J. P., Wolchok, J. D. & Hughes, H. Monoclonal antibodies in cancer therapy. **12**, 1–8 (2012).

33. J Golay, M Manganini, V Facchinetti, R Gramigna, R Broady, G Borleri, A Rambaldi, M. I. Rituximab-mediated antibody-dependent cellular cytotoxicity against neoplastic B cells is stimulated strongly by interleukin-2. *Haematologica*

**88**, 1002–1012 (2003).

34. Dotan, E., Aggarwal, C. & Smith, M. R. Impact of Rituximab ( Rituxan ) on the Treatment of B-Cell Non-Hodgkin ' s Lymphoma. **35**, 148–157 (2010).

35. Shi, Y. *et al.* Trastuzumab Triggers Phagocytic Killing of High HER2 Cancer Cells In Vitro and In Vivo by Interaction with Fc γ Receptors on Macrophages. (2017). doi:10.4049/jimmunol.1402891

36. Blank, C. U. & Enk, A. Therapeutic use of anti-CTLA-4 antibodies. *Int. Immunol.* **27**, 3–10 (2014).

37. Buchbinder, E. I. & Desai, A. CTLA-4 and PD-1 Pathways:Similarities, Differences, and Implications of Their Inhibition. *Am. J. Clin. Oncol.* **39**, 98–106 (2016).

38. Chen, L. & Han, X. Anti – PD-1 / PD-L1 therapy of human cancer : past , present , and future. *J. Clin. Invest.* **125**, 3384–3391 (2015).

39. Nagaraj, D. I. G. and S. Myeloid-derived-suppressor cells as regulators of the immune system. *Nat Rev Immunol* **9**, 162–174 (2010).

40. Dilek, N., de Silly, R. V., Blancho, G. & Vanhove, B. Myeloid-derived suppressor cells: Mechanisms of action and recent advances in their role in transplant tolerance. *Front. Immunol.* **3**, 1–9 (2012).

41. Suzanne Ostrand-Rosenberg and Pratima Sinha. Myeloid-Derived Suppressor Cells: Linking Inflammation and Cancer. *J Immunol* **182**, 4499–4506 (2009).

42. Casares, N. *et al.* A peptide inhibitor of FOXP3 impairs regulatory T cell activity and improves vaccine efficacy in mice. *J. Immunol.* **185**, 5150–9 (2010).

43. Tanaka, A. & Sakaguchi, S. Regulatory T cells in cancer immunotherapy. *Cell Res.* **27**, 109–118 (2016).

44. Schirrmann, T. & Hust, M. Phage display-derived human antibodies in clinical development and therapy. *MAbs* **8**, 1177–1194 (2016).

45. Vaughan, A. T., Cragg, M. S. & Beers, S. A. Antibody modulation: Limiting the efficacy of therapeutic antibodies. *Pharmacol. Res.* **99**, 269–275 (2015).

46. Wang, Y. & Fan, Z. Nanobody-derived nanobiotechnology tool kits for diverse biomedical and biotechnology applications. *Int. J. Nanomedicine* **11**, 3287–3303 (2016).

47. Dorresteijn, B. Nanobody-based cancer therapy of solid tumors. *Nanomedicine (Lond.)* **10**, 161–174 (2015).

48. Meyer, T. De, Muyldermans, S. & Depicker, A. Nanobody-based products as research and diagnostic tools. *Trends Biotechnol.* **32**, 263–270 (2014).

49. Danquah, W. *et al.* Nanobodies that block gating of the P2X7 ion channel ameliorate inflammation. *Sci. Transl. Med.* **8**, (2016).

50. Frejd, F. Y. & Kim, K. T. Affibody molecules as engineered protein drugs. *Exp. Mol. Med.* **49**, e306-8 (2017).

51. Löfblom, J. *et al.* Affibody molecules : Engineered proteins for therapeutic ,

diagnostic and biotechnological applications. *FEBS Lett.* **584**, 2670–2680 (2010).

52. Wu, B. & Sun, Y. Pharmacokinetics of Peptide – Fc Fusion Proteins. *J. Pharm. Sci.* **103**, 53–64 (2014).

53. Mcenaney, P. J. *et al.* Chemically Synthesized Molecules with the Targeting and Effector Functions of Antibodies. *J. Am. Chem. Soc.* **136**, 18034−18043 (2014).

54. Weiner, G. J. Building better monoclonal antibody-based therapeutics. *Nat. Rev. Cancer* **15**, 361–370 (2015).

55. Dekkers, G. *et al.* Affinity of human IgG subclasses to mouse Fc gamma receptors. *MAbs* **9**, 767–773 (2017).

56. Overdijk, M. B. *et al.* Crosstalk between Human IgG Isotypes and Murine Effector Cells. *J. Immunol.* **189**, 3430–8 (2012).

57. Beck, A., Goetsch, L., Dumontet, C. & Corva ä, N. Strategies and challenges for the next generation of antibody-drug conjugates. *Nat. Rev. Drug Discov.* **16**, 315–337 (2017).

58. Overdijk, M. B. *et al.* Crosstalk between Human IgG Isotypes and Murine Effector Cells. (2016). doi:10.4049/jimmunol.1200356

59. Foy, K. C. *et al.* Peptide Vaccines and Peptidomimetics of EGFR (HER-1) Ligand Binding Domain Inhibit Cancer Cell Growth In Vitro and In Vivo. *J Immunol* **191**, 11 (2015).

60. Park, B. *et al.* Rationally designed anti-HER2 / neu peptide mimetic disables P185

HER2 / neu tyrosine kinases in vitro and in vivo. **18**, (2000).

61. Murali, R. & Greene, M. I. Structure Based Antibody-Like Peptidomimetics. 209–235 (2012). doi:10.3390/ph5020209

62. Brown, K. C., Gray, B. P. & Li, S. From Phage Display to Nanoparticle Delivery: Functionalizing Liposomes with Multivalent Peptides Improves Targeting to a Cancer Biomarker. *Bioconjug Chem* **24**, 85–96 (2012).

63. Eugene W. M. Ng, David T. Shima, Perry Calias, Emmett T. Cunningham Jr., D. R. G. & A. P. A. Pegaptanib, a targeted anti-VEGF aptamer for ocular vascular disease. *Nat. Rev. Drug Discov.* **5**, 123–132 (2006).

64. Schneider, M. R. & Wolf, E. The epidermal growth factor receptor ligands at a glance. *J. Cell. Physiol.* **218**, 460–466 (2009).

65. Dickgiesser, S. *et al.* Self-Assembled Hybrid Aptamer-Fc Conjugates for Targeted Delivery: A Modular Chemoenzymatic Approach. *ACS Chem. Biol.* **10**, 2158–2165 (2015).

66. Lee, T., Lin, C., Kuo, S., Chang, D. & Wu, H. Peptide-Mediated Targeting to Tumor Blood Vessels of Lung Cancer for Drug Delivery. *Cancer Res.* **67**, 10958–10966 (2007).

67. Bruno, J. G., Carrillo, M. P. & Crowell, R. Preliminary development of DNA aptamer-Fc conjugate opsonins. *J. Biomed. Mater. Res. - Part A* **90**, 1152–1161 (2009).

68. Montet, X., Funovics, M., Montet-Abou, K., Weissleder, R. & Josephson, L. Multivalent effects of RGD peptides obtained by nanoparticle display. *J. Med. Chem.* **49**, 6087–6093 (2006).

69. Curk, T., Dobnikar, J. & Frenkel, D. Optimal multivalent targeting of membranes with many distinct receptors. *Proc. Natl. Acad. Sci.* **114**, 7210–7215 (2017).

70. Dalal, C. & Jana, N. R. Multivalency Effect of TAT-Peptide-Functionalized Nanoparticle in Cellular Endocytosis and Subcellular Trafficking. *J. Phys. Chem. B* **121**, 2942–2951 (2017).

71. Lin, J. *et al.* TIRF imaging of Fc gamma receptor microclusters dynamics and signaling on macrophages during frustrated phagocytosis. *BMC Immunol.* 1–9 (2016). doi:10.1186/s12865-016-0143-2

72. Safenkova, I. V, Zherdev, A. V & Dzantiev, B. B. Correlation between the composition of multivalent antibody conjugates with colloidal gold nanoparticles and their af fi nity. **357**, 17–25 (2010).

73. Jesse Popov, Anita I Kapanen, Christopher Turner, Rebecca Ng, Catherine Tucker, Gigi Chiu, Richard Klasa, M. B. B. & Chikh, & G. Multivalent rituximab lipid nanoparticles as improved lymphoma therapies : indirect mechanisms of action and in vivo activity R eseaRch a Rticle. *Nanomedicine* **6**, 1575–1592 (2011).

74. Martinez-Veracoechea, F. J. & Frenkel, D. Designing super selectivity in multivalent nano-particle binding. *Proc. Natl. Acad. Sci.* **108**, 10963–10968 (2011).

75. Vikash P. Chauhan, Triantafyllos Stylianopoulos, John D. Martin, Zoran Popović, Ou Chen, Walid S. Kamoun, Moungi G. Bawendi, Dai Fukumura, and R. K. J. Normalization of tumour blood vessels improves the delivery of nanomedicines in a size-dependent manner. *Nat Nanotechnol* **7**, 383–388 (2012).

76. Cabral, H. *et al.* Systemic Targeting of Lymph Node Metastasis through the Blood Vascular System by Using Size-Controlled Nanocarriers. *ACS Nano* **9**, 4957–4967 (2015).

77. Mu, Q. *et al.* Anti-HER2/neu peptide-conjugated Iron oxide nanoparticles for targeted delivery of paclitaxel to breast cancer cells. *Nanoscale* **7**, 18010–18014 (2015).

78. Kawamura, W. *et al.* Density-tunable conjugation of cyclic RGD ligands with polyion complex vesicles for the neovascular imaging of orthotopic glioblastomas Density-tunable conjugation of cyclic RGD ligands with polyion complex vesicles for the neovascular imaging of orthotop. *Sci. Technol. Adv. Mater.* **16**, 1–13 (2015).

79. Lin, A. Y. *et al.* Gold Nanoparticle Delivery of Modified CpG Stimulates Macrophages and Inhibits Tumor Growth for Enhanced Immunotherapy. **8**, (2013).

80. Almeida, J. P. M. *et al.* In vivo immune cell distribution of gold nanoparticles in naïve and tumor bearing mice. *Small* **10**, 812–9 (2014).

81. Avram, M. *et al.* Gold Nanoparticle Uptake by Tumour Cells of B16 Mouse Melanoma. *Plasmonics* **7**, 717–724 (2012).

82. Rauta, P. R., Hallur, P. M. & Chaubey, A. Gold nanoparticle-based rapid detection and isolation of cells using ligand-receptor chemistry. *Sci. Rep.* 1–13 (2018). doi:10.1038/s41598-018-21068-8

83. Mocan, T. *et al.* In Vitro Administration of Gold Nanoparticles Functionalized with MUC-1 Protein Fragment Generates Anticancer Vaccine Response via Macrophage Activation and Polarization Mechanism. *J. Cancer* **6**, 583–92 (2015).

84. Dimitriou, N. M. *et al.* Gold nanoparticles, radiations and the immune system: Current insights into the physical mechanisms and the biological interactions of this new alliance towards cancer therapy. *Pharmacol. Ther.* **178**, 1–17 (2017).

85. Narges Elahi, Mehdi Kamali, M. H. B. Recent biomedical applications of gold nanoparticles: A review. *Talanta* **184**, 537–556 (2018).

86. Hadis Daraee, Ali Eatemadi, Elham Abbasi, Sedigheh Fekri Aval, M. K. & A. A. Application of gold nanoparticles in biomedical and drug delivery. *J. Artif. Cells, Nanomedicine, Biotechnol.* **44**, 410–422 (2016).

87. Farooq, M. U. *et al.* Gold Nanoparticles-enabled Efficient Dual Delivery of Anticancer Therapeutics to HeLa Cells. *Sci. Rep.* **8**, 1–12 (2018).

88. Yang, H., Fung, S. Y. & Liu, M. Programming the cellular uptake of physiologically stable peptide-gold nanoparticle hybrids with single amino acids. *Angew. Chemie - Int. Ed.* **50**, 9643–9646 (2011).

89. Kaewsaneha, C., Tangboriboonrat, P., Polpanich, D., Eissa, M. & Elaissari, A.

Janus Colloidal Particles : Preparation , Properties , and Biomedical Applications. (2013).

90. Hu, J., Zhou, S., Sun, Y., Fang, X. & Wu, L. Fabrication, properties and applications of Janus particles. *Chem. Soc. Rev.* **41**, 4356–4378 (2012).

91. M. D. McConnell, M. J. Kraeutler, S. Y. and R. J. C. Patchy and multiregion janus particles with tunable optical properties. *Nano Lett.* **10**, 603–609 (2010).

92. J. Herrikhuyzen, G. Portale, J. C. Gielen, P. C. M. Christianen, N. A. J. M. Sommerdijk, S. C. J. M. and A. P. H. J. S. Disk micelles from amphiphilic Janus gold nanoparticles. *Chem. Commun.* 697–699 (2008).

93. Peiris, P. M. *et al.* Treatment of cancer micrometastasis using a multicomponent chain-like nanoparticle. *J. Control* **173**, 1–18 (2014).

94. Peiris, P. M. *et al.* Imaging Metastasis Using an Integrin-Targeting Chain-Shaped Nanoparticle. *ACS Nano* **6**, 8783–8795 (2012).

95. Yi, Y., Sanchez, L., Gao, Y., Lee, K. & Yu, Y. Interrogating Cellular Functions with Designer Janus Particles. *Chem. Mater.* **29**, 1448–1460 (2017).

96. Chen, B. *et al.* Janus particles as artificial antigen-presenting cells for T cell activation. *ACS Appl. Mater. Interfaces* **6**, 18435–18439 (2014).

97. Tang, J. L., Schoenwald, K., Potter, D., White, D. & Sulchek, T. Bifunctional janus microparticles with spatially segregated proteins. *Langmuir* **28**, 10033–10039 (2012).

98. Ma, C. *et al.* Anti-Gr-1 antibody depletion fails to eliminate hepatic myeloid-derived suppressor cells in tumor-bearing mice. *J. Leukoc. Biol.* **92**, 1199–206 (2012).

99. Matsuzaki, Junko , Tsuji, Takemasa , Chamoto, Kenji , Takeshima, Tsuguhide , Sendo, Fujiro , and Nishimuraa, T. Successful elimination of memory-type CD8+ T cell subsets by the administration of anti-Gr-1 monoclonal antibody in vivo. - PubMed - NCBI. *Cell. Immunol.* **223**, 8 (2003).

100. Sukhatme, Vikas P.; Husain, Z. Cancer Therapy Targeting Tetraspanin 33 (Tspan33) IN Myeloid Derived Suppressor Cells. 93 (2016).

101. Luu, V. P. *et al.* TSPAN33 is a novel marker of activated and malignant B cells. *Clin. Immunol.* **149**, 388–399 (2013).

102. Donnelly, E. M., Kubelick, K. P., Dumani, D. S. & Emelianov, S. Y. Photoacoustic Image-Guided Delivery of Plasmonic-Nanoparticle-Labeled Mesenchymal Stem Cells to the Spinal Cord. *Nano Lett.* **18**, 6625–6632 (2018).

103. W., L. & X., C. Gold nanoparticles for photoacoustic imaging. *Nanomedicine* **10**, 299–320 (2015).

104. Cieslewicz, M. *et al.* Targeted delivery of proapoptotic peptides to tumor-associated macrophages improves survival. *Proc. Natl. Acad. Sci. U. S. A.* **110**, 15919–24 (2013).

105. Kumar, V., Patel, S., Tcyganov, E. & Gabrilovich, D. I. The Nature of Myeloid-

Derived Suppressor Cells in the Tumor Microenvironment. *Trends in Immunology* **37**, (2016).

106. Bronte, V. *et al.* Recommendations for myeloid-derived suppressor cell nomenclature and characterization standards. *Nature Communications* **7**, (2016).

107. Gabrilovich, D. I. Myeloid-derived suppressor cells. *Cancer Immunol. Res.* **5**, 3–8 (2017).

108. Louise A. Elliott, Glen A. Doherty, Kieran Sheahan, and E. J. R. Human Tumor-Infiltrating Myeloid Cells: Phenotypic and Functional Diversity. *Front. Immunol.* **8**, (2017).

109. Pluta, M. D. *et al.* Granulocytic myeloid - derived suppressor cells suppress virus - specific -T cell responses during acute Friend retrovirus infection. *Retrovirology* 1–14 (2017). doi:10.1186/s12977-017-0364-3

110. Li, H., Han, Y., Guo, Q., Zhang, M. & Cao, X. Cancer-expanded myeloid-derived suppressor cells induce anergy of NK cells through membrane-bound TGF-beta 1. *J. Immunol.* **182**, 240–249 (2009).

111. Srinivas Nagaraj, Adam G. Schrum, Hyun-Il Cho, Esteban Celis, and D. I. & Gabrilovich. Mechanism of T-cell tolerance induced by myeloid-derived suppressor cells. *J Immunol. 2010* **184**, 3106–3116 (2011).

112. Umansky, V., Blattner, C., Gebhardt, C. & Utikal, J. The Role of Myeloid-Derived Suppressor Cells ( MDSC ) in Cancer Progression. *Vaccine* **4**, (2016).

113. Ostrand-Rosenberg, S., Sinha, P., Chornoguz, O. & Ecker, C. Regulating the suppressors: Apoptosis and inflammation govern the survival of tumor-induced myeloid-derived suppressor cells (MDSC). *Cancer Immunol. Immunother.* **61**, 1319–1325 (2012).

114. Forghani, P., Khorramizadeh, M. R. & Waller, E. K. Silibinin inhibits accumulation of myeloid-derived suppressor cells and tumor growth of murine breast cancer. *Cancer Med.* 1–10 (2014). doi:10.1002/cam4.186

115. Srivastava, M. K. *et al.* Myeloid suppressor cell depletion augments antitumor activity in lung cancer. *PLoS One* **7**, (2012).

116. Alizadeh, D. *et al.* Doxorubicin eliminates myeloid-derived suppressor cells and enhances the efficacy of adoptive T-cell transfer in breast cancer. *Cancer Res.* **74**, 104–118 (2014).

117. KiBem Kim, Andrew D. Skora, Zhaobo Li, Qiang Liu, Ada J. Tam, R. L. B. & Luis A. Diaz, Jr., Nickolas Papadopoulos, Kenneth W. Kinzler, Bert Vogelstein, and S. Z. Eradication of metastatic mouse cancers resistant to immune checkpoint blockade by suppression of myeloid-derived cells. *PNAS* **111**, 11774–11779 (2014).

118. Henau, O. De *et al.* Overcoming resistance to checkpoint blockade therapy by targeting PI3Kγ in myeloid cells. *Nat. Publ. Gr.* **539**, 443–447 (2016).

119. Vincent, J. *et al.* 5-Fluorouracil Selectively Kills Tumor-Associated Myeloid-Derived Suppressor Cells Resulting in Enhanced T Cell-Dependent Antitumor

Immunity. *Cancer Res.* **70**, 3052–3061 (2010).

120. Braun, G. B. *et al.* Etchable plasmonic nanoparticle probes to image and quantify cellular internalization. *Nat. Mater.* **13**, 1–19 (2014).

121. Averill, M. M. *et al.* S100A9 Differentially Modifies Phenotypic States of Neutrophils, Macrophages, and Dendritic Cells: Implications for Atherosclerosis and Adipose Tissue Inflammation. *Circulation* **123**, 1216–1226 (2012).

122. Mie Ichikawa, Roy Williams, Ling Wang, Thomas Vogl, and G. S. S100A8/A9 activate key genes and pathways in colon tumor progression. *Mol Cancer Res* **9**, 133–148 (2011).

123. Anne R. Bresnick, David J. Weber, and D. B. Z. S100 proteins in cancer. *Nat. Rev. Cancer* **15**, 96–109 (2015).

124. Zhao, F. *et al.* S100A9 a new marker for monocytic human myeloid-derived suppressor cells. *Immunology* **136**, 176–183 (2012).

125. Xia, C., Braunstein, Z., Toomey, A. C., Zhong, J. & Rao, X. S100 Proteins As an Important Regulator of Macrophage Inflammation. *Front. Immunol.* **8**, 1–11 (2018).

126. Qin, H. *et al.* Generation of a new therapeutic peptide that depletes myeloid-derived suppressor cells in tumor-bearing mice. *Nat. Med.* **20**, 676–81 (2014).

127. Sinha, P. *et al.* Proinflammatory S100 Proteins Regulate the Accumulation of Myeloid-Derived Suppressor Cells. *J Immunol.* **181**, 4666–4675 (2008).

128. Brun V, Masselon C, Garin J, D. A. Isotope dilution strategies for absolute quantitative proteomics. *J Proteomics* **72**, 740–748 (2009).

129. Rinker TE, Philbrick BD, Hettiaratchi MH, Smalley DM, McDevitt TC, T. J. Microparticle-mediated sequestration of cell-secreted proteins to modulate chondrocytic differentiation. *Acta Biomater.* **68**, 125–136 (2018).

130. MacLean B, Tomazela DM, Shulman N, Chambers M, Finney GL, Frewen B, Kern R, Tabb DL, Liebler DC, M. M. Skyline: an open source document editor for creating and analyzing targeted proteomics experiments. *Bioinformatics* **26**, 966–973 (2010).

131. Peiris, P. M. *et al.* Enhanced Delivery of Chemotherapy to Tumors Using a Multicomponent Nanochain with Radio-Frequency- Tunable Drug Release. 4157–4168 (2012).

132. Kute, T. *et al.* Understanding key assay parameters that affect measurements of trastuzumab-mediated ADCC against Her2 positive breast cancer cells. *Oncoimmunology* **1**, 810–821 (2012).

133. Yamashita, M. *et al.* A novel method for evaluating antibody-dependent cell-mediated cytotoxicity by flowcytometry using cryopreserved human peripheral blood mononuclear cells. *Sci. Rep.* **6**, 1–10 (2016).

134. Brandsma, A. M., Jacobino, S. R., Meyer, S., ten Broeke, T. & Leusen, J. H. W. Fc receptor inside-out signaling and possible impact on antibody therapy. *Immunol. Rev.* **268**, 74–87 (2015).

135. Nimmerjahn, F., Gordan, S. & Lux, A. FcγR dependent mechanisms of cytotoxic, agonistic, and neutralizing antibody activities. *Trends Immunol.* **36**, 325–336 (2015).

136. Curnow, S. J., Glennie, M. J. & Stevenson, G. T. The role of apoptosis in antibody-dependent cellular cytotoxicity. *Cancer Immunol. Immunother.* **36**, 149–155 (1993).

137. DiLillo, D. J. & Ravetch, J. V. Fc-Receptor Interactions Regulate Both Cytotoxic and Immunomodulatory Therapeutic Antibody Effector Functions. *Cancer Immunol. Res.* **3**, 704–713 (2015).

138. Wang, W., Erbe, A. K., Hank, J. A., Morris, Z. S. & Sondel, P. M. NK cell-mediated antibody-dependent cellular cytotoxicity in cancer immunotherapy. *Front. Immunol.* **6**, (2015).

139. Clynes, R. A., Towers, T. L., Presta, L. G. & Ravetch, J. V. Inhibitory Fc receptors modulate in vivo cytoxicity against tumor targets. *Nat. Med.* **6**, 443–446 (2000).

140. Uchida, J. *et al.* The Innate Mononuclear Phagocyte Network Depletes B Lymphocytes through Fc Receptor-dependent Mechanisms during Anti-CD20 Antibody Immunotherapy. *Cancer Res.* **199**, 1659–1669 (2004).

141. Hamaguchi, Y., Xiu, Y., Komura, K., Nimmerjahn, F. & Tedder, T. F. Antibody isotype-specific engagement of Fcγ receptors regulates B lymphocyte depletion during CD20 immunotherapy. *J. Exp. Med.* **203**, 743–753 (2006).

142. Lazar, G. A. *et al.* Engineered antibody Fc variants with enhanced effector function. *Proc. Natl. Acad. Sci.* **103**, 4005–4010 (2006).

143. Donnelly, E. M., Kubelick, K. P., Dumani, D. S. & Emelianov, S. Y. Photoacoustic Image-Guided Delivery of Plasmonic-Nanoparticle-Labeled Mesenchymal Stem Cells to the Spinal Cord. *Nano Lett.* **18**, 6625–6632 (2018).

144. Korndörfer I P, Brueckner F, S. A. The crystal structure of the human (S100A8/S100A9) 2 heterotetramer, calprotectin, illustrates how conformational changes of interacting α-helices can determine specific association of two EF-hand proteins. *J. Mol. Biol.* **370**, 887–898 (2007).

145. Jorgensen WL, Chandrasekhar J, Madura JD, Impey RW, K. M. Comparison of simple potential functions for simulating liquid water. *J Chem Phys* **79**, 926–935 (1983).

146. Humphrey W, Dalke A, S. K. VMD: Visual molecular dynamics. *J Mol Graph* **14**, 33–38 (1996).

147. Jing Huang, Sarah Rauscher, Grzegorz Nawrocki, Ting Ran, Michael Feig, Bert L de Groot, H. G. & A. D. M. J. CHARMM36m: an improved force field for folded and intrinsically disordered proteins. *Nat. Methods* **14**, 71–73 (2017).

148. Vanommeslaeghe K, Hatcher E, Acharya C, Kundu S, Zhong S, Shim J, Darian E, Guvench O, Lopes P, Vorobyov I, M. A. J. CHARMM general force field: A force field for drug-like molecules compatible with the CHARMM all-atom additive biological force fields. Journal of computational chemistry. *J Comput Chem.* **31**,

671–690 (2010).

149. Rebecca S. Bamert, Karl Lundquist, Hyea Hwang, Chaille T. Webb, Takoya Shiota, Christopher J. Stubenrauch, Mathew J. Belousoff, Robert J. A. Goode, Ralf B. Schittenhelm, Richard Zimmerman, Martin Jung, James C. Gumbart, and T. L. Structural basis for substrate selection by the translocation and assembly module of the β-barrel assembly machinery. *Mol. Microbiol.* **106**, 142–156 (2017).

150. Martyna GJ, Tobias DJ, K. M. Constant pressure molecular dynamics algorithms. *J Chem Phys* **101**, 4177–4189 (1994).

151. Darden T, York D, P. L. Particle mesh Ewald: An N· log (N) method for Ewald sums in large systems. *J. Chem. Phys.* **98**, 10089–10092 (1993).

152. Phillips JC, Braun R, Wang W, Gumbart J, Tajkhorshid E, Villa E, Chipot C, Skeel RD, Kalé L, S. K. Scalable molecular dynamics with NAMD. *J Comput Chem* **26**, 1781–1802 (2005).

153. Narumi, K. *et al.* Proinflammatory Proteins S100A8/S100A9 Activate NK Cells via Interaction with RAGE. *J. Immunol.* **194**, 5539–5548 (2015).

154. Ivashkiv, L. B. A signal switch hypothesis for cross-regulation of cytokine and TLR signalling pathways. *Nat Rev Immunol* **8**, 816–822 (2009).

155. Joshi, T., Butchar, J. & Tridandapani, S. Fcγ Receptor Signaling in Phagocytes. *Int. J. Hematol.* **84**, 210–216 (2006).

156. B Thaci, AU Ahmed, IV Ulasov, DA Wainwright, P Nigam, B Auffinger, AL

Tobias, Y Han, L Zhang, K-S Moon, and M. L. Depletion of myeloid-derived suppressor cells during interleukin-12 immunogene therapy does not confer a survival advantage in experimental malignant glioma. *Cancer Gene Ther.* **21**, 38–44 (2014).

157. Stylianos Bournazos, Taia T. Wang, and J. V. R. The Role and Function of Fcγ Receptors on Myeloid Cells. *Microbiol Spectr* **4**, (2016).

158. Garc á-Garc á, E. & Rosales, C. Signal transduction during Fc receptor-mediated phagocytosis. *J. Leukoc. Biol.* **72**, 1092–1108 (2002).

159. Ortiz, D. F. *et al.* Elucidating the interplay between IgG-Fc valency and Fc g R activation for the design of immune complex inhibitors. *Sci. Transl. Med.* **8**, 13 (2016).

160. Hickey, J. W., Vicente, F. P., Howard, G. P., Mao, H. Q. & Schneck, J. P. Biologically Inspired Design of Nanoparticle Artificial Antigen-Presenting Cells for Immunomodulation. *Nano Lett.* **17**, 7045–7054 (2017).

161. Moynihan, K. D. *et al.* Eradication of large established tumors in mice by combination immunotherapy that engages innate and adaptive immune responses. (2016). doi:10.1038/nm.4200

162. Wesolowski, R., Markowitz, J. & Carson, W. E. Myeloid derived suppressor cells - a new therapeutic target in the treatment of cancer. *J. Immunother. cancer* **1**, 10 (2013).

163. Liu, Y. *et al.* Triple negative breast cancer therapy with CDK1 siRNA delivered by cationic lipid assisted PEG-PLA nanoparticles. *J. Control. Release* **192**, 114–121 (2014).

164. Lebert, J. M., Lester, R., Powell, E., Seal, M. & McCarthy, J. Advances in the systemic treatment of triple-negative breast cancer. *Curr. Oncol.* **25**, S142–S150 (2018).

165. Matucci, A., Vultaggio, A. & Danesi, R. The use of intravenous versus subcutaneous monoclonal antibodies in the treatment of severe asthma: A review. *Respir. Res.* **19**, 1–10 (2018).

166. Robin K Hartman, Kristina A Hallam, E. M. D. and S. Y. E. Photoacoustic imaging of gold nanorods in the brain delivered via microbubble-assisted focused ultrasound: a tool for in vivo molecular neuroimaging. *Laser Phys. Lett.* **16**, (2019).

167. YS Chen, W Frey, S Kim, P Kruizinga, K Homan, S. E. Silica-coated gold nanorods as photoacoustic signal nanoamplifiers. *Nano Lett.* **11**, 348–354 (2011).

168. Tabrizi, M., Bornstein, G. G. & Suria, H. Biodistribution Mechanisms of Therapeutic Monoclonal Antibodies in Health and Disease. *AAPS J.* **12**, 33–43 (2009).

169. Shi M, Li M, Cui Y, Adachi Y, I. S. Gr-1 Ab administered after bone marrow transplantation plus thymus transplantation suppresses tumor growth by depleting granulocytic myeloid-derived suppressor cells. *PLoS One* **9**, e97908 (2014).

170. Bulliard, Y. *et al.* Activating Fc γ receptors contribute to the antitumor activities of immunoregulatory receptor-targeting antibodies. *J. Exp. Med.* **210**, 1685–93 (2013).

171. Lucas Silva Carvalho, Otávio Bravim da Silva, Gabriela Carneiro de Almeida, J. D. de O. & Carmo, N. S. P. and T. S. Production Processes for Monoclonal Antibodies. in *Fermentation Processes* 182–197 (2017).

172. Ackerman, M. E., Pawlowski, D. & Wittrup, K. D. Effect of antigen turnover rate and expression level on antibody penetration into tumor spheroids. *Mol. Cancer Ther.* **7**, 2233–2240 (2008).

173. Wang, A. Z. *et al.* Biofunctionalized targeted nanoparticles for therapeutic applications. *Expert Opin. Biol. Ther.* **8**, 1063–70 (2008).

174. Ellis, S. E., Newlands, G. F. J., Nisbet, A. J. & Matthews, J. B. Phage-display library biopanning as a novel approach to identifying nematode vaccine antigens. *Parasite Immunol.* **34**, 285–295 (2012).

175. Shadidi, M. & Sioud, M. Identification of novel carrier peptides for the specific delivery of therapeutics into cancer cells. *FASEB J.* **17**, 256–258 (2003).

176. Pacheco, P., White, D. & Sulchek, T. Effects of Microparticle Size and Fc Density on Macrophage Phagocytosis. *PLoS One* **8**, 1–9 (2013).

177. Nie, Z., Li, W., Seo, M., Xu, S. & Kumacheva, E. Janus and ternary particles generated by microfluidic synthesis: Design, synthesis, and self-assembly. *J. Am.*

*Chem. Soc.* **128**, 9408–9412 (2006).

178. Lone, S. & Cheong, I. W. Fabrication of polymeric Janus particles by droplet microfluidics. *RSC Adv.* **4**, 13322–13333 (2014).

179. Wenxiu Li, ab Hua Dong, Guannan Tang, T. M. and X. C. Controllable microfluidic fabrication of Janus and microcapsule particles for drug delivery applications. *RSC Adv.* 23181–23188 (2015).

180. Herd, H. L., Bartlett, K. T., Gustafson, J. A., McGill, L. D. & Ghandehari, H. Macrophage silica nanoparticle response is phenotypically dependent. *Biomaterials* **53**, 574–582 (2015).

181. Shang, L. *et al.* Nanoparticle interactions with live cells: Quantitative fluorescence microscopy of nanoparticle size effects. *Beilstein J. Nanotechnol.* **5**, 2388–97 (2014).

182. Luk, B. T. *et al.* Interfacial interactions between natural RBC membranes and synthetic polymeric nanoparticles. *Nanoscale* **6**, 2730–7 (2014).

183. HC Kolb, MG Finn, K. S. Click chemistry: diverse chemical function from a few good reactions. *Angew. Chemie Int. Ed.* **40**, 2004–2021 (2001).

184. Stanislav I. Presolski, Vu Phong Hong, and M. G. F. Copper-Catalyzed Azide–Alkyne Click Chemistry for Bioconjugation. *Curr Protoc Chem Biol.* **3**, 153–162 (2011).

185. Brian M. Zeglis, Charles B. Davis, Robert Aggeler, Hee Chol Kang, Aimei Chen,

Brian J. Agnew, and J. S. L. An Enzyme-Mediated Methodology for the Site-Specific Radiolabeling of Antibodies Based on Catalyst-Free Click Chemistry. *Bioconjug Chem* **24**, 1057–1067 (2013).

186. Wagner, K. *et al.* Bispecific antibody generated with sortase and click chemistry has broad antiinfluenza virus activity. *Proc. Natl. Acad. Sci.* **111**, 16820–16825 (2014).

187. Moraveji, S. R. and M. K. Microfluidic assisted synthesis of PLGA drug delivery systems. *RSC Adv.* **9**, 2055–2072 (2019).

188. Edyta Swider, Olga Koshkina, Jurjen Tel, Luis J.Cruz, I. Jolanda M.de Vries, M. S. Customizing poly(lactic-co-glycolic acid) particles for biomedical applications. *Acta Biomater.* **73**, 38–51 (2018).

189. Nicolete, R., Santos, D. F. Dos & Faccioli, L. H. The uptake of PLGA micro or nanoparticles by macrophages provokes distinct in vitro inflammatory response. *Int. Immunopharmacol.* **11**, 1557–1563 (2011).

190. Chen, X. & Gao, C. Influences of size and surface coating of gold nanoparticles on inflammatory activation of macrophages. *Colloids Surfaces B Biointerfaces* **160**, 372–380 (2017).

191. Kononenko, V., Narat, M. & Drobne, D. Nanoparticle interaction with the immune system. *Arh. Hig. Rada Toksikol.* **66**, 97–108 (2015).

192. Thomas, S. N., Vokali, E., Lund, A. W., Hubbell, J. A. & Swartz, M. A. Targeting

the tumor-draining lymph node with adjuvanted nanoparticles reshapes the anti-tumor immune response. *Biomaterials* **35**, 814–824 (2014).

193. Cleary, K. L. S., Chan, H. T. C., James, S., Glennie, M. J. & Cragg, M. S. Antibody Distance from the Cell Membrane Regulates Antibody Effector Mechanisms. *J. Immunol.* **198**, 3999–4011 (2017).

194. Lucarelli M, Gatti AM, Savarino G, Quattroni P, Martinelli L, Monari E, B. D. Innate defence functions of macrophages can be biased by nano-sized ceramic and metallic particles. *Eur Cytokine Netw* **13**, 339–346 (2004).

195. Miller, S. D., Getts, D. R., Shea, L. D., Miller, S. D. & King, N. J. C. Harnessing nanoparticles for immune modulation Harnessing nanoparticles for immune modulationfile:///C:/Users/Usuari/Downloads/ar500190q.pdf. *Trends Immunol.* **36**, 419–427 (2015).

196. Fadeel, B. Hide and Seek: Nanomaterial Interactions With the Immune System. *Front. Immunol.* **10**, 133 (2019).

197. Luo, Y.-H., Chang, L. W. & Lin, P. Metal-Based Nanoparticles and the Immune System: Activation, Inflammation, and Potential Applications. *Biomed Res. Int.* **2015**, 1–12 (2015).

198. Dykman, L. A. & Khlebtsov, N. G. Immunological properties of gold nanoparticles. *Chem. Sci.* **8**, 1719–1735 (2017).

199. Nagashima, H. *et al.* Tandemly repeated Fc domain augments binding avidities of

antibodies for Fcγ receptors, resulting in enhanced antibody-dependent cellular cytotoxicity. *Mol. Immunol.* **45**, 2752–2763 (2008).

200. Zhang, Y., Hoppe, A. D. & Swanson, J. a. Coordination of Fc receptor signaling regulates cellular commitment to phagocytosis. *Proc. Natl. Acad. Sci. U. S. A.* **107**, 19332–19337 (2010).

201. Slamon Dennis J, Lelyland-Jones Brian, Shak Steven, N. L. Use of Chemotherapy Plus a Monoclonal Antibody Against Her2 For Metastatic Breast Cancer That Overexpresses Her2. *N. Engl. J. Med.* **344**, 783–792 (2001).

202. Evert J Van Limbergen, Dirk K De Ruysscher, Veronica Olivo Pimentel, Dami ënne Marcus, Maaike Berbee, Ann Hoeben, Nicolle Rekers, Jan Theys, Ala Yaromina, Ludwig J Dubois, and P. L. Combining radiotherapy with immunotherapy: the past, the present and the future. *Br J Radiol.* **90**, (2017).

203. Formenti, S. C. *et al.* Radiotherapy induces responses of lung cancer to CTLA-4 blockade. *Nat. Med.* doi:10.1038/s41591-018-0232-2

204. Gandhi SJ, Minn AJ, Vonderheide RH, Wherry EJ4, Hahn SM, M. A. Awakening the immune system with radiation: Optimal dose and fractionation. *Cancer Lett* **368**, 185–190 (2015).

205. M.J., S. *et al.* Transcriptomic analyses of murine resolution-phase macrophages. *Blood* **118**, e192–e208 (2011).

206. Nimmerjahn, F. & Ravetch, J. V. Antibodies, Fc receptors and cancer. *Curr. Opin.*

*Immunol.* **19**, 239–245 (2007).

207. Luo, Y., Pollard, J. W. & Casadevall, A. Fcγ receptor cross-linking stimulates cell proliferation of macrophages via the ERK pathway. *J. Biol. Chem.* **285**, 4232–4242 (2010).